

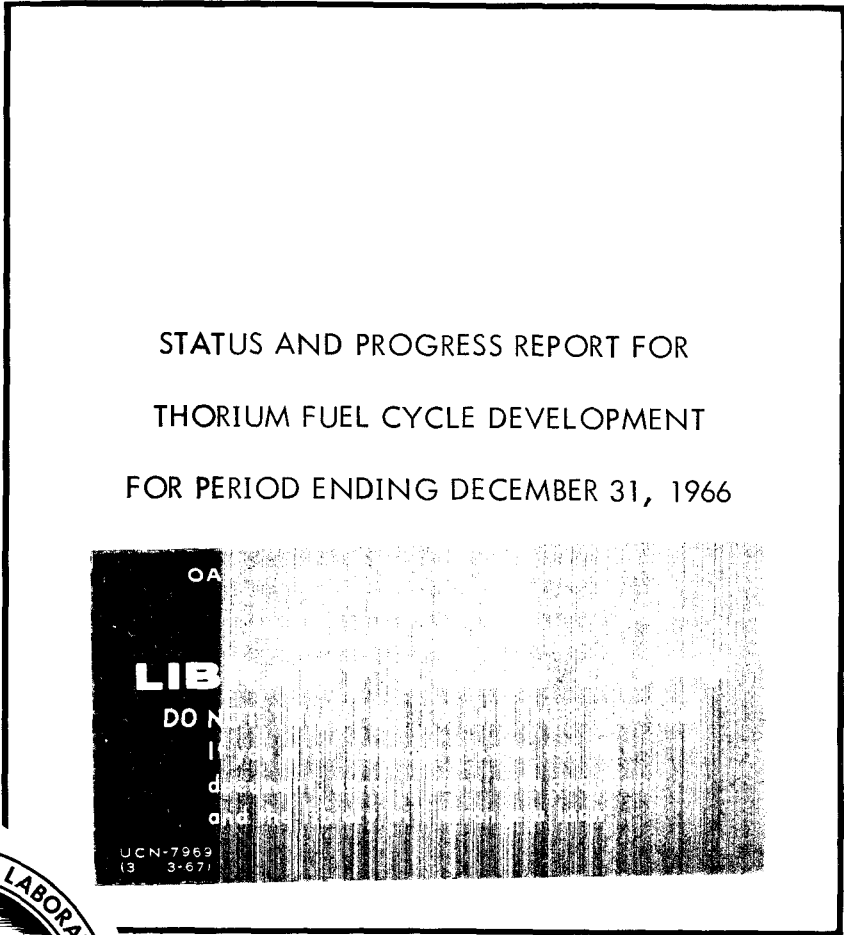


3 4456 0450117 1

CENTRAL RESEARCH LIBRARY,
DOCUMENT COLLECTION

1

ORNL-4275
UC-25 - Metals, Ceramics, and Materials



OAK RIDGE NATIONAL LABORATORY
operated by
UNION CARBIDE CORPORATION
for the
U.S. ATOMIC ENERGY COMMISSION

Printed in the United States of America. Available from Clearinghouse for Federal
Scientific and Technical Information, National Bureau of Standards,
U.S. Department of Commerce, Springfield, Virginia 22151
Price: Printed Copy \$3.00; Microfiche \$0.65

LEGAL NOTICE

This report was prepared as an account of Government sponsored work. Neither the United States, nor the Commission, nor any person acting on behalf of the Commission:

- A. Makes any warranty or representation, expressed or implied, with respect to the accuracy, completeness, or usefulness of the information contained in this report, or that the use of any information, apparatus, method, or process disclosed in this report may not infringe privately owned rights; or
- B. Assumes any liabilities with respect to the use of, or for damages resulting from the use of any information, apparatus, method, or process disclosed in this report.

As used in the above, "person acting on behalf of the Commission" includes any employee or contractor of the Commission, or employee of such contractor, to the extent that such employee or contractor of the Commission, or employee of such contractor prepares, disseminates, or provides access to, any information pursuant to his employment or contract with the Commission, or his employment with such contractor.

ORNL-4275

Contract No. W-7405-eng-26

CHEMICAL TECHNOLOGY DIVISION
METALS AND CERAMICS DIVISION

STATUS AND PROGRESS REPORT FOR THORIUM FUEL CYCLE DEVELOPMENT
FOR PERIOD ENDING DECEMBER 31, 1966

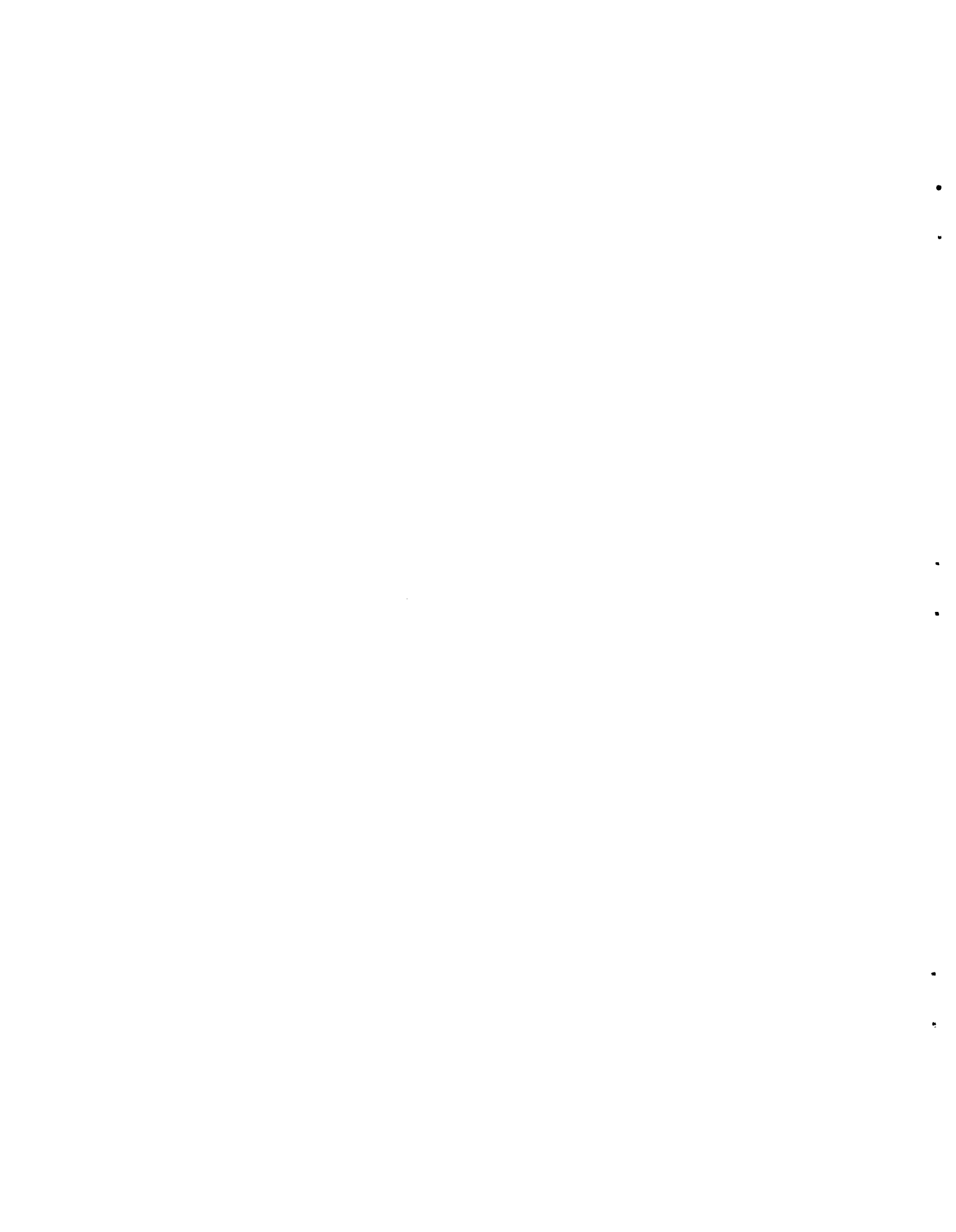
Compiled by
R. G. Wymer and A. L. Lotts

JANUARY 1969



3 4456 0450117 1

OAK RIDGE NATIONAL LABORATORY
Oak Ridge, Tennessee
operated by
UNION CARBIDE CORPORATION
for the
U.S. ATOMIC ENERGY COMMISSION



CONTENTS

1.	PROCESS DEMONSTRATION AND ^{233}U DISTRIBUTION.....	1
	Storage and Distribution Facilities.....	1
	Distribution Activities Summary.....	1
2.	THORIUM-URANIUM RECYCLE FACILITY.....	4
	TURF Construction.....	4
	Design of Sol-Gel Process Equipment.....	8
	Fueled-Graphite Refabrication Equipment.....	11
3.	SOL-GEL PROCESS DEVELOPMENT.....	15
	Preparation of Urania Sols by a Precipitation-Peptization Process.....	15
	Sol Preparation by Amine Extraction.....	27
	Preparation of Mixed Oxide Sols.....	33
	Microsphere Preparation Process Development.....	39
	Microsphere Preparation Column Chemistry.....	51
4.	FUELED-GRAPHITE DEVELOPMENT.....	57
	Particle Handling.....	57
	Particle Coating.....	61
	Particle Inspection.....	78
	Blending and Bonding Fuel Particles.....	81
5.	IRRADIATION OF COATED-PARTICLE FUELS.....	88
	Comparison of Test Results with Model Predictions.....	88
	Comparison of Sol-Gel-Derived Microspheres with Sintered Spheroidal Fuel Kernels.....	91
	Summary of Irradiation Tests on Sol-Gel-Derived Fuels as Coated Particles.....	94
6.	BULK OXIDE PROCESS DEVELOPMENT.....	99
	Pelletizing.....	100
	Sol-Gel Extrusion.....	104
	Vibratory Compaction of Microspheres by the Sphere-Pac Technique.....	118
7.	IRRADIATION OF BULK OXIDE FUELS.....	121
	Irradiation of Thorium-Bearing Bulk Oxide Fuels.....	121
	Irradiation Testing of Sol-Gel-Derived Urania-Base Fuels.....	129

8. ADVANCED SOL-GEL STUDIES.....	135
Preparation of Thorium and Uranium Carbides.....	135
Porous Oxides.....	149
Properties of Carbon-Metal Oxide Sols.....	152
9. DRYING, SINTERING, AND GAS EVOLUTION STUDIES ON SOL-GEL UO ₂ MICROSPHERES.....	157
Isothermal Shrinkage of Sol-Gel Urania Microspheres.....	158
Changes of Crystallite Size, BET Surface Area, and Bulk Density During Drying and Sintering of Urania Microspheres....	159
Differential Thermal Analyses of Sol-Gel Urania.....	162
UO ₂ Oxidation Studies by Thermogravimetric Analysis.....	165
Firing in Various Atmospheres.....	166
Drying and Sintering Schedule for Sol-Gel Urania Microspheres.....	169
Gas Evolution from Sol-Gel Microspheres.....	173

1. PROCESS DEMONSTRATION AND ^{233}U DISTRIBUTION

J. R. Parrott

Storage and Distribution Facilities

With its high yield of 2.29 neutrons per thermal neutron absorbed, ^{233}U is attractive as a breeder reactor fuel. Thorium is abundant in nature, and because the use of the ^{233}U produced from it avoids the need for uranium isotope separation, there is a strong interest in the thorium fuel cycle. During the past year the AEC increased by 114 kg the amount of ^{233}U available from the ORNL national storage facilities for use by experimentalists and others. This ^{233}U was made by irradiating ThO_2 to low burnup to produce material with a low ^{232}U content (less than 5 ppm), thus greatly reducing the handling problems usually associated with ^{233}U as a result of the high-energy gamma-emitting daughters of ^{232}U .

The Building 3019 facilities for storage, dissolution, and purification were discussed in detail previously¹ and will not be further discussed here.

Distribution Activities Summary

During 1966, 41 shipments containing 128 kg of ^{233}U were received by ORNL. During the same period, 54 shipments containing a total of 128 kg of ^{233}U were made. The bulk of the material was received as freshly purified nitrate solution and transferred to other sites without re-purification. Approximately 73 kg of ^{233}U was exchanged with Nuclear Fuels Services, Erwin, Tennessee. Nuclear Fuels Services is the fuel fabrication contractor for the Bettis Light-Water Breeder Reactor program. The material originally allotted to this program was slightly lower in isotopic enrichment than that returned to the ORNL pool.

Approximately 73 kg of ^{233}U as uranyl nitrate was temporarily transferred to the Neutron Physics Division for use in criticality experiments.

During the year, four solvent extraction runs were made for the purification of 40 kg of ^{233}U .

The activities of the ^{233}U handling group for 1966 are compared with previous years in Fig. 1.1. The inventory of material at the end of 1966 is shown in Table 1.1.

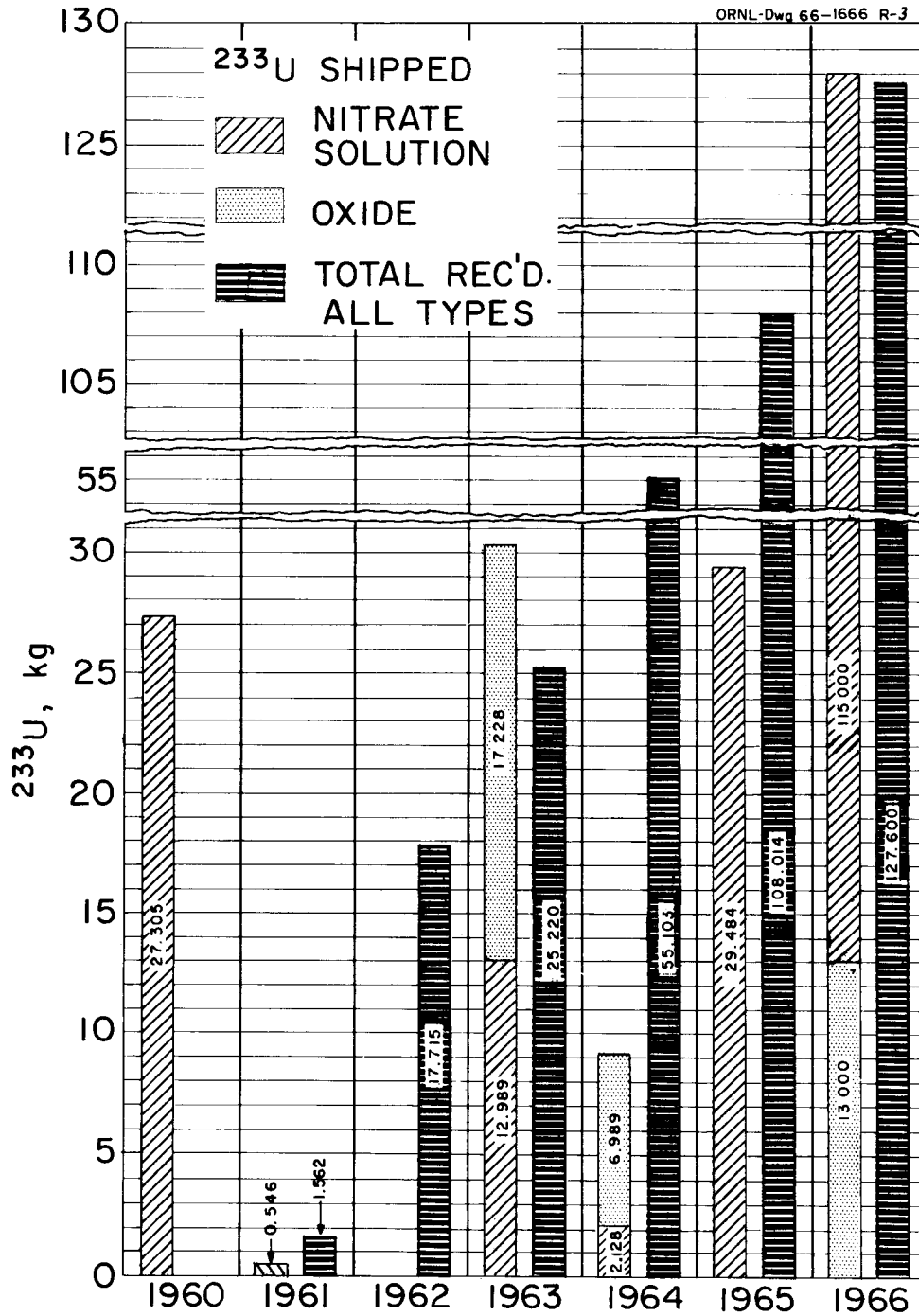


Fig. 1.1. Uranium-233 Receipts and Shipment.

Table 1.1. Inventory of ^{233}U in Building 3019

Quantity (kg)	Form	Isotopic Purity (% ^{233}U)	^{232}U Content (ppm)
0.546	Nitrate	91	50
2.276	$\text{UO}_2\text{-ThO}_2$	91	50
98.013	UO_2	91	250
19.312	Nitrate	97	~42
2.179	Scrap (slag, UO_2 , etc.)	91-98	5-50
13.647	UO_2	97	50
13.954	Nitrate	98	5
72.700	Nitrate (temporarily assigned to Neutron Physics)	98	5
23.794	UO_2	93-98	5
2.205	UO_2	78	23
5.052	^{233}U metal	98	5
<hr/>			
Total:	253.678		

REFERENCE

¹J. R. Parrott, Status and Progress Report for Thorium Fuel Cycle Development for Period Ending December 31, 1965, ORNL-4001, pp. 1-10.

2. THORIUM-URANIUM RECYCLE FACILITY

A. R. Irvine

The engineering-scale demonstration of processes developed on the bench scale requires design decisions, prototype construction, drawings for plant and equipment layout, and estimates of cost. A major design effort is being devoted to the TURF.

The TURF is to afford adequate shielded space for development of remote processing and fabrication equipment for Th-²³³U fuels of various types. Sufficient shielding (5.5 ft of normal concrete) is being provided so that highly irradiated fuel assemblies can be accommodated after a three-month decay period. The heavy shielding also avoids limitations on ²³²U content or decay time after removal of ²³²U decay products and permits the fabrication of fuels from irradiated uranium and thorium that have been only partially decontaminated from fission products. The four operating cells in the facility are each 20 ft wide and have a combined length of 106 ft.

TURF Construction

J. W. Anderson D. M. Shepherd J. P. Jarvis

A contract for the construction of the Thorium-Uranium Recycle Facility was signed with Blount Brothers Construction Company of Montgomery, Alabama, on May 6, 1965.

At the end of 1965, the facility was estimated to be 39.5% complete. The exterior walls of concrete block were essentially complete, and the roof was nearly complete. Cell F and the concrete for the fuel storage basin had been completed. Underground piping and ductwork below the cell floors had been nearly completed. Some of the processing cell floors were complete, and three of the cell E walls had been poured up to elevation 851 ft even, just above the first floor level. The first course of stainless steel liner plates had been placed on the walls in cells C and G.

During 1966, facility construction work progressed to 93% completion. Figures 2.1 and 2.2 show the east cell operating area and the

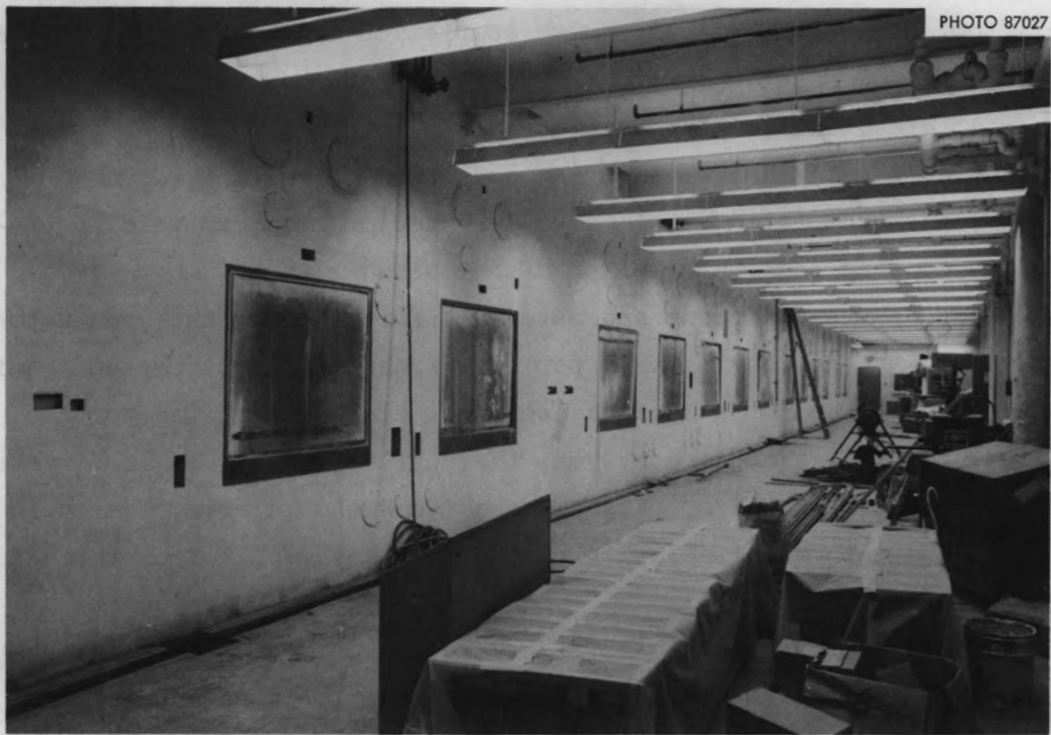


PHOTO 87027

Fig. 2.1. East Cell Operating Area in TURF.

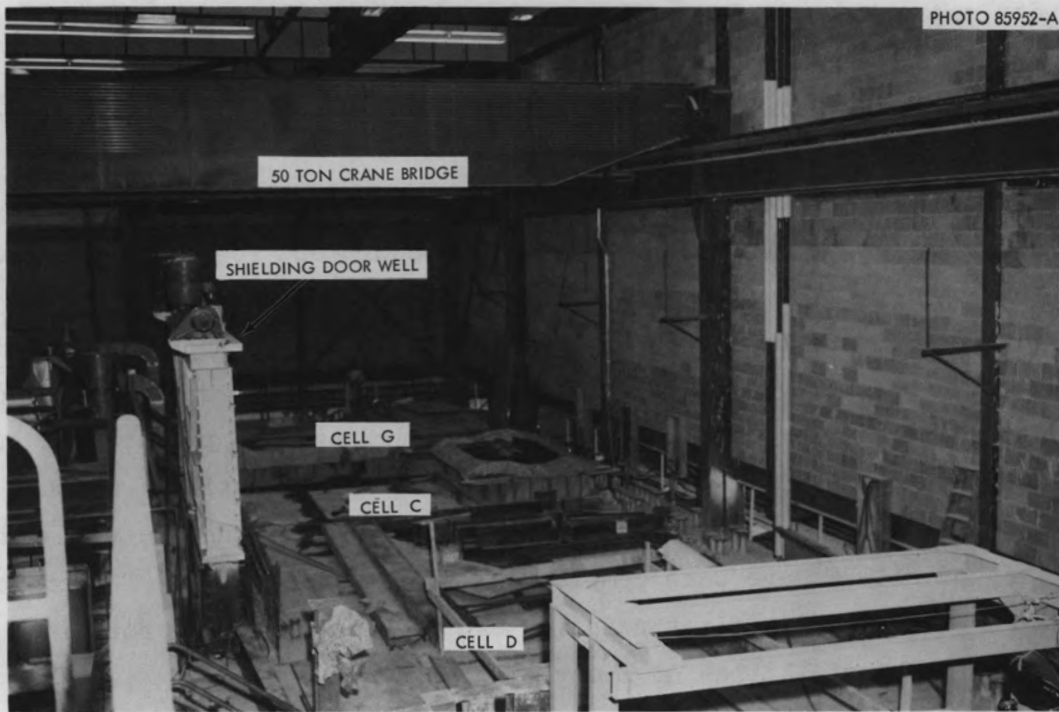


PHOTO 85952-A

Fig. 2.2. Cell Roof Area in TURF.

cell roof area, respectively, with completion of the outside walls and roof. Outside painting, with the exception of the usual touch-up work, was completed. All cell concrete, except for the cell B roof, was poured. All cell liners, with the exception of cells B, C, and D floors, were completed. Cell A was erected and is now awaiting protective coating and installation of the windows.

Most of the equipment and materials furnished by the contractor arrived on the job during this period. Exceptions were certain equipment for cell A and the airlock, the fuel element transfer port for cell E, the fuel element conveyor, the Vogt valves for the CO₂ system, and valves for the filter pits. These items should arrive early in 1967. Some delay in completion of the TURF may result from their late delivery.

Except for certain small, floor-slab areas near cell B on the third floor, the interior walls and floors were completed throughout the building. Electrical work included the installation of panels, motors, transformers, motor control centers, multiconductor cables and cable trays, lighting, and the emergency generator set. Mechanical work included major items such as fabrication of the CO₂ fire-protection system piping, installation of the waste tank pit, installation of heating and ventilating units with associated ductwork, and miscellaneous mechanical services.

Protective coating was applied in certain areas of the building, principally the mechanical and electrical equipment rooms, cell F and cell F corridor, the warm shop, and the chemical makeup room. Other large areas of the building have been prepared for the application of protective coating. The preparation work includes the installation of transite enclosures on the trusses on the high bay and preparation of the concrete walls of cell E to receive protective coating. Of the areas that have been coated, only the waste tank pit and the walls and ceiling of cell F have been completed with the final coat. The office area has received its first painting and is being prepared for final painting and installation of floor tile.

Shield doors 1, 2, and 3, furnished by ORNL rather than by the contractor, were installed and tested. The doors were delivered at a later date than had been scheduled, due to difficulties at the manufacturer's plant, resulting in a setback in construction completion date and additional expense. Completion of the facility is now scheduled for the latter part of May 1967. Contract extensions to that time were granted to the contractor because of delay in delivery of shield doors and because of various work stoppages. All of the remaining materials furnished by ORNL for installation by the fixed-price contractor were delivered during 1966 and either have been given to the contractor or are being held by ORNL until the contractor is ready to install them.

A considerable number of other items that will be installed by the local contractor or ORNL were also procured during this period. These include the lead-glass viewing windows and the partial delivery of the copper-lined, zinc bromide window tanks. There were problems with these tanks - primarily with the copper material and welding - which now appear to be resolved; the tanks are now being fabricated without difficulty.

Portions of the cell crane and manipulator system were completed, tested, and delivered. These portions included the equipment for cells F, E, and A. Tests of crane and manipulator systems for cells B, C, and D in November indicated that certain modifications and corrective work are required. Completion of these systems is expected early in 1967. A large quantity of motor control cable, associated with the installation of the cell crane and manipulator systems, was ordered because we anticipated that the copper shortage would delay delivery. Approximately 75% of this cable has now been delivered.

Other items procured during this period include master-slave manipulators, the waste tank sampling station, Raschig rings for installation in the waste tanks, cell service shield and seal plugs and dust covers of 4-in. bent service sleeve, equipment mounting pads fabricated from 17-4 PH stainless steel, and special in-cell filters.

Design of Sol-Gel Process Equipment

A. R. Irvine J. M. Chandler F. L. Hannon J. W. Snider

The design group is providing counsel on process alternatives and assisting the development groups by designing test equipment. The status of the various process steps is discussed below.

Uranyl Nitrate Solution Storage and Dispensing

We designed a system for the storing and dispensing of accurately measured quantities of uranyl nitrate solution. It is now being constructed and will be installed in the TURF. The main reason for fabricating this equipment now is to gain experience with the special design features for remote handling and operability. The cost of fabricating this equipment has been excessive, but we have discovered means to materially reduce the difficulty of construction. We have designed and partially tested with encouraging results a prototype device, which consists of an "acid-egg," or blow-case, which can be emptied at a controlled rate to provide a metered flow. More work is needed before this is ready for plant use.

Uranium Reduction

Both methods for making a urania sol (i.e., precipitation-peptization and solvent extraction) require a feed of uranium(IV) solution. The procedures now used in laboratory and engineering-scale equipment for reduction of uranium(VI) to (IV) are undesirable for plant operation because of either difficult separations of solids and liquids or the many problems imposed by high-pressure operation. Preliminary tests have indicated that a process operating at atmospheric pressure and employing catalyst deposited on large particles can be developed to avoid these problems. Present development and design work is directed to attaining these goals.

Reduction of hexavalent uranium requires intimate contact between gas, solid, and liquid. Methods being considered to achieve this are: (1) a trickle column in which uranyl nitrate solution would flow over a bed of catalyst particles while in a hydrogen atmosphere, and

(2) several forms of a slurry reactor in which the liquid phase would be continuous with catalyst particles in suspension and hydrogen gas bubbled through the mixture.

Sol Preparation

We are considering two methods for use in the TURF for preparation of urania-thoria sols having 0.1 to 0.25 mole fraction urania: (1) blending separately prepared urania and thoria sols and (2) amine extraction of nitrate from a solution of uranium and thorium nitrates.

Blended sols would be composed of urania sol - prepared by precipitation, washing of the precipitate, and peptization of the washed solids - and thoria sol prepared by steam denitration of thorium nitrate and dispersion of the resultant thoria in water. This procedure has been used to make all the large quantities (i.e., kilogram batches) of urania-thoria microspheres of high urania content prepared at ORNL to date. We reported previously¹ the design of a system to substitute fluid handling operations for the solids handling operations required by filtration techniques used earlier in preparing urania sol by precipitation-peptization. Design personnel observed and assisted in the operation of this equipment for precipitation-peptization and counter-current decantation. It was redesigned several times in an eventually successful effort to avoid problems with plugging of transfer lines and difficulties in pumping a slurry of the precipitate. Success was attained largely by changing from small tortuous tubes to much larger straight tubes and by restricting pumping to only relatively dilute (~ 0.2 M) slurries.

The design and construction of engineering-scale equipment for development of the amine extraction process for sol preparation was completed. This equipment, while performing quite well in cold service, must be modified for remote in-cell operations. In particular, a more compact design for the mixer-settlers is required.

Of the two processes for preparation of mixed sols, amine extraction is preferred as an engineering operation. The apparent major advantages are these:

1. such sols have essentially no undispersed material;
2. there is less difficulty with controlling and measuring uranium-to-thorium ratio in blending nitrate solutions, which are used as feed to the extractors, than in blending sols;
3. mechanical and control problems are less difficult.

Sphere Forming

The process and equipment development for sphere forming is farther advanced than any of the other aspects of microsphere preparation; hence, the TURF equipment design for this aspect will be started first, in January 1967. A single pump will circulate 2-ethyl-1-hexanol, and the equipment will be arranged to permit use of a wide variety of drop formers. Other than the drop former, the major remaining mechanical problem is inspection of the spheres, either as they are formed or as they leave the sphere-forming column. Optical and photoelectric methods are being considered. The optical method may reveal flaws in particle structure and size, whereas the photoelectric device can report only the diameter of the particles.

Drying and Firing

Study of drying and firing techniques has led to the conclusion that batch operation is preferable for the TURF. Both the dryer and the furnace would use fluidized transfer of particles into and out of the process vessels. A movable product-withdrawal tube may be needed to assure removal of particles. We have designed and constructed a unit that cannot contaminate the outside of the equipment and does not have sliding seals. A dryer that can attain a temperature of 260°C and dry up to 15 kg per batch was designed for use in engineering studies. This unit employs an integral electrically driven steam generator to supply heat at a known and controllable temperature. We have planned a furnace consisting of an alumina vessel fitted with a number of nozzles, heated by molybdenum resistors, and housed in a gas-tight, insulated metal container. A prototype ceramic vessel is on order; it will be tested for leak rate and durability.

Fueled-Graphite Refabrication Equipment

J. D. Sease S. E. Bolt²

We began to develop and design a remote fabrication line that will be installed in the TURF to demonstrate the refabrication technology of High-Temperature Gas-Cooled Reactor (HTGR) fuel elements. Advanced HTGR fuel elements consist of graphite blocks with fuel holes and holes for the passage of the coolant gas. The fuel holes are filled with pyrolytic-carbon-coated microspheres of thoria and urania in a carbonaceous matrix. For the design of the fabrication line, the reference fuel element is based on the proposed design of the Public Service of Colorado Company Fort St. Vrain Reactor (PSC) fuel element and consists of a 3.5-in.-diam hexagonal block modified to fit the existing Peach Bottom core. A segment of the reference fuel element, including the pertinent design features, is shown in Fig. 2.3. Even though the modified Peach Bottom element will be the design reference, the process equipment will be such that only minimum retooling will be required to make the larger elements for PSC (14.5-in.-diam hexagonal block containing 216 fuel holes). The design production rate for the fabrication line has been established at 10 kg/day each of fissile and fertile material. The flexibility of the design will permit handling and fabricating any combination of $^{235}\text{UO}_2$, $^{236}\text{UO}_2$, and ThO_2 that may be selected for the optimum fuel cycle. The production capacity of the present design in a 24-hr day, with a 70% plant factor, is approximately 30 Peach Bottom segments 30 in. long or two PSC elements 29 in. long.

The process flow diagram for the TURF fueled-graphite refabrication line is shown in Fig. 2.4. A general division of this process line in the TURF hot cells based on contamination levels is represented by the shading around segments of the flowsheet; the operations that involve potential contamination or direct contact with fuel particles will be carried on in cell D; the relatively clean operations of element assembly and inspection will be carried on in cell E.

The refabrication process can be divided into three general operations: particle selection and coating, fuel-stick fabrication, and element assembly. Particle selection and coating will be done on a

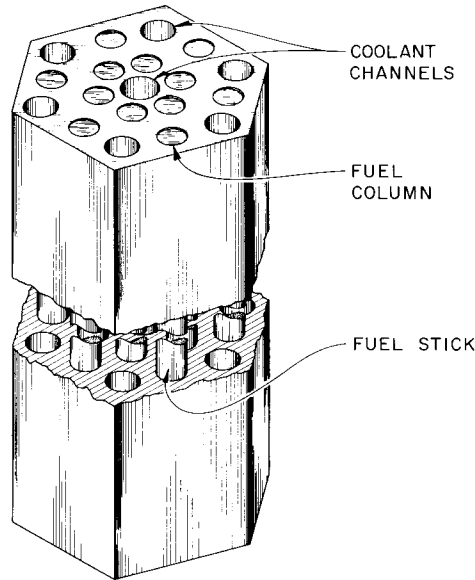


Fig. 2.3. Modified PSC Element for the Peach Bottom Reactor.

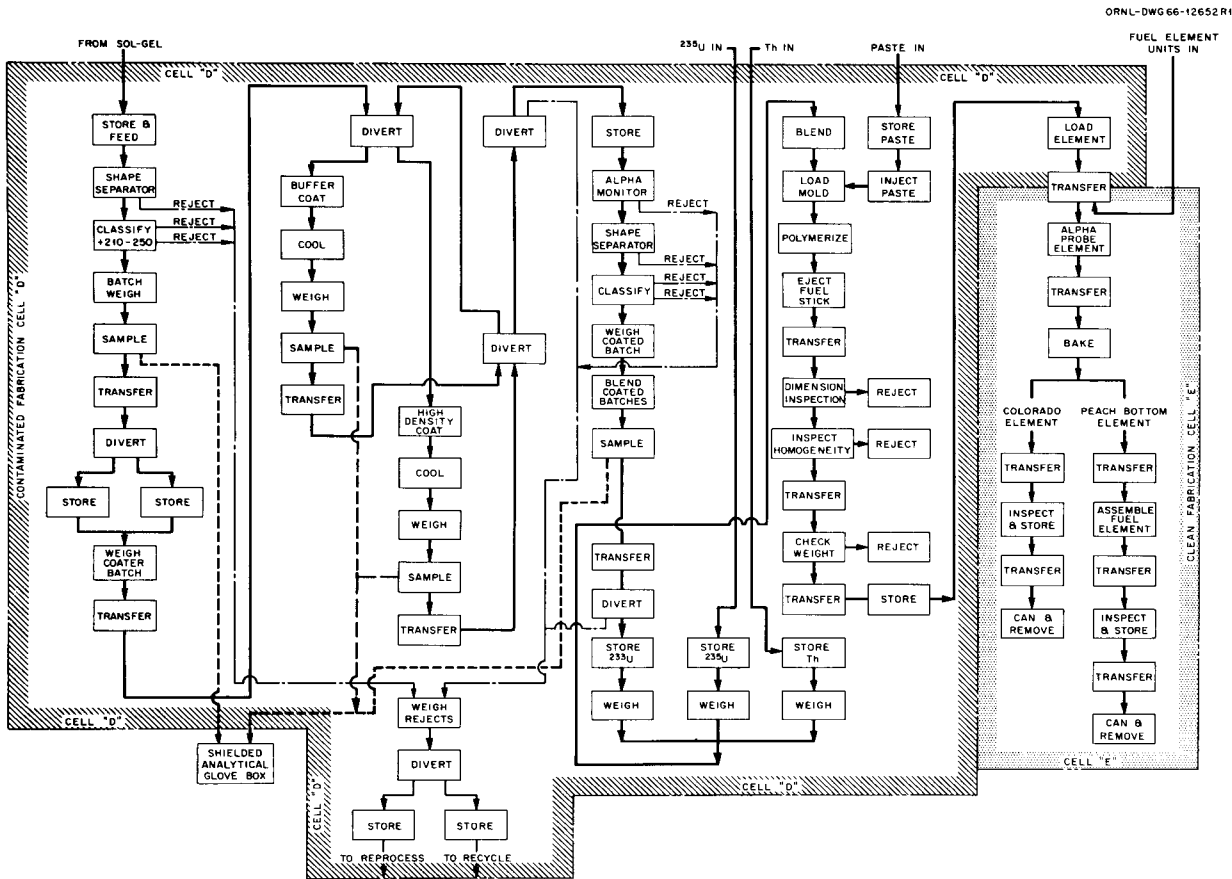


Fig. 2.4. Process Flow Diagram for Recycle HTGR Fuel in TURF.

batch basis. First, bare sol-gel microspheres in the approximate size range of 210 to 250 μ in diameter will be culled to remove any irregularly shaped or broken particles and classified to remove out-of-size microspheres. A batch weight will next be taken for inventory, samples will be taken to qualify the batch, and the batches will be stored. The basic batch weight to this point will be 10 kg. For coating, microspheres will be weighed out in approximately 1-kg increments and first transferred to the buffer coating furnace, where a pyrolytic carbon coating of 1.0 g/cm^3 and approximately 50 μ thick will be deposited. The quality of the buffer coating will be checked on a sample with an in-cell particle analyzer. A high-density coating of approximately 2.0 g/cm^3 and approximately 50 μ thick will be applied over the low-density buffer coating. The product will then be analyzed for quality with an in-cell particle analyzer. The duplex-coated product will be monitored for surface alpha contamination, shape separated, and classified to remove out-of-shape and out-of-size particles. Then all of the coater batches from a given sol-gel batch will be collected, blended, and sampled to qualify the composite coating properties for the batch.

In stick fabrication, the coated fissile particles made in the TURF will be weighed out in batch quantities for one fuel stick loading and then blended with weighed quantities of coated particles containing ^{235}U and thorium from an outside source to make up the loading for one fuel stick. The fuel will be fed into a stick mold, and a paste containing charcoal and a polymer will be injected into the interstices of the packed bed of fuel particles. The compound in the paste will then be polymerized to form a hard stick of fuel particles in a carbonaceous matrix. After ejection from the mold, the stick, approximately 0.450 in. in diameter \times 29 in. long, will be checked for surface contamination with a direct-probe alpha monitor, inspected for homogeneity by a gamma or x-ray attenuation system, and weighed.

In element assembly, the fuel sticks will be first inserted into the fuel holes of a premachined graphite fuel element block. After alpha monitoring for surface contamination, the element will be baked at approximately 1000°C to carbonize the polymer in the fuel sticks.

In the case of the modified Peach Bottom element, fuel element segments will be assembled into a 12-ft-long fuel element that is compatible with the existing Peach Bottom core and core-loading system.

We have developed a working flow diagram and have completed conceptual designs for most of the process equipment. Most of the design effort has been concentrated on a prototype remote coating system (see Chap. 4), which is now being fabricated. A critical-path schedule has been developed and will be used in the execution of this project. The scheduled date for the equipment to be fabricated and installed in the TURF, ready for "cold" shakedown runs, is late 1969. A detailed description of the development work in support of the TURF fueled graphite fabrication line is contained in Chap. 4.

REFERENCES

¹A. R. Irvine, J. W. Snider, and J. M. Chandler, Status and Progress Report for Thorium Fuel Cycle Development for Period Ending December 31, 1965, ORNL-4001, pp. 14-18.

²On loan from Reactor Division.

3. SOL-GEL PROCESS DEVELOPMENT

W. D. Bond P. A. Haas

The sol-gel process consists of three principal operations: (1) preparing an aqueous sol, (2) removing water from the sol to give gel particles, and (3) drying and firing at controlled conditions and according to a definite program to remove volatile compounds, sinter the particles to a controlled density (usually to essentially the theoretically attainable density), and cause any necessary chemical reductions or conversions. The development of the sol-gel process for the thorium fuel cycle has recently emphasized production of microspheres of mixed thoria-urania sols containing greater than 10% UO_2 . Such mixed sols may be prepared either by mixing urania and thoria sols or directly from a mixed solution of thorium and uranyl nitrates. Gelation of sol drops by extraction of water to give small spherical particles (microspheres) is the adaptation of the sol-gel process of greatest current interest. Continuing development of equipment and process chemistry studies are reported in this chapter.

Preparation of Urania Sols by a Precipitation-Peptization Process

P. A. Haas J. P. McBride

The several precipitation-peptization flowsheets for preparation of aqueous urania sols consist of the same principal operations. The differences are in the chemical conditions of individual operations (the pH, the addition and concentration of formic acid, etc.) introduced to simplify or improve the process steps. The principal operations are:

1. reduction of uranyl nitrate by hydrogen in the presence of a hydrogenation catalyst, such as platinum on alumina, to yield a partially hydrolyzed uranous nitrate;
2. precipitation of uranous hydroxide by ammonia;
3. washing the precipitate to remove adsorbed and occluded salts such as ammonium nitrate;
4. dispersion of the washed precipitate with NO_3^- as the peptizing ion to form a concentrated sol.

Chemical development of urania sol preparation has proceeded in two stages. The first was the development of a laboratory process for preparing aqueous urania sols by a precipitation-peptization method and the production by this method of kilogram quantities of urania microspheres, some containing fully enriched uranium.^{1,2} The second stage has been modification of the laboratory process to make it amenable to engineering scaleup.

Laboratory Preparation of Urania Sol

A flowsheet for the laboratory preparation of urania sol is given in Fig. 3.1. It begins with the preparation of a uranous nitrate solution by the catalytic reduction of a uranyl nitrate solution containing excess nitric acid. The solution is filtered to remove the catalyst. In this flowsheet (the nitrate-formate flowsheet) formic acid is added to the filtered solution, and the hydrous oxide is formed by precipitating uranium(IV) with an aqueous ammonia solution containing hydrazine. The precipitate is collected by filtration and washed to remove excess electrolytes. The washed filter cake is then heated at 60 to 65° to produce a fluid, stable sol. Sufficient nitrate ion is left in the washed cake to cause it to peptize to a sol upon heating. Precautions are taken to protect the material from air oxidation by the use of a blanket gas (argon) during all stages of the process following the reduction. Sol concentrations of 1.2 to 1.6 M U are achieved. Ammonia must be added in the precipitation step until a pH between 7 and 8 is reached if the washed filter cake is to be transformed to a sol by heating. The addition of formic acid to the uranium(IV) nitrate solution is necessary to maintain a high uranium(IV) content (more than 85% of the total uranium) in the precipitate and the subsequent sol. Both formate and nitrate are present in the final sol (Table 3.1). In the absence of formic acid, the uranium(IV) content of the hydrous oxide would be down to about 80% of the total uranium, which is in contrast to the more than 99% total uranium which is present in the original uranium(IV) nitrate solution. In addition, the formic acid simplifies pH control in the precipitation step and decreases the amount of water needed for washing the filter cake.

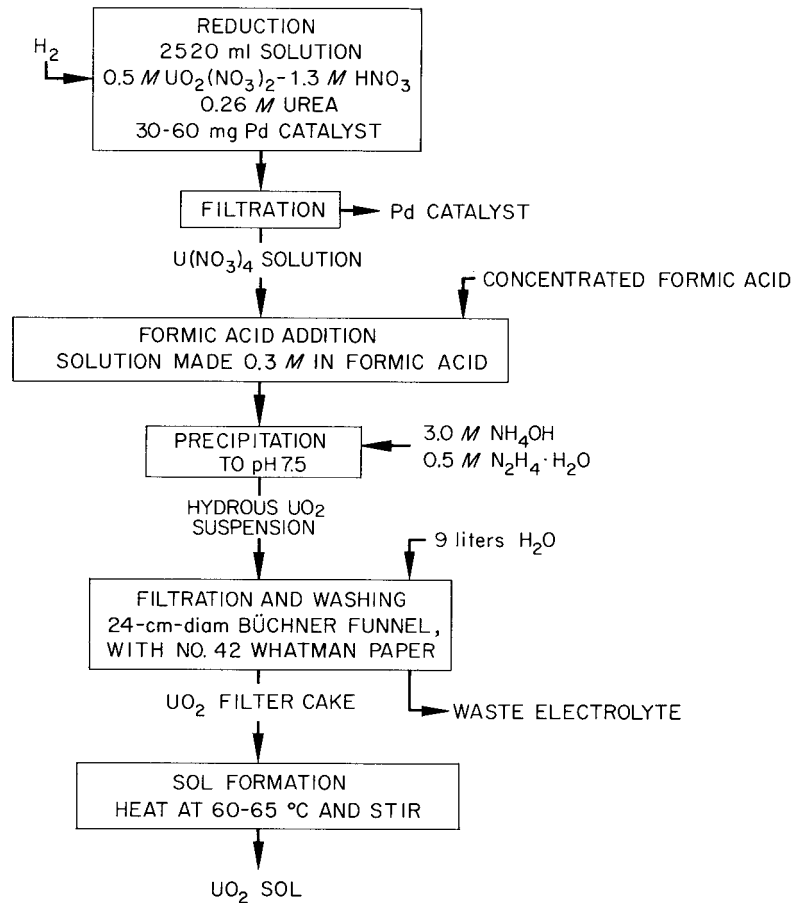


Fig. 3.1. Flowsheet for the Laboratory Preparation of Urania Sol by Precipitation-Peptization.

Table 3.1. Properties of Urania Sols Prepared by the Laboratory Precipitation-Peptization Method

Uranium Concentration (M)	U(IV) Content (% of U)	NO ₃ ⁻ /U Ratio	HCOO ⁻ /U Ratio	Specific Gravity (g/cm ³)
1.23	87	0.13	0.44	1.317
1.27	85	0.07	0.38	1.319
1.48	86		0.45	1.369
1.49	84	0.14	0.45	1.373
1.61	86	0.11	0.31	1.404
1.62	87	0.11		1.405

Development of an Engineering-Scale Flowsheet

Development of a process for the continuous production of urania sol (enriched in ^{235}U) at the rate of several kilograms per day in criticality-proof equipment required modification of the laboratory process. The filtering and washing steps in the laboratory process posed criticality and handling problems and made difficult the production of sols having a prescribed nitrate-to-uranium ratio. Hence, we directed attention to development of a process in which the hydrous oxide was precipitated, washed completely free of electrolyte by decantation, and peptized by the addition of a controlled amount of the peptizing electrolyte, nitric acid.

The current flowsheet for the engineering-scale preparation of urania sol is Fig. 3.2. A uranium(IV) solution is prepared by the catalytic reduction with hydrogen of a $0.5 \text{ M } \text{UO}_2^{2+}$ solution containing $1 \text{ M } \text{NO}_3^-$ and $0.25 \text{ M } \text{HCOO}^-$. After reduction and catalyst removal, concentrated formic acid is added to the reduced solution to give a formate-to-uranium ratio between 0.6 and 1.0 (this adjustment is necessary because part of the original formate is lost in the reduction step). The hydrous oxide is then precipitated by the addition of $3.5 \text{ M } \text{NH}_4\text{OH}$ or $3.0 \text{ M } \text{NH}_4\text{OH}-0.5 \text{ M } \text{N}_2\text{H}_4 \cdot \text{H}_2\text{O}$ to about pH 9.0. The pH should not exceed 9, but may be as low as 8. The resulting precipitate is washed free of electrolyte by decantation with either water or $0.01 \text{ M } \text{N}_2\text{H}_4 \cdot \text{H}_2\text{O}$ (see below). The washed precipitate is resuspended, nitric and formic acids are added, and the suspension is stirred at 60 to 65°C until peptized.

The use of a uranium(VI) feed solution containing a lower nitrate-to-uranium ratio than that used in the laboratory process was prompted by development studies showing that a stable uranium(IV) solution containing a nitrate-to-uranium ratio of 2 could be prepared if a small amount of formic acid were added before reduction.² It should be noted that when the uranium is completely reduced, the solution is acid-deficient [the amount of nitrate ion present is less than that required to be stoichiometrically equivalent to the uranium(IV)]. The use of hydrazine in the precipitation and washing steps and the addition of formic in addition to nitric acid in the peptization step are to control

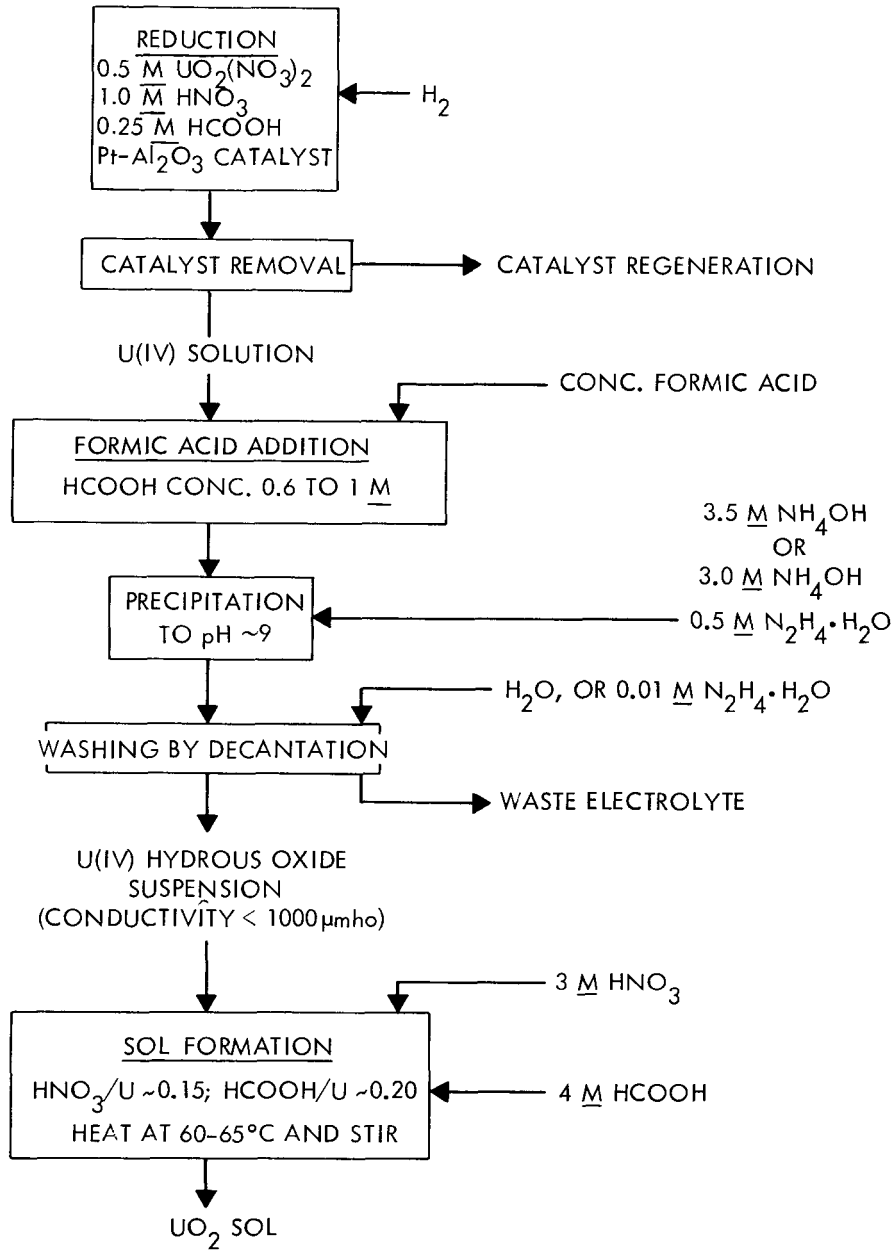


Fig. 3.2. Flowsheet for the Engineering-Scale Preparation of Urania Sol by Precipitation-Peptization.

aging in the precipitate and to increase sol yields. Laboratory studies on the engineering flowsheet using ammonia as the precipitating reagent, water as the wash solution, and decantation washing, where the period between precipitation and peptization was as long as 48 hr, showed an apparent aging in the precipitate such that peptization was not always achieved and sol yields were not as high as desired (i.e., there was too much undispersed precipitate). Out of ten preparation attempts, only six produced good sols. The use of hydrazine in the precipitation and washing steps and formic acid in the peptizing step has made the process more reproducible and increased sol yields to greater than 90%.

Table 3.2 shows the effects of the precipitating reagent and wash solution on sol yields and sol properties where the hydrous oxide precipitate was washed by decantation and peptized by the addition of nitric acid. Observe that with ammonia as the precipitating reagent and either hydrazine formate or hydrazine as the wash solution we obtained marked increases in sol yield. The use of ammonia and hydrazine mixtures as the precipitants also resulted in high yield. Highest yields of sol were obtained with 3.5 \underline{M} NH_4OH solution as the precipitant and 0.01 \underline{M} $\text{N}_2\text{H}_4 \cdot \text{H}_2\text{O}$ wash (UNR-5) and with 3.0 \underline{M} NH_4OH -0.5 \underline{M} $\text{N}_2\text{H}_4 \cdot \text{H}_2\text{O}$ and 0.01 \underline{M} $\text{N}_2\text{H}_5\text{COOH}$ wash.

The use of both formic and nitric acids in the peptizing step was suggested by a series of laboratory experiments in which the hydrous oxide was recovered by filtration and washed in place on a filter to minimize the time required for washing, and in which the washed precipitate was peptized with various additions of electrolyte. In a typical preparation, we reduced with hydrogen 300 g of uranium in a 0.5 \underline{M} $\text{UO}_2(\text{NO}_3)_2$ -0.25 \underline{M} HCOOH solution, using a palladium-on-thoria catalyst. Formic acid was added to increase its concentration; the reduced solution was divided into two portions and precipitated with either 3.5 \underline{M} NH_4OH or 3.0 \underline{M} NH_4OH -0.5 \underline{M} $\text{N}_2\text{H}_4 \cdot \text{H}_2\text{O}$. The resulting precipitate was washed with 9 liters of distilled water on a Büchner funnel, using No. 42 Whatman paper. Nitric acid or nitric-formic acid solutions were then added to the precipitate to form sol. (For most preparations, the time between precipitation and peptization was less than 1 hr.)

Table 3.2. Effect of Precipitation Conditions on Urania Sol Preparation by Decantation Washing^a

Preparation	Precipitation Conditions		Wash Solution	Sol Yield (%)	Sol Properties			
	Formate-to-Uranium Mole Ratio in Feed	Reagent			Uranium Concentration (M)	U(IV) Content (% of U)	Nitrate-to-Uranium Mole Ratio	Formate-to-Uranium Mole Ratio ^b
NUFD-13A	0.94	3.5 M NH ₄ OH	H ₂ O	72 ^c	0.70	86	0.18	0.33
NUFD-13B	0.98	3.5 M NH ₄ OH	0.05 M HCOOH	69	0.87	84	0.22	0.50
NUFD-14A	0.87	3.5 M NH ₄ OH	0.013 M HCOOH	79	0.75	87	0.17	0.40
NUFD-14B	0.53	3.5 M NH ₄ OH	0.007 M HCOOH	59	0.45	88	0.29	0.30
NUFD-16A	0.79	3.5 M NH ₄ OH	0.01 M NH ₄ COOH	66	0.58	83	0.16	
NUFD-16B	0.77	3.5 M NH ₄ OH	0.01 M N ₂ H ₅ COOH	86	0.71	87	0.23	0.16
UNR-2	0.82	3.5 M NH ₄ OH	0.01 M N ₂ H ₅ COOH	84	0.74	88	0.23	0.19
UNR-5	0.59	3.5 M NH ₄ OH	0.01 M N ₂ H ₄ · H ₂ O	95	0.65	85	0.16	0.06
UNR-7	0.61	3.5 M NH ₄ OH, 0.2 M N ₂ H ₄ · H ₂ O	0.01 M N ₂ H ₅ COOH	92	0.85	87	0.16	0.13
UNR-9M	0.84	3.5 M NH ₄ OH, 0.2 M N ₂ H ₄ · H ₂ O	0.02 M N ₂ H ₅ COOH	94	0.88	87	0.11	0.29
UNR-6	0.61	2.5 M NH ₄ OH, 1.0 M N ₂ H ₄ · H ₂ O	0.01 M N ₂ H ₅ COOH	>90	0.62	84	0.16	0.12
UNR-1	0.79	3.0 M NH ₄ OH, 0.5 M N ₂ H ₄ · H ₂ O	0.01 M N ₂ H ₅ COOH	96	0.54	87	0.23	0.16

^aSol preparation conditions: 0.5 M U(IV) solution; NO₃⁻/U mole ratio of 2.0; precipitate to pH 9, wash by decantation, peptize by addition of HNO₃ (NO₃⁻/U mole ratio = 0.14) and stirring at 60 to 65°C.

^bAnalyzed as carbon.

^cPeptized with HNO₃ and HCOOH; NO₃⁻/U mole ratio = 0.14; HCOO⁻/U mole ratio = 0.20.

Table 3.3 shows the effect of the precipitating reagent and peptizing conditions on sol yield and sol properties.

The highest yields of sol were obtained by adding both nitric and formic acids to the sol at ratios to the uranium of 0.15 and 0.20, respectively, independent of the precipitation conditions. When the ratio of nitrate to uranium was high in the reduced solution (preparation A-3403-115), the sol yield was acceptable but the uranium(IV) content of the final sol was lower than in the other preparations.

Urania Sol Characteristics

Urania sols produced by the laboratory flowsheet are generally very fluid and exhibit good stability on standing several months. Those prepared by the engineering flowsheet, although fluid when prepared, have shown various degrees of stability. While some have remained fluid for as long as four months, others have thickened and gelled on standing four days, even though they differ very little from the fluid sols in their chemical properties. The thickened sols exhibit a long-term thixotropy in that they may be shaken to restore fluidity and do not thicken again until after standing several days. Studies to relate sol properties and reproducibility to various process variables and to delineate sol characteristics associated with the thickening process are under way.

Studies on the x-ray crystallite sizes of sols produced by the engineering flowsheet have shown that they are affected by the precipitation conditions. Those preparations in which 3.5 M NH_4OH was used as the precipitant have crystallite sizes varying between 62 and 84 A, regardless of whether hydrazine was used in the wash solution. When 3.0 M NH_4OH -0.5 M $\text{N}_2\text{H}_4 \cdot \text{H}_2\text{O}$ was used as the precipitating reagent, the crystallite sizes varied between 90 and 96 A.

Equipment Development and Urania Sol Production

The laboratory flowsheets for urania sol preparation are used in three ways: to prepare sols for use in preparation of UO_2 microspheres for irradiation specimens; to prepare sol for use in development of the

Table 3.3. Effect of Precipitation Conditions on Urania Sol Preparation Using Filtration-Washing^a

Preparation	Precipitating Reagent	Peptization Conditions		Sol Yield (%)	Sol Properties			
		Nitric Acid-to-Uranium Adjustment	Formic Acid-to-Uranium Adjustment		Uranium Concentration (M)	U(IV) Content (% of U)	Nitrate-to-Uranium Mole Ratio	Formate-to-Uranium Mole Ratio
A-3403-83 ^b	3.0 M NH ₄ OH, 0.5 M N ₂ H ₄ · H ₂ O	0.1	0	82 ^c	1.13	84	0.13	0.05
A-3403-85	3.0 M NH ₄ OH, 0.5 M N ₂ H ₄ · H ₂ O	0.1	0	59 ^c	0.95	86	0.12	0.01
A-3403-90	3.0 M NH ₄ OH, 0.5 M N ₂ H ₄ · H ₂ O	0.1	0.2	96	1.60	89	0.14	0.30
A-3403-96	3.5 M NH ₄ OH	0.1	0.2	72	1.26	88	0.13	0.24
A-3403-97	3.0 M NH ₄ OH, 0.5 M N ₂ H ₄ · H ₂ O	0.15	0.2	98	1.62	88	0.17	0.24
A-3403-100	3.0 M NH ₄ OH, 0.5 M N ₂ H ₄ · H ₂ O	0.15	0.2	99	1.40	85	0.15	0.23
A-3403-107	3.5 M NH ₄ OH	0.15	0.2	99	1.27	82	0.21	0.24
A-3403-111	3.5 M NH ₄ OH	0.19	0 ^d	92	1.19	82	0.17	
A-3403-115 ^b	3.5 M NH ₄ OH, 0.5 M N ₂ H ₄ · H ₂ O	0.15	0.2	96	1.04	79	0.15	0.008

^aSol preparation conditions: 0.5 M U(IV) solution; NO₃⁻/U mole ratio = 2, HCOO⁻/U mole ratio ~0.5; precipitate to pH 9; filter and wash in place; add HNO₃ or HNO₃-HCOOH and peptize by heating and stirring at 60 to 65°C. Time between precipitation and peptization <1 hr.

^b0.5 M U(IV) solution; NO₃⁻/U mole ratio = 4.6; HCOO⁻/U mole ratio = 0.6.

^c18 hr between precipitation and peptization.

^d0.01 M N₂H₅COOH wash.

process for forming UO_2 microspheres; to provide a basis for development of remotely operated equipment for preparation of urania sols in the TURF. The flowsheets for these several applications have been somewhat different, depending on the use intended and the scale of the work.

The reduction of uranyl nitrate to uranous nitrate is a necessary preliminary step and is relatively independent of the remaining precipitation-peptization flowsheet. Reduction at atmospheric pressure with a finely divided catalyst was used for batch preparations in laboratory apparatus. At present the larger scale reduction operations are at 300 psig, using 0.5% Pt on 1/8-in. alumina pellets. The reduction operation is continuous; uranyl nitrate is fed by a diaphragm pump. This system is not entirely adequate, and we have work in progress to develop an improved reduction flowsheet for remote operation.

The first reproducible sol-gel flowsheet for urania was applied to preparation of microspheres for irradiation specimens, and over 10 kg of enriched urania has been made into sols. Criticality was prevented by limiting batch size to 300 g of uranium. Laboratory apparatus was practical and convenient for this batch size; therefore, the enriched urania microspheres presently in irradiation specimens were all made in batch laboratory apparatus, using the flowsheet for precipitation to pH of 7 to 7.5. This combination will not be used in the future: some additional precipitations of enriched urania sols will be with the pH 9 flowsheet in the batch laboratory apparatus.

Most of the natural urania sols formed into microspheres during the year were prepared in a batch apparatus with a capacity of 1 kg of UO_2 , using the pH 9 flowsheet. We did all the precipitation, washing, and dispersion operations in a single vessel, which had a porous 12-in.-diam stainless steel plate as the bottom and a slow-speed, paddle-type agitator. The supernate was removed by filtration after precipitation and after each of four washing steps. For each wash, we agitated 10 liters of water with 5 liters of slurry or cake remaining on the filter. We peptized by a combination of agitation and heating after addition of nitric and formic acids.

We designed and fabricated a continuous urania sol preparation system (Fig. 3.3) to meet the requirements for both remote operation and large-scale, critically safe operation with enriched uranium. This system consists of two continuous precipitators, six countercurrent mixer-decanter stages, and two continuous peptizers. The wash water flows by gravity, while the solids are transferred by gas-operated pumps. The initially installed precipitators, gas-operated pumps, and peptizers were inadequate for transfer of precipitates and were replaced by units of modified design. After two 70-hr runs with natural uranium we concluded the following.

1. The continuous precipitators are mechanically and chemically acceptable.

2. Precipitation can be controlled by metered flow, but pH indicators in the slurry are not dependable for indicating end point.

3. Washing is excellent if the proper flows of slurry and wash liquid are maintained.

4. The transfer of slurry between stages is still a source of trouble. The operation during the second 70-hr run was acceptable for direct operation and visual observation, but would have been too difficult for remote operation.

5. The pump we are now using for transfer of settled, washed precipitate from the final washer to the continuous peptizers is not acceptable.

6. The continuous peptizers can probably produce adequately dispersed sols of acceptable compositions if the slurry, nitric acid, and formic acid flows can be controlled. (These requirements were not met for any extended period of operation.) However, the as-produced sols are too dilute for use in preparing microspheres.

7. Compaction of the washed precipitate to give a uranium concentration greater than 0.7 M in the sol will be very difficult to achieve; either a sol concentration step such as evaporation or dewatering (squeezing) the precipitate on a filter will probably be necessary.

A 12-ft-high, 4-in.-ID column was tested as an alternative to the decantation-settlers for countercurrent washing of the uranous hydroxide precipitate. The wash column tests showed good mechanical operation and adequately satisfied the chemical flowsheet requirements for either a

PHOTO 84359

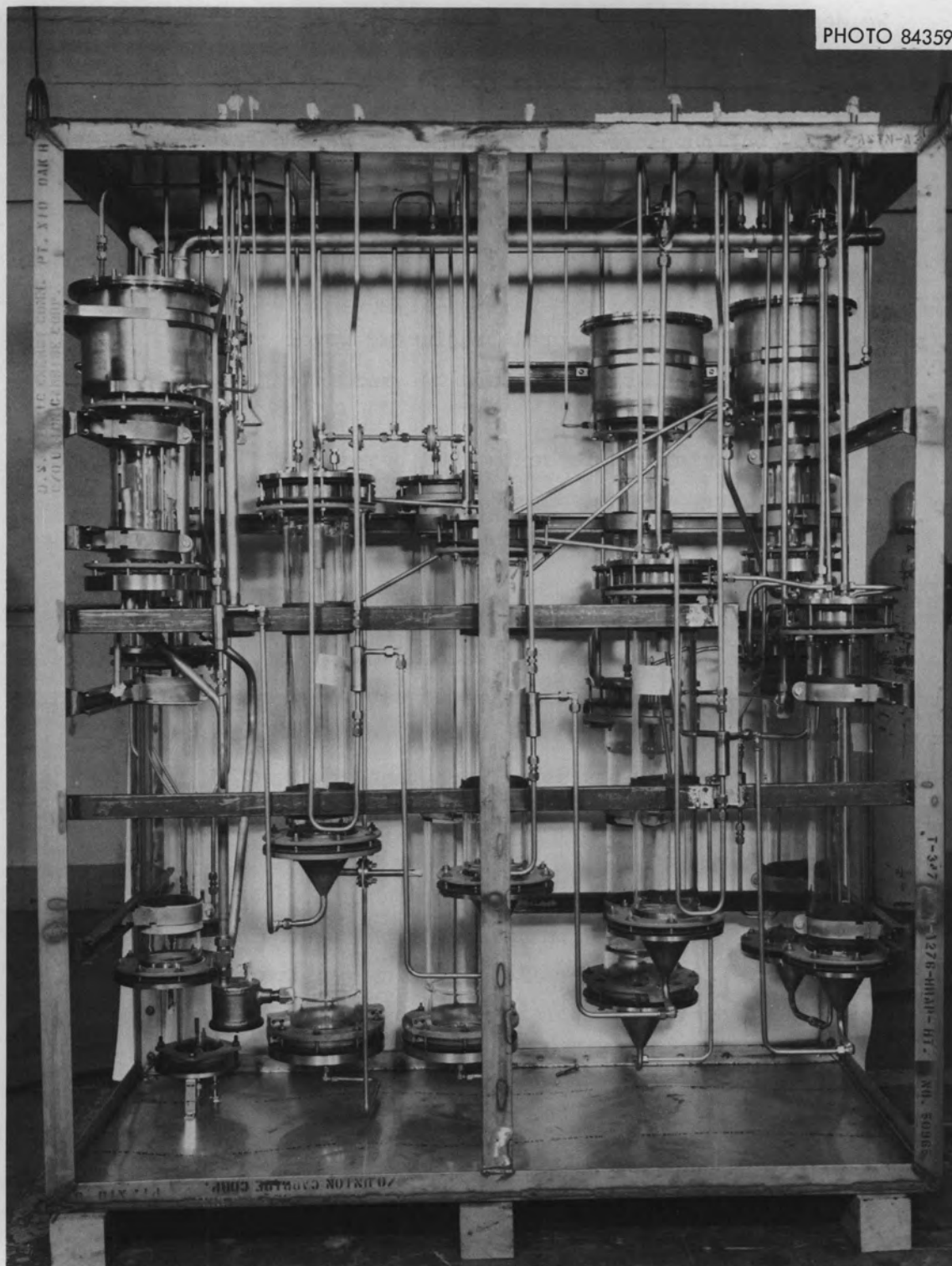


Fig. 3.3. Equipment Used for the Production of Urania Sol.

batch precipitator or continuous precipitators. The wash column has the advantage of shorter residence time and less material holdup than the equipment shown in Fig. 3.3.

Sol Preparation by Amine Extraction

J. G. Moore

We have developed and demonstrated on a laboratory scale a simple solvent extraction process to extract nitrate from aqueous solutions of thorium and uranyl nitrate mixtures by long-chain aliphatic amines, allowing mixed thorium-uranium oxide sols to be prepared directly from aqueous solutions containing 0 to 68 mole % $\text{UO}_2(\text{NO}_3)_2$. Figure 3.4 shows, as a typical example, the flowsheet conditions used in this amine denitration process³ to prepare a sol and subsequent oxide microspheres with a thorium-to-uranium atom ratio of about 3.5, one of the compositions being studied for high-temperature gas-cooled reactor fuels.

One volume of an aqueous solution about 0.21 M in $\text{Th}(\text{NO}_3)_4$ and 0.06 M in $\text{UO}_2(\text{NO}_3)_2$ is contacted for at least 2 min with about 1.9 volumes of 0.75 M Amberlite LA-2 (the highly branched secondary amine n-lauryltrialkylmethylamine) in n-paraffin, the commercial equivalent of n-dodecane. To ensure rapid phase separation, the extraction is made at 50 to 60°C with the organic phase continuous. The elevated temperature also decreases uranium losses by decreasing the amount of uranium extracted by the amine. In the first stage, 80 to 90% of the total nitrate is extracted. After the phases separate, the aqueous phase is heated at least 10 min at 95 to 100°C. This digestion changes the aqueous phase from yellow-orange to dark red. Simultaneously, nitrate is released, which is then extracted by the amine in a second stage. Greater than 91% of the total nitrate is removed in the two stages, yielding a sol with a nitrate-to-metal mole ratio of about 0.2. In this particular example, we evaporated the sol to give a final sol that was 1.10 M in thorium, 0.32 M in uranium, 0.30 M in nitrate, and 0.01 M in carbon in an unspecified form.

The crystallite size according to x-ray analysis was 35 to 40 Å. Spheres were formed by injecting this sol into 2-ethyl-1-hexanol con-

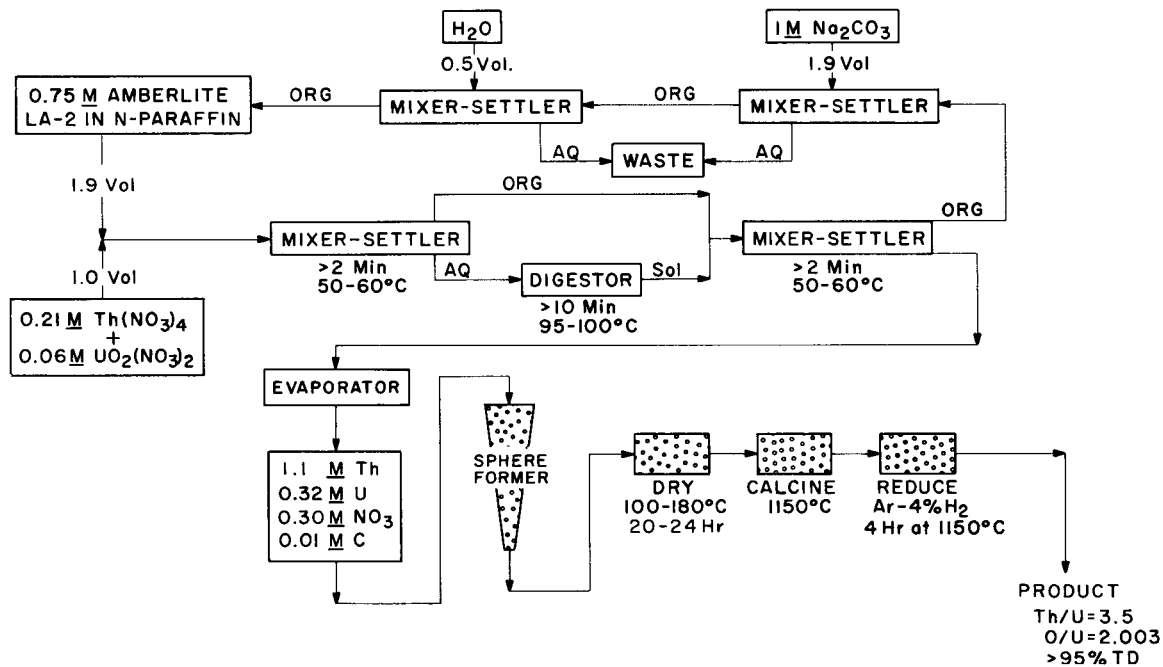


Fig. 3.4. Amine Denitration Process.

taining 0.5 vol % H_2O and suitable surfactants. The gelled spheres were dried overnight at 100°C , held at 170 to 180°C for about 5 hr, then calcined in air at 1150°C . Finally, the uranium was reduced by firing in Ar-4% H_2 for 4 hr at 1150°C . The resulting spheres were shiny black and had an oxygen-to-uranium ratio of 2.003. The density of the product microspheres was greater than 95% of theoretical. Individual spheres 150 to 350 μ in diameter resisted crushing forces of 940 to 2000 g.

After the nitrate extraction is completed in the last stage, the amine nitrate is converted back to free amine by contact with at least 1.05 moles of sodium carbonate per mole of amine nitrate. In this example, the 1.9 volumes of organic phase would be contacted with about 1 volume of 1 M Na_2CO_3 ; this would be followed by a wash with 0.5 volume of H_2O . The amine would then be ready for use again in the first extraction stage.

To date, the overall process has been demonstrated on a laboratory scale with sols having 17 to 26 mole % U; however, the amine denitration procedure has been used to prepare stable thorium-uranium sols with 0 to 68 mole % U (Table 3.4). A multiple contact procedure was used to ensure that nitrate equilibrium had been reached. From 98 to 99.6% of the extractable nitrate was extracted in the first two extraction stages. The amount of extractable nitrate ranged from 93 to 95% of the total aqueous nitrate.

The nitrate-to-metal mole ratio after the first extraction decreased with increasing uranium content from 0 to 50 mole % U. The equilibrium nitrate value also varied regularly with uranium, but only up to about 25 mole % and then, under these conditions, remained at a value of about 0.16 mole of nitrate per mole of total metal.

We have also prepared sols with such amines as Adogen 364, Di-tridecyl P, 1-nonyldecylamine, and Primine JM-T; however, most of our development work used the Amberlite IA-2, an effective extractant, which does not require any additive to the diluent and is commercially available. An equimolar amount of the amine per initial nitrate would be sufficient to extract the nitrate in a contactor with perfect efficiency; however, we used 1.2 to 1.5 moles of amine per mole of nitrate to ensure nitrate equilibrium.

Several diluents were used: n-dodecane, n-paraffin, di-isopropylbenzene, diethylbenzene, and Amsco 125-82. Most of the development work used 0.6 to 0.75 M amine in n-dodecane or n-paraffin, since these solutions had slightly better phase separation characteristics and handling properties than more concentrated solutions or other diluents. The control of concentration of the aqueous phase is more critical; it must be less than 0.6 M in total metal ions to prevent the formation of solids during extraction. Although these solids will liquefy on heating, they could become a source of trouble in a continuous process.

Equilibrium is achieved very rapidly in the extraction stages, and 1 min of thorough mixing is sufficient to compensate for possible mixing variations; however, a minimum of 2 min contact time was used in all the extraction steps. A 5-min contact at a temperature of 50 to 60°C reduced the thorium and uranium extraction losses to less than 0.02 and 0.01%, respectively.

Table 3.4. Solvent Extraction of Nitrate Ion from Thoria-Urania Sols^a

U/(U + Th) (mole %)	First Extraction		Second Extraction		Third Extraction		Fourth Extraction	
	NO ₃ ⁻ /metal	pH						
0	0.73	4.46	0.31	4.33	0.28	4.99	0.28	4.31
2.5	0.68	4.24	0.30	3.93	0.28	4.74	0.26	4.47
5.3	0.67	5.00	0.28	4.09	0.24	4.57	0.25	4.65
9.4	0.62	4.71	0.25	4.61	0.24	4.84	0.23	4.88
18	0.55	4.84	0.21	5.02	0.20	4.38	0.19	4.46
26	0.45	4.13	0.19	4.27	0.16	4.46	0.16	4.50
35	0.39	4.76	0.23	4.67	0.19	4.67	0.16	4.77
53	0.26	4.92	0.20	5.12	0.20	5.14	0.18	5.06
68	0.25	5.06	0.16	5.46	Gelled			

^aStarting solution: 0.22 to 0.3 M Th(NO₃)₄ with sufficient UO₂(NO₃)₂ to give the indicated mole percentage of UO₂ in the final product. Procedure: four 6-min contacts at 50 to 60°C separated by 20-min digestions at about 100°C. Amine: 0.77 M Amberlite LA-2 in *n*-paraffin, 1.5 moles per mole nitrate ion. Cocurrent flow.

It is necessary to heat the aqueous phase after partial denitration in the first extraction stage to form a sol and release more extractable nitrate. For maximum effectiveness, a digestion period of 8 to 10 min at 95 to 100°C is necessary. Shorter digestions yield sols that, after a second amine extraction, have nitrate-to-metal mole ratios of about 0.3, compared to about 0.17 after 10 min or more. Similarly, a higher nitrate value is obtained if the digestion temperature is lowered to 80 or 90°C.

Microspheres are formed by injecting the thoria-urania sols into a dehydrating medium such as 2-ethyl-1-hexanol containing suitable surfactants to prevent the droplets from coalescing or clustering. The sols prepared by the amine denitration process were especially sensitive to the type and concentration of surfactant used in the sphere-forming column. For example,⁴ in the formation of microspheres from a ThO₂-UO₂ sol formed by blending thoria and urania sols in the ratio 3.5 to 1, we used 2-ethyl-1-hexanol containing 0.3 vol % Span 80 (sorbitan monooleate) and 0.5 vol % Ethomeen S-15 (a condensation product of a primary fatty amine with ethylene oxide). In contrast, as little as 0.1 vol % of either the Span 80 or Ethomeen S-15 caused severe cracking or flaws in spheres formed from a sol of similar composition produced by the amine denitration process. Surfactant concentrations of around 0.04 vol % produced excellent spheres. Other surfactants that produced good spheres and were not quite as critical in their concentration levels were Alkanol OE, a long-chain alcohol-ethylene oxide condensation product, and bis(2-ethoxyethyl)phthalate.

The sphere-forming characteristics of the sols are dependent on the temperature used before, during, and after evaporation of the sol as well as on the rate of drying and the final nitrate-to-metal mole ratio. For example, sols that were evaporated under vacuum at 30 to 38°C were much more sensitive to column conditions than sols that had been evaporated slowly at atmospheric pressure and reflux temperature (~100°C); however, the former became more amenable to sphere formation if digested at a temperature of 70 to 100°C after the evaporation (Table 3.5). These spheres were made by use of 2-ethyl-1-hexanol containing 1 vol % H₂O and equal concentrations of Span 80 and Ethomeen

S-15. The sol was evaporated under vacuum and then digested for 30 min at either 70 to 80°C or 100°C. The effect of surfactant concentration on the percentage yield of whole spheres after drying was used as a measure of sensitivity. Only 0.08 vol % of each of the surfactants was required to reduce the yield from undigested sol to 50%, but 0.15 vol % was required for the same effect after the sol had been digested at 70 to 80°C. At this concentration the yield was still about 90% for the refluxed sol. Similarly, less sensitivity was observed with sols with lower nitrate-to-metal ratios. For example, sols with a ratio of 0.20 were less sensitive than those with a ratio of 0.29. However, the sensitivity of the latter could be reduced by decreasing the rate of dehydration of the spheres in the forming column by simply raising the water content of the 2-ethyl-1-hexanol to 1.5 or even 1.8 vol %.

Table 3.5. Effect of Surfactant Concentration and Sol Digestion on Microsphere Yield

Surfactant (vol %) ^a		Yield (%) ^b		
		Undigested	Digested at	
Span 80	Ethomeen S-15		70-80°	100°
0.04	0.04	97	90	97
0.06	0.06	85	85	90
0.08	0.08	50	90	98
0.10	0.10	25	90	95
0.15	0.15		50	90

^aDehydrating medium: 2-ethyl-1-hexanol containing 1 vol % H₂O and the listed surfactants.

^bApproximate.

Preparation of Mixed Oxide Sols

A. B. Meservey

We have studied coprecipitation of thorium and uranium hydroxides as an alternate approach to the sol-gel preparation of thoria-urania fuels. This approach uses uranium(VI) and emphasizes attaining thorium-to-uranium ratios of about 3 in the final oxide, since this is about the value for what appear to be the most useful fuels for reactors that utilize thorium. The original ORNL sol-gel process^{5,6} is limited to uranium concentrations less than about 10%. We also determined the accuracy with which we could mix sols to make a desired composition and characterized microspheres made with this method of sol preparation.

Sol-Gel Process Employing Mixed UO₂-ThO₂ Sols

We have examined two approaches to the preparation of UO₂-ThO₂ sols for all compositions. One involves simply mixing UC₂ sols prepared by the formate method (described above) with ThO₂ sols prepared from steam-denitrated thoria.⁵ The other method involves coprecipitating thorium-uranium(IV) hydroxides and then peptizing them to a stable sol. Because of the promise of the solvent-extraction process for UO₂-ThO₂ sol preparation, no work beyond demonstration that sols could be prepared by the coprecipitation approach was performed. We demonstrated the mixed sol method through final product microsphere evaluation and prepared irradiation test specimens from these materials.

We thought that one of the major problems with the sol mixing method would be close control of the thorium-to-uranium ratio; however, this was not the case. We demonstrated that fuel composition can be controlled very closely (Table 3.6). The preparations were demonstrated on the 150-g scale. The sols were mixed in calibrated glassware. To obtain the different degrees of uranium enrichment required for some applications, the UO₂ sols that were mixed with the thoria sol were prepared by mixing a UO₂ sol of 93.18% enrichment with a natural UO₂ sol. The UO₂-ThO₂ sols were formed into gel microspheres in a typical sphere-forming operation, and 40 to 60% of the microspheres were in the desired 210- to 297- μ -diam range (after calcination) and were of ex-

Table 3.6. Properties of Fired ThO₂-UO₂ Microspheres Prepared from Mixed ThO₂-UO₂ Sols^a

Prep. Code	Th/U Weight Ratio		Uranium Enrichment		Density		Surface Area (m ² /g)	C (ppm)	Gas Release to 1200°C in Vacuum (cm ³ /g)
	Desired	Measured	Desired (%)	Measured (%)	g/cm ³	% of Theoretical			
OL-2	0.3333	0.3337	43.5	43.3	10.34	96.5	0.004	<20	0.02
OL-3	1.000	1.005	65.3	65.04	10.31	98.3	0.006	30	0.01
OL-4	1.857	1.886	93.18		10.08	97.5	0.005	20	0.011

^aDiameter: 250-297 μ; firing conditions: Ar-4% H₂ to 650°C at 300°C/hr; CO₂ to 1100°C at 200°C/hr; Ar-4% H₂ at 1100°C for 4 hr.

cellent quality. High density and low carbon content of fuel particles were achieved for each preparation; this is typical of this preparation method.

We have demonstrated⁷ the preparative method on the kilogram-scale for UO_2 - ThO_2 microspheres in which thorium:uranium atom ratios were 4.8 and 3.4. These microspheres were prepared from highly enriched uranium and are being used in coated-particle irradiation tests in the Dragon Reactor. The spheres had very high density, good crushing strengths, and essentially "geometric" surface area (Table 3.7). X-ray diffraction measurements showed that solid solution was achieved. The spheres produced by the 1400°C firing in hydrogen were amber colored and transparent, unlike spheres fired at 1100°C in Ar-4% H_2 . Typical metallographic sections of the 1400°C -fired spheres are shown in Fig. 3.5.

A number of interesting color effects, which are not understood, were noted throughout the firings. After the 1100°C firing, the microspheres were not transparent and were pale green and black in about equal numbers. The density was 97 to 98% of theoretical, and the oxygen-to-uranium ratio was less than 2.006. These values are acceptable. However, we decided to refire the spheres in pure hydrogen in case the color difference was caused by minor variations in the oxygen-to-uranium ratio or degree of solid solution among the individual spheres. A test sample was fired to 1150°C in hydrogen and held for 4 hr, and three different colors of spheres resulted. In addition to the blacks and pale greens, half of the spheres were amber colored and transparent. The material was then fired to 1400°C in hydrogen; all of the spheres were converted to the amber-colored transparent type.

Sol-Gel Process Employing Coprecipitated UO_2 - ThO_2 Sols

We developed a coprecipitation method for the preparation of UO_2 - ThO_2 sols and demonstrated this process on a laboratory scale through the final dense UO_2 - ThO_2 calcined microsphere product for a thorium-to-uranium atom ratio of 3. Other precipitation approaches that we tried included peptization of thorium hydroxide precipitates with uranyl nitrate and addition of UO_3 to sols prepared from precipitated thorium hydroxide. Although sols could be readily formed by these methods,

Table 3.7. Analyses of $\text{UO}_2\text{-ThO}_2$ Microspheres (97.69% ^{235}U) After Firing

First firing — fired to 1100°C and reduced for 2 hr in Ar-4% H_2 ; cooled to 25°C in Ar
 Second firing — the 210- to 297- μ -diam fraction from the first firing was fired to 1400°C
 and reduced 4 hr in H_2 ; cooled to 25°C in Ar

	Sample No. ^a		
	3371-78-1400 ^b	3371-80-1400	3371-82-1400
Sol preparation No.	47-27-97	47-27-97	47-49A-97
Th/U atom ratio ^c	3.41	3.41	4.79
U, %	10.95	10.95	8.18
Th, %	37.3	37.3	39.2
Hg porosimetry			
Density, g/cm^3	10.13	10.17	10.11
Density, % of theoretical	99.3	99.7	99.6
Porosity, %	<1	<1	<1
Resistance to crushing, g	1152	1008	907
Surface area, ^d m^2/g	0.004	0.003	0.004
X-ray crystallite size, A	1537	1280	1348
Lattice parameter	5.5679	5.5680	5.5679
Carbon, ppm	<10	<10	<10
Aluminum, ppm	100	110	110
Gas release to 1200°C in vacuum			
Total volume, cm^3/g	0.011	0.007	0.007
Composition, vol %			
H_2	91.4	68.8	81.1
H_2O	0.69	5.24	2.16
$\text{N}_2 + \text{CO}$	7.92	13.4	16.2
Ar		0.26	0.27
CO_2		12.0	0.27
O_2		0.26	
Weight of 210- to 297- μ -diam fraction, g	439.2	539.3	1295.1
Screen analysis, ^e wt %			
>297 μ	20.6	9.2	15.5
249-297 μ	65.9	74.9	69.0
210-249 μ	0.6	1.7	3.2
<210 μ	12.9	14.2	12.2

^aAll analyses on 1400°C -fired material except as indicated.

^bContained some "cherry-pitted" spheres.

^cAnalysis on coated particles.

^dCalculated geometric surface area of 210- to 297- μ -diam spheres is $2.0\text{--}2.8 \times 10^{-3} \text{ m}^2/\text{g}$.

^eAfter 1100°C firing.

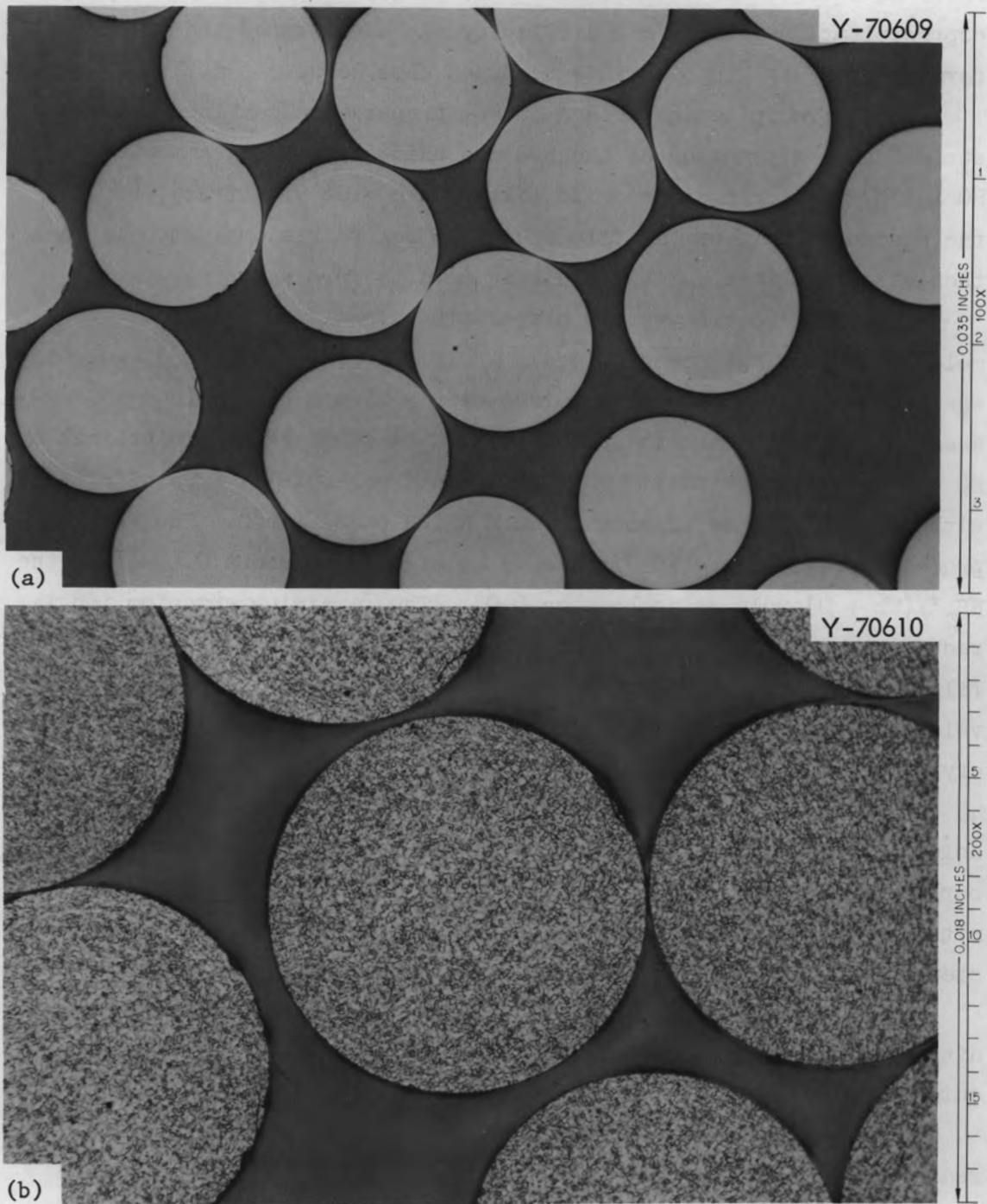


Fig. 3.5. Metallographic Sections of Sol-Gel $\text{UO}_2\text{-ThO}_2$ Preparation 3371-82-1400. (a) As polished; the halos are light effects from the transparent spheres. (b) Etched with $\text{H}_3\text{PO}_4\text{-HF}$. Grain structure is visible.

their nitrate-to-metal ratios were higher than those obtained by the coprecipitation method, and difficulty was encountered in the sphere forming process. This work is reported elsewhere.⁸

The coprecipitation method of sol preparation combines "reverse strike" coprecipitating of the hydrous oxides in excess ammonia at $80 \pm 5^\circ\text{C}$, washing hydrous oxide filter cake free of nitrate, boiling the aqueous slurry of the filter cake to remove residual ammonia, and then dispersing the cake with nitric acid to form a sol.

Typical laboratory-scale preparation of sols consisted of 0.5-mole batches of the mixed oxides. A $0.5 \text{ M } \text{UO}_2(\text{NO}_3)_2\text{-Th}(\text{NO}_3)_4$ solution was added at a nearly constant rate over a 20-min period to a 75% excess of $3 \text{ M } \text{NH}_4\text{OH}$, and the precipitation temperature was maintained at $80 \pm 5^\circ\text{C}$. The precipitate was then washed essentially free of nitrate with 10 cake volumes of about $0.08 \text{ M } \text{NH}_4\text{OH}$ at $80 \pm 5^\circ\text{C}$. The washing procedure reduces the $\text{NO}_3^-/(\text{Th} + \text{U})$ mole ratio to about 0.003, and the $\text{NH}_4^+ / (\text{Th} + \text{U})$ mole ratio becomes 0.05. The remaining ammonium ion is reduced to the range 10 to 30 ppm by boiling an aqueous slurry of the filter cake until the pH of the condensed steam drops from its initial value of approximately 10 to about 6. The hydrous oxides have an x-ray crystallite size less than 30 Å.

A three-step process is used to disperse the hydrous oxides to sols to attain nitrate-to-metal ratios low enough for use of the sol in our conventional sphere forming process. The three-step process gives nitrate-to-metal oxide mole ratios of 0.13 to 0.14, whereas a single step gives 0.19. The three-step dispersion process follows:

1. One-third of the hydroxide slurry is boiled with sufficient nitric acid to give a nitrate-to-metal ratio of 0.40; a clear red sol quickly forms.
2. The second one-third of the hydroxide slurry is added to the red sol and boiled for about 20 min; this peptizes all of the added hydroxides, and a nitrate-to-metal ratio of 0.20 is obtained.
3. The remaining third of the hydroxides is then added, and boiling is continued at reflux for about 8 hr or until the sol becomes a clear dark red. The final nitrate-to-metal ratio is 0.13 to 0.14.

The sol may then be concentrated by evaporation to 1.5 M (Th + U). The x-ray crystallite sizes of the dispersed particles of the sol are 40 to 45 A.

The sol is easily formed into microspheres by the standard method (using 2-ethyl-1-hexanol containing 1.1% H₂O, 0.3% Span 80, and 0.5% Ethomeen S/15). The gel spheres are converted to theoretically dense ThO₂-UO₂ microspheres by firing in air to 1200°C and then reducing for 4 hr with Ar-4% H₂. Temperature rise rates greater than about 20°C/hr caused cracking during heating to 300°C, but cracking could be eliminated entirely by using a slower rate. The crushing strength of 177- to 250-μ-diam fired spheres was about 1700 g.

Microsphere Preparation Process Development

S. D. Clinton P. A. Haas

We have developed a process for converting sols into gel microspheres of closely controlled size in the range 50 to 700 μ in diameter. In this process, drops of sol are gelled by extraction of water into an immiscible organic liquid such as 2-ethyl-1-hexanol. The following five operations are required:

1. dispersion of the sol into droplets,
2. suspension in an immiscible liquid that will extract water to cause gelation,
3. separation of the gel microspheres from the liquid,
4. recovery of the immiscible liquid for reuse,
5. drying of the gel microspheres.

The size of the product microspheres is determined in the first step. In the second step, the extraction of water causes gelation and thus converts the droplet of sol into a solid sphere. Interfacial tension holds the drop in a spherical shape. The maximum droplet size is limited, since very large drops (> 1000 μ) will distort. Slow extraction of the water is essential to obtaining a dense strong microsphere. If the water is extracted too rapidly, the drop breaks into fragments or forms a hollow particle. A surfactant must be dissolved in the immiscible liquid to prevent coalescence of the sol drops, destruction

of the sol drops on the vessel wall, and clustering of partially dried drops. The remaining three operations are simple in principle. The dried gel spheres may be calcined to give oxide spheres of near-theoretical densities.

Sol Disperser Development

Many sphere-forming column operating difficulties would be minimized if we produced even more uniform sol drop sizes; therefore, we have tested a variety of sol dispersion devices. Drops can be formed from a sol mass by applying one or more forces such as gravity, centrifugal field, shear, inertia, interfacial tension, and electrostatic repulsion. To obtain uniform drops and controlled diameters, both the force and the configuration of the sol where the force is applied must be uniform, and one or both must be controllable. For all dispersers tested the sol is fed through orifices or capillaries 0.004 to 0.030 in. in diameter. The two-fluid nozzles have been the most useful sol dispersion devices because they are reliable, they give good uniformity, and droplet size is easily controlled over the whole sol drop size range of interest (200 to 2000 μ in diameter).

A new type of sol disperser is being developed in which a hypodermic needle or capillary is mechanically connected to a loudspeaker and vibrated by it. Power is supplied to the speaker in the form of a sine wave at a controlled frequency and amplitude. The mechanical support from the speaker cone to the sol-feeding capillary must be either rigid or supported vertically in such a manner as to minimize any secondary vibrations that might be imposed on the vibrating sol stream. In our work a piece of thin-walled steel tubing was fastened to a Lucite disk, which was glued to the inner cone of the speaker. The capillary was mounted on the end of the tubing, and the whole assembly was vibrated by the speaker coil. The tubing support was bent at a 90° angle so that the end of the vibrating capillary would be submerged in 2-ethyl-1-hexanol at the top of the tapered column. The sol droplet size was controlled by fixing the sol flow rate and vibration frequency (see Fig. 3.6). We adjusted the vibration amplitude to produce a stable sol dispersion of either one or two equally sized drops per cycle and to

PHOTO 85526

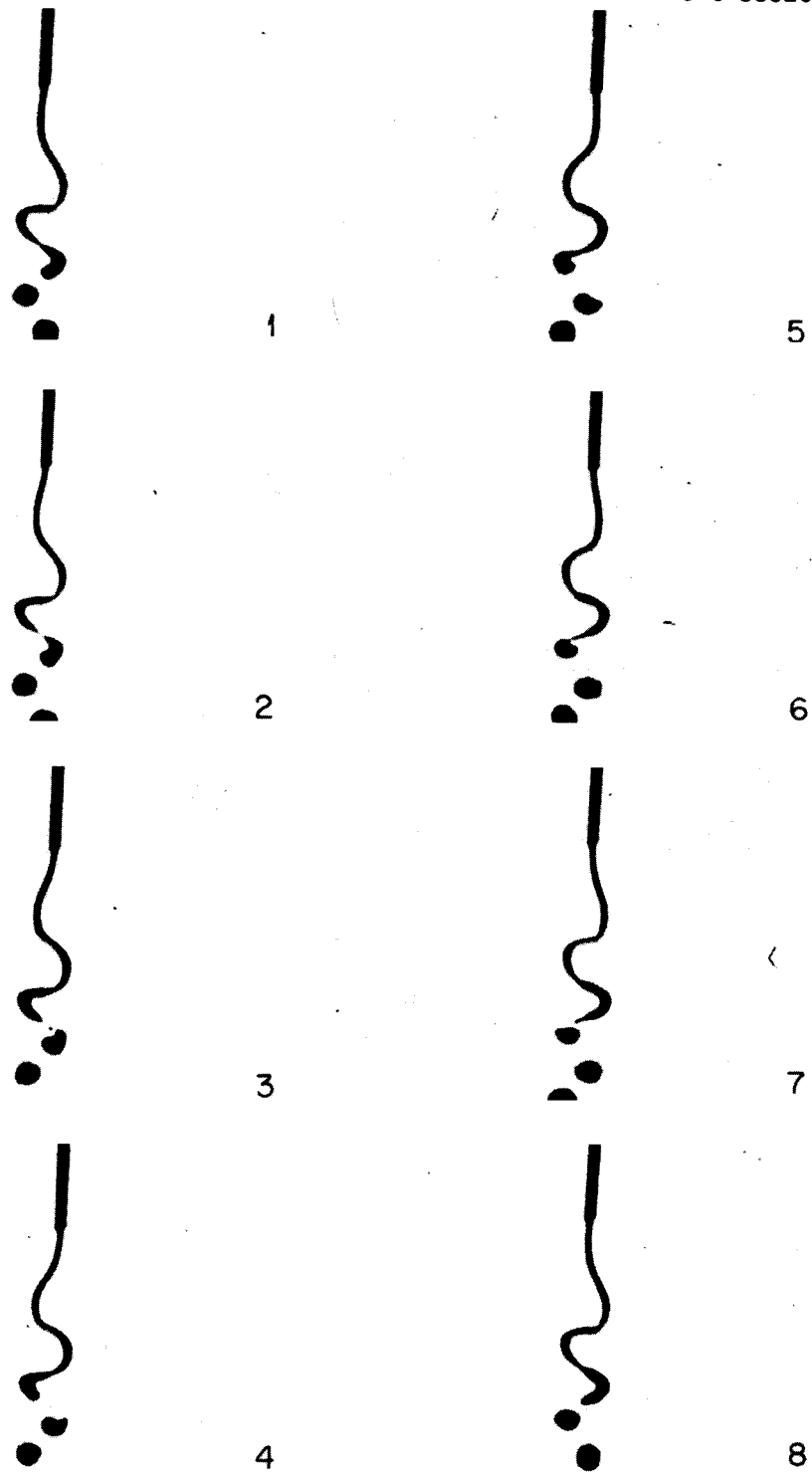


Fig. 3.6. Single Capillary Vibrating at 60 Hz to Disperse 9.6 cm^3 of UO_2 Sol per Minute into $1370\text{-}\mu$ -diam Droplets.

eliminate satellite droplets. During certain conditions at increased amplitudes, four drops per cycle of apparently uniform size could be formed, but in general this mode of operation was not stable. The total capillary displacement for forming two drops per cycle ranged from about 1/4 in. at 20 Hz down to 1/32 in. at 200 Hz.

We made initial speaker vibration tests using a Lucite orifice plate to disperse the sol, but the vibrational energy seemed to have little or no effect on the droplet formation. Subsequent tests with a vibrating No. 22 hypodermic needle produced size distributions that compared favorably with the best results from the two-fluid nozzle (Table 3.8). During the first vibrating needle test, the predicted mean particle size was the same as a 40 mesh-screen, and the screen analysis indicated 94 wt % of the product was between 45 and 35 mesh. Two more vibrating needle tests produced 98 wt % of the calcined oxide spheres within two adjacent screen sizes. The amplitude of vibration for these three tests ranged from 1.5 to 4.0 v. During the initial vibrational runs, the amplitude or voltage was very dependent on the mechanical coupling from the speaker and the method of holding the rubber tubing connecting the sol pump to the vibrating needle.

The first attempt at scale-up of sol flow rate was to vibrate four 15-mil-ID capillaries attached in parallel to a speaker and to use one infusion pump for the sol feed (see Fig. 3.7). Four runs using this approach produced size distributions of calcined spheres at least comparable to past experiences with the two-fluid nozzle (Table 3.9). Although the size uniformity for four vibrating capillaries was not as good as for a single vibrating needle, the size distribution results were encouraging, and no difficulty was encountered with plugging of any of the four parallel capillaries. By comparing pressure drop-flow rate characteristics through the capillaries with water, we determined the apparent viscosity of the 3.0 μ thoria feed sol to be 4 to 5 centipoises. With apparent viscosities of about 5 centipoises, the rheology of the sol probably favors a Newtonian behavior, which would produce equal sol flow rates through equal parallel resistances. If the sol has a tendency to be thixotropic, the vibrational energy in the capillaries could be beneficial in lowering the effective sol viscosity.

Table 3.8. Comparison of Product Sizes of Calcined Thoria Microspheres from a Vibrating Hypodermic Needle and from a Two-Fluid Nozzle

Conditions	Single Vibrating Needle			Two-Fluid Nozzle
Sol feed rate, ^a cm ³ /min	1.2	1.2	4.8	1.2
Vibration frequency, Hz	20	40	70	
Mode of sol dispersion, drops/cycle	2	2	1	
Predicted mean size, μ	420	330	550	270
Product distributions, wt %				
-30 + 35 ^b or 500 to 590 μ			97.8	
-35 + 40 or 420 to 500 μ	49.0		2.2	
-40 + 45 or 350 to 420 μ	45.4	0.2		
-45 + 50 or 297 to 350 μ	5.6	98.3		2.9
-50 + 60 or 250 to 297 μ		1.5		92.0
-60 or < 250 μ				5.3

^aTotal Thoria sol is 3.0 M Th.

^bU.S. sieve mesh.

Table 3.9. Product Sizes of Calcined Thoria Microspheres from Four Vibrating Capillaries in Parallel

Conditions	Run I	Run II	Run III	Run IV
Sol feed rate, ^a cm ³ /min	4.8	9.6	9.6	19.2
Vibration frequency, Hz	50	50	50	200
Mode of sol dispersion, drops/cycle	2	2	2	2
Predicted mean size, μ	310	390	390	310
Weight of product, g	266	346	720	314
Product distribution, wt %				
-35 + 40 ^b or 420 to 500 μ		1.4	0.1	
-40 + 45 or 350 to 420 μ	0.8	70.1	61.9	
-45 + 50 or 297 to 350 μ	27.3	23.5	37.6	30.4
-50 + 60 or 250 to 297 μ	68.9	4.9	0.4	62.6
-60 or < 250 μ	2.9			7.0

^aTotal to four capillaries.

^bU.S. sieve mesh.

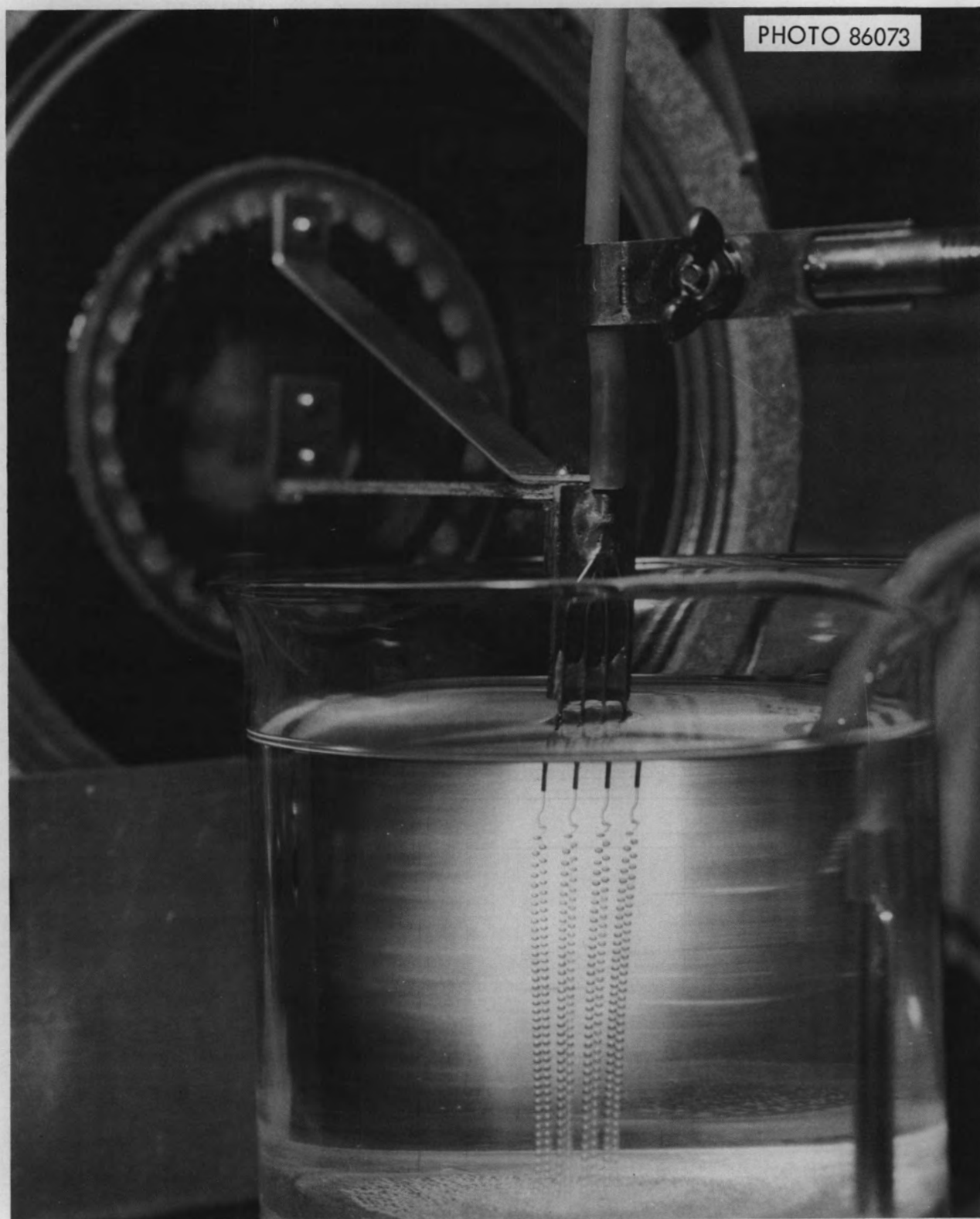


Fig. 3.7. Four Parallel Capillaries Vibrating at 90 Hz to Disperse $20 \text{ cm}^3/\text{min}$ of ThO_2 -25% UO_3 Sol into $960\text{-}\mu$ -diam Droplets.

With the multiple vibrating capillaries it was difficult to determine the mode of sol dispersion through each capillary. During the four previously mentioned tests, we increased the vibrational amplitude until all of the sol streams were producing two drops per cycle. Because of differences in mechanical coupling from the speaker or slight differences in sol flow rates, the change from one to two drops per cycle from each capillary did not always occur at exactly the same amplitude. We determined the mode of sol dispersion visually with the aid of a stroboscope. As the vibrational frequency was increased, the number of sol droplet streams produced by the multiple capillaries become more difficult to resolve.

We made a vibration test using a single needle with the 2-ethyl-1-hexanol in the tapered column at a temperature of 60°C instead of the normal 25 to 30°C. The sol flow rate was 2.4 cm³/min, the vibration frequency was 90 Hz, and the mode of sol dispersion was two drops per cycle. The predicted mean product size was 325 μ, and 93 wt % of the fired spheres were between 297 and 350 μ. There was essentially no cracking of the calcined oxide, and the particle density was within 98% of theoretical. The gelation time for the thoria sol droplets in the organic liquid at 60°C was about half that required at the normal operating temperature. Since there was no evidence of increased particle cracking, the higher temperature could essentially double the capacity of a given column. We attempted to make a 500-μ-diam product at 60°C, but we had to terminate the run because of increased droplet coalescence and particle clustering.

The results certainly indicate that the effect of higher organic temperature on the gelation of sol drops should be a subject for further study. The residual carbon problem in urania gel spheres could conceivably be minimized by shorter contact time between the sol droplets and organic solvent.

Thoria and urania sols with apparent viscosities between 15 and 20 centipoises proved to be difficult to disperse into uniformly sized droplets with the existing vibration system. The voice coils of three 12-in.-diam speakers were burned out in our attempts to disperse sols

of higher viscosities. A recently acquired 8-in.-diam two-way diffraxial speaker seems to have more resistance to burnout with increasing load on the speaker cone, but a more reliable source of vibration will be required in the future to prove the effectiveness of vibrating capillaries as a sol dispersion method. An electronic shaking device designed to vibrate under specified loads was ordered for these studies. We will continue tests of this type of sol disperser.

Preparation of Microspheres by Dispersion and Suspension Through Mechanical Agitation

Sol-gel microspheres of relatively nonuniform diameter and less than 80 μ in mean diameter can be prepared easily and efficiently by use of mechanical agitation to disperse and suspend the droplets into 2-ethyl-1-hexanol (2EH) during the extraction of water. The procedures previously tested⁹ were applied to preparation of 2.5 kg of -325 mesh (< 44- μ -diam) thoria microspheres.

The yields from three tests (Table 3.10) show the need for an improved product collection system. In the first two tests, the mixer discharged into the microsphere preparation column, which is 6 in. in diameter at the top. The third test used a flat 11-3/4 \times 13-3/4 in. settler. The losses tabulated are nearly all from entrainment of fine microspheres out of the settlers. The lost material was probably essentially all -325 mesh, and the yields of the second and third tests on this basis are consistent with the agitator speeds used. The much larger area of the paddle agitator actually provided a higher average agitation for the first test than for the other tests with smaller paddles at higher speeds. However, the higher localized agitation for the smaller paddles dispersed the sol into smaller drops.

Microsphere Preparation Without Fluidization - Concatenated Column

Operation of a continuous fluidized-bed column requires uniform sol drop sizes and an accurate matching of the fluidizing flows to the drop size. Also, the accumulation of sol or gel spheres in a fluidized bed may increase the clustering or coalescence. We considered alternatives to the fluidized bed in a column for suspending sol drops during

Table 3.10. Yields from Mechanical Agitator Systems for Preparing Thoria Microspheres^a

Agitator			
Number of paddles	4	3	3
Paddle dimensions	1-1/4 × 1 in. high	3/4 in. diam ^b	3/4 in. diam ^b
Speed, rpm	660	1250	1250
Settler			
2EH to mixer, cm ³ /min	Column	Column	11-3/4 × 13-3/4 in. pan
Average mixer holdup time, min	390	390	550
2EH flow to column, cm ³ /min	5	5	6
ThO ₂ feed, g	400	400	
ThO ₂ collected, g	1150	1200	900
% of feed	822	644	782
< 44 μ collected, % of feed	72	54	87
< 44 μ produced, ^c % of feed	26	49	70
44-53 μ collected, % of feed	54	95	83
53-74 μ collected, % of feed	19	3	10
> 74 μ collected, % of feed	19	1	3
	8	0.5	4

^aFeed: 4.8 cm³/min of 2.5 M ThO₂ sol.

^bThree round paddles attached to shaft at 120° with 2 in. maximum OD of assembly.

^cAssuming all material not collected was spheres smaller than 44 μ lost by entrainment.

the extraction of water to cause gelation with the expectation of avoiding one or both of these limitations. A "fall-through" column that is long enough to give the required holdup time without fluidization is practical and attractive for small microspheres,¹⁰ but is not practical for gelation of the larger ($\geq 800 \mu$) thoria or urania sol drops, which are usually the preferred size.

Therefore, we tested apparatus with cocurrent flow of sol drops and 2EH for suspending larger sol drops for the longer times necessary for gelation. Simple coils of small diameter tubing were not satisfactory.¹⁰ Staged columns with cocurrent flow through both upflow and downflow stages appear more practical for larger sol drops than simple "fall-through" columns without fluidization. Considering the stringent requirements for uniform product and for flexibility with respect to product diameter and composition, we find the regular fluidized bed type of microsphere column more suitable for use in the TURF. The cocurrent multistage columns will not be tested further at present.

One cocurrent multistage column tested was a "concatenated" glass column with six 8-ft-high stages - three 2-in.-ID downflow stages and three 3/4-in.-ID upflow stages. The stages were connected by 3/8-in.-ID bends with 2-in.-long tapered sections for the diameter changes. A two-fluid nozzle fed sol drops into the top of the first downflow stage along with an added flow of 2EH to give the selected total flow of 2EH. The sol drops or gel spheres moved through the downflow stages at a velocity equal to the sum of their settling velocity and the 2EH velocity. In the upflow stages, their velocity was the 2EH velocity minus their settling velocity. The concatenated column produced good samples of thoria microspheres.

We must select the design of the column and the operating conditions to avoid the following difficulties:

1. discharge of incompletely gelled drops because of inadequate holdup time,
2. accumulation of drops because of inadequate 2EH velocities and then coalescence or clustering of the accumulated drops,
3. breakup of drops because of excessive turbulence,
4. deposition of drops on the walls at regions of turbulence or impingement.

Smooth tapers without any sudden diameter changes are necessary to avoid the second and third difficulties. The dimensions described and a 2EH flow rate of about 1 liter/min were adequate to avoid the accumulation of gel spheres for thoria sol drops that yielded 300- or 400- μ calcined ThO₂ microspheres. The drops from the first top end sections tested broke because of excessive turbulence at a sudden increase in tubing diameter from 3/8 in. to 2 in. Tapered enlargements eliminated the breakup at this point. About 500- μ -diam ThO₂ microspheres after calcination (or 1100- μ sol drops) were the maximum size possible with the six stages described. To prepare larger products, longer holdup times would be necessary to ensure gelation, and higher velocities would be needed to avoid accumulation in the column. Thus many more or longer stages would be required.

The concatenated column reduces the clustering, coalescence, and deposition on walls, but it is not a complete solution to these problems. In one test with a urania sol in the regular column, clustering and deposition on the walls were very bad. These problems were insignificant in the main sections of the concatenated column, but there were small amounts of clustering or deposition in regions of turbulence or low velocity. The urania sol drops (720 μ initial diameter) were not adequately dried when they left the column, and they coalesced in the product collector. This is much slower drying than we found with thoria sol drops of the same size. The slower drying of urania or mixed sols as compared with thoria had been noticeable in other studies, but this test was the clearest example of the slower drying.

In general, the potential advantages of the concatenated column are realized only if the end sections are carefully designed to give smooth, gradual tapers without any significant discontinuities or turbulence. Since the cocurrent flow of 2EH must be rapid enough to avoid settling out of drops at any location, the holdup time per stage will be much less than the holdup time of a "fall-through" column of the same length. Thus the total length of concatenated column stages must be much greater than the length of a simple "fall-through" column before larger spheres can be prepared.

Drying of Thoria Gel Spheres

We investigated empirically conditions to avoid cracking of thoria gel microspheres during firing. In general, the factors that minimize cracking are those that minimize composition gradients within the gel microspheres. The drying conditions were the important variables, and the best conditions were superheated steam to a final drying temperature of 200°C. The principal observations made during drying of gel spheres prepared from regular thoria sols were as follows:

1. The sphere diameter is a principal variable; the tendency toward cracking increases as the diameter increases. If the fired products are larger than 500 μ in diameter, the optimum drying conditions (superheated steam to a final drying temperature of 200°C) are necessary to minimize cracking. For calcined product diameters less than 250 μ , the optimum conditions are not necessary. The amount of cracking for diameters of 250 to 500 μ is variable; the best drying conditions can usually be compromised without excessive cracking.

2. The amount of cracking in the fired spheres decreases as the maximum drying temperature increases from 100°C to 200°C.

3. The presence of superheated steam in the drying atmosphere promotes the removal of 2EH from the gel and reduces the amount of cracking during firing. Drying in air may permit an exothermic oxidation reaction while relatively large amounts of 2EH remain on the gel and thus give very rapid temperature rises and excessive cracking. Inert atmospheres (argon or nitrogen) without steam remove 2EH rapidly only at temperatures exceeding 180°C, as compared with rapid stripping at 120 to 140°C by steam.

For thoria microspheres, the presently preferred drying and firing conditions are:

Drying	Argon atmosphere	25 to 110°C in 1 hr
	Argon plus steam atmosphere	110 to 200°C in 6 hr
Firing	Air atmosphere	100 to 500°C at 100°C/hr
	Air atmosphere	500 to 1150°C at 300°C/hr
	Air atmosphere	At 1150°C for 4 hr

Microsphere Preparation Column Chemistry

A. T. Kleinstauber¹¹

In the microsphere forming process, gel microspheres are formed by dispersing sol droplets into the organic solvent 2-ethyl-1-hexanol, which extracts water from the droplets to form the microspheres. To stabilize the droplets during water extraction, we use small amounts of surfactants. The current choice of surfactants is Span 80 and Ethomeen S/15. The organic solvent is recycled for column operation after removal of water by continuous distillation at pot temperatures of 140 to 155°C.

We do not understand the chemical behavior of the various species in the solvent, nor do we know the effects of the distillation process on them. We have obtained control of the microsphere forming by empirical methods, which have been very successful in most instances. We began this investigation with the hope that it would provide information for improvement of column operation and, in particular, that it would lead to conditions permitting long-term operation with the same solvent. Since surfactants are depleted both by adsorption on the microspheres and by degradation during operation, and periodic addition of surfactants is required, we examined the changes that occur during operation. We examined analytical methods that might be used to measure surfactant concentrations, changes that occur during solvent purification by distillation, and extraction of components from the organic medium into the sol and gel spheres.

Analytical Methods

We examined measurements of surface tension and conductivity as possibilities to rapidly analyze surfactant concentration during operation. These measurements, if meaningful, could be used routinely to determine surfactant concentration and to ascertain when surfactant should be added. Surface tension measurements were not sufficiently sensitive to surfactant concentration to be useful, but the conductivity measurement was sufficiently sensitive to be used to measure Ethomeen S/15 concentration.

There was essentially no change in the surface tension, as measured against an air interface, of water-saturated 2-ethyl-1-hexanol containing

either Span 80 or Ethomeen S/15 from 0 to 0.5 vol % of surfactant. Interfacial tension measurements were somewhat more sensitive (Fig. 3.8), but were not sufficiently so. Ethomeen S/15 gave results similar to those shown for Span 80 in Fig. 3.8. We measured with a ring tensiometer and observed viscoelastic films at all surfactant concentrations, which covered the range 0.05 to 2.0 vol %. With the du Noüy ring method, the film does not break sharply but stretches considerably before the break. The measured values were not very reproducible, and the smoothed curve is an averaging of points.

Conductance was a sensitive measure of Ethomeen S/15 concentration (Table 3.11). Ethomeen S/15 in water-saturated 2-ethyl-1-hexanol is essentially nonconductive, but when equilibrated with nitric acid, which is extracted by the Ethomeen S/15, it is sufficiently conductive to provide a useful measurement. A small amount of nitric acid is always in equilibrium with the sols, and additional HNO_3 can be equilibrated with a sample of the alcohol containing surfactants if desirable.

Solvent Changes During Distillation

To simulate the distillation, dilute nitric acid (pH = 2.0) was continuously infused into boiling 2EH that contained Span 80 and Ethomeen S/15 surfactants. Nitric acid is known to be extracted into 2EH to a slight extent from the nitric-acid-stabilized sols. We then determined the Span 80 concentration by infrared analysis for its carbonyl group and determined the amine and nitrate contents chemically. The

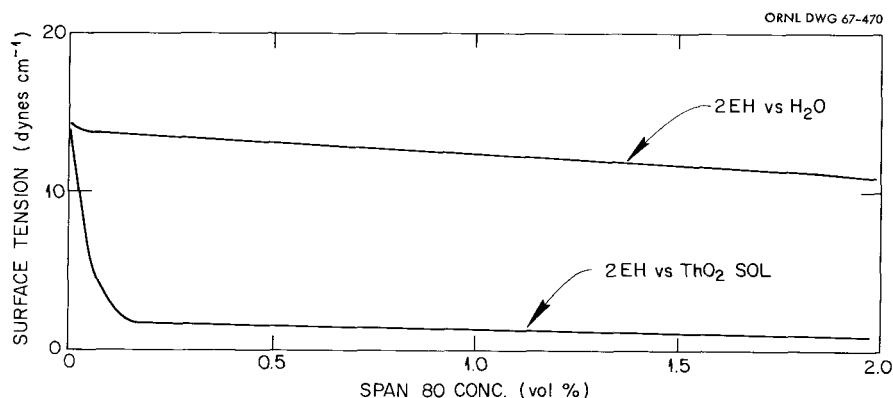


Fig. 3.8. Effect of Span 80 Concentration on Interfacial Tension.

results showed that nitrate and amine disappeared (Table 3.12). The Span 80 concentration apparently increased. We interpret this result to show that some organic species, probably the 2EH, is oxidizing to form carbonyl groups. Since some of the oxidation may have been a result of our failure to exclude air in this experiment, we performed a second set of experiments. In one of the experiments, the 2EH containing only Ethomeen S/15 was boiled in air, and in another, the 2EH containing nitric acid and Ethomeen S/15 was boiled under argon. The re-

Table 3.11. Conductance of 2-Ethyl-1-hexanol Solutions Containing Ethomeen^a

Ethomeen S/15 Concentration (vol %)	Relative Conductance
0	0.714
0.3	2.71
0.4	3.56
0.6	4.98
1.6	8.13

^aConditions: 20 volumes of HNO₃ at pH = 2.00 equilibrated with 1 volume of alcohol before measurement.

Table 3.12. Changes in Boiling^a 2-Ethyl-1-hexanol During Continuous Infusion of Nitric Acid

Boiling Time (days)	HNO ₃ Added ^b (millimoles)	Content (millimoles)		
		NO ₃ ⁻	Span 80	Ethomeen S/15
0	0.0	0.0	15.1	8.8
1	1.1	0.52	19.5	9.0
2	2.8	0.34	20.0	7.0
3	9.6	0.05	26.6	2.8
4	14.3	0.23	31.4	1.8
5	17.1	0.48	37.9	2.0

^aSolution boiled in 140 to 160°C range.

^bpH = 2.0.

sults show that both air and nitric acid cause oxidation (Table 3.13). The Ethomeen S/15 in 2-ethyl-1-hexanol was stable in the absence of nitric acid. Analysis of the organic phase throughout the course of a continuous microsphere forming run shows the same general trends as in our distillation experiments (Fig. 3.9). The implications of these results on long-term operation of a continuous sphere forming column are not clear, but it may be necessary to have better knowledge as well as control of the composition of the 2-ethyl-1-hexanol phase than we now have.

Equilibration Studies with ThO₂ Sols and Gels

The object of several experiments was to determine if Span 80 or Ethomeen S/15 were adsorbed on a ThO₂ surface. The results indicate that only very small amounts, if any, are adsorbed. Span 80 in concentrations ranging from 0.13 to 2 vol % was equilibrated with sol and with dried gel for periods of one day. Within the limits of accuracy of the measurements, no Span 80 was adsorbed (Table 3.14). Infrared adsorption of the carbonyl group at 1727 cm⁻¹ was used as the analytical method for Span 80. In similar equilibration experiments with Ethomeen S/15, similar results were obtained (Table 3.15). Extraction of residual nitric acid from the ThO₂ gel is a very slow process, as indicated by the nitrate-to-amine ratios.

Table 3.13. Oxidation of 2-Ethyl-1-hexanol

Boiling Time (days)	Atmosphere	HNO ₃ Added (millimoles)	Content (millimoles)		
			NO ₃ ⁻	Carbonyl Group	Ethomeen S/15
0	Air	0.0	0.0	0.00	8.4
1.5	Air	0.0	0.0	0.00	8.4
2.5	Air	0.0	0.0	1.12	8.4
0	Argon	0.0	0.0	0.00	8.4
1.5	Argon	6.7	0.73	2.9	5.2
2.5	Argon	14.1	0.13	5.4	0.9

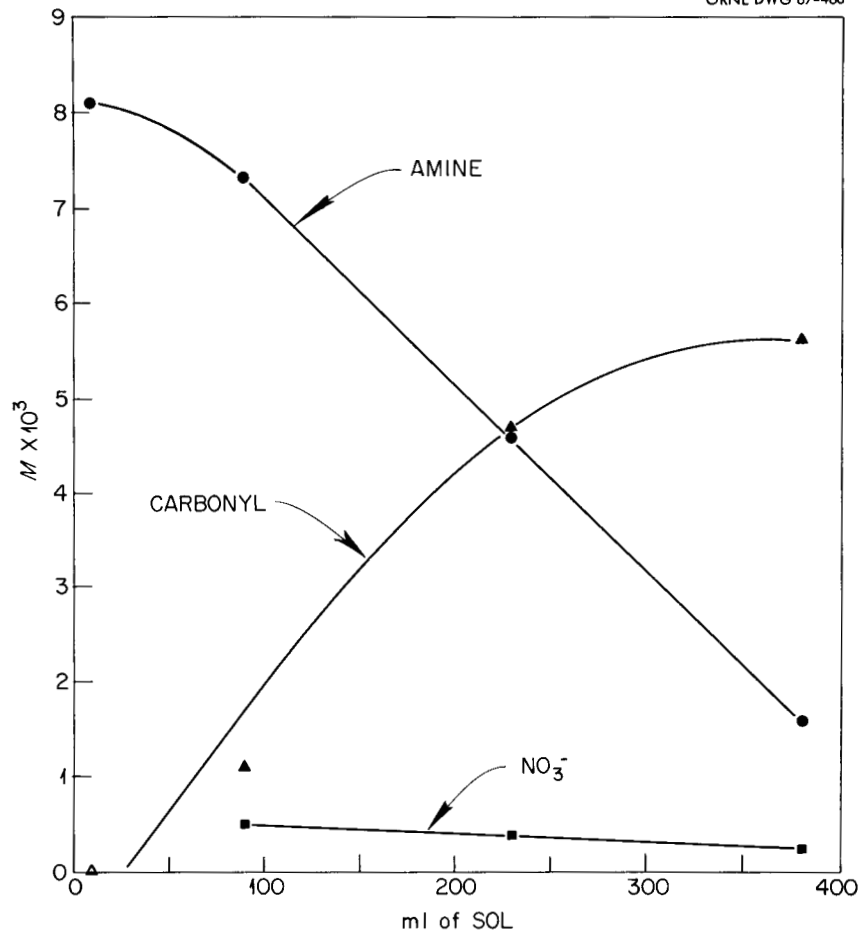


Fig. 3.9. Changes in Organic Solvent During Continuous Operation of a Sphere-Forming Column.

Table 3.14. Equilibration of 2EH Containing Span 80 with ThO_2 Sols and Gels

Conditions: One-day equilibration with 2 M ThO_2 sol or 110°C dried gel

ThO_2	Span 80 Concentration in 2EH, vol %	
	Initial	Final
Sol	0.13	0.16
	0.80	0.81
	2.0	2.0
Gel	0.13	0.16
	0.80	0.87
	2.00	2.04

Table 3.15. Composition of 2EH Containing Ethomeen S/15 After Equilibration with ThO₂ Sols

Equilibration Time (days)	Molarity of ThO ₂	Ethomeen Concentration (M)		Final Nitrate : Amine Ratio
		Initial	Final	
3.5	2.0	0.018	0.016	0.30
		0.019	0.019	0.18
		0.035	0.031	0.30
10	7.3	0.0086	0.0086	0.86
	8.6	0.0086	0.0085	0.61
	9.6	0.0086	0.0085	0.94

REFERENCES

- ¹J. P. McBride et al., Preparation of UO₂ Microspheres by a Sol-Gel Technique, ORNL-3874 (February 1966).
- ²Chem. Technol. Div. Ann. Progr. Rept. May 31, 1966, ORNL-3945, p. 161.
- ³J. G. Moore, A Sol-Gel Process for Preparing ThO₂-UO₂ Sols from Nitrate Solutions by Solvent Extraction with Amines, ORNL-4095 (October 1967).
- ⁴W. D. Bond, A. B. Meservey, and A. T. Kleinstuber, Status and Progress Report for Thorium Fuel Cycle Development Dec. 31, 1965, ORNL-4001, p. 42.
- ⁵D. E. Ferguson (Compiler), Status and Progress Report for Thorium Fuel Cycle Development Dec. 31, 1962, ORNL-3385.
- ⁶C. C. Haws, J. L. Matherne, F. W. Miles, and J. E. Van Cleve, Summary of the Kilorod Project - A Semiremote 10-kg/Day Demonstration of ²³³UO₂-ThO₂ Fuel-Element Fabrication by the ORNL Sol-Gel Vibratory-Compaction Method, ORNL-3681 (August 1965).
- ⁷W. D. Bond et al., Preparation of ²³³UO₂-ThO₂ Microspheres by a Sol-Gel Method, ORNL-TM-1601 (August 1966).
- ⁸A. B. Meservey, UO₂-ThO₂ and UO₃-ThO₂ Sols Prepared by Precipitation-Peptization Processes, ORNL-TM-1782 (March 20, 1967).
- ⁹S. D. Clinton and P. A. Haas, Unit Operations Section Quart. Progr. Rept. July-Sept. 1965, ORNL-3916, pp. 44-50.
- ¹⁰P. A. Haas, S. D. Clinton, and W. D. Bond, Status and Progress Report for Thorium Fuel Cycle Development Dec. 31, 1965, ORNL-4001, pp. 61-64.
- ¹¹Deceased.

4. FUELED-GRAPHITE DEVELOPMENT

J. D. Sease

We are designing processing equipment for installation in the Thorium-Uranium Recycle Facility (TURF) to demonstrate refabrication technology of HTGR fuel elements. The design of the TURF refabrication line requires a thorough understanding of the processing steps required in fabricating fueled-graphite elements. Preliminary studies and the critical-path schedule have indicated that before a large portion of the detailed design of the line can be undertaken, a number of steps in the process must be further delineated and developed. In some cases, we must develop special processes to satisfy the requirement of remote operation in the TURF. In developing processes for the fabrication line, our main objective is to develop processes that will result in the lowest possible fuel cycle cost for the remote fueled-graphite line. This objective is being met by a comprehensive development program in direct support of the TURF fueled-graphite design effort. The progress of this work during the last year is reported in four main categories: particle handling, particle coating, particle inspection, and particle blending and bonding. No development work has been done on assembly and inspection of the fuel element.

Particle Handling

J. T. Meador S. E. Bolt¹ F. C. Davis

Each day 10 kg or 10^8 particles of recycle fissile material must be stored, weighed, transferred, coated, classified, shape-separated, inspected, blended, and dispersed in passage through the fabrication line. Fertile material is added at the blending and dispensing step. We must design equipment and develop techniques that permit remote operation of the production line in a manner consistent with the very high degree of quality control required to produce acceptable fuel elements. Most of the commercially available equipment cannot satisfy our requirements; either it is designed to handle tonnage quantities or it is laboratory equipment and thus not readily adaptable to remote or

automatic operation. Also, conventional bulk-handling equipment would impart too much mechanical damage to the coated particles.

Fuel Transfer System

We are developing a pneumatic system, using an air jet to transfer particles in the TURF. In preliminary tests we developed a system that can transfer microspheres 25 ft horizontally and 7 ft vertically. We have developed a loop system and will use it to develop fully the transfer and valving systems required for the design of the TURF fueled-graphite line.

Shape Separation

A few imperfectly coated or out-of-round particles are invariably produced in the sphere formation and coating processes. To reject cupped, faceted, or ovate material and to minimize the amount of acceptable kernels or coated fuel in the reject material, a shape separation system is being developed. The first system that was investigated and the system generally used for sphere shape separation employs a flat plate mounted on a vibratory feeder slightly in line with, but opposite in direction to, the feeding action of the vibrator. Particles are fed onto the middle of the plate; nonspherical particles are moved up the plate by the vibratory force, while spherical particles, which are relatively unaffected by the vibratory feeding action, roll down the plate. Since the spheres roll down the incline, interference with the nonspheres is prevalent. At higher feed rates, the degree of interference increases.

We developed a new system that obtains separation when the incline down which the spherical particles roll is oriented about 90° with respect to the line of action of the vibration. The general arrangement of this setup is shown in Fig. 4.1. With this arrangement, the particles form a massed array at the point of feed onto the plate and separate as the mass spreads out. Separation occurs in only 2 to 3 in. of travel, and about 400 g/hr can be processed at the single feed point. With multiple feed points the system can be easily scaled to several kilograms per hour.

Classification

Development of a main-line size classification system capable of grading coated fuel microspheres within $\pm 5 \mu$ is required to eliminate the badly oversize or undersize microspheres. Tests and study of commercially available classification equipment indicated that inadequate sizing is usually caused by inaccurate screen openings or by "blinding" of the openings by the particles being processed. From a remote processing standpoint, blinding of the screen openings is of great concern. A system that will accurately classify shape-separated microspheres has been developed, using a vibratory feeder and square-holed etched micro-mesh sieves. This test assembly can virtually eliminate blinding for a limited flow rate, but it has not yet been scaled up to the larger sieve areas required for the TURF process equipment. The general arrangement of the classification system is shown in Fig. 4.2.

The angle between the surface of the micro-mesh and the center line of the magnet ($\beta + \gamma$) was set so that the mesh is pulled from under the microspheres, and yet, on the upward or return stroke the mesh imparts a minimum of impact as it hits the falling particle in midair. The upper limit of the angle $\beta + \gamma$ was estimated with the displacement diagram shown in Fig. 4.3. Experimentally, blinding was minimized with the vertical component of the mesh displacement between 0.040 and 0.045 in. With the angle used, the magnet literally jerks the micro-mesh from under a stationary microsphere. With γ at too steep an angle, bouncing of the microspheres leads to poor classification. Data on the degree of classification of coated fuel are now being taken.

Particle Singularizer

The successful operation of an in-line particle counter and size analyzer (see next subsection) requires that the particles be fed to the optical window of the instrument in single file and spaced at discrete intervals without coincidence of more than one particle in the window. We have developed a device that can feed 417- to 500- μ -diam glass beads in single file at a rate of 120,000/min. High-speed photographs of the particles as they emerge from the feeder showed that the spacing between

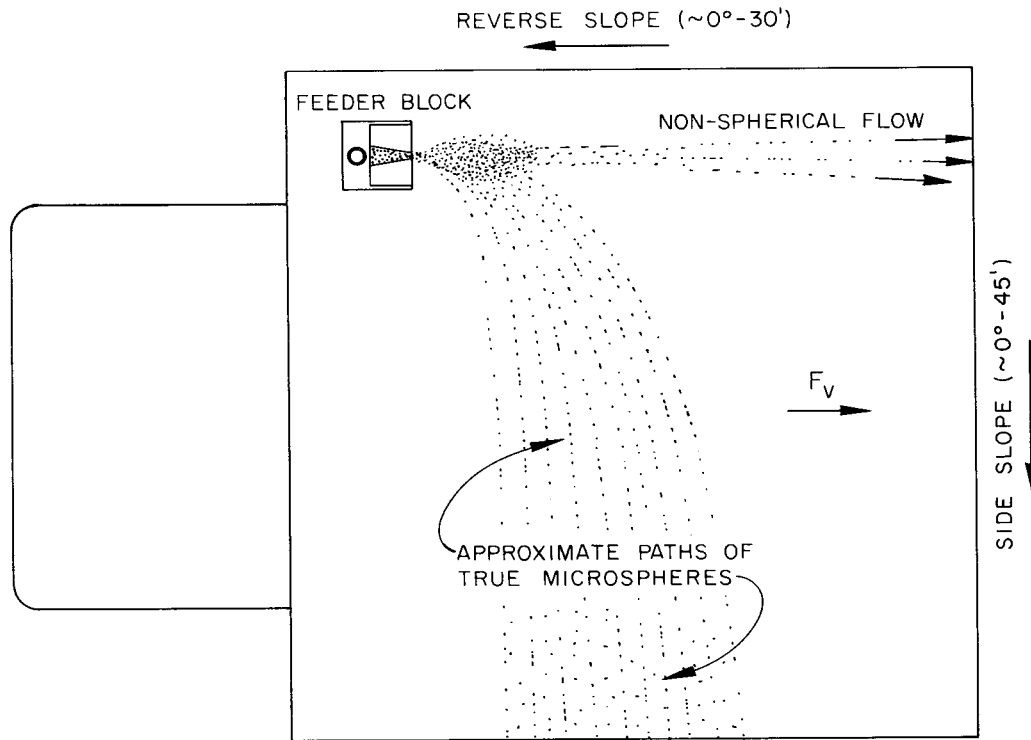


Fig. 4.1. Shape Separation System.

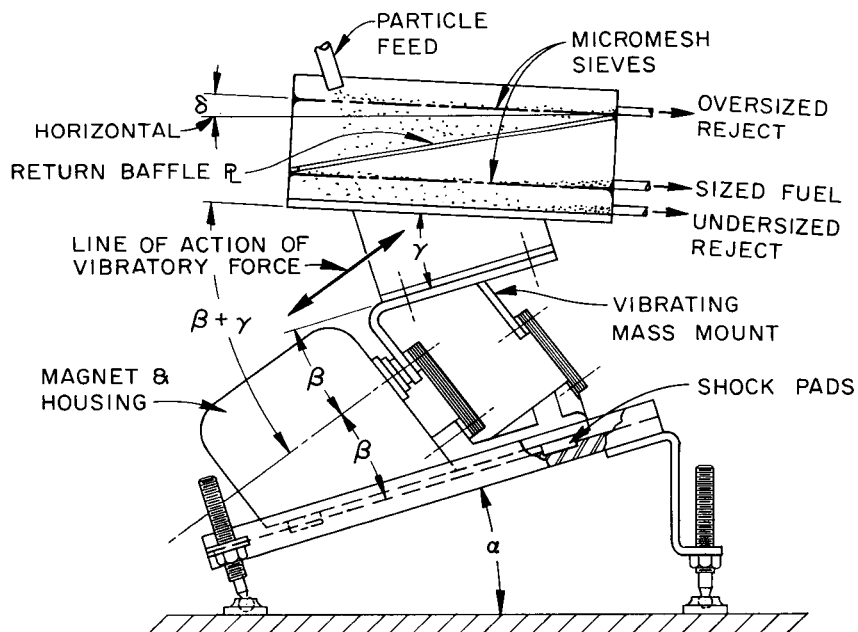


Fig. 4.2. Micro-Mesh Classifier. α is the angle of the vibrator. β is the angle of the magnetic field with respect to the feeder mount bracket or the base of the feeder and is fixed for a particular vibratory feeder. γ is the angle of the micro-mesh with the mount. δ is the angle of incline of the mesh with the horizontal.

particles is at least 0.1 in., which is adequate to prevent coincidence in the instrument. The device, which is quite simple (Fig. 4.4), consists of a controlled air jet in the bottom of a hopper and directed toward a restricted discharge port.

Particle Coating

R. B. Pratt S. E. Bolt¹

The coating of nuclear fuel particles with pyrolytic carbon is probably the most expensive step in fabricating HTGR fuel elements. The principal requirement for these coatings in the tentative specifications for the Peach Bottom hex-block fuel element is that the particles should have duplex pyrolytic carbon coatings. The interior layer is less dense than 1.2 g/cm^3 and the outer layer is to be isotropic and denser than 2.0 g/cm^3 . We are directing our developmental work toward describing the best combinations of processing parameters, gases, and equipment required for remotely coating fuel particles to these specifications. We have investigated three coating systems: fluidized bed, entrained bed, and a rotary drum. Since July we have concentrated our efforts on the fluidized-bed system and the design of a remote prototype.

Fluidized-Bed Coating Development

The fluidized-bed coating system appears to be the most suitable system for remote application and is the system we intend to install in the TURF. Our major progress this year in direct support of the engineering of the TURF remote fueled-graphite line was the development of operating parameters and techniques for making the low-density buffer coatings with acetylene in a 5-in. fluidized-bed coating system. We demonstrated the deposition of buffer coatings with controlled densities from 0.5 to 1.3 g/cm^3 at processing rates of about 10 kg/day in our laboratory-type equipment on $230\text{-}\mu$ -diam fuel particles. In addition, we made cursory runs to produce high-density isotropic coatings from methane, propane, and propylene, using both single- and multiorifice gas nozzles.

ORNL-DWG 67-3135

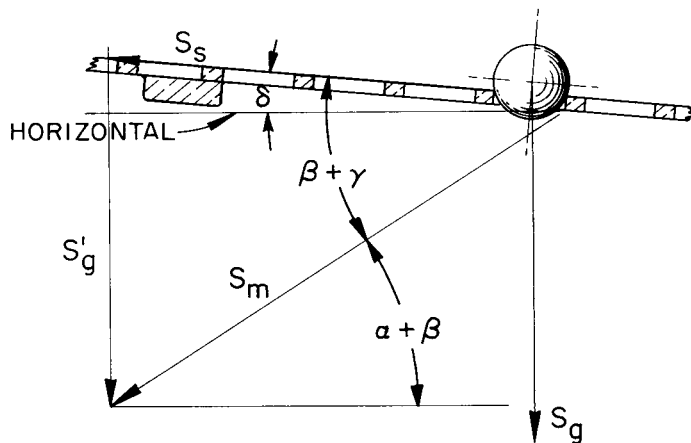


Fig. 4.3. Displacement Diagram. S_g is the distance of free fall of a particle from rest in $1/60$ sec (0.0535 in.). S_m is the vibratory amplitude of the magnet, about 0.070 in. S_s is the displacement along the surface of the sieve.

ORNL-DWG 67-4634

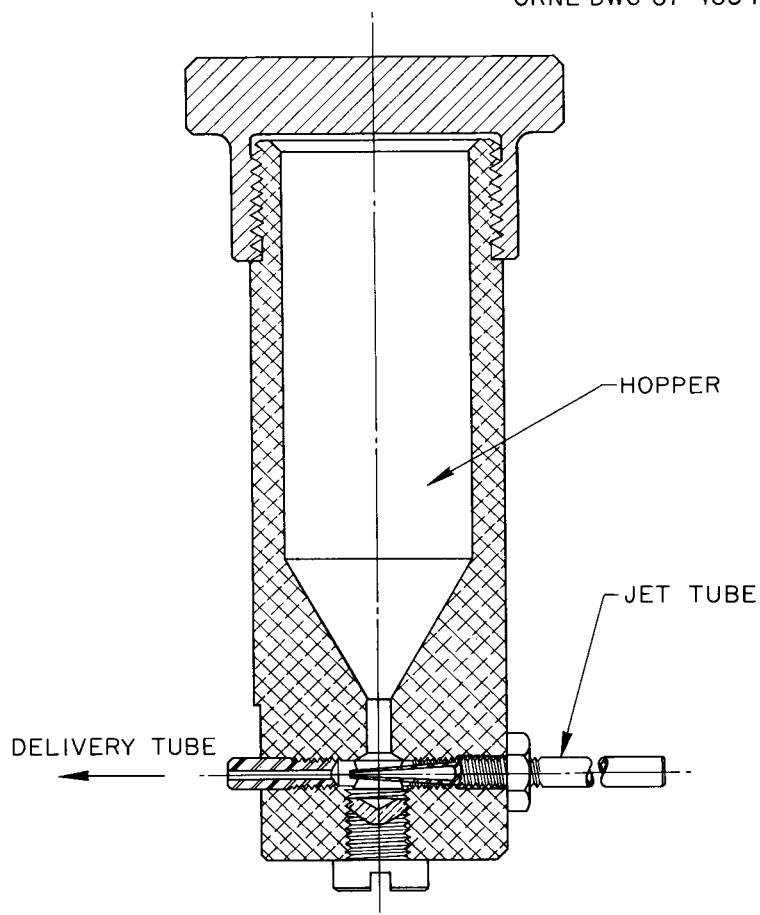


Fig. 4.4. Particle Singularizer.

Equipment and Procedures. - The fluidized-bed particle coating work has been done in the Coated-Particle Development Laboratory (CPDL),² which is equipped with hood-type enclosures for control of alpha contamination. Within the CPDL, prepared thoria-urania sols are converted into microspheres by the sol-gel microsphere process, calcined for densification, and then coated with pyrolytic carbon in a fluidized-bed furnace. The last of these is our concern here. The high-temperature graphite-element resistance furnace is the principal component of the coating systems. The coating furnace in its current configuration is shown in Fig. 4.5. A single-inlet nozzle has replaced the previously used multi-orifice nozzle because it allows bottom unloading and is comparatively more simple. This figure also illustrates a top unloading system, which mechanically thrusts a suction tube into the fluidized bed and evacuates the particles to a cooling chamber. Although the top unloading system functions as intended, we prefer bottom unloading.

We made a number of modifications and additions to coating systems during the past year. A bag filter system for soot removal was installed and has given very satisfactory service. There has been no down time because of filter blockage in over 200 coating runs. A water-cooled baffle and heat exchanger were installed above the hydrogen burnoff flame to cool the exhaust gases to permit high hydrocarbon gas flows. A furnace-top component consisting of a 15-in.-diam water-cooled metal chamber was installed to facilitate maintenance and to support the coater internals. This system uses an existing jackscrew system for component disassembly to minimize handling of components during cleanup. A mechanical drive system for the suction sampling and unloading tube and bed thermocouple is mounted on top of the water-cooled chamber. We installed a new gas flow control panel, which enables us to adjust coating gas flow rates while venting it to the exhaust burner and levitate the particles with an inert carrier gas while the fluidized bed is being stabilized at the desired temperature. A timer-controlled, three-way valve controls the hydrocarbon gas and carrier gas. Multiple flow paths and ranges for six gases provide flexibility.

The first step in coating in the fluidized bed is to load the desired charge of sol-gel microspheres pneumatically into the reaction

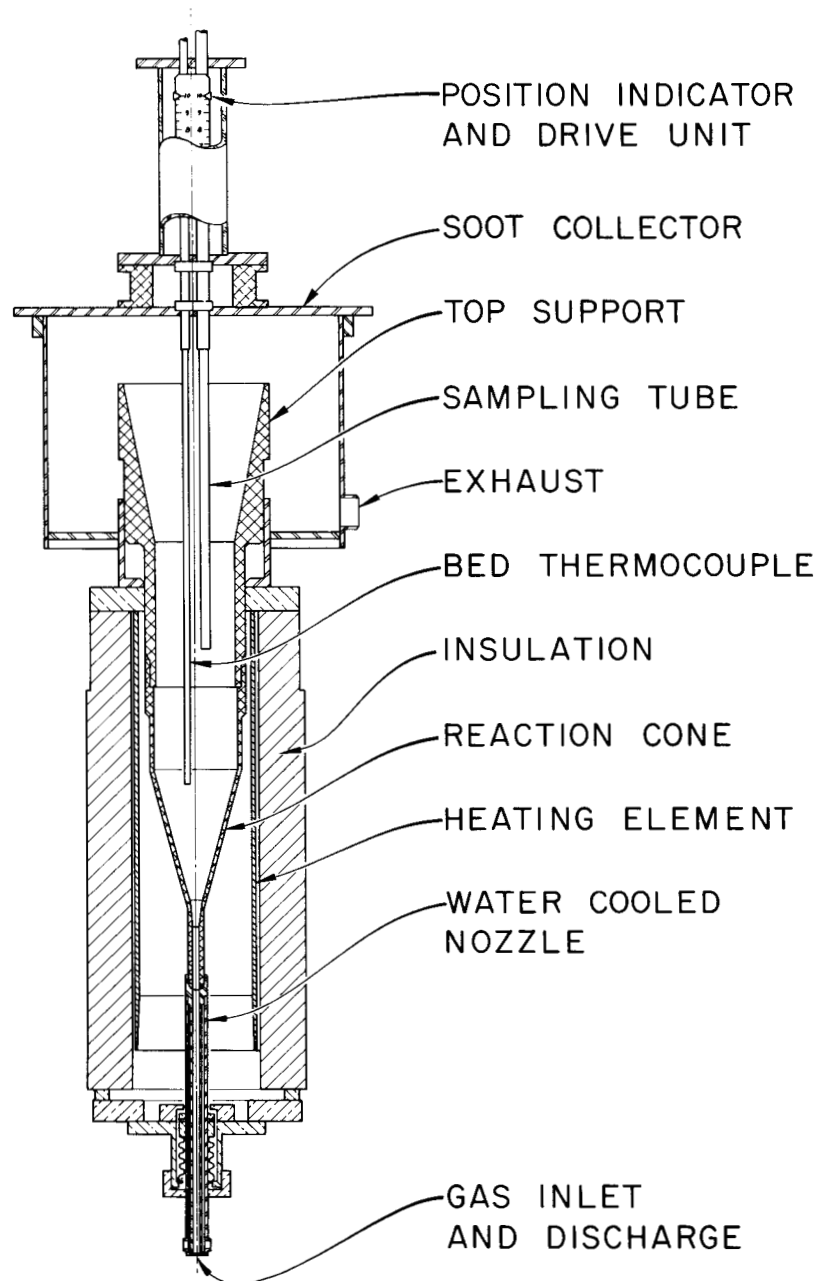


Fig. 4.5. Current Configuration of the 5-in. Coating System,
Showing Pertinent Components.

cone of the furnace, in which they are levitated by an appropriate carrier gas flow. We then establish temperature equilibrium and introduce the coating gas. The gases enter the reaction cone through a nozzle, which controls the degree of bed fluidization and particle motion within the system. When the system is at temperatures above 1000°C, the hydrocarbon cracks and deposits pyrolytic carbon on the sol-gel microspheres. The process also produces soot and hydrogen, which are removed from the furnace as waste. A graphite sleeve above the reaction cone accommodates the increase in charge volume as the coating progresses. Above the sleeve is a deentrainment region, where lower gas velocities allow entrained particles to fall back into the reaction cone.

We control coating temperatures by controlling the wall temperature of the reaction cone, which is measured by a thermocouple and an optical pyrometer. We select the control point from a calibration curve that establishes the relationship between the bed and wall temperatures for the charge size and flow rate of interest. In general, the reaction cone wall temperature under stabilized conditions is 100 to 120°C higher than the bed temperature.

For acetylene coating runs of short duration, we maintain the furnace power at a constant setting because temperature adjustments are impractical for the short run times. For other hydrocarbons, the endothermic reaction requires that input power be adjusted to maintain a constant reaction cone wall temperature.

In all of our experiments, the mean diameter of the charge material, sol-gel ThO₂ microspheres, was 230 μ. This material was obtained by classifying the incoming material into 10-μ increments with precision micro-mesh screens³ and blending controlled proportions to give a constant mean particle diameter. Analytical techniques used for evaluating coatings include microradiography for determination of kernel diameter and coating thickness, mercury displacement for determination of coating volumes, and weights before and after burning off the carbon for determination of coating weights. Coating densities are calculated from these weights and volumes. A more detailed description of particle inspection is contained later in this chapter.

Coating Results. — Our investigation of coating processes included work with the previously described⁴ multiorifice nozzle systems and single-inlet nozzle systems and the investigation of coating properties on coatings deposited from methane, propane, and acetylene.

Initially, we employed a multiorifice dual-flow nozzle system, the design of which was based upon previous room-temperature model studies. In our initial efforts, we established the effect of temperature on coating density for coatings deposited from methane in the 5-in. coating furnace. The results are shown in Fig. 4.6. To deposit coatings at temperatures above 2150°C, we had to deposit a seal coating of 1.6 to 1.8 g/cm³ for the ThO₂ microspheres to prevent conversion to ThC₂. High-density pyrolytic carbon coatings can be deposited from methane in the 5-in. coating furnace on charges as large as 2000 g. Coating densities as high as 1.96 g/cm³ can be deposited at temperatures near 2300°C.

The object of cursory experiments using propane as the hydrocarbon gas in the multiorifice nozzle system was to find a process that could deposit high-density coatings at lower temperatures. The effect of temperature on propane coating properties is shown in Fig. 4.7. Coating densities near 2.0 g/cm³ were achieved, and the coating density was relatively insensitive to temperature and gas flux variations in the range investigated. Coating rate and deposition efficiency are increased by increasing the gas flux and temperature. Although the figure does not show it, the coating thickness variation within a batch characterized by the unit standard deviation is very small. It ranges from 5 to 8% of the coating thickness.

Low-density coatings are of interest for use as an inner buffer coating placed adjacent to the nuclear fuel kernel. The purpose of this coating is to provide void volume for fission gases and to protect the outer high-density coating from fission product recoil damage.

Low-density coatings in the range of interest, less than 1.2 g/cm³, are deposited from acetylene. In experiments using the multiorifice nozzle system we demonstrated that acetylene coatings can be deposited in a 5-in. coater without excessive temperature problems because of the exothermic reaction of acetylene. The heat of reaction of acetylene is represented by

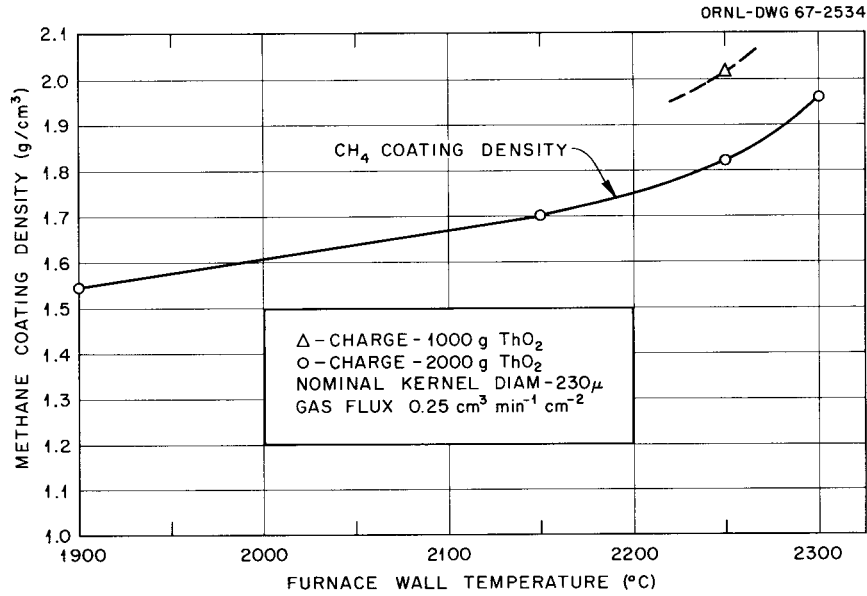


Fig. 4.6. Effect of Temperature on the Density of Coatings Deposited from Methane in a 5-in. Fluidized-Bed Coating Furnace.

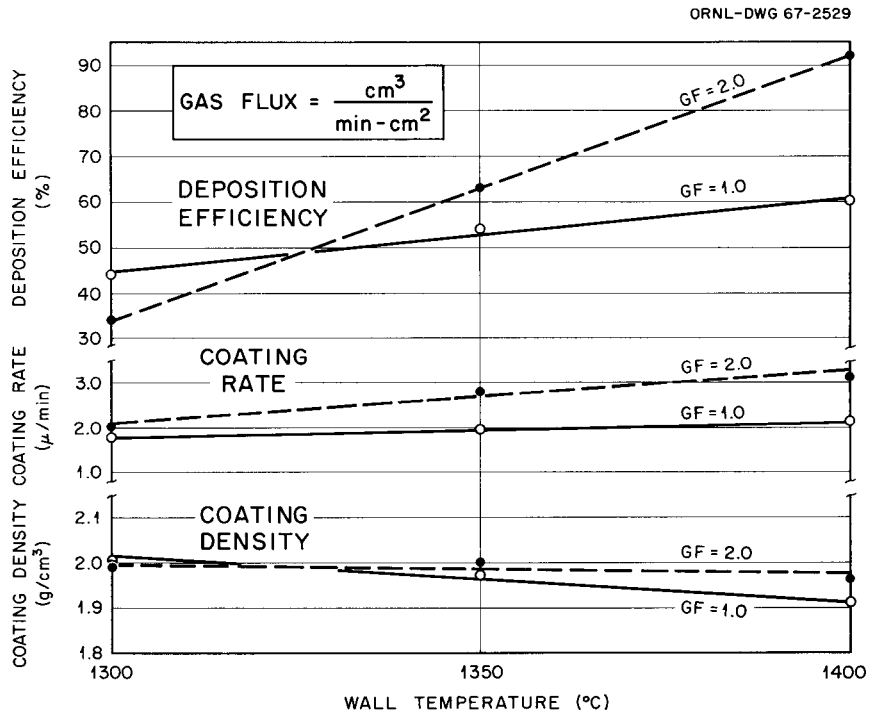
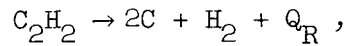


Fig. 4.7. Effect of Temperature on the Propane Coating Properties. Gas flux is given in cm³/min per square centimeter of particle surface.



where

$$Q_{\text{R}} = Q_{\text{O}} - \int_{T_{\text{O}}}^{T_{\text{R}}} \Delta C_{\text{P}} dT,$$

Q_{R} = heat of reaction at T_{R} ,

T_{R} = reaction temperature,

Q_{O} = heat of reaction at T_{O} ,

Q_{O} at $25^{\circ}\text{C} = 3747$ Btu/lb,

Q_{R} at $1100^{\circ}\text{C} = 2140$ Btu/lb.

In general, during coating with acetylene the exothermic reaction heat represented by Q_{R} causes the mean bed temperature to increase if the power input is kept constant. During the course of the runs, observed wall temperature increases ranged from 20 to 30°C . The heat input of the acetylene is not significant in comparison to the total furnace power input. The experimental conditions were as follows: the bed temperature was stabilized at 1100°C before acetylene was introduced; the acetylene flow was 39 liters/min. For these conditions the power input to the furnace was 2300 Btu/min and the heat supplied by the acetylene reaction was 220 Btu/min. Other furnace conditions would produce somewhat different results.

We obtained additional data using a single-inlet nozzle system. Coatings produced by the multiorifice system showed no significant advantages over the single-inlet nozzle systems, which have the capability of bottom unloading. In addition, the single-inlet systems are easier to construct and operate. All of the following results were obtained with the single-inlet system.

The effect of temperature on the density of coatings produced from acetylene is shown in Fig. 4.8. Results are shown for three gas flow conditions, two of which use pure acetylene and one C_2H_2 -33 mole % He. The charge size and kernel diameter remain constant for each flow condition. Flow rates are expressed in terms of gas flux, which is expressed in cubic centimeters of gas per minute per square centimeter of

kernel surface area. Gas fluxes of 2.0 and $3.0 \text{ cm}^3 \text{ min}^{-1} \text{ cm}^{-2}$ represent the latitude of flows with $230\text{-}\mu$ kernels and 500-g charges in this system. With gas fluxes greater than $3.0 \text{ cm}^3 \text{ min}^{-1} \text{ cm}^{-2}$, particles are entrained and blown out of the system. Below a gas flux of $2.0 \text{ cm}^3 \text{ min}^{-1} \text{ cm}^{-2}$ the particles are incompletely fluidized.

The density in all cases increases with temperature. The difference in densities obtained from undiluted acetylene with gas fluxes of 2.0 and 3.0 and those from helium dilution is most probably caused by differences in the rate of hydrogen evolution during polymerization-carbonization of the acetylene. For these runs, the coating efficiency (ratio of amount of carbon deposited to carbon supplied) increased gradually from 50 to 60% as the temperature was increased from 900 to 1200°C , with no particular differences noted among the three flow conditions.

A more detailed study on the effect of helium dilution on the acetylene coating density is shown in Fig. 4.9. Variation of the helium dilution from 0 to 50 mole % can produce coating densities from 0.5 to 1.3 g/cm^3 . The coating efficiency remains essentially constant at approximately 55% throughout the temperature range. Since the deposition efficiency remains constant, an increase in coating density is reflected by a decrease in coating rate as the amount of dilution is increased.

As shown in Fig. 4.10, increasing the charge weight has little effect on the coating properties. The coating density increased slightly and the average coating rate decreased slightly while the coating efficiency remained essentially constant. The slight density increase with charge size is probably a result of increased excess heat from the acetylene decomposition. The coating thickness variation within a batch, as represented by unit standard deviation, improves with increased charge size. A desirable characteristic of large charge sizes is an increase in gas inlet velocity, which results in significantly less pyrolytic carbon buildup on the reaction cone and its parts. Charges greater than 1500 g would require equipment modification.

The sphericity of all the acetylene-derived coatings has been exceptionally good. A typical microradiograph of particles coated from

ORNL-DWG 67-2531R

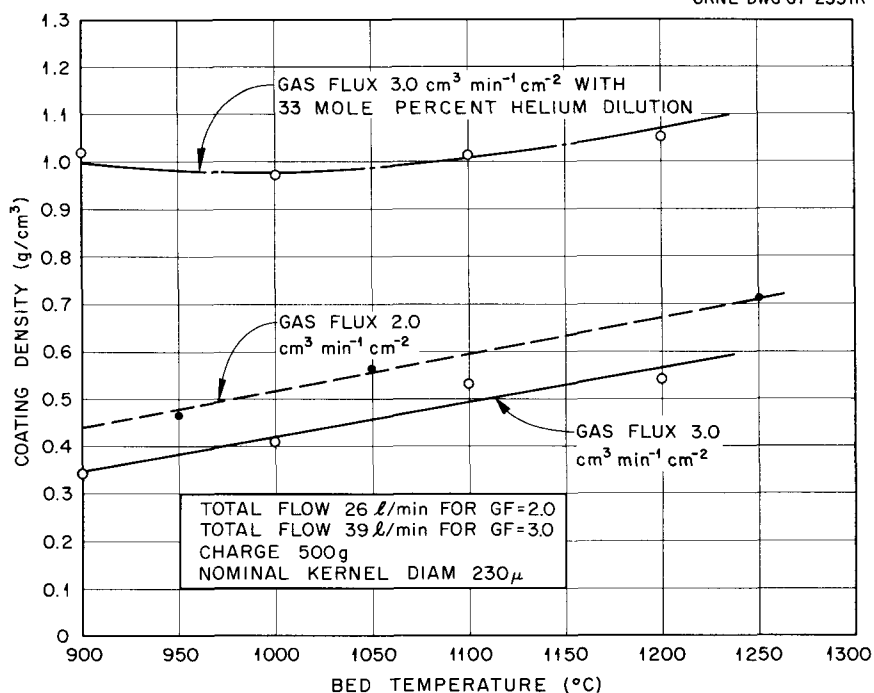


Fig. 4.8. Effect of Temperature on Density of Coatings Deposited from Undiluted Acetylene at Gas Fluxes of 2.0 and 3.0 and for a Gas Flux of $3.0\text{ cm}^3/\text{min}$ per Square Centimeter of Particle Surface with 33 mole % He Dilution.

ORNL-DWG 67-2532

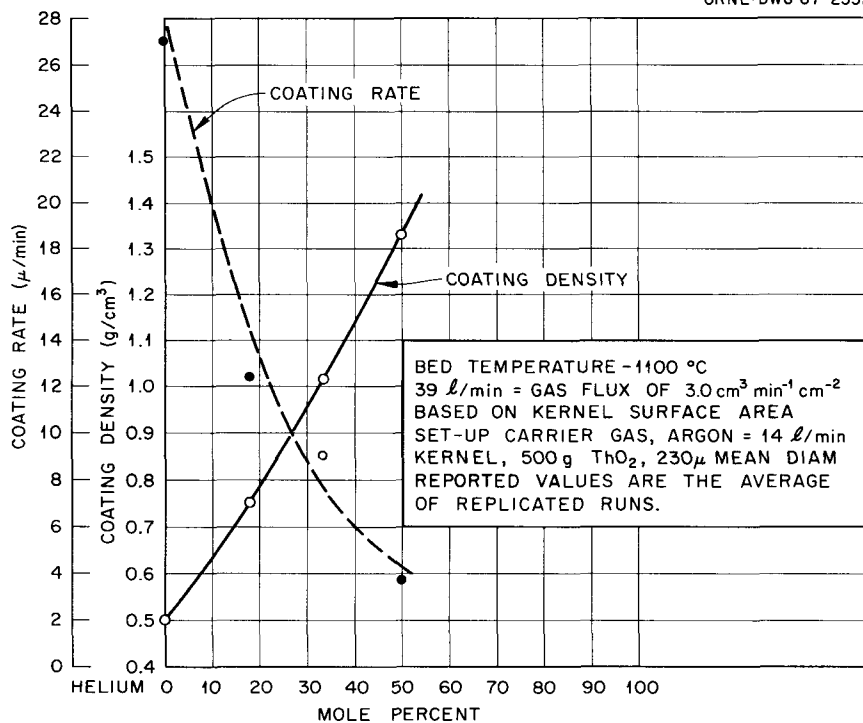


Fig. 4.9. Effect of Helium Dilution on Acetylene Coating Properties for a Constant Gas Flow of 39 liters/min.

acetylene is shown in Fig. 4.11. Photomicrographs of typical low-density-coated particles taken in bright field and polarized light are seen in Fig. 4.12. The pore size, as determined by mercury porosimetry, is approximately 0.2μ .

Drum Coater

We designed the drum coater⁵ to coat very large particles and to handle large charge sizes. The process consists in passing a hydrocarbon gas over a charge of nuclear fuel particles in a heated cylindrical drum rotating about a horizontal axis. Thus, mechanical motion is imparted to the particles in a manner that is not greatly affected by particle size or charge size.

Most of our effort was shakedown operation of the equipment. We conducted preliminary runs with very irregular silicon carbide particles in the 800- to 1400- μ size range. The 14 exploratory runs conducted did point out the limitations and deficiencies of the equipment as designed. Some of the mechanical deficiencies were eliminated by minor modifications. Evaluation of the results of these runs was qualitative rather than quantitative because of the irregularity in shape and the composition (SiC) of the substrate.

Four runs were made with sol-gel thoria microspheres in the 500- to 700- μ -diam size range. None was successful in meeting the objective of depositing a substantial layer of pyrolytic carbon on the particles. The mechanism for transferring the heat from the drum wall to the particles and thence to the coating gas to cause pyrolysis was inadequate. Most of the gas passed through the apparatus undecomposed. The coating deposition rate and efficiency with methane and propane were very low, as seen in Table 4.1.

Further effort with the rotary drum coater was abandoned. The conclusions drawn from this effort are:

1. The scale of the experiment (charge size 5 to 10 kg) was much too great to embark upon without the advantage of controlled laboratory-scale studies of the process and development of the basic equipment.

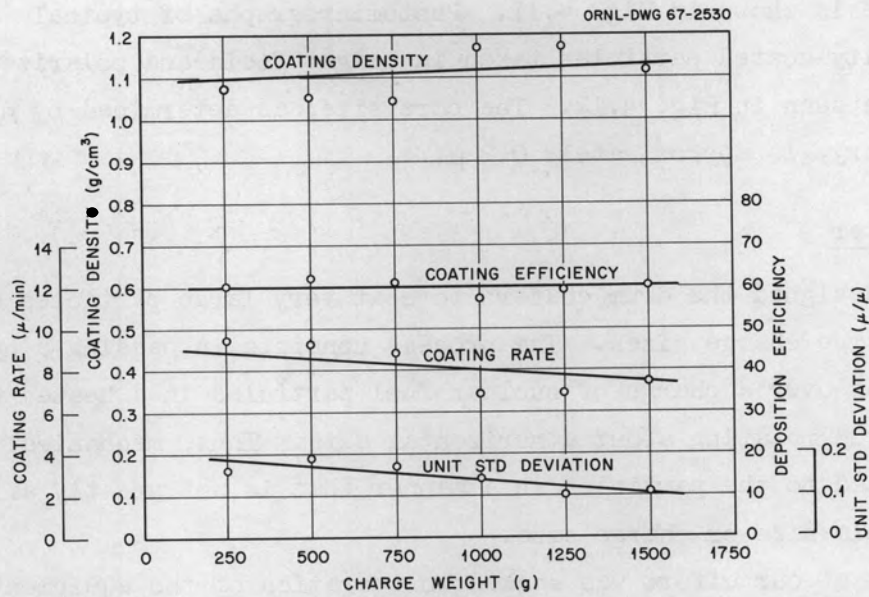


Fig. 4.10. Effect of Charge Weight on Acetylene Coating Properties.

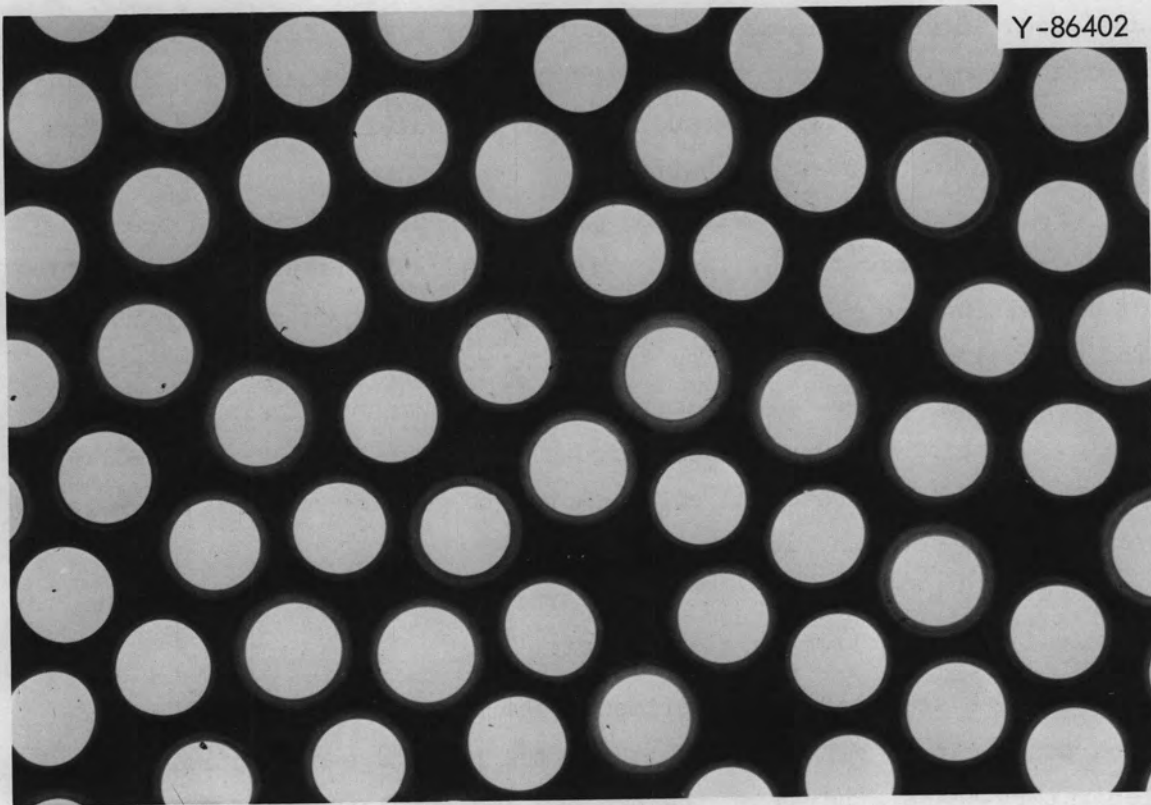


Fig. 4.11. Typical Microradiograph of Particles Coated from Acetylene.

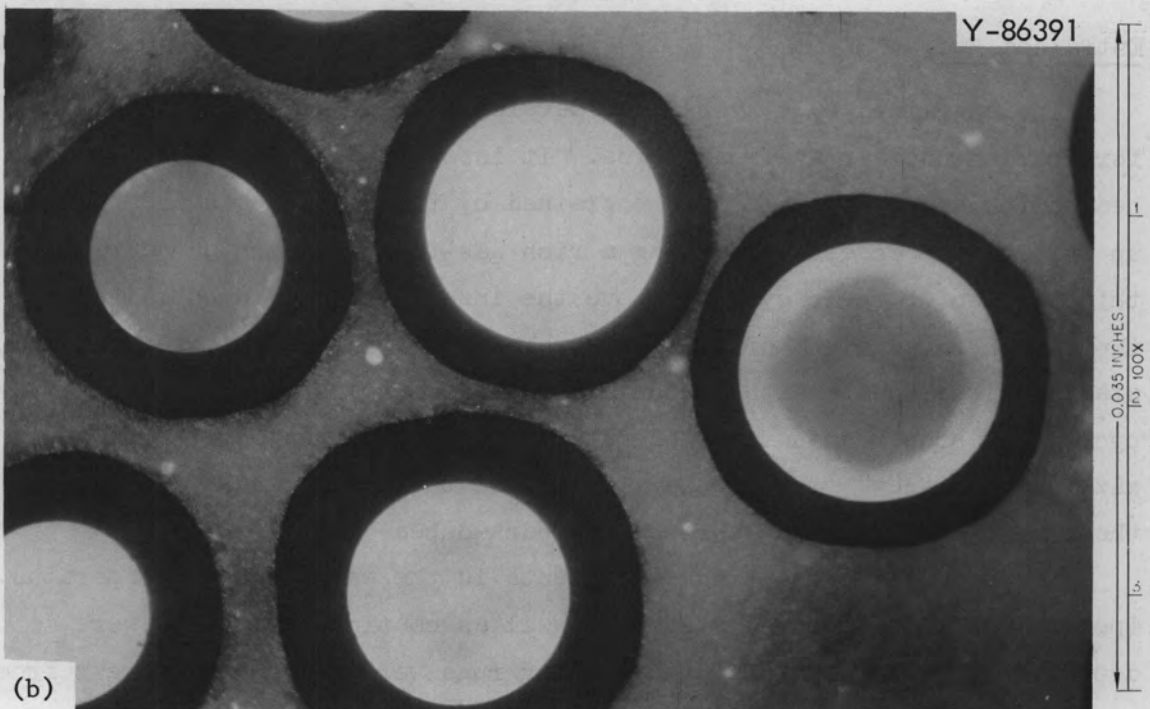
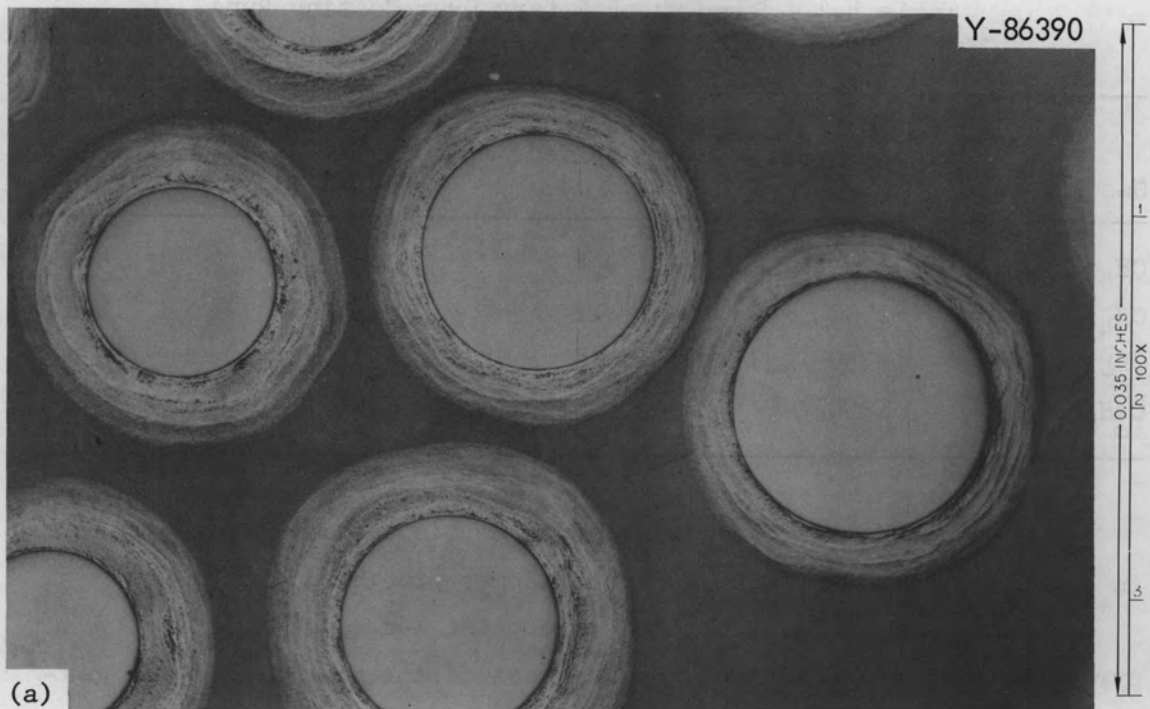


Fig. 4.12. Typical Particles with Low-Density Coatings.
(a) Bright field. (b) Polarized light.

Table 4.1. Summary of Rotary Drum Coating Runs

Gas	Temperature (°C)	Coating Applied (μ)	Coating Rate (μ /hr)	Efficiency (%)
CH ₄	1700	4	0.8	5
CH ₄	1700	11	4.9	15
CH ₄	1350	8	2.1	10
C ₃ H ₈	1350	5	1.7	3

2. Development of an efficient pyrolytic carbon coating process in a horizontal rotary drum does not appear practical.

3. It is most difficult to prevent the large accumulation of pyrolytic carbon deposits on the surfaces of the drum and in the gas-flow passages.

Entrained Bed

The entrained bed⁵ system was developed as an alternate technique for coating nuclear fuel particles. It is operated in an electrically heated furnace. Particles are entrained by the coating gas and carried up through the insert, providing a rich gas-to-solids contact during this portion of their cycle. Above the insert they are deentrained by the sudden enlargement of flow area. They fall into the packed bed and start their downward path to the area of entrainment to begin another cycle. By proper adjustment of insert height with respect to charge size and gas flow, very little, if any, of the coating gas will bypass the insert and travel up through the packed bed.

We conducted 34 coating experiments in the entrained bed apparatus. Operational limits of the system as well as coating parameters were determined. The results of the coating runs were not too different from those obtained in the fluidized or spouting bed.

The entrained bed does appear to have the capability of satisfactorily coating slightly larger charge sizes than the fluidized bed.

However, this increase in charge capacity is gained at the expense of an additional piece of hardware (the insert) within the bed. The insert and its supporting structure are quite susceptible to the deposition of carbon upon them, requiring frequent maintenance. Thus, any charge size advantage is negated if this problem cannot be overcome.

The entrained-bed experiments were conducted in the same furnace as the fluidized-bed experiments. The conflict over use of the furnace and auxiliary supporting facilities began to become a real hindrance to the evaluation of the coating process in either system. Accordingly, the entrained bed effort was terminated without prejudice in favor of the simpler fluidized or spouting bed system. A report describing this work has been written.⁶

The conclusions drawn from the entrained bed coating experiments were:

1. Satisfactory high-density pyrolytic carbon coatings can be obtained by use of methane or propane as the coating gas.
2. The insert required within the bed is quite susceptible to carbon buildup, which interferes with proper movement of the coating gas. We doubt that product quality control can be ensured without frequent maintenance or replacement of the insert.

Prototype Remote Fluidized-Bed Coater

We completed the design of a remote prototype coater. This unit will permit development of operational and maintenance techniques that are directly applicable to the fueled graphite line to be installed in the TURF.

The coating system consists of a 5-in.-diam fluidized-bed coater and its furnace, services, loading and unloading system, and instrumentation to monitor and control the process. The design is based on the low-temperature coating process in which propane or propylene is used for the high-density coating and acetylene for the low-density coating. However, the coater will accommodate the high-temperature process using methane if this should be necessary.

The design of the coater, its furnace, and service disconnects is shown in Fig. 4.13. The assembly consists of the following functional

modules: the base; the subbase, including disconnect blocks; the water-cooled shell and the furnace internals, including the coating chamber; the gas-injector manifold; and the heating element. The design of these modules reflects our thinking that the coater will require more maintenance than other pieces of equipment in the production line. For example, the coating chamber may have to be replaced frequently. To permit this, air-operated clamps release the top head, and the head is lifted off by the in-cell manipulator withdrawing with it the deentrainment chamber and the coating chamber. This operation is shown as the first separation in Fig. 4.14. A replacement assembly is inserted, and the clamps are closed to complete the operation. The replaced sub-assembly is moved into the decontamination cell for cleanup and then into the glove-maintenance area for repair or renovation. With the coating chamber and furnace shell removed from the base at the second separation line, the gas injector can be simply pulled up out of its socket and replaced with another unit. Because of the fragile construction of the heating element we plan to move the furnace shell, including internals, to the glove-box facility for normal replacement of this item. However, the heating element can be replaced without moving the furnace shell.

All services enter the furnace through the service block and subbase. The release of three tie bolts and two service block bolts with an impact wrench will permit removal of the furnace and internals from the subbase assembly. The replacement of the subbase or base will require more effort, but these units are expected to require only infrequent maintenance. In summary, the coating system design reflects a maintenance philosophy of in-cell modular replacement coupled with renovation in the glove-maintenance area of the TURF.

We are now designing an effluent disposal system amenable for remote application for the prototype coater. The effluents from the coating operations will have a wide range of composition of uncracked hydrocarbons, as well as hydrogen and soot. The system being designed will remove the particulate matter in roughing and absolute filters and pass the gaseous products into the atmosphere above the building.

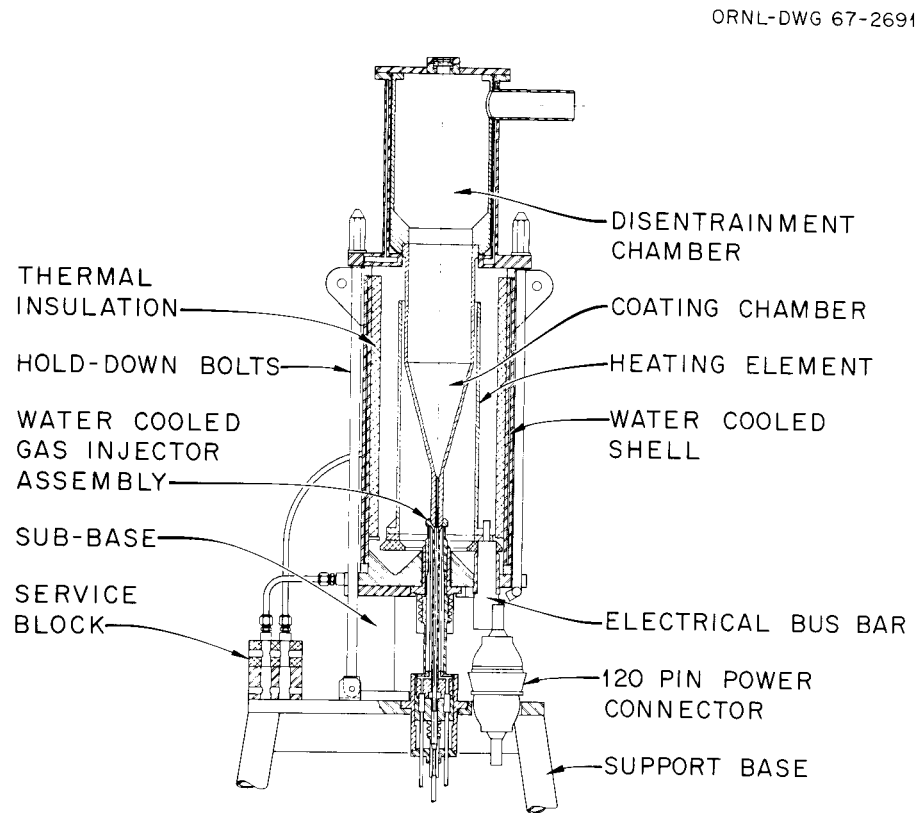


Fig. 4.13. Prototype Remote Fluidized-Bed Coater.

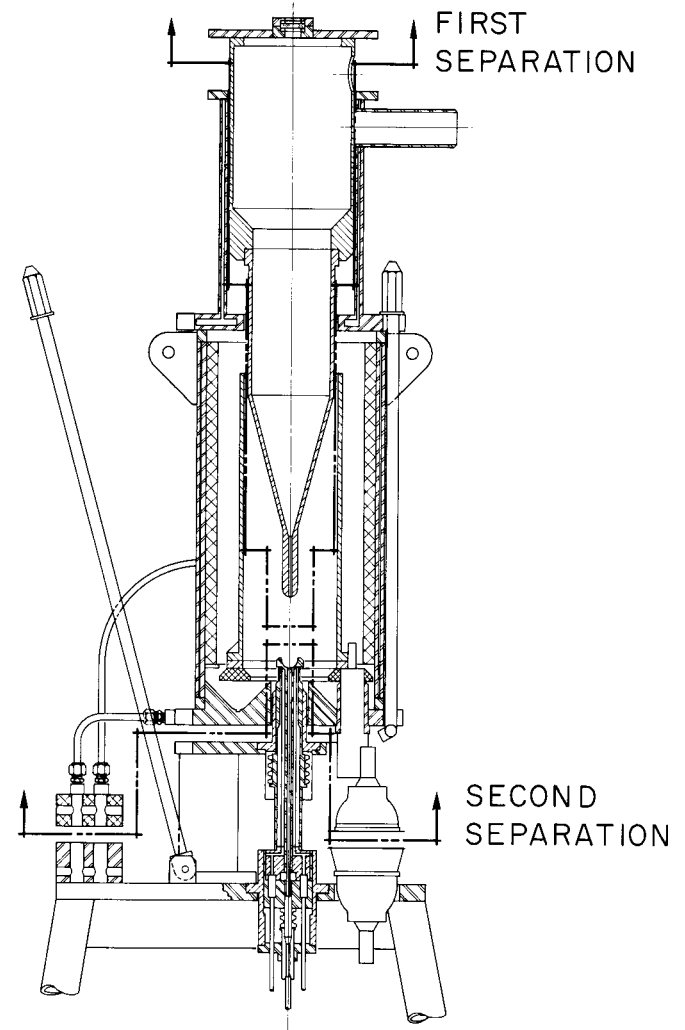


Fig. 4.14. Disassembly of Prototype Coater for Maintenance.

Continuous monitoring of the system and its environment for hazardous mixtures of gases coupled with a system of interlocks that automatically initiate emergency actions to eliminate the hazard make up a major part of this design. The instrumentation of the prototype coater and effluent disposal system is being designed for automatic and remote operation. The instruments will be compatible with the data logging and handling system planned for the TURF.

Particle Inspection

W. H. Pechin B. E. Foster S. D. Snyder S. E. Bolt⁷

In the present concept of particle inspection, the batch-to-batch control of the coating process will be based on samples fed to an on-stream sensor for determination of particle size distribution and number of particles per unit weight. Just before the fuel element filling step, another sample will be taken and transferred to an analytical glove box, in which various inspections necessary for quality control, such as determination of coating densities and particle size and shape, will be made. We have ordered equipment for on-stream inspection.

Low-Density Coatings

One of the difficulties in determining the characteristics of the process for applying low-density coatings was the lack of a scheme for measuring the densities of these coatings. Because of the porous nature of the coating, gas displacement and most liquid displacement methods of measuring volume produced values that were nearer to the volume of the matrix than to the bulk volume of the coating. We attempted to calculate the coating volume from coating thicknesses measured from microradiographs of the coated particles. However, since the calculations involve cubing the linear measurements and thus magnifying the errors, this method produced too great a scatter in the data to properly evaluate the coating conditions.

The method now being used successfully consists in determining the volume of the coated particle with a mercury porosimeter and determining the weight of the coating by burning off the carbon. These data can also

be used to calculate the coating thickness, but determining the standard deviation of the coating thickness still requires measurement from a microradiograph.

High-Density Coatings

The required properties of the high-density coating are the density, the anisotropy, and the crystallite size. We presently determine the density by an extension of the method for low-density coatings. This will require some modification to correct for infiltration of the low-density coating with carbon during the application of the outer coating.

In the past, the anisotropy of the high-density coating has been measured on coatings stripped from carbon disks placed in the bed during the coating run. We started to determine the feasibility of measuring anisotropy and crystallite size directly from the coated particles.

Carbon Coating Thickness Determination

We are developing an x-ray attenuation technique and associated equipment for use as an in-line process monitor for determining the average carbon coating thickness on a small batch of ThO_2 microspheres. The developmental equipment and accessories, shown in Fig. 4.15, consist of a 2-curie ^{241}Am radiation source, NaI(Tl) photomultiplier-detector combination, mechanical scanner, high-voltage power supply, digital voltmeter, signal processing instrumentation, and microsphere hopper or containment cell.

The microspheres are placed in the trough-shaped hopper shown in the center of Fig. 4.15 and are directed into the vertically oriented containment cell. The cell is 1/16 in. thick, 1 in. high, and 2 in. long with 0.020-in. beryllium side windows. The radiation from the source is collimated to 3/8 in. in diameter at the surface of the beryllium window. The microsphere kernel transmits very little of the 60-keV gamma radiation. Most of the radiation passes through the carbon coating, which effectively separates the kernels in the containment cell. As the coating thickness increases, the kernels are farther apart; therefore, the quantity of radiation transmitted through the cell of microspheres

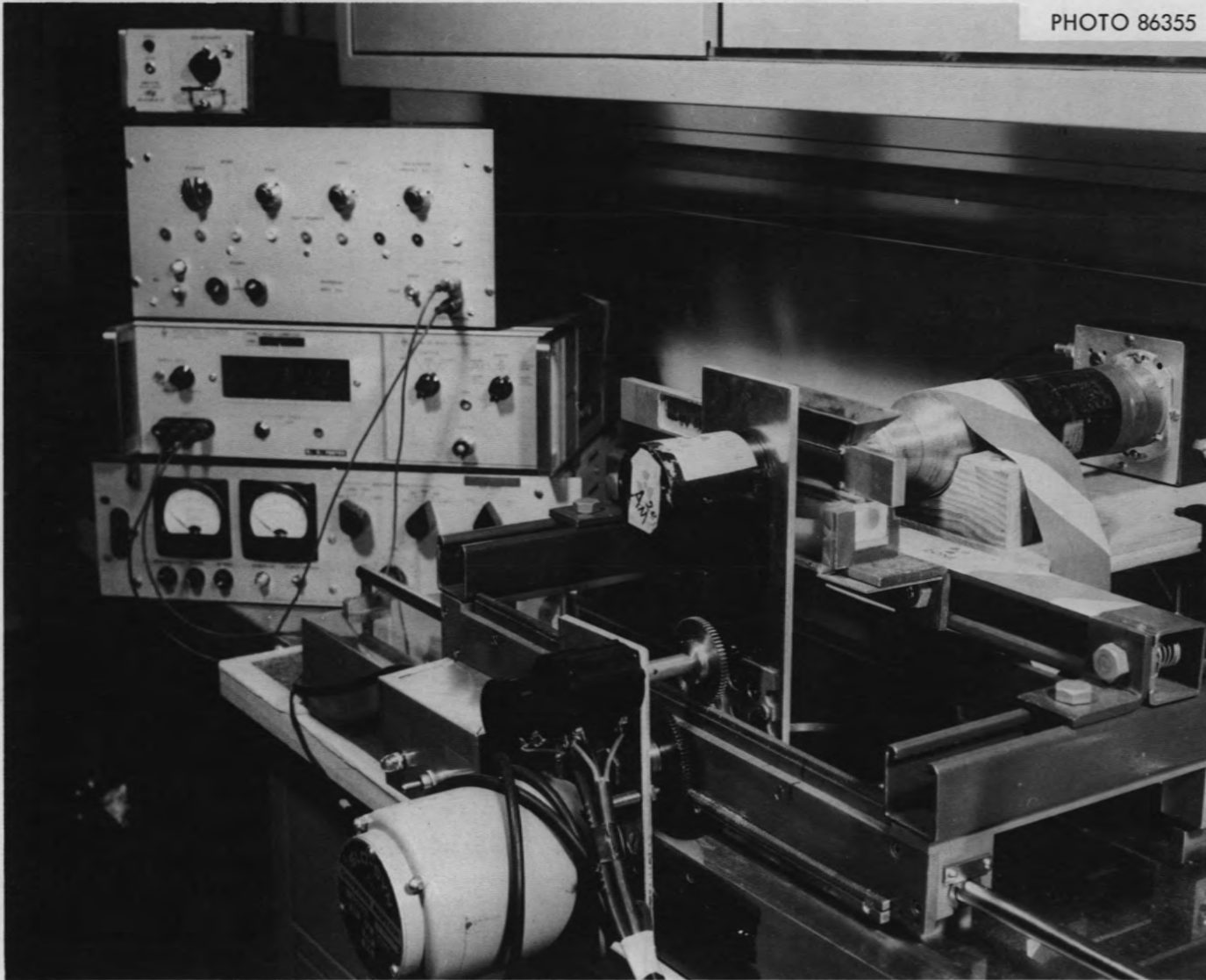


Fig. 4.15. Apparatus for Measuring Coating Density.

is a function of the carbon coating thickness. The detector monitors the transmitted radiation, and the digital voltmeter displays the resultant signal.

We obtained a calibration curve of voltmeter readout vs coating thickness for microspheres with a nominal kernel diameter of 230 μ and coating thickness ranging from 13 to 172 μ . The precision of this measuring technique is about ± 2 μ throughout the full range.

We are presently developing calibration curves for kernel diameters of 223 and 250 μ with coating thicknesses ranging from 10 to 170 μ .

Size Analysis and Counting

Determination of particle size and of the number of particles in a given weight of material is necessary in the fabrication line for process and quality control and for material balance. Rapid determination and evaluation of this information at several steps in the process are important. We are procuring a particle counting and measuring system consisting of (1) an optical sensing unit, (2) amplification assembly, (3) ten counter-display units, (4) range selectors, and (5) scanner and printer assembly. It will be able to count particles at a rate of 3000/sec, determine the size, register each count in the proper size range, and give a printed record of the analysis. The counter-display units provide ten minor size ranges at 10- μ -diam intervals; four major ranges available will be 200, 300, 400, and 500 μ . The system will permit us to quickly determine the number and size distribution of particles in very large samples.

Blending and Bonding Fuel Particles

J. M. Robbins R. L. Hamner

We are developing techniques for loading the fuel holes according to the tentative specifications set for the PSC initial core. These require that the coated fissile and fertile fuel particles be of two different sizes (approx 400 and 600 μ in diameter), be homogeneously blended and loaded in the fuel holes to a packing density of 60 to 64 vol %, and be bonded together so that they will not spill freely into

the reactor in case a fuel element is broken. Also, as much carbon as possible should be provided in the bonding material for cesium absorption.

Our main problems for study, based on the specifications for fuel loading, have been the bonding and the blending of fuel particles. These have been approached separately since neither depends upon the other.

Blending Studies

We evaluate blends of two size fractions of fuel particles by screening samples to their original size fractions, weighing the screened fractions, and calculating the weight ratio of screened fractions from each sample. In our blending studies, we used batches of pyrolytic-carbon-coated ThO_2 microspheres having average diameters of 400 and 600 μ . These were blended in a weight ratio, large-to-small, of 1.5.

We employed various conventional means of blending, such as tumbling in a cylindrical container or in a "V" blender, without success. The particles are extremely free-flowing and segregate readily during such blending operations. We improved the results of conventional blending by applying a film of resin to the particles to make them slightly sticky and thereby reduce their freeness of flow. This proved to be impractical because of the difficulty in controlling the application of the resin film.

Our most encouraging approach to the blending problem has been to blend the particles by feed control. This method requires that given weights of particles of two different sizes be fed simultaneously in some manner into a common collector. We demonstrated the feasibility of this method by adjusting the orifices of two feed hoppers, one containing 40 g of 400- μ -diam particles and the other containing 60 g of 600- μ -diam particles, so that the feed times of the particles from the hoppers into a collector tube were coincident. In blends obtained by this technique, the largest deviation from the ideal blend was 8% in the samples taken at 1-in. intervals from a 15-in.-long collector tube; 95% of the deviation values obtained were below 5%. We attributed these deviations primarily to the orifice shape. We observed that particles flowing from hoppers with round orifices sometimes bridged for

a fraction of a second. This caused a layer of particles from one hopper to form in the collector tube during the time of bridging in the other hopper. This is illustrated in Fig. 4.16, which shows a radiographed section of a fuel stick. During loading of this stick, the large particles fed from one hopper bridged at intervals during the feed, resulting in a deposit of small particles from the other hopper during the time of bridging.

We are currently experimenting with feed control of particles through rectangular orifices. These show little tendency to permit bridging provided the orifice opening in the smaller dimension is at least three particle diameters.

Bonding Studies

In most of our bonding experiments, we used pyrolytic-carbon-coated $(Th,U)C_2$ particles having an average diameter of $400\ \mu$. Approximately 0.5-in.-ID graphite tubes were used as simulated fuel holes in preliminary experiments.

In our initial studies, we demonstrated that a liquid phenolic resin⁸ surrounding the particles provides a satisfactory bond after carbonizing at $1000^\circ C$ in a helium atmosphere. However, the residual carbon provided by the bond resin alone, approximately $0.55\ g/cm^3$, may not be sufficient to meet the requirements for cesium absorption.

PHOTO 88302



Fig. 4.16. Radiograph of Fuel Stick Section Containing 400- and 600- μ Coated Fuel Particles Blended by Feed Control. Dark bands show layers of the smaller particles deposited during bridging of the larger particles in the feed hopper. 3X.

To provide matrix carbon in the fuel bed in addition to that provided by the resin, we attempted to vibrate various forms of powdered carbon into the interstices of the fuel particles before addition of the resin. This approach was not successful because the low-density powders packed at the top of the fuel bed and penetrated the bed only slightly.

We attempted to form a high-carbon-content bond from a polyacenaphthylene pitch, which has a low melting point (110°C) and a high coking value (60%). The pitch was introduced in solid form as a coating on the particles. We applied this coating by tumbling the fuel particles with pitch ground to a -80-mesh powder and consistently obtained about 9 wt % of pitch on the fuel particles. Pouring the pitch-coated particles into the fuel holes and heating at 1000°C for carbonization formed an excellent bond; however, the pitch when added in this manner expanded the fuel bed and decreased the fuel loading from 64 to 53 vol %.

A better approach to the bonding problem was to pour the fuel particles into a graphite tube and inject a mixture of liquid phenolic resin and 15 wt % charcoal powder into the fuel bed with a conventional grease gun. By this method, we obtained good bonding of particles in fuel beds up to 15 in. long, with a 64 vol % fuel loading, and 0.7-g/cm^3 matrix carbon content. Figure 4.17 is a polished section from a fuel bed showing the nature of the bond formed in this manner. The bonding carbon obviously shrinks during carbonization, but the shrinkage apparently does not damage the methane-deposited coatings on the fuel particles.

The direct loading and bonding of fuel particles into a graphite fuel block by the injection technique described poses at least three major problems: (1) mistakes made during the course of loading the fuel block could not be easily rectified, and the fuel block would probably have to be rejected; (2) we foresee no satisfactory means of inspecting individual fuel holes in a multihole fuel block for fuel loading and homogeneity; (3) the graphite fuel block absorbs resin during injection, and either it must be saturated with resin before fuel loading, or the walls of the fuel holes must be sealed in some manner to prevent resin absorption.

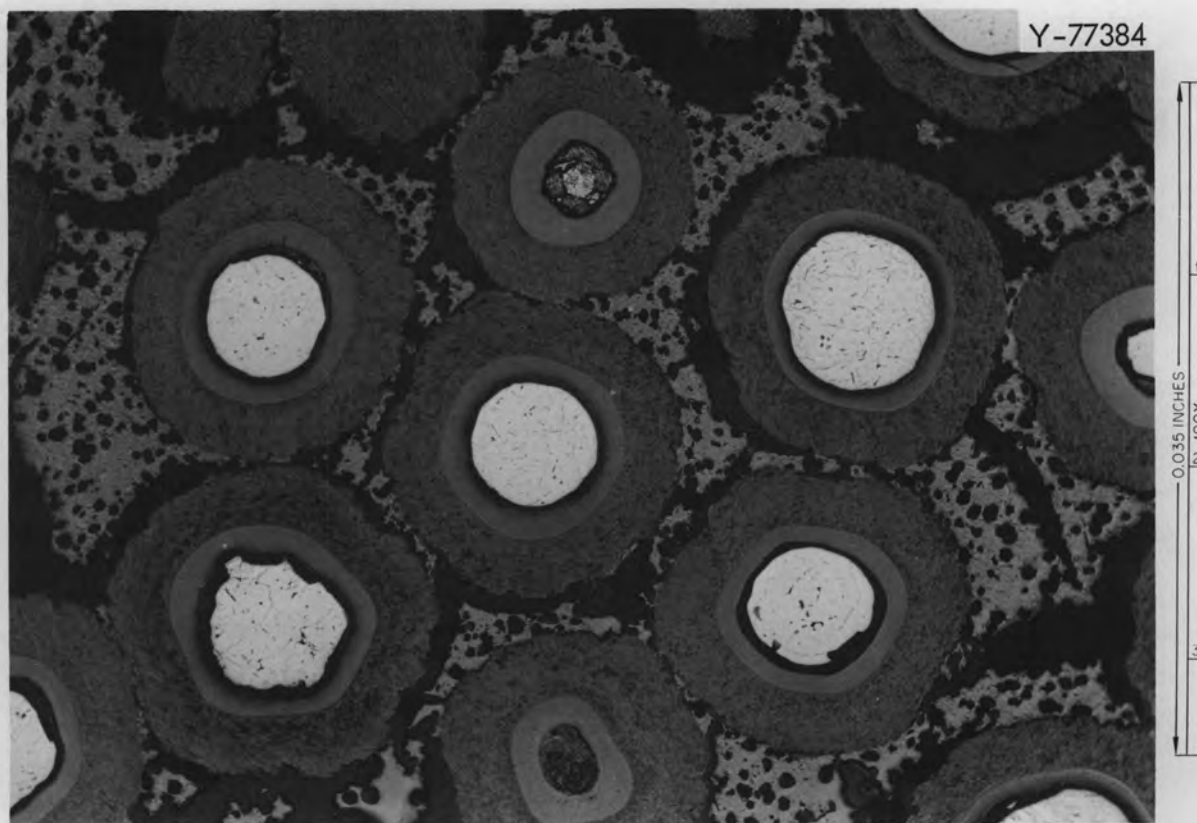


Fig. 4.17. Microstructure of a Bed of $(\text{Th,U})\text{C}_2$ Particles Coated with a Methane-Deposited, Pyrolytic Carbon Coating and Bonded with a Phenolic Resin Mixed with 15 wt % Charcoal. The light gray phase between the particles is the bonding matrix after carbonization at 1000°C in helium. The black areas are voids in the matrix carbon. The dark gray phase surrounding the particles is metallographic mounting resin. As polished.

To eliminate these problems, our present approach to bonded fuel beds is to mold fuel sticks, which can then be inspected and inserted into the fuel holes in the element. The fuel sticks are prepared by pouring the fuel particles into a split metal mold and injecting the resin-charcoal mixture into the bed as previously described. The assembly is then heated at 80°C for 40 hr to polymerize (cure) the resin. The fuel sticks thus formed are rigid and strong and may be readily inspected before insertion into the fuel block. Figure 4.18 shows a 12-in.-long fuel stick, as cured, formed by the molding technique.

The fuel sticks may be inserted into the graphite fuel block after carbonization, or they may be inserted into the fuel block and then



Fig. 4.18. Fuel Stick, in the As-Cured State, with a 64 vol % Loading of Pyrolytic-Carbon-Coated Thoria Microspheres and a Matrix Carbon Content of 0.8 g/cm^3 .

carbonized; we prefer the latter approach, since the fuel sticks in the as-cured state are in their strongest form and since they frequently warp during carbonization unless restrained.

We are currently improving our mold design for more efficient operation in the remote fabrication process. We are also trying to decrease the time required for curing the resin. It requires 40 hr at 80°C , the temperature that we have used in preparing fuel sticks. Such a long curing time is undesirable for fabricating fuel elements in production quantities. We hope to decrease the resin curing time to a range of 2 to 3 hr. Our studies will include the effects of time, temperature, prepolymerization, and vacuum treatment on the curing of the resin.

REFERENCES

- ¹On loan from the Reactor Division.
- ²R. B. Pratt, T. N. Washburn, and J. W. Snider, Status and Progress Report for Thorium Fuel Cycle Development Dec. 31, 1965, ORNL-4001, pp. 19-33.
- ³These are precision screens with nominal openings of 200, 210, 220, 230, 240, and 250 μ . The tolerance on each of these screens is $+2 \mu$. Developed and manufactured by Buckbee-Mears Co., St. Paul, Minnesota.
- ⁴R. B. Pratt, T. N. Washburn, and C. C. Haws, Jr., Status and Progress Report for Thorium Fuel Cycle Development Dec. 31, 1965, ORNL-4001, pp. 33-40.

⁵R. L. Pilloton, R. B. Pratt, and H. J. Flamm, Status and Progress Report for Thorium Fuel Cycle Development Dec. 31, 1965, ORNL-4001, pp. 78-92.

⁶H. J. Flamm, An Entrained-Fluidized-Bed System for Pyrolytic Carbon Coating of Microspheres, ORNL-TM-2113 (April 1968).

⁷On loan from the Reactor Division.

⁸P-514, Great Lakes Carbon Corp.

5. IRRADIATION OF COATED-PARTICLE FUELS

A. R. Olsen J. H. Coobs J. W. Prados¹

Coated-particle fuels for use in high-temperature gas-cooled reactors have been irradiation tested for a number of years. Recently the ability of pyrolytic-carbon-coated (Th,U)C₂ and (Th,U)O₂ microspheres to meet the performance requirements of several demonstration reactors has been demonstrated.²⁻⁸ As part of a cooperative effort with the Gas-Cooled Reactor Program at ORNL, we have been testing the performance of sol-gel-derived UO₂ and (Th,U)O₂ microspheres. In these experiments, the results are compared with the results of tests on similar coated particles having sintered fuel kernels. All tests are compared with predicted performance based on our mathematical model of coated-particle behavior.^{9,10} Some early results on the irradiation performance of sol-gel-derived microspheres were reported previously.¹¹ The program has been expanded to investigate fuel kernel variations, such as diameter and composition, to improve our estimates of model parameters.

To supplement the static and purged instrumented capsules used for irradiation tests in the past, we began a series of irradiations using a static noninstrumented capsule designed for simultaneous high- and low-temperature testing of annular arrays of loose coated particles in individual containers within the capsule. The basic design of the capsule used with the first two tests in this series is shown in Fig. 5.1. The desired operating fuel temperatures of 400 and 1400°C are obtained by varying the dimensions of a helium-filled gap between the graphite sleeves and the metal tube. We include a series of melt wires to provide an estimate of the temperatures achieved. A stainless steel tape, which extends the full length of the capsule, monitors the neutron flux.

Comparison of Test Results with Model Predictions

The first capsule in this series of tests, designated ORNL 43-89, contained two different batches of coated particles prepared at ORNL with two-layer coatings on highly enriched fuel kernels of sintered UO₂ and melted UC₂. Coating density, anisotropy, crystallite size, and

microstructure were systematically varied by controlling the deposition conditions.^{12,13} Inner coatings, nominally 50 μ thick, were low-density isotropic, porous, low-density laminar, or high-density laminar pyrolytic carbon deposits. The outer coatings, nominally 70 μ thick, were high-density isotropic or granular pyrolytic carbon deposits. The capsule was irradiated in an ETR X-basket facility for three reactor cycles at a peak thermal flux of 1×10^{14} neutrons $\text{cm}^{-2} \text{sec}^{-1}$ and accumulated a peak unperturbed dose of 5.92×10^{20} neutrons/ cm^2 .

We evaluated the performance of the various coated particles by visual and metallographic examination. Details of the preirradiation and postirradiation examinations have been reported elsewhere.¹⁴⁻¹⁷ Based on an examination of the melt wires and the fuel burnup levels, the temperature regimes during irradiation were approximately 1000°C in the high-temperature containers and 400°C in the low-temperature containers. Fuel burnup in the experiment ranged from 11 to 23% FIMA (fissions per initial heavy metal atom). Figure 5.2 graphically compares the observed results with those predicted by our mathematical model.

If the model assumptions were comprehensive, the parameters were known accurately, and there were no variations in coated-particle properties in a given batch, all symbols above the shaded boundary should be filled, and all below the boundary should be open. Only three batches of coated particles, as represented by four points on the plot, showed failures (<10%) at burnup levels significantly below the predicted values. The one oxide batch had a low-density laminar inner layer that was severely damaged and failed to protect the outer layer from fission-fragment damage. In the case of the two UC_2 batches, apparently a combination of fuel migration and an inadequate inner-layer thickness (<30 μ) on some particles led to fission-fragment damage of the outer coating and premature failure.

The model includes a number of poorly known parameters, such as fuel swelling, fission-gas release, pyrolytic-carbon densification, pyrolytic-carbon mechanical properties, and the effects of fast neutron damage as manifested in stress-inducing dimensional changes from anisotropic growth and irradiation-induced creep. If one considers the uncertainties in these parameters, together with the known particle-to-particle variation

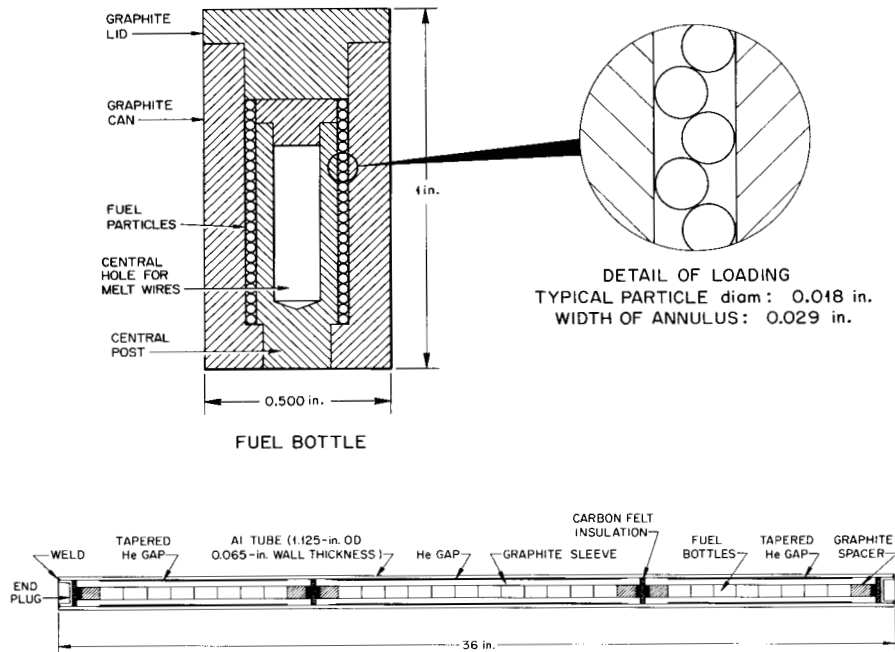


Fig. 5.1. Schematic Drawing of Components for Uninstrumented Irradiation Capsule.

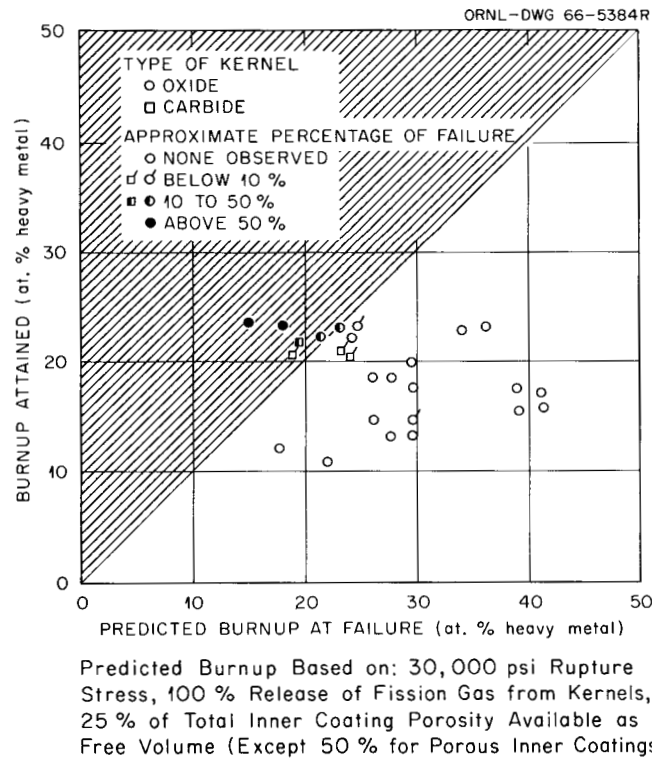


Fig. 5.2. Comparison of Mathematical Model Predictions with Observed Coated-Particle Failures in ETR X-Basket Irradiation Experiment.

in properties of pyrolytic carbon deposits within a single coating batch, the observed agreement between predictions and experimental results is highly gratifying.

Comparison of Sol-Gel-Derived Microspheres with Sintered Spheroidal Fuel Kernels

Ideal kernels for coated-particle fuels are spherical ceramic bodies of controlled density and composition. The sol-gel process will produce nearly perfect microspheres of UO_2 and $(\text{Th,U})\text{O}_2$ with controlled size and composition. During the past year, two tests with sol-gel UO_2 coated with carefully characterized pyrolytic carbon deposits were conducted to burnup levels of approximately 25 and 50% FIMA.

Enriched UO_2 microspheres used in these tests had an average diameter of 220 μ and were prepared in two batches having densities 90 and 94% of theoretical. The lower burnup experiment was essentially a duplicate of the noninstrumented irradiation capsule test described above. A variety of two-layer coatings similar to those used on the sintered fuel kernels was used. The inner layers were laminar, isotropic, or porous deposits of various thicknesses and densities, while the outer layers were all high-density granular or isotropic deposits also of varying thickness. The particles irradiated to the higher burnup were coated with three layers: 49 μ of porous, 20 μ of high-density laminar, and 60 μ of high-density granular pyrolytic carbon.

Particles with the two-layer coatings on sol-gel microspheres were irradiated in the ETR as experiment ORNL 43-97 for three reactor cycles at a peak thermal flux of 1×10^{14} neutrons $\text{cm}^{-2} \text{sec}^{-1}$; they accumulated a peak unperturbed dose of 5.75×10^{20} neutrons/ cm^2 . The particles coated with three layers were irradiated in a specially designed instrumented sweep capsule¹⁸ in a lattice position in the ORR. The fuel temperature in this experiment gradually changed from 1350 to 1100°C in achieving approximately 50% FIMA. The fission-gas release measurements and detailed irradiation history for this experiment have been reported elsewhere.¹⁹⁻²¹ Performance of the various coated-particle samples was evaluated by macroscopic and metallographic examination. We compared

the results with previous experiments and with the predicted behavior based on our mathematical model.

The examination and evaluation of experiment 43-97 (the non-instrumented capsule) is not complete in that the final burnup analyses are not available. The available data indicate a burnup range from approximately 11 to 27% FIMA, which is comparable to experiment 43-89 with sintered fuel kernels. Evidence that the intended operating temperatures of 400 and 1400°C were achieved is derived from the melt wires and the distinct plasticity of the UO_2 fuel kernels. The sol-gel-derived particles performed as well as the previous sintered fuels with similar coatings. Based on the preliminary burnup data, the particles in the noninstrumented capsule reaffirmed the model predictions, with little or no damage seen for those samples predicted to survive, while the samples designed to fracture showed failure percentages ranging from 10 to 100%.

The three-layer coated particles showed no failures; and only 1 of 100 particles examined metallographically showed detectable damage. None of the sol-gel UO_2 fuel particles in either experiment developed any grain structure, but all contained the shiny metallic inclusions and pores typical of UO_2 after appreciable burnup. This can be seen in Figure 5.3, which compares the pre- and postirradiation microstructures for the sol-gel fuel kernels in this experiment.

The results of evaluations of all the tests completed to date lead to the following conclusions:

1. Coated particles must incorporate at least three features to ensure adequate irradiation stability: provision for shielding the outer coating from direct fission recoil damage, adequate volume in or adjacent to the fuel kernel, and mechanical decoupling (a distinct physical separation) between inner and outer coating layers.

2. Properly designed two-layer pyrolytic carbon coatings on oxide and dicarbide fuel kernels will provide excellent performance at burnup levels in excess of 25% FIMA.

3. Dense sol-gel-derived UO_2 microspheres will perform as well as sintered UO_2 or bed-melted UC_2 fuel kernels when coated with properly designed pyrolytic carbon coatings.

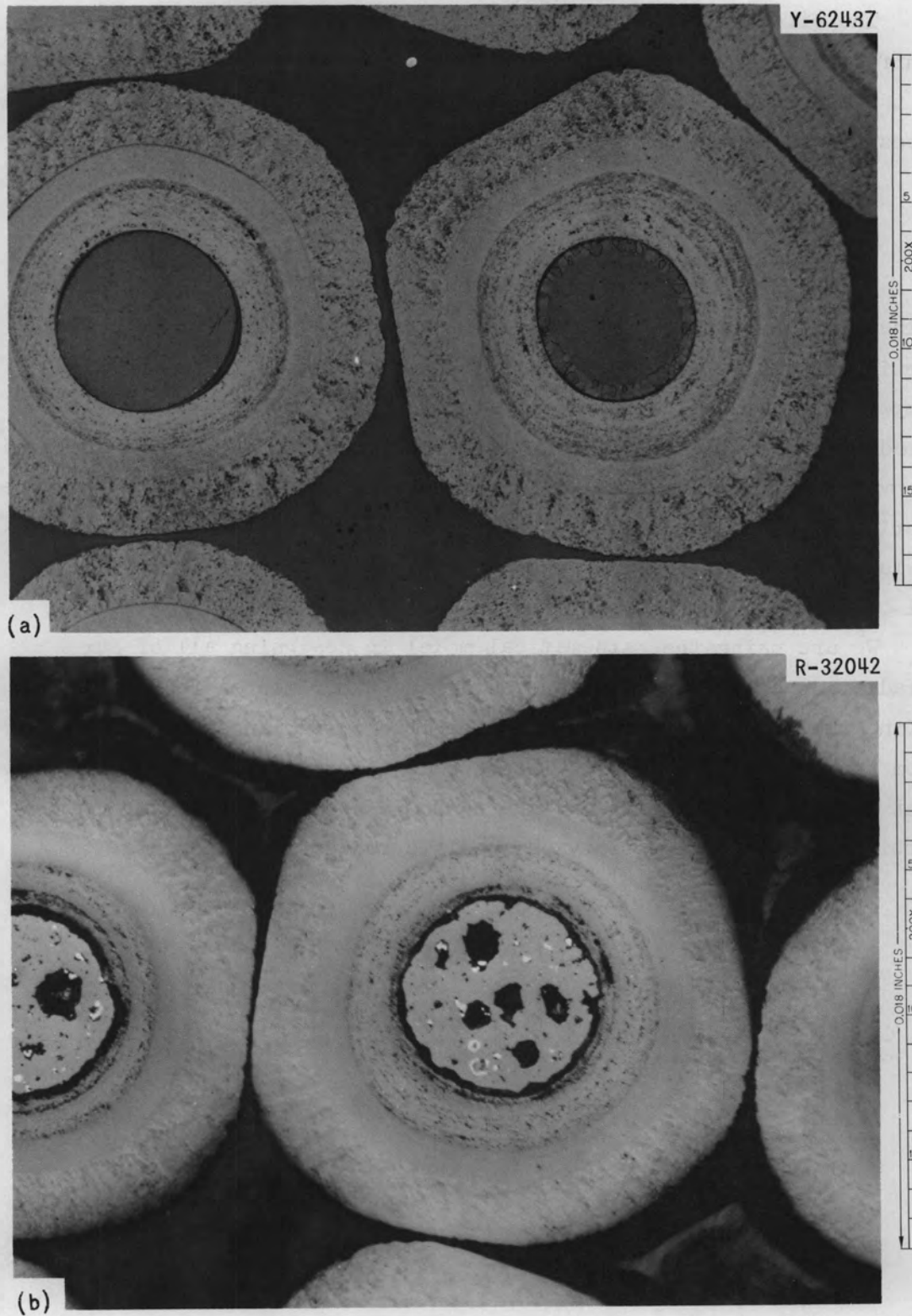


Fig. 5.3. Pyrolytic-Carbon-Coated Sol-Gel UO_2 Particles. (a) Unirradiated; etched. (b) Irradiated to 50 at. % burnup at 1100 to 1350°C in F9 High-Burnup Experiment. As polished.

The effects of fast-neutron damage on coating performance, as manifested in stress-inducing dimensional changes, could not be tested in the experiments completed to date because the fast-neutron (>0.2 Mev) doses attained were all less than 10^{20} neutrons/cm².

Summary of Irradiation Tests on Sol-Gel-Derived Fuels as Coated Particles

In the irradiation tests completed, we have established the usefulness of the mathematical model for predicting behavior of coated particles with sol-gel-derived fuel kernels. In an operating high-temperature gas-cooled reactor, both the fuel composition and the irradiation conditions will vary with core position. We have analyzed the various parameters included in the mathematical model and developed a critical-path schedule for timely irradiation tests required to evaluate these parameters. The experiments in this program involving sol-gel-derived fuels are listed in Table 5.1.

We are using the mathematical model in designing all of our irradiation experiments and are using the experimental results to refine the model parameters. The specific performance predictions from the mathematical model will be used together with the process development results to establish optimum economic specifications for coated-particle fuels for a variety of specific reactor requirements.

Table 5.1. Summary of Irradiation Tests on Coated-Particle Sol-Gel Fuels

Experiment	Fuel Varieties	Fuel Kernel Size (μ)	Coated Particle Variations ^a	Type of Experiment ^b	Fuel Irradiation Temperature ($^{\circ}$ C)	Fission Gas Release Rate ^c	Peak Burnup (% FIMA ^d)	Status	Objective
43-89	Sintered UO ₂ and bed-melted UC ₂	220	12	1	400, 1000		25	Examined	Compare coated particle model performance characteristics with fuel performance
43-97	Sol-gel and sintered UO ₂	210	13	1	400, 1400		27	Being examined	Compare sol-gel microsphere performance with sintered spheroids
43-98	Sol-gel (U,Th)O ₂	280	15	1	400, 1400		20	In-reactor	Test fuel particles prepared for irradiation in Dragon; investigate coating optimization and fast-flux effects on particle performance
43-104	Sol-gel (U,Th)O ₂ and sol-gel UO ₂	230	10	1	400, 1400		25	In-reactor	Determine the effects of the Th/U ratio on fuels with a constant fissile content
43-105	Sol-gel (Th,U)O ₂	450	11	1	400, 1400		25	In preparation	Evaluate the performance of fertile fuels and fast-flux effects, including radiation creep on coated-particle behavior
Loop 1-14	Sol-gel ThO ₂ and (U,Th)O ₂	240, 210	2	4	1350, 675	4.2×10^{-5}	2.7	Examined	Evaluate the performance of large beds of loose coated particles and the performance and fission-gas retention of coated sol-gel oxide kernels
Loop 1-15	Sol-gel ThO ₂ and (U,Th)O ₂ Bed-melted UC ₂ and (U,Th)C ₂	230, 340 380, 180	4	4	1400, 675	2×10^{-6} to 2×10^{-4}	12	Being examined	Same as Loop 1-14, with controlled coolant purity and a preliminary test of a lightly bonded bed of coated particles
B 9-19	Sol-gel (Th,U)O ₂	210	1	3	1200	2×10^{-6}	0.7	Examined	Test stability of sol-gel oxide as a coated particle

Table 5.1. (continued)

Experiment	Fuel Varieties	Fuel Kernel Size (μ)	Coated Particle Variations ^a	Type of Experiment ^b	Fuel Irradiation Temperature ($^{\circ}\text{C}$)	Fission Gas Release Rate ^c	Peak Burnup (% FIMA ^d)	Status	Objective
O 1-3	Sol-gel (Th,U) O_2 and bed-melted (Th,U) C_2	210	1	2	1130		0.03	Examined	Test fueled graphite sphere containing loose coated particles within an array of machined holes
F-9 HIBUP	Sol-gel UO_2 Bed-melted UC_2	150 125	2	3	1400 to 1100	10^{-6} to 10^{-4}	50	Being examined	Evaluate the fission-product retention and irradiation stability of coated particles at extended burnup levels
F-9 HIBUP-2	Sol-gel UO_2 Bed-melted UC_2	265-150 190	9	3	1400	2×10^{-4}	12	In-reactor	Same as F-9 HIBUP including some SiC coatings
B 9-31	Sol-gel UO_2	210	1	3	1400	10^{-6} to 6×10^{-4}	23	Being examined	Test of mathematical model failure predictions under monitored gas-release conditions
B 9-32	Sol-gel UO_2	280	1	3	1400	1×10^{-4}	25	In-reactor	Evaluate low-temperature performance of pyrolytic carbon coatings
A 9-3	Sol-gel UO_2	270	2	3	1400	1×10^{-7}	15	In-reactor	Same as B 9-32
A 9-9	Sol-gel UO_2 Bed-melted UC_2	240 210	8	3	1000			In preparation	Test retention of solid fission products
Dragon	Sol-gel (Th,U) O_2	280	2	5	700 to 1100			In-reactor Dec. 1966 to May 1968	Evaluate sol-gel oxide fuels as coated particles in a fuel element of an operating High-Temperature Gas-Cooled Test Reactor

^aCoated particle variations include both coating parameter and fuel composition variables to make up the different types of coated particles in a test.

^b1. Noninstrumented static-atmosphere capsules. 2. Instrumented static-atmosphere capsules. 3. Instrumented sweep-gas capsules. 4. Instrumented circulated gas loop experiments. 5. Test reactor fuel rods.

^cRelease-to-birth rate ratio for ^{88}Kr .

^dFissions per initial metal atom.

REFERENCES

- ¹Consultant from the University of Tennessee.
- ²J. M. Blocher, Jr., et al., "Properties of Ceramic-Coated Nuclear-Fuel Particles," Nucl. Sci. Eng. 20, 153-70 (1964).
- ³C. W. Townley et al., "Irradiation Studies of Ceramic-Coated Nuclear Fuel Particles," Nucl. Sci. Eng. 20, 171-79 (1964).
- ⁴F. L. Carlsen, Jr., E. S. Bomar, and W. O. Harms, "Development of Fueled Graphite Containing Pyrolytic-Carbon-Coated Carbide Particles for Nonpurged, Gas-Cooled Reactor Systems," Nucl. Sci. Eng. 20, 180-200 (1964).
- ⁵W. V. Goedel, "Development and Utilization of Pyrolytic-Carbon-Coated Carbide Fuel for the High-Temperature Gas-Cooled Reactor," Nucl. Sci. Eng. 20, 201-18 (1964).
- ⁶R. A. Reuter, "Duplex Carbon-Coated Fuel Particles," Nucl. Sci. Eng. 20, 219-26 (1964).
- ⁷H. G. Sowman, R. L. Surver, and J. R. Johnson, "The Development of Spherical Pyrolytic-Carbon-Coated UC₂ and UThC₂ Fuel Particles," Nucl. Sci. Eng. 20, 227-34 (1964).
- ⁸R. A. U. Huddle, P. Barr, G. Hauser, C. Vivante, and J. H. Coobs, "Recent High-Temperature Irradiation Experiments on Coated Particle Fuel for the Dragon Reactor," Trans. Am. Nucl. Soc. 7, 450-51 (1964).
- ⁹J. W. Prados and J. L. Scott, Mathematical Model for Predicting Coated-Particle Behavior, Nucl. Appl. 2, 402-14 (1966).
- ¹⁰J. W. Prados, "Calculation of Creep in Spherical Shells Under Combined Radiation Damage and Internal Pressure," Nucl. Appl. 3, 488-94 (1967).
- ¹¹R. G. Wymer and J. H. Coobs, "Preparation, Coating, Evaluation and Irradiation Testing of Sol-Gel Oxide Microspheres," Proc. Brit. Ceram. Soc. 7, 61-79 (February 1967).
- ¹²R. G. Wymer and D. A. Douglas, Jr. (compilers), Status and Progress Report for Thorium Fuel Cycle Development Dec. 31, 1964, ORNL-3831, pp. 116-26.
- ¹³R. L. Beatty, F. L. Carlsen, Jr., and J. L. Cook, "Pyrolytic-Carbon Coatings on Ceramic Fuel Particles," Nucl. Appl. 1, 560-66 (1965).
- ¹⁴H. Beutler, R. L. Beatty, and J. H. Coobs, "Low Density Pyrolytic-Carbon Coatings for Nuclear Fuel Particles," Electrochem. Technol. 5, 189-94 (1967).

¹⁵J. H. Coobs, GCR Program Semiann. Progr. Rept. Sept. 30, 1965,
ORNL-3885, pp. 50-52.

¹⁶A. R. Olsen, H. L. Krautwedel, J. H. Coobs, and E. L. Long, Jr.,
GCR Program Semiann. Progr. Rept. Mar. 31, 1966, ORNL-3951, pp. 41-53.

¹⁷J. H. Coobs et al., GCR Program Semiann. Progr. Rept. Sept. 30,
1966, ORNL-4036, pp. 31-45.

¹⁸J. H. Coobs, R. L. Beatty, A. R. Olsen, H. L. Krautwedel,
J. W. Prados, and J. L. Scott, "Testing of a Design Analysis for
Coated-Particle Fuels," Trans. Am. Nucl. Soc. 9(2), 421-422 (1966).

¹⁹A. W. Longest and J. A. Conlin, Design of an Irradiation
Experiment to Test Coated-Particle Fuels to High Burnup, ORNL-TM-1427
(May 1966).

²⁰J. A. Conlin et al., GCR Program Semiann. Progr. Rept. Mar. 31,
1966, ORNL-3951, pp. 69-73.

²¹A. W. Longest et al., GCR Program Semiann. Progr. Rept.
Sept. 30, 1966, ORNL-4036, pp. 72-78.

6. BULK OXIDE PROCESS DEVELOPMENT

R. B. Fitts

Bulk oxides in the form of pellets are the predominant fuel employed in today's power reactors. They are also the leading fuel candidates for some of the most promising advanced reactor concepts. This is due principally to their excellent in-reactor performance. Since they may be operated to high burnup and fuel pellets cost relatively little to produce, the fuel fabrication cost per unit of power generated is low. There is, however, always an incentive to develop a more economical fuel fabrication process, and this becomes a necessity for the advanced reactors for which fuel fabrication is a more significant part of the total power cost.

Development of new methods, such as vibratory compaction of powders, has been attempted in the past for the fabrication of bulk oxides for use in present power reactors. None have been adopted commercially because they offered little, if any, economic advantage over the standard pelletization technique. However, two factors provide renewed incentive to search for better ways of fabricating these materials.

The sol-gel process is one new factor. It permits fabrication of oxide fuels by at least two new routes (compaction of microspheres and extrusion), and it may produce a better pelletization process. The other factor is the new set of physical requirements for oxide fuel to be used in advanced reactors. For instance, liquid-metal-cooled fast breeder reactors require oxide having lower density and fabricated to much smaller diameter than present fuels. In addition, their recycled fuels must be fabricated remotely because of high radioactivity. These changes in fuel preparation and specifications can have significant effects on the economics of fuel fabrication.

We are therefore investigating various new methods of fabricating bulk oxides, and the most promising of these techniques are discussed below.

Pelletizing

J. G. Stradley J. M. Robbins

Our study of the use of sol-gel-derived oxide fuel powders has continued.^{1,2} Sol-gel-derived materials are of interest for pelletizing because of the relatively low-temperature sintering required to attain moderate densities, the homogeneous nature of the mixtures of fertile and fissile materials, and the suitability of the sol-gel process to the recycle of fuels.

This year, we emphasized the fabrication of small specimens for the determination of mechanical properties and large specimens for studies of thermal conductivity. We made all of these specimens from conventional sol-gel material. Chemical analyses of the as-received materials are shown in Table 6.1.

Table 6.1. Chemical Analyses of Sol-Gel-Derived Materials Used for Fabricating Test Specimens

Batch	Uranium (wt %)	Thorium (wt %)	Oxygen-to-Uranium Ratio
TU-2	5.5	78.9	2.99
TU-4	6.5	77.3	3.00

We fabricated 18 large specimens (approximately 2.6 in. in diameter x 0.5 in. long) for conductivity measurements as shown in Table 6.2. A typical specimen is shown in Fig. 6.1. The general fabrication scheme for all specimens consisted of:

1. grinding the dried sol to -200 mesh,
2. calcining the -200 mesh powder,
3. adding water as a lubricant,
4. cold forming in a steel die,
5. isostatically pressing at 20,000 psi,
6. sintering in air at 1450°C,
7. reducing in hydrogen at 1450°C.

Table 6.2. Fabrication History and Results on (Th,U)O₂ Sol-Gel
Thermal Conductivity Specimens

Specimen	Batch	Powder Calcining Temperature (°C)	Water Added (wt %)	Bulk Density (g/cm ³)		
				Isostatically Pressed	Air-Sintered ^a	Hydrogen- Reduced ^b
A	TU-2	300	6	5.03	9.29	9.33
F	TU-2	300	6	5.04	9.19	9.15
E	TU-2	300	6	5.02	9.12	9.11
C	TU-2	400	9	4.79	8.71	8.76
S ^c	TU-2	400	6	4.87	8.70	8.67
U ^c	TU-2	400	6	4.87	8.71	8.68
T ^c	TU-2	400	6	4.87	8.71	8.67
V ^c	TU-2	400	6	4.87	8.70	8.72
No number	TU-2	650	6	4.62	8.55	8.53
L' ^c	TU-2	650	6	4.82	8.60	8.59
N' ^c	TU-2	650	6	4.88	8.61	8.61
M'	TU-2	650	6	4.83	8.63	8.55
K'	TU-2	650	6	4.88	8.58	8.57
2	TU-4	Not calcined	Dry	4.94	8.79	8.85
3	TU-4	200	3	5.26	9.17	9.20
5	TU-4	200	5	5.08	9.17	9.13
6	TU-4	200	5	5.08	9.16	9.13
7	TU-4	200	6	5.18	9.21	9.21

^a1450°C, 1 hr.

^b1450°C, 40 min.

^cSelected for thermal conductivity measurements

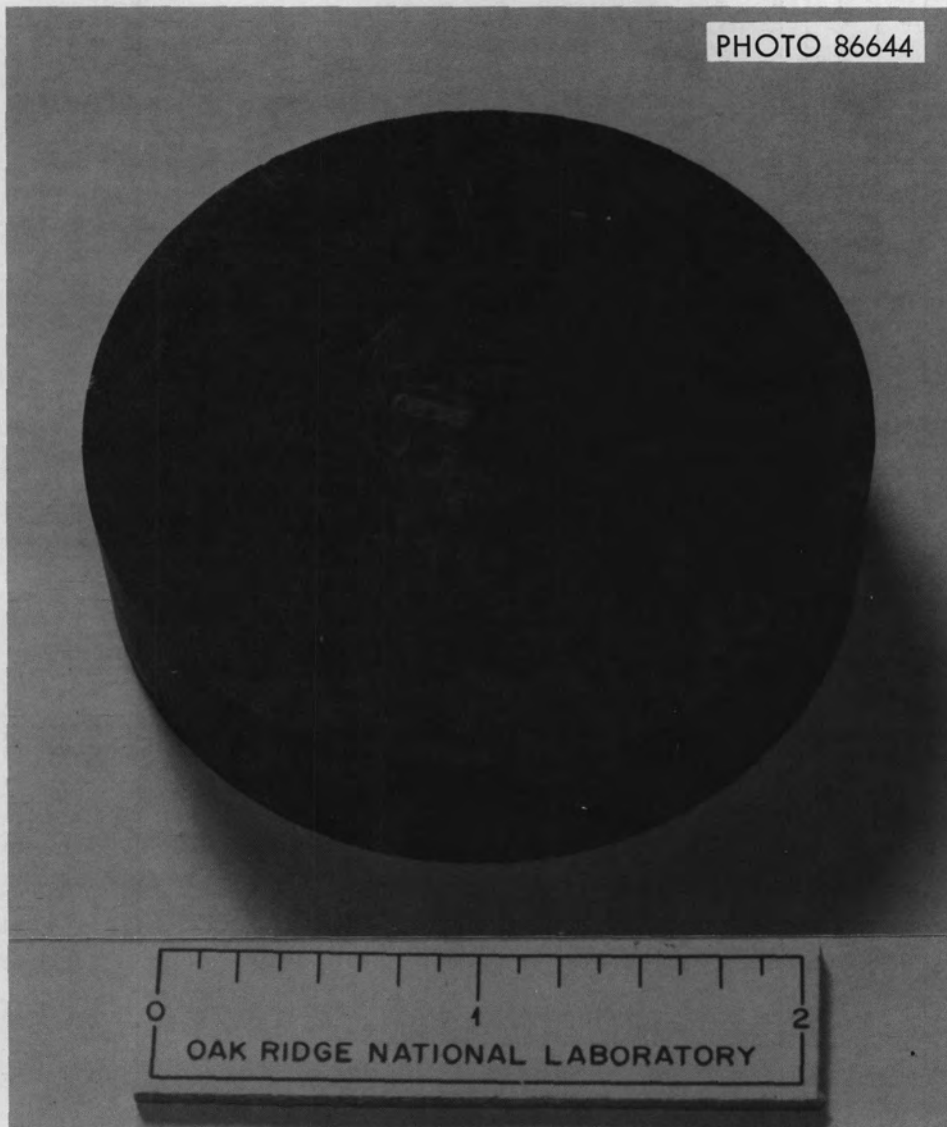


Fig. 6.1. Typical Sol-Gel (Th,U)O₂ Specimen Fabricated for Thermal Conductivity Measurements.

Six pellets are required for measuring thermal conductivity at a given density. An adequate number of the specimens fabricated fell into the proper density range to be used for measurements at 8.65 g/cm^3 . The remaining specimens will be used as spacers to provide the proper stack height. Ultimately we will supply six specimens each at a lower and a higher density. Thus, the conductivity at three densities can be measured to establish the variation of thermal conductivity of sol-gel-derived $(\text{Th,U})\text{O}_2$ with density.

We fabricated 24 small pellets (approximately 0.2 in. in diameter x 0.3 in. long) from sol-gel-derived $(\text{Th,U})\text{O}_2$ and ThO_2 . We mixed approximately 6 wt % water with -200 mesh powder and cold formed the mixture in a steel die. We then isostatically pressed the uniaxially formed pellets at 60,000 psi and sintered them in two steps. First we heated them to 1450°C in air to take advantage of the higher density obtainable¹ by sintering in air. Then we heated the ThO_2 to 1750°C and the $(\text{Th,U})\text{O}_2$ to 1450°C in hydrogen. In this manner we reduced the oxygen-to-uranium ratio to stoichiometric in the urania-bearing pellets and further densified the pure ThO_2 pellets. Typical fabrication details are shown in Table 6.3.

Table 6.3. Fabrication History and Results on ThO_2 and $(\text{Th,U})\text{O}_2$ Sol-Gel Thermal Creep Specimens

Material	Batch	Powder Calcining Temperature ($^\circ\text{C}$)	Bulk Density (g/cm^3)	
			Isostatically Pressed	Sintered
ThO_2	TU-5	400	5.25^{a}	8.8^{b}
$(\text{Th,U})\text{O}_2$	TU-4	None	5.76^{c}	9.57^{c}

^aAverage for 2 pellets.

^bAverage for 3 pellets.

^cAverage for 6 pellets.

A comparison of Tables 6.2 and 6.3 shows that the small pellets of $(\text{Th,U})\text{O}_2$ sintered to a higher density than the large specimens. However, the larger specimens were isostatically pressed at a lower pressure than the small pellets because of equipment limitation. Also, the large pellets tend to crack during sintering when they are fabricated to high densities.

The ThO_2 sol-gel specimens reached only 88% of theoretical density, even though they were isostatically pressed at 60,000 psi. However, Daniels and Wadsworth³ have reported similar results for sol-gel ThO_2 . Their procedure was to crush, screen, press, and sinter specimens that were only 84% of theoretical density. They found that the individual gel particles sintered to nearly theoretical density, but they were too large to sinter together to eliminate the bulk porosity.

Sol-Gel Extrusion

We are developing extrusion as a fabrication technique for sol-gel-derived materials such as ThO_2 , $(\text{Th,U})\text{O}_2$, UO_2 , and $(\text{U,Pu})\text{O}_2$. The extrusion process is a low-cost, high-rate-of-production method for forming ceramics, even in complex shapes. This fabrication technique offers advantages for the production of long small-diameter fuel pieces with good control of the diameter. Distinct reductions in grinding, inspection, and handling costs are possible. Sol-gel materials, in addition to their low sintering temperature and inherent homogeneity, are attractive for extrusion because of the plastic properties of the "sol-gel clay" that allow fabrication by a novel extrusion technique without the addition of extraneous organic binders or plasticizers. Thus, we are forming essentially pure fuel. This process readily incorporates direct recycle of scrap materials and allows the fabrication of fuels having a wide range of density.

Preparation of Thoria Sol-Gel "Clay" (A. B. Meservey)

The material that is fundamental to the sol-gel extrusion process and that makes it a unique process, is the sol-gel clay. In the thoria system, this clay is produced by the aqueous digestion of steam-denitrated thoria powder with a slight excess of nitric acid over that required to form a sol. The thoria goes through a sol stage and then, as evaporation proceeds, coagulates to a finely divided precipitate. This precipitate, when separated by filtration, is the sol-gel clay.

The material exhibits most of the physical and mechanical characteristics of a natural clay. It differs from the material used in ordinary ceramic extrusion, as applied to high-purity oxides, in that the particles are held together by complex bonds between water, acid, and the particles. In other techniques, organic plasticizers are added to powders of much larger particle size to produce a plastic mass. The utilization of sol-gel clay as the extrusion mass permits the extrusion of what is essentially a pure oxide material containing only a dilute acid.

Thoria Sol-Gel Extrusion (R. B. Fitts)

The working material in the initial development work on the sol-gel extrusion process was thoria. The advanced state of thoria sol-gel work in general, as compared to other materials such as urania, meant that substantial quantities could be made available for the work.

Extrusion is used extensively in commercial fabrication and consists in pressing a plastic mass through a die. The flow sheet, Fig. 6.2, illustrates the general technique of forming ceramic bodies from sol-gel clay. If we follow the process route given by the left-hand side of this figure, the clay is extruded and air dried at room temperature and then calcined at 1150°C to yield 99%-dense ThO_2 . This density has been obtained for solid rods up to 0.080 in. in diameter and cored rods with wall thickness up to 0.050 in. Thicknesses greater than 0.050 to 0.080 in. made from pure clay yield excessively cracked finished products.

An alternate approach to the direct extrusion of clay material, which is indicated on the right-hand side of Fig. 6.2, is to mix the clay with various powders. Powders that we have studied include fired material, such as recycled scrap, and lightly calcined material, such as dried scrap that has been heated to 600°C for 1 hr. These powders may also be obtained directly from dried sol-gel material by grinding and an appropriate heat treatment. A mixture of one or both types of powder with the clay when processed (extruded, air dried, and calcined at 1150°C) will yield compacts having from 70 to 98% of theoretical density. We have fabricated thoria extrusions up to 0.3 in. in diameter over this

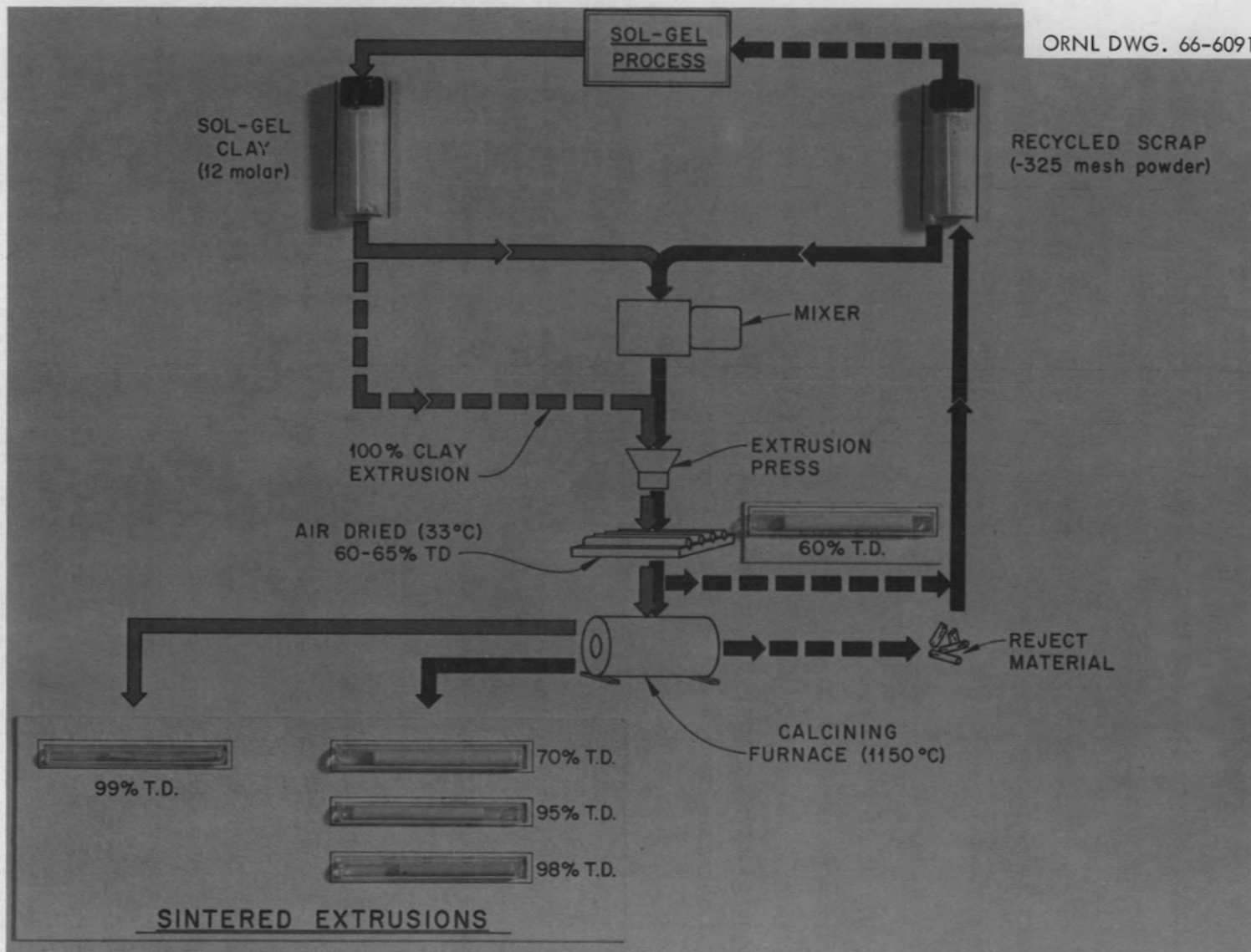


Fig. 6.2. Extrusion of Sol-Gel-Derived Ceramic Fuel Compacts.

entire density range, and we have produced 0.430-in.-diam pieces at 95% of theoretical density by this route.

We conducted all of our experiments to date, with the exception of the 0.430-in.-diam pieces mentioned above, with the simplest type of laboratory extrusion apparatus. This consisted of a small laboratory press, a 1-in. powder die that was adapted for extrusion, and a laboratory-scale sigma mixer. Most of this work has used 10 to 12 \underline{M} ThO₂ clay as the working material. Some testing of 10 \underline{M} ThO₂-5% UO₂ clays indicates no difference in the handling properties of the two materials.

Initial results from tests on extrusion of pure as-received clays revealed 16% diametral shrinkage on drying and a similar amount of firing shrinkage. These samples showed high sintered density (99% of theoretical) and good mechanical strength; however, in diameters over about 0.080 in. these specimens contain a network of fine cracks, as shown in Fig. 6.3. We have attempted to reduce or eliminate this cracking by adjusting the moisture content of the pure clay, by isostatic pressing of the dried extrusion, by trying various drying techniques, and by adding powders to the clay. Adjustment of water content from 14.9 to 22.6% by weight by either addition of water or evaporation appeared to have little effect on the final fired structure. Isostatic pressing following extrusion also appeared to have little if any effect.

We made several preliminary attempts to reduce cracking of extrusions by varying the conditions of drying. Samples are normally dried lying on a cotton pad in normal room air. We varied the moisture content of the drying air, the temperature of drying, and the method of sample support during drying. Sample bowing was markedly reduced where drying was uniform, but none of the things we tried had a significant effect on internal cracking. Samples dried in a low-moisture atmosphere broke apart rather violently when exposed to ambient room air before firing. They completely disintegrated in 1 to 2 min. We attribute this behavior to rehydration of the gel.

Our experience indicates that addition of powders to the clay before extrusion is the best method for reduction of sample cracking. We have investigated the effects of powder particle size, morphology, and heat

treatment on the effectiveness of powder additions to the clay. Particle sizes greater than 325 mesh (44μ) lead to some surface roughening and a reduction in the green strength of the extrusions. For this reason, most of our work has been with particle sizes less than 325 mesh (smaller than 44μ).

We have added powders (1) in the as-dried and crushed condition, (2) after a 600°C 1-hr calcining heat treatment, and (3) in the fully sintered condition. Addition of over 5 to 10% of the as-dried powder leads to a clay-powder mixture that is too dry to extrude. Lightly calcined (600°C) powder additions in the amounts of 15 to 30% by weight of the clay-powder mixture yield an extrusion mass with much greater plasticity than in any of the other mixtures. This plasticity greatly assists the production of crack-free extrusions, possibly because of the enhanced ability of the stresses to relax in the extruded body during drying.

Fully sintered powder fired at 1150°C for 1 hr may be used in the as-crushed condition or may be ball-milled before use. The addition of crushed powder to the clay caused the greatest reduction in drying and firing shrinkage and also yielded extrusions of lower density and with more angular porosity, as shown in Fig. 6.4. The addition of ball-milled powder, wet-milled to a "stable" particle size distribution, reduced shrinkage but not as markedly as did addition of the angular crushed particles. This material stabilizes the extrusions with respect to cracking almost as well as does the angular powder. It also yields a denser product with more rounded porosity, but with lower strength. Examples of results of various mixtures with the shrinkage and density obtained are shown in Table 6.4.

From a process standpoint, powder additions to the clays offer several advantages. They provide a means to control the final fired density, reduce the amount of drying and firing shrinkage and thus increase the dimensional control, and improve the economy of the fuel cycle by utilizing scrap materials for the powder additions.

We made useful extrusions of two types by this process for use in irradiation capsules. First, we made ThO_2 buckets to hold wires (of various compositions) that melt to indicate central temperature in a

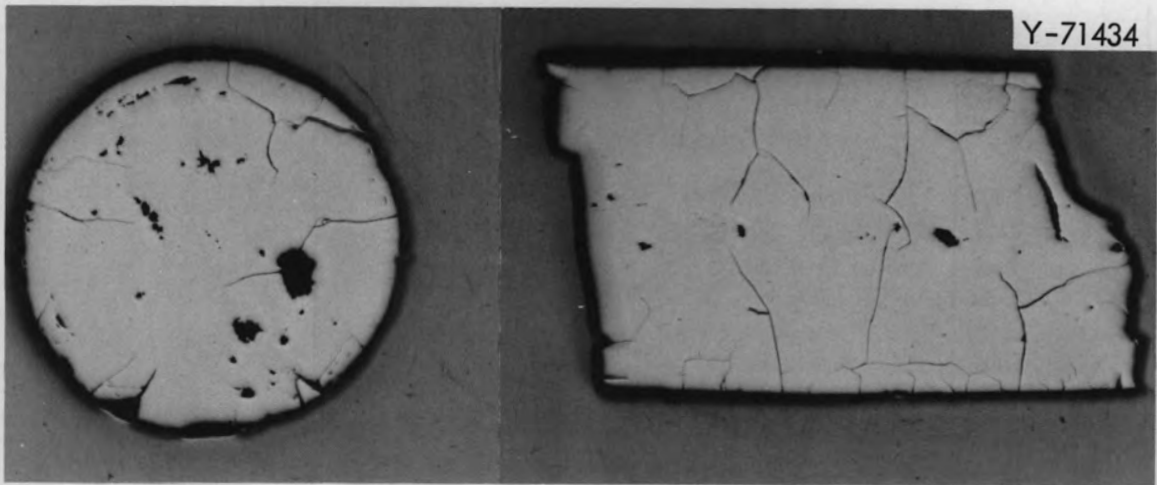


Fig. 6.3. Pure ThO_2 Clay Extrusion After Firing to 0.117 in. in Diameter and 99% of Theoretical Density. 12X.

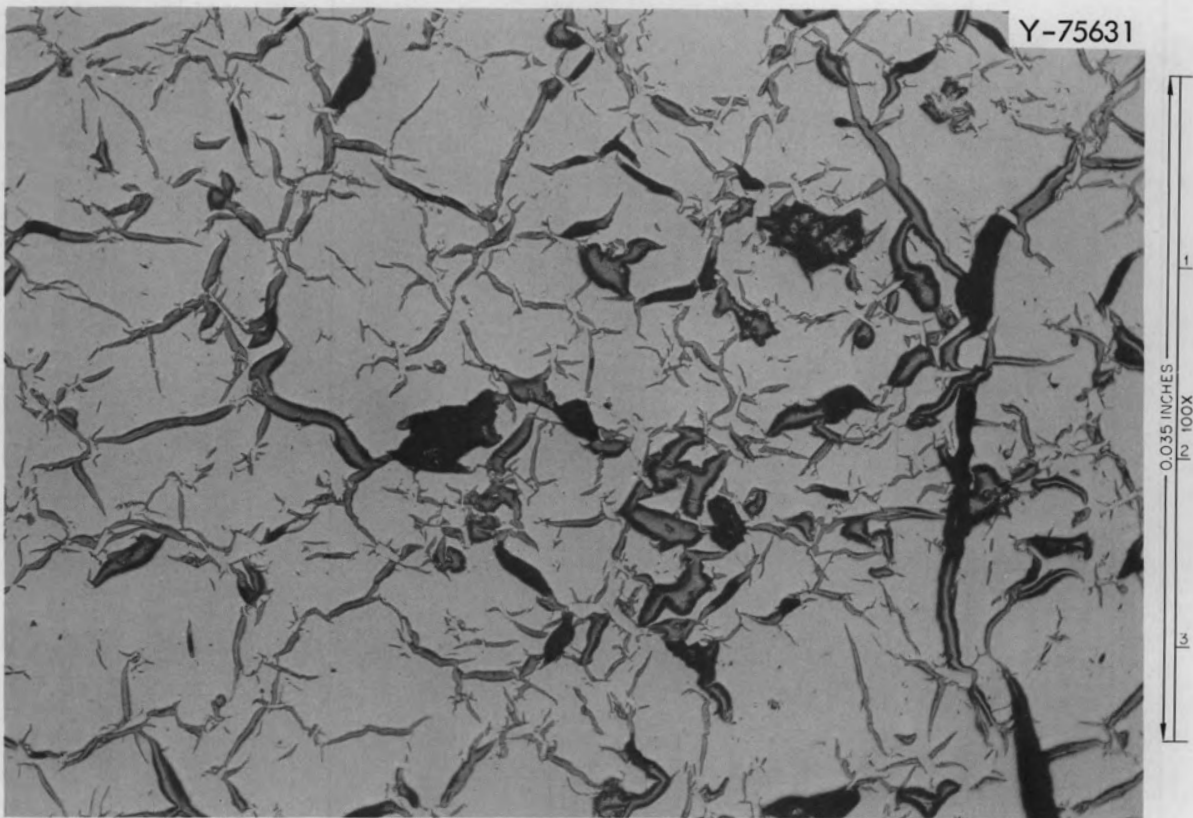


Fig. 6.4. Fired ThO_2 Extrusion (95% Clay Plus 5% Fired Crushed Powder), 0.182 in. in Diameter, 83% of Theoretical Density.

Table 6.4. Sol-Gel Thoria Clay and Powder Extrusion Mixture

Clay	Starting Composition (%)			Fired Diam (%)	Drying Shrinkage (%) ^b	Green Density (g/cm ³)	Firing Shrinkage (%) ^b	Fired Density (g/cm ³)	Total Shrinkage (%) ^b
	600°C Calcined Powder	Fired Crushed Powder ^a	Fired Ball-Milled Powder ^a						
100				0.117 ^c	16.0 ^c	d	16 ^c	9.92	32.0
95		5		0.182	14.4	5.63	12.8	8.34	27.2
90		10		0.188	14.0	5.72	10.8	7.85	24.8
80		20		0.1965	14.0	5.85	7.4	6.97	21.4
95	5			0.1735	d	5.54	d	9.90	30.6
90	10			0.175	d	5.41	d	9.94	30.0
75	25			0.176	d	5.17	d	9.80	29.6
95			5	0.1745	d	5.70	d	9.87	30.2
90			10	0.1775	d	5.78	d	9.89	29.0
75			25	0.186	d	6.195	d	9.60	25.6
71	24		5	0.125 ^e	d	d	d	9.65	27.3
45	15	40		0.230 ^f	11.1 ^f	6.44	3.7 ^f	7.20	14.8

^aAll powders -325 mesh.

^bShrinkage in percent of extruded diameter. Extruded diameter is 0.250 in. unless noted otherwise.

^cExtruded diameter of 0.172 in.

^dNot determined.

^eExtruded diameter of 0.172 in., final extrusion has 60-mil-diam hole down the center.

^fExtruded diameter of 0.270 in.

coated-particle irradiation experiment. These buckets were 96.5% dense and 3/8 in. tall x 0.125 in. OD x 0.060 in. ID. The structure may be seen in Fig. 6.5.

We also made 72%-dense ThO_2 insulators for use at the end of the fuel column in irradiation tests of vibratorily compacted microsphere fuel. These were made 1/4 in. tall x 0.229 ± 0.001 in. in diameter. They were made by cutting the extruded rod to length after it had dried, smoothing the ends, and then firing. These extrusions, although low in density, are very hard and show no tendency to spall or "chalk." Their structure is shown in Fig. 6.6.

The results to date indicate that pure thoria and thoria-urania sol clays can be extruded without additions to produce high-density fuels containing some fine internal cracking. These same clays with powder additions will produce high- or low-density fuels with no internal cracking. Although we have made little effort to control diameter and bow, we have produced 3-in.-long, 80%-dense, 0.230-in.-diam extrusions that varied less than 0.0005 in. in diameter from end to end. The outward appearance and microstructure of this type of extrusion are shown in Fig. 6.7. The dark area in the center of the pellet microstructure is caused by the lack of penetration of mounting material to this region. Nearly all of the porosity in these extrusions, either high or low density, is surface connected.

Urania Sol-Gel Clay (K. H. McCorkle, J. P. McBride)

Practical reactor application of the sol-gel extrusion process requires its extension to the urania system. We expect that the most difficult part of this work will be the preparation of a satisfactory sol-gel clay. Once such a material is obtained, the general type of process employed in the thoria-base work (see above) should yield satisfactory results.

Our initial work with urania indicates that pastes prepared from chloride-stabilized systems will form sol-gel clay satisfactory for extrusion, whereas those prepared from nitrate-stabilized systems will not. One can prepare chloride sols that are 4 to 5 times as concentrated

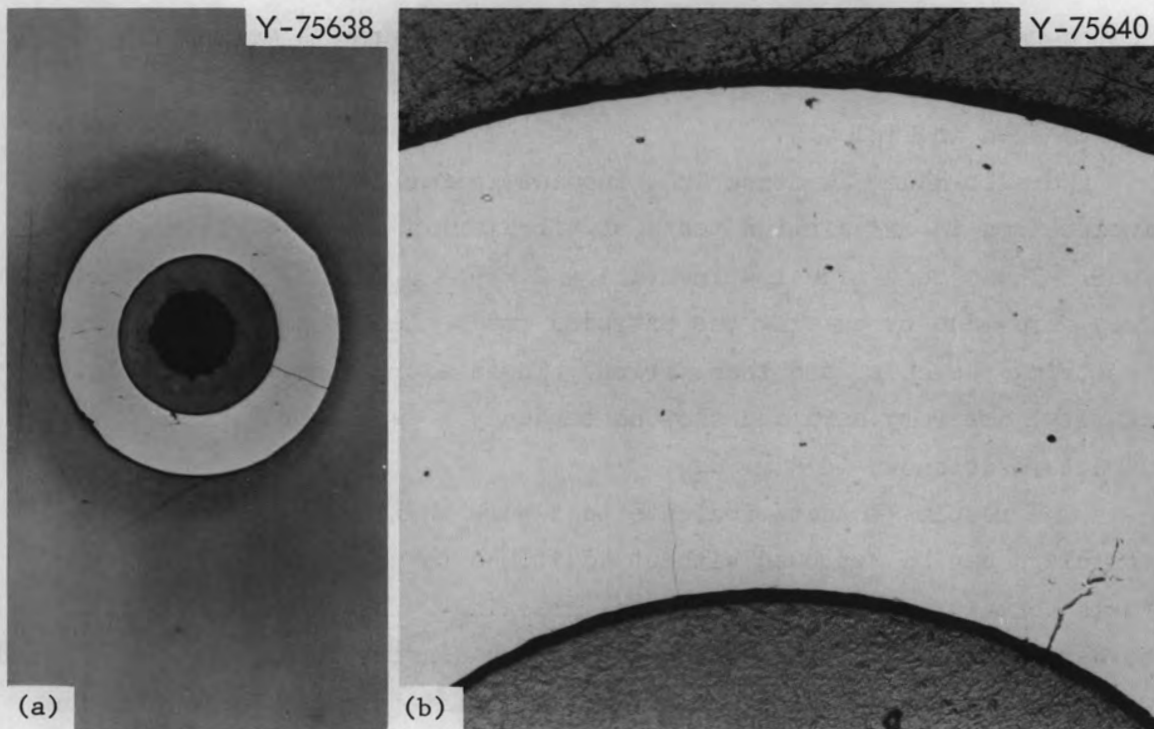


Fig. 6.5. Extruded Clay Bucket (71% Clay, 24% Calcined Powder, 5% Fired Ball-Milled Powder), 0.125-in.-OD, 0.060-in.-ID, 96.5% of Theoretical Density. (a) 12X. (b) 100X.

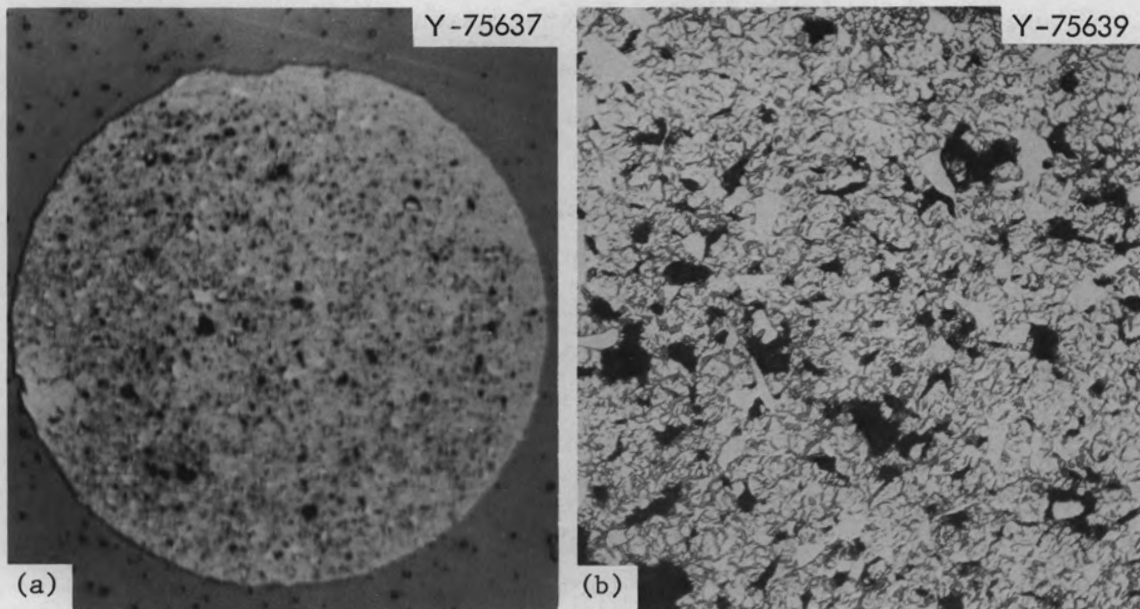


Fig. 6.6. Insulator Extruded from 45% Clay, 15% Calcined Powder, and 40% Fired Crushed Powder. 72% of theoretical density, 0.230-in.-OD. (a) 12X. (b) 100X.

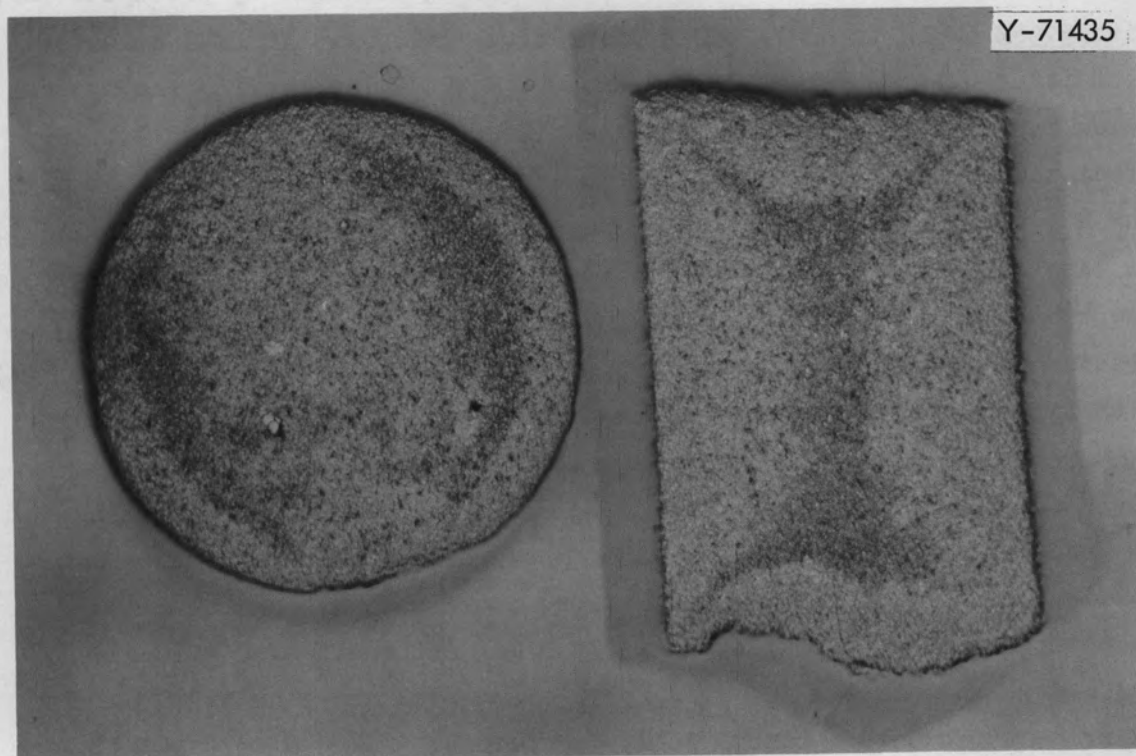
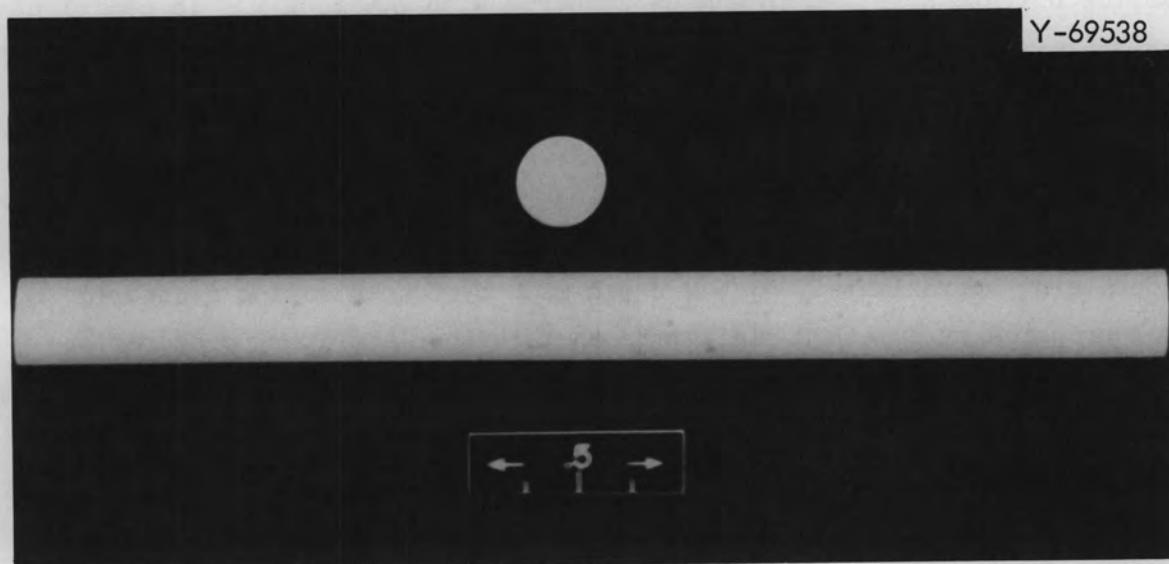


Fig. 6.7. Extruded ThO₂ Made from ThO₂ Gel with Addition of 40 wt % -325-mesh High-Fired ThO₂. Final sintered density is 70% of theoretical. (a) Overall view. (b) Structure at 12X.

as the nitrate sols: 6 to 9 M as compared with 1.5 to 2 M. In addition, the chloride sols may be dried directly to give concentrated clays (approximately 9.8 M), while the nitrate systems thicken and gel at about 2 M. Using a modified sol-gel process, we prepared nitrate-stabilized pastes containing uranium concentrations of 4.6 and 4.8 M, but the results of extrusion tests were not encouraging. A chloride-stabilized clay containing approximately 9.75 M U was made by concentrating a chloride sol prepared by a method similar to that in the laboratory preparation flowsheet for urania (see Fig. 3.1), but with chloride substituted for nitrate. This clay when blended with a sol-gel-prepared UO_2 powder that had been calcined at 400°C formed a material having the kind of plasticity and smoothness that characterized the thoria sol-gel clay and most conventional extrusion materials.

The first nitrate-stabilized paste (NP-1) was made by precipitating, with 3.5 M NH_4OH to pH 7, 300 g of uranium from a uranium(IV) solution containing 0.51 M U, 1.0 M NO_3^- , and 0.2 M HCO_2H , recovering the hydrous oxide by filtration, and washing the filter cake in place with 9 liters of distilled water and 2 liters of acetone. The cake was heated at 62°C for 2.5 hr under an argon flush, which carried out about 250 ml of liquid. We then added 100 ml of water, stirred and heated the mixture, and allowed the resultant sol or fine suspension to stand. After 60 hr, all the urania had settled to a sludge containing 51 wt % U (approximately 4.6 M) with nitrate-to-uranium and carbon-to-uranium mole ratios of 0.06 and 1.14 respectively. The recovered urania sludge was a stiff paste, showing a slight dilatancy and considered suitable for extrusion testing.

We initiated the preparation of the second paste (NP-2) by precipitating the hydrous urania as described above and washing the filter cake with 9 liters of water and 2 liters of methanol. The filter cake was heated and stirred in argon for 1 hr at 60°C and 4 hr at 70°C . The experiment produced a runny "jelly" containing 3.54 M U [87% U(IV)] with nitrate-to-uranium and carbon-to-uranium mole ratios of 0.04 and 0.55 respectively; and the jelly showed an x-ray crystallite size of 80 Å. To stiffen the jelly, a urania powder was prepared and added at a ratio of about 1 to 3 of the original jelly. The resulting paste was moved easily with a spatula, showed no dilatancy, and held its shape. The

paste contained 58 wt % U (approximately 4.84 M), had a uranium(IV) content of 81% of the total uranium, and nitrate-to-uranium and carbon-to-uranium mole ratios of 0.09 and 0.04 respectively. The carbon analyses appear to be in error.

The urania powder was prepared by precipitating the hydrous urania from a uranium(IV) solution containing 0.5 M U-1.0 M NO_3^- -0.25 M HCO_2H -0.66 M urea with 3.5 M NH_4OH to pH 9. The hydrous oxide was recovered by filtration and washed in place with 9 liters of 0.01 M $\text{N}_2\text{H}_4 \cdot \text{H}_2\text{O}$ and 2 liters of methanol. The wet cake was dried under argon at 100°C for 28 hr to give a lumpy, black powder. The powder contained 74 wt % U [87% U(IV)], had nitrate-to-uranium and carbon-to-uranium mole ratios of 0.02 and 0.16, respectively, and had an x-ray crystallite size of 33 Å.

For the preparation of the chloride-stabilized paste or clay (CP-1), the hydrous urania was precipitated from a uranium(IV) chloride solution containing 0.51 M U[99.1% U(IV)]-2.21 M Cl^- by the addition of 3.5 M NH_4OH to pH 7.5. The precipitate, containing 300 g of uranium, was recovered by filtration on a 24-in. Büchner funnel and washed with 8 liters of water (in 1-liter increments) until incipient peptization occurred. The washed filter cake contained 13.78% U and had a uranium(IV) content 98% of the total uranium and a chloride-to-uranium ratio of 0.395. This cake was heated at 61°C for 1 hr and allowed to settle 64 hr. About half the total volume was heel. The sol was heated to 67°C for 1 hr and allowed to settle for 20 hr. This time there was no heel.

The analysis for this sol was U, 0.667 M; U(IV), 99% of total uranium; Cl^-/U mole ratio, 0.375; density, 1.673 g/liter; x-ray crystallite size, 31 Å.

The sol was evaporated from 0.667 M to 2.4 M under vacuum, at which point it began to thicken. Uranium trioxide was added to this sol at a mole ratio of 0.03 to the total uranium to restore fluidity (a peculiar phenomenon observed with chloride-stabilized sols), and evaporation continued under 29 in. of vacuum at 60 to 65°C.

Analysis of the resulting material was U, 67.82 wt % (\approx 9.75 M); U(IV), 88.9% of total uranium; Cl^- , 3.6 wt %; Cl^-/U mole ratio, 0.358.

Initial extrusion tests with the above clay were very encouraging, and, for the present, preparation work will concentrate on chloride-dispersed systems. Insofar as possible, the paste preparation methods investigated will be those most easily adapted to the urania sol-gel processes under current investigation.

Urania Sol-Gel Extrusion (J. M. Robbins, J. G. Stradley, R. L. Hamner)

We are investigating the feasibility of extruding UO_2 clays with the anticipation that this work can be extended to UO_2 - PuO_2 materials for fast-reactor fuel studies. Our extrusion operations were essentially the same as those for the extrusion of conventional materials; that is, the clays were placed in a steel die case fitted with an extrusion die, evacuated to remove air, then forced through the die opening under pressure with a steel punch. Most of the materials were extruded vertically through die openings of 1/16 or 1/8 in. in diameter.

The materials for extrusion were stored under an argon atmosphere until ready for use to prevent excessive oxidation by air. The extrusion operations, which require only a short time (approximately 15 min), were performed in air.

The materials for experimental extrusions were of four different types: (1) a UO_2 sol approximately 0.7 M, (2) a hydrous UO_2 filter cake (NP-1) approximately 4.6 M, formed by interrupting the usual nitrate-formate flowsheet for sol preparation before a sol was formed, (3) a hydrous UO_2 filter cake containing approximately 30 wt % of the same material dried and powdered (NP-2), and (4) a UO_2 clay (CP-1) approximately 9.75 M, prepared from chloride.

We failed to form a clay from the 0.7 M urania sol by evaporation in vacuum; as the material approached the consistency for extrusion (approximately 15 wt % liquids), large gel fragments began to form and the materials could not be extruded. The preparation of the last three materials is described above.

The first extrusions from the hydrous UO_2 filter cake (NP-1), as-received, cracked rapidly during drying, probably because of rapid and excessive shrinkage. We dried, powdered (to 325 mesh), and calcined

some of this material at 400°C in Ar-4% H₂ for addition to the batch to reduce shrinkage. We blended 30 wt % of the calcined powder with the as-received batch in a Waring Blendor, using 3 cm³ of acetone per gram of solids as the vehicle. Since we found that the oxygen-to-uranium ratio of this material increased only from 2.201 to 2.267 during a two-day exposure to air at room temperature, the operations of blending and evaporation to extrusion consistency were done in air. The extrusions from this material did not crack during drying, but they had rough surfaces and deformed readily. After a sintering treatment at 1000°C for 1 hr in Ar-4% H₂, the extrusions exhibited a linear shrinkage of 41% from the extruded state. The final density was 6.2 g/cm³ (56.2% of theoretical).

We could not extrude the hydrous UO₂ filter cake containing dried, powdered material (NP-2). The solids and liquids in this material separated under pressure and the liquid was forced from the die, leaving a compacted mass of solids behind.

Our most encouraging results were obtained from the chloride-prepared clay (CP-1). Extrusions of this material, as-received, were unsatisfactory; they broke into sections during extrusion and developed shrinkage and drying cracks very quickly. Self-loading of the weak, heavy extrusions as they came from the vertically positioned die probably contributed to the breaking phenomenon. We blended 30 wt % of sol-gel urania powder (325 mesh) calcined at 400°C with the concentrated sol in methyl alcohol, evaporated the mixture to a 13 wt % liquid content, and extruded the material in a horizontal position. This eliminated both the breaking and cracking of the extrusions. The extrusions were sintered at 1000°C for 1 hr in Ar-4% H₂. A soak period of 2 hr at 325°C during heating was employed to suppress a strong exotherm beginning at 350°C as shown by differential thermal analysis. Characterization of the extrusions is given below.

Density, g/cm ³ , % of theoretical	
Green, after drying at room temperature	5.5, 50.1
Sintered	6.94, 63
Linear shrinkage, after sintering, from the as-extruded state, %	27
Residual chlorine content after sintering, %	0.14
Oxygen-to-uranium ratio after sintering	2.086
Visual examination after sintering	Some micro- cracking observed

The chloride material was the only clay prepared for extrusion that approached plasticity; the other clays were nonplastic and had a "gluelike" quality, which made them extremely difficult to handle. Also, the extrusions from the chloride sol were the only ones to have smooth surfaces and to exhibit the property of "toughness" that is observed in most conventional oxide extrusions.

The extrusion of sol-derived urania, at present, must be considered to be in the preliminary stage of development. The preparation of suitable clays is complex, and the extrusion of such materials is very much in the "art" stage. We conclude from our preliminary experiments:

1. Clay preparation directly from nitrate-derived sols is unsatisfactory because of the gelling problem encountered during sol concentration.
2. Hydrous UO_2 filter cakes are nonplastic and the extrusions from such materials have rough surfaces and consistencies resembling toothpaste.
3. A chloride-sol-derived clay appears to be suitable for extrusion because it exhibits a characteristic approaching plasticity, which is a basic requirement for good extrusions. However, the high residual chlorine content in the extrusions after sintering at $1000^\circ C$ cannot be tolerated, and developmental studies must be made to obtain a chlorine-free product.

Vibratory Compaction of Microspheres
by the Sphere-Pac Technique

A. R. Olsen

The feasibility of utilizing high-energy vibratory compaction with sol-gel-derived dense fuel fragments to fabricate fuel rods has been established.⁴ Preliminary economic evaluations have shown that this process is cheaper than standard pellet processes, particularly for remote fabrication. It does, however, require complicated remote equipment for crushing, grinding, and sizing operations. The use of sol-gel microspheres with low-energy vibratory compaction, Sphere-Pac, offers an alternate process. Elimination of the powder preparation equipment with its attendant dusting problems would improve inventory control and reduce equipment maintenance problems. The disadvantages of this process are the need for a two-step loading procedure, the limit on practical loading

densities, and uncertainties about in-reactor performance characteristics, particularly the thermal conductivity of a packed bed.

During the past year, we conducted limited laboratory experiments using available sol-gel microspheres to investigate loading procedures, equipment requirements, time cycles, and attainable packing densities. This investigation of sphere packing in cylindrical containers was based on reported work of others,^{5,6} and was aimed at providing fuel rods for irradiation testing of the performance characteristics.

In the work, we used spheres in two size fractions. The coarse size fraction has been -35 +40 mesh (500- to 420- μ -diam) microspheres produced by the sol-gel column-forming technique,⁷ while the fine fraction was -325 mesh (< 44- μ -diam) microspheres produced by the sol-gel "stirred-pot" forming technique.⁸

We have found that sequential loading in which the coarse fraction is first loaded into the tube and the fine fraction then infiltrated from the top produces the highest density and most uniform packing. We tested a variety of energy inputs and vibrational frequencies. Frequency had little effect on density, but 60 Hz provides the highest loading rate. Energy input with less than 15g acceleration is adequate. The vibrational modes that included lateral components provided more rapid and denser packing than purely axial vibration. A light follower rod on top of the fine-particle bed during infiltration will prevent expansion of the coarse-particle bed and the attendant segregation; but to minimize contamination of the upper part of the tube, we use a funnel with a screen in the bottom to restrain the coarse bed. We have not optimized all of the variables. However, by using the two size fractions, we routinely attain packed densities from 83 to 85% using a coarse-to-fine size fraction volume ratio of 2.7. Higher volume packing densities are attainable with ternary loadings, and we shall investigate these.

The current target density for high-burnup oxide fuels for liquid-metal fast breeder reactor fuel elements is 85%; so we are fabricating and testing fuel rods containing packed beds of microspheres of (Th,Pu) O_2 and (U,Pu) O_2 . These tests are discussed in Chapter 7.

In addition to the irradiation tests, we have begun to determine the thermal conductivity of packed beds of microspheres. Initial tests were made on 98%-dense ThO_2 microspheres with a packed bed fuel density of 82.2% of theoretical in a helium atmosphere. Thermal conductivity has been measured up to 900°C in a radial heat flow apparatus. Although there were some anomalies in the first test, the bed conductivity ranged between $0.0135 \text{ w cm}^{-1} (\text{C})^{-1}$ at 300°C and $0.0118 \text{ w cm}^{-1} (\text{C})^{-1}$ at 200°C . These measurements are being repeated and extended to 1100°C to investigate an apparent increase in conductivity at the higher temperatures. We also plan to measure the conductivity of packed beds of microspheres of UO_2 and $(\text{U,Pu})\text{O}_2$.

REFERENCES

- ¹R. G. Wymer and D. A. Douglas (compilers), Status and Progress Report for Thorium Fuel Cycle Development Dec. 31, 1964, ORNL-3831, pp. 134-37.
- ²J. D. Sease, A. L. Lotts, and J. M. Robbins, Status and Progress Report for Thorium Fuel Cycle Development Dec. 31, 1965, ORNL-4001, pp. 98-101.
- ³A. U. Daniels and M. E. Wadsworth, Densification and Sintering of Thoria and Thoria Gel, Technical Report Number XXVIII, TID-22491, pp. 58-59 (Dec. 15, 1965).
- ⁴J. E. Van Cleve and A. L. Lotts, "Operating Experience in a Semi-Remote Facility for Preparation of Fuel Rods Containing $(\text{U}^{233}, \text{Th})\text{O}_2$," pp. 257-71 in Proceedings of the 12th Conference on Remote Systems Technology, American Nuclear Society, Hinsdale, Ill., November 1964.
- ⁵R. K. McGearry, J. Am. Ceram. Soc. 44(10), 513-22 (October 1961).
- ⁶J. E. Ayer and F. E. Soppet, J. Am. Ceram. Soc. 48(4), 180-83 (April 1965).
- ⁷P. A. Haas and S. D. Clinton, Ind. Engr. Chem. Prod. Res. Develop. 5, 236-44 (September 1966).
- ⁸S. D. Clinton and P. A. Haas, Unit Operations Section Quarterly Progress Report July-September 1965, ORNL-3916, pp. 43-50.

7. IRRADIATION OF BULK OXIDE FUELS

A. R. Olsen

R. B. Fitts

As part of the evaluation of processes under development for preparing nuclear fuels and fabricating the fuel elements, a continuing program for testing the irradiation performance is essential. In the Thorium Fuel Cycle Program we have been testing coated-particle fuels as reported in Chap. 5 and continuing the irradiation of bulk thorium-base fuels as pellets or particles vibratorily compacted into tubes.^{1,2} During the past year, we started an irradiation program to characterize sol-gel-derived fuels that show promise for fast reactors.

Irradiation of Thorium-Bearing Bulk Oxide Fuels

We continued the irradiation testing of powder-compacted sol-gel oxide and pelletized fuels. We also began the irradiation of low-energy vibratorily compacted sol-gel oxide microspheres. The tests currently in-reactor or under examination are outlined in Table 7.1.

Effects of Extended Burnup

Three rods containing pellets of ThO_2 -4.4% UO_2 fuel attained an estimated burnup of 150,000 Mwd/MT Th + U. The rods are similar to those reported earlier.³ They were removed from the reactor in December, and postirradiation examination is scheduled for early 1967.

We examined the last rod of the MTR-1 group containing vibratorily compacted sol-gel ThO_2 -4.5% UO_2 . This test group was started in 1961 to compare sol-gel-derived powder fuels with similar arc-cast powder fuels and pelletized fuels. Burnup values and fission-gas release data are compared in Table 7.2.

The irradiation performance of all three fuel types is comparable according to the results of these tests. There are some variations in the fission-gas release rates. These may be associated with variations in the test conditions over the prolonged exposure periods. The similarity in performance and the effects of extended burnup have been discussed previously.^{2,4-6}

Table 7.1. Thorium Fuel Cycle Program Powder-Packed Rods Currently Being Irradiated or Being Examined^a

Designation	Number of Rods	Type of Oxide	Density (% of Theoretical)	Fuel Rod Dimensions (cm)			Linear Heat Rating (w/cm)	Peak Burnup (Mwd per tonne of metal)	Objective	Status
				Length	OD	Wall				
MTR-II	2	Sol-Gel S ThO ₂ -4.5% UO ₂ Vi-Pac	88 to 89	57	0.8	0.06	600	100,000	Obtain higher heat rating by increasing enrichment	Being examined
MTR-III	6	Sol-Gel 35 ThO ₂ -4.5% UO ₂ Vi-Pac	86 to 89	30	1.1	0.06	820	100,000	Compare oxide calcining atmospheres and higher heat ratings obtained by increasing diameter	In reactor
ETR-II	6	BNL Sol-Gel ThO ₂ -4% ²³³ UO ₂ Vi-Pac	90	48	1.3	0.09	630	30,000 to 100,000	Study effects of remote fabrication and oxide recalcining	1 Being examined 5 In reactor
ETR-III	7	Sol-Gel ThO ₂	88	48	1.3	0.09	770	10,000 to 70,000	Study ThO ₂ blanket material with gradually increasing heat rating and provide high-protactinium low-fission-product material for chemical processing	3 Rods in process 4 Rods in reactor
ETR-IV	6	Sol Gel	84	24	1.3	0.09	650 to 7000	20,000 to 100,000	Study sol-gel ThO ₂ -PuO ₂ microsphere performance as vibratorily compacted beds at various heat ratings and burnup levels	In reactor
Sphere-Pac	4	Sol-Gel ThO ₂ -5% PuO ₂ Sphere-Pac	84	19	0.64	0.025	650 to 1000	10,000	Test sol-gel ThO ₂ -PuO ₂ microspheres with high cladding temperatures	Being examined
Pellet Rods	3	ThO ₂ -4.5% UO ₂	91	11.4	0.79	0.06	400	150,000	Investigate swelling and gas release of ThO ₂ -base fuels at very high burnup	Being examined

^aETR-II, ETR-III, and ETR-IV rods are clad with Zircaloy-2; all other fuel rods are clad with type 304 stainless steel.

Table 7.2. Comparative Operating Conditions for Various ThO₂-UO₂ Fuels (MTR-I Group)

Fuel	Fuel Form	Irradiation Time (Reactor Full Power Days)	Maximum Burnup		Time-Averaged Peak Linear Heat Rating (w/cm)	$\int_{T_o}^{T_c} kd\theta$ (w/cm)	⁸⁵ Kr Release (%)
			(fissions/cm ³)	(% FIMA)			
			$\times 10^{20}$				
Arc-fused ThO ₂ -4.5% UO ₂	Vi-Pac ^a	110	2.5	1.2	299	33.8	2.4
	Vi-Pac	376	8.6	4.2	297	33.7	7.2
	Vi-Pac	707	14.4	7.1	267	31.6	6.4
Sol-gel ThO ₂ -4.5% UO ₂	Vi-Pac	110	2.9	1.4	341	37.8	0.5
	Vi-Pac	375	8.2	4.0	286	32.8	13.2
	Vi-Pac	691	16.5	8.1	311	34.6	17.0
	Vi-Pac	1107	26.4	12.5	303	34.2	2.6
Pressed and sintered ThO ₂ -4.5% UO ₂	Pellet ^b	905	26.4	12.0	420	44.8	22.8
	Pellet	660	21.1	9.6	461	48.2	12.4
	Pellet	497	8.1	3.7	270	31.5	c
	Pellet	406	11.0	5.0	394	42.6	c

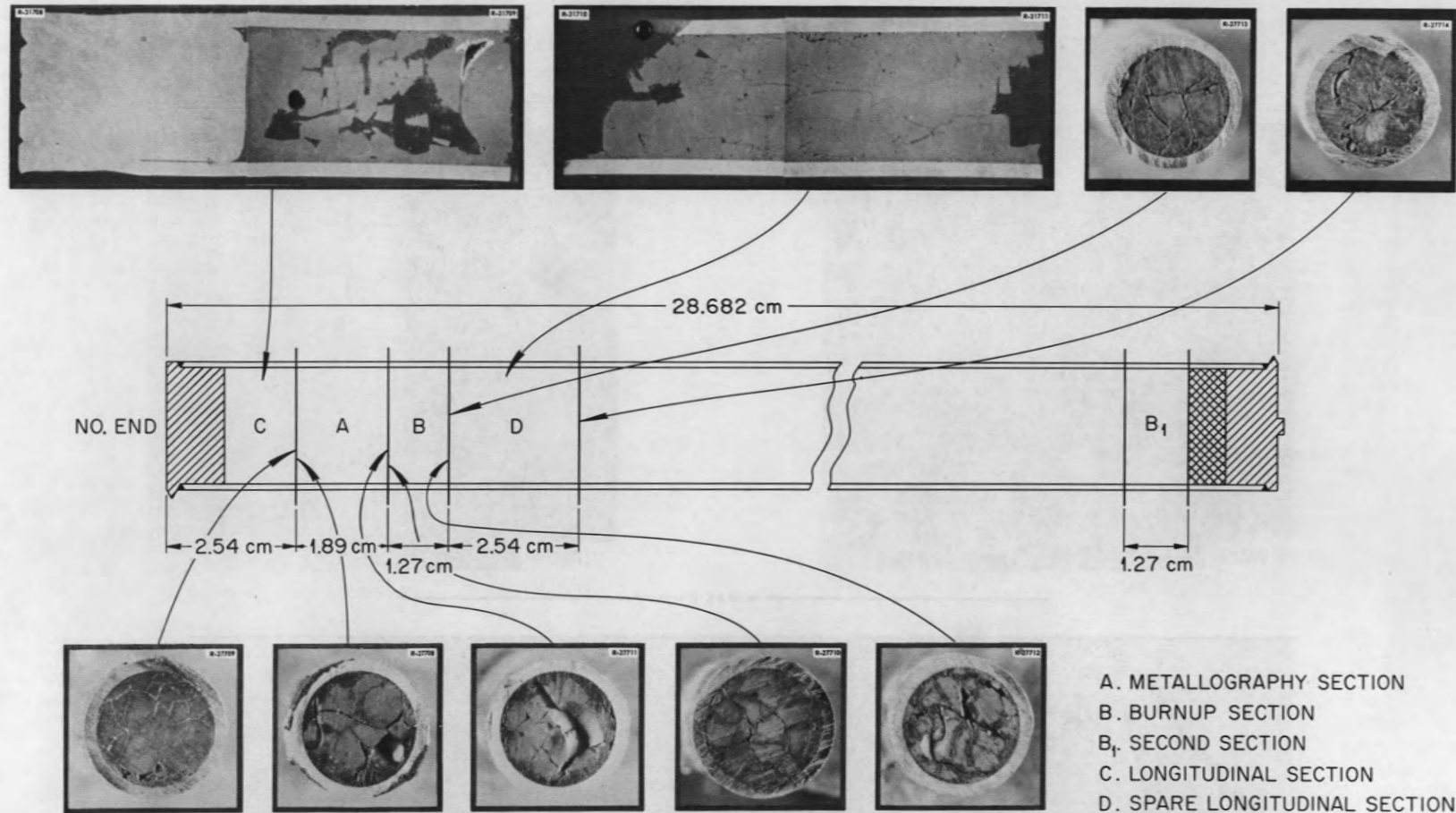
^aVibratorily compacted to a density 85 to 87% of theoretical.

^bPellets pressed from coprecipitated powders and sintered to 93% of theoretical density.

^cGas samples diluted with air in sampling and partially lost.

One striking feature has been a macrostructural phenomenon. At the operating conditions of these tests the fuel temperatures are such that sintering and grain growth occur initially in the center. Under the cyclic operating conditions, this leads to the formation and gradual migration of a circumferentially oriented crack in the fuel. At low burnup this crack is near the fuel center, and it moves out toward the cladding as burnup progresses. In the latest test examined, the compacted powder sol-gel fuel had sintered all the way out to the cladding. This can be seen in the macroscopic views shown in Fig. 7.1. This condition exists throughout the length of the fuel column from the peak burnup section at 126,000 Mwd/MT of metal (26.4×10^{20} fissions/cm³) to the low burnup end at only 24,000 Mwd/MT of metal. This suggests that the sintering is not strongly influenced by burnup but that it is strongly dependent on the time at operating temperatures.

A composite photomicrograph of the fuel from the high-burnup end of this rod is shown in Fig. 7.2. This shows not only the sintering but also the more or less uniform distribution of porosity from the surface to the center of the fuel. Previous tests with this fuel material had indicated a growth of equiaxed grains in the fuel center area. We did not observe an equiaxed grain growth region in the fuel of this very-high-burnup rod. Although no clear explanation of this difference is available, the widespread internal porosity in the fuel and the low gas release values indicate that low central fuel temperatures prevailed during the later stages of irradiation. Lower temperatures would not only reduce the rate of grain growth, but would also allow trapped fission-gas bubbles to disrupt any previously established grain structure. A similar distribution of porosity and lack of grain growth was seen in the highest burnup pelletized fuel rods examined to date, but the gas release was an order of magnitude higher. Examination of some of the sol-gel powder-packed rods and the very-high-burnup pellet rods should provide a better understanding of these structural changes.



MTR Group I, Capsule U-5, Macroscopic Views of Selected Section Locations, as Cut.

Fig. 7.1. Sections of Irradiated $\text{ThO}_2\text{-UO}_2$ Rod Made by Compacting Sol-Gel Powder.

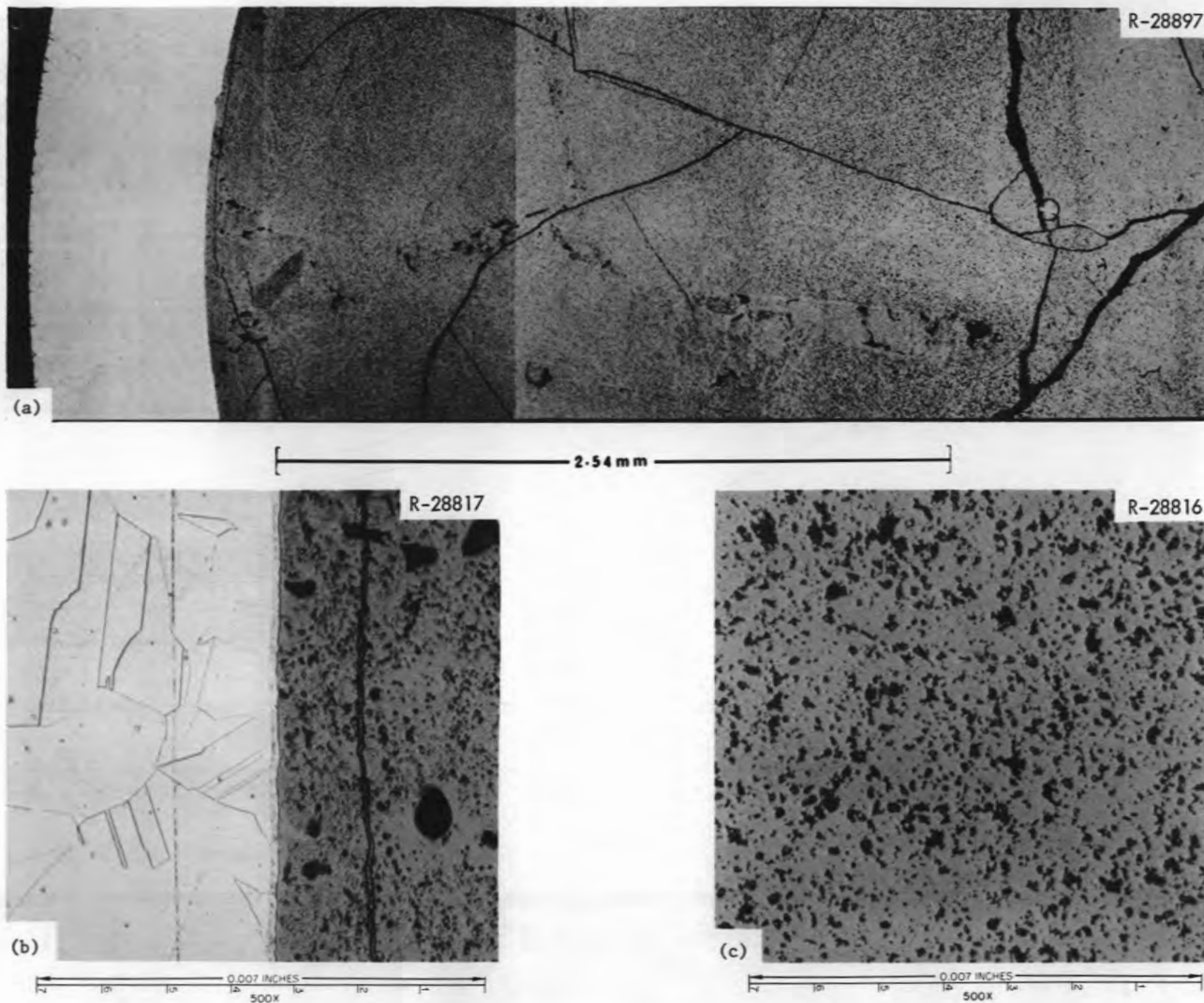


Fig. 7.2. Transverse Section of Vibratorily Compacted Sol-Gel ThO_2 -4.5% UO_2 Irradiated to 26.4×10^{20} fissions/cm³ (125,000 Mwd/MT metal). (a) Composite showing radial area from the cladding to the center of the fuel. (b) Typical fuel-cladding interface. (c) Fuel central region.

Effects of Higher Heat Ratings and Calcining Atmospheres

The effects of higher heat ratings during irradiation and the influence of processing variables such as fuel firing atmospheres are being studied in a series of tests. The results of very high heat ratings from ETR group I tests at 1000 w/cm were discussed previously.⁷ Two rods, constituting the MTR-II group, were operated at intermediate linear heat ratings of 600 w/cm to a burnup of 100,000 Mwd/MT of heavy element. These rods were removed from the reactor in December 1966 and are scheduled for examination early in 1967.

None of the fuel rods from MTR group III, which contain sol-gel powder-packed fuels fired in air, nitrogen, or Ar-5% H₂ have attained the scheduled burnup levels. These rods will provide information on the effects of the calcining atmosphere used in the sol-gel-process firing stage. All rods in this group have attained burnup levels in excess of 60,000 Mwd/MT of metal and are functioning without incident.

Performance of Remotely Fabricated Fuel Rods

At the end of the Kilorod Program, to demonstrate semiremote fabrication of vibratorily compacted (²³³U,Th)₂O₂ fuel rods,^{8,9} we fabricated a group of irradiation test rods in the Kilorod facility. We inserted six of these rods in the Engineering Test Reactor as irradiation test group ETR II. The details of the fabrication procedures and preirradiation examinations have been reported elsewhere.¹⁰

We are currently examining one of these rods - experiment 43-83. This experiment failed in the reactor after a peak unperturbed dose of 20×10^{20} neutrons/cm². The peak burnup in this rod, which operated at a time-averaged linear heat rating of 690 w/cm, was 21,000 Mwd/MT of metal, about 70% of the scheduled exposure. The failure apparently occurred in the gas plenum region about 1 in. below the top weld and approximately 2 in. above the fuel column. We probably cannot precisely determine the cause of failure, since the rod was severely damaged in postirradiation handling at the reactor site. The top end plug weld was sheared, and the plug was forced down into the gas plenum region, causing additional fracture of the tube wall. The microstructure of the

Zircaloy-2 at the failure area shows a normal hydride content. The only unusual feature seems to be a relatively high concentration of twinning in localized regions, indicating possibly a postanneal straightening operation during tube fabrication. Examination of other tubing from the same lot of material showed similar areas, although somewhat reduced in extent.

Macroscopic examination of sections through the fueled portion of the rod showed no unusual features that might have caused the failure. However, in preparing one of these sections for metallographic examination we discovered a crack in the Zircaloy-2 cladding. When first noted, it was located only midway through the cladding. Subsequent polishing revealed a crack extending from the inside surface 90% of the way through the cladding. There is no evidence of reaction products or other peculiarities in the fuel adjacent to the crack. This cladding failure may be a result of the severe mechanical stressing during postirradiation handling.

Although the examination of this rod is not complete, it now appears that the failure resulted from a spot in the cladding with undetected poor corrosion resistance. The fact that the other five rods in this group are still in the reactor and performing without incident at peak unperturbed exposure levels in excess of 33×10^{20} neutrons/cm² tends to support this preliminary conclusion.

Tests of (Th,Pu)O₂ Sol-Gel-Derived Fuels

The use of plutonium from current power reactor fuels has been proposed for the fissile enrichment in thorium-base fuels. The advantages offered are potentially both economical and technological. Pending the development of fast breeder reactors, plutonium may be less expensive than highly enriched ²³⁵U. In addition, bred ²³³U can be separated from the plutonium during reprocessing; thus the ²³⁶U contamination associated with ²³⁵U fissile enrichment is avoided.

We have previously¹¹ tested, with some success, sol-gel-derived thoria shards mixed with PuO₂ powder in vibratorily compacted fuel rods. The development of a sol-gel process for PuO₂ has made possible a sol-gel-derived (Th,Pu)O₂ fuel.

We are currently completing the fabrication of six irradiation test rods, ETR group IV, in which sol-gel ThO_2 -5% PuO_2 microspheres are being loaded by the Sphere-Pac process (Chap. 6). These rods will be 0.500-in.-diam x 0.035-in.-wall Zircaloy-2 tubes containing a 6.75-in. fuel column. These tests are scheduled for insertion in the ETR early in 1967 under conditions outlined in Table 7.3.

Irradiation Testing of Sol-Gel-Derived Urania-Base Fuels

The versatility of the sol-gel process in producing a variety of different forms for fuel rod fabrication and the resultant intimate mixtures of components make it a potential process for producing $(\text{U,Pu})\text{O}_2$ fuels for fast reactors.

We began a series of noninstrumented screening irradiation tests on sol-gel-derived $(\text{U,Pu})\text{O}_2$ fuels. Although our program will eventually include all of the fabrication processes discussed in Chap. 6, the initial tests will investigate the performance limitations of sol-gel microspheres fabricated into test rods by the Sphere-Pac process. The first two capsules in this series of tests, identified as 43-99 and 43-100, contained both $(\text{Th,Pu})\text{O}_2$ and $(\text{U,Pu})\text{O}_2$ fuels.

The new capsule design shown in Fig. 7.3 permits operation with low cladding restraint and surface temperatures on the cladding between

Table 7.3. Irradiation Conditions Planned for Sol-Gel-Derived ThO_2 -4% PuO_2 , Test Group ETR-IV

Experiment	Peak Linear Heat Rating (w/cm)	Peak Target Burnup (Mwd/MT of metal)
106	650	20,000
107	1000	20,000
108	850	50,000
109	1000	100,000
110	850	100,000
111	650	100,000

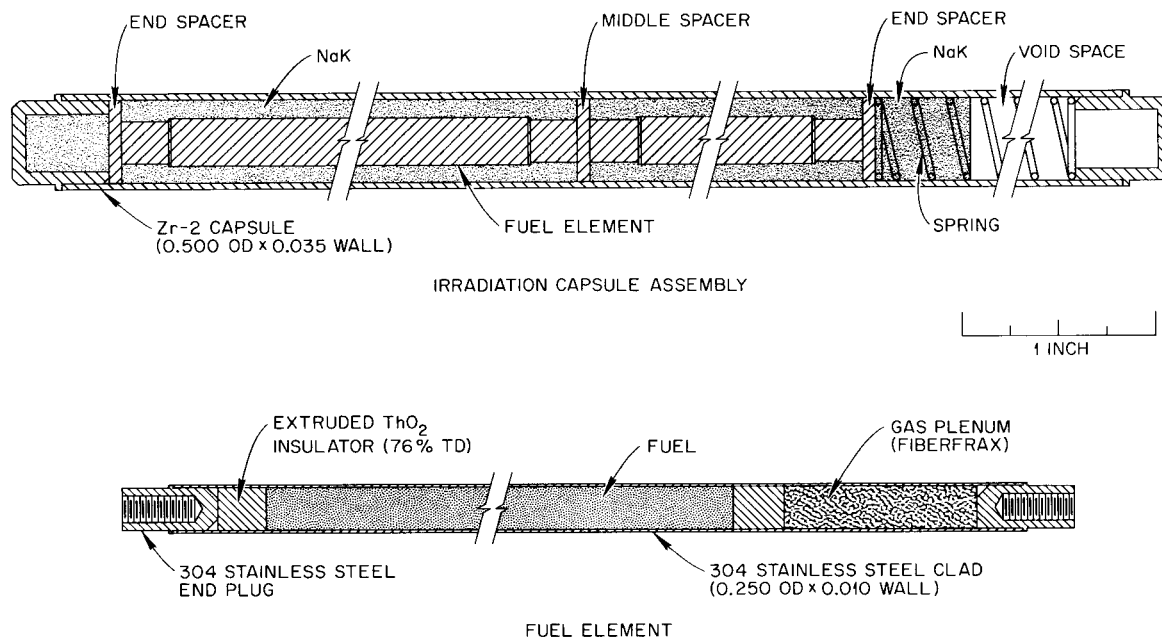


Fig. 7.3. Capsule for Irradiation Tests.

450 and 600°C. Four fuel rods are in each capsule, separated by stainless steel spacers. Capsules 43-99 and 43-100 were loaded identically, as shown in Table 7.4. The sol-gel fuel characteristics are shown in Table 7.5. Both capsules were inserted in separate X-basket positions in the ETR at the start of cycle 85. The maximum linear heat rating, which occurs in the 93%-enriched U-20% Pu fuel, was calculated to be 650 w/cm. On December 13, 1966, near the end of ETR cycle 85, capsule 43-99 failed. The reactor history just before the failure included 16 continuous days of full-power operation, interrupted by a short zero-power cycle and a return to full power for 2 hr. The reactor operators report that the failure was abrupt. Cooling water analyses indicated essentially total loss of NaK and failure of a rod containing $(\text{Th}, \text{Pu})\text{O}_2$ but no $(\text{U}, \text{Pu})\text{O}_2$. A limited preliminary examination of the capsule in the Idaho hot cells revealed a 1/8-in.-diam hole in the Zircaloy capsule wall some 16 in. from the bottom of the capsule. This would place the failure near the middle spacer between fuel rods 2 and 3. The rest of the capsule appeared to be in excellent condition. Further examination

Table 7.4. Vibratorily Compacted Fuel Rods for Irradiation Capsules 43-99 and 43-100

Rod	Irradiation Capsule and Position ^a	Fuel Material	Fuel Height (in.)	Average Fuel Density ^b (g/cm ³)	Fuel Density Variation ^c (% , <u>±</u>)
2	43-99-2	(Th-5% Pu)O ₂	3.15	8.40	2
3	43-99-4	(Th-5% Pu)O ₂	3.16	8.38	1
4	43-100-2	(Th-5% Pu)O ₂	3.13	8.45	1
5	43-100-2	(Th-5% Pu)O ₂	3.15	8.39	1.5
7	43-99-3	(U-20% Pu)O ₂	3.14	8.38	1
8	43-99-1	(U-20% Pu)O ₂	3.13	8.41	4
9	43-100-1	(U-20% Pu)O ₂	3.14	8.39	1
10	43-100-3	(U-20% Pu)O ₂	3.13	8.39	1

^aLast number indicates position in capsule numbered from bottom up.

^bCalculated from height, weight, and inside diameter of cladding.

^cDetermined by transmission gamma scan along fuel rod.

Table 7.5. Characteristics of Sol-Gel Fuel for Capsules 43-99 and 43-100

Material	Sphere Size (μ)	Density		Surface Area (m^2/g)	Carbon (ppm)	Gas Release at 1200°C (cm^3/g)
		(g/cm^3)	(% of theoretical)			
ThO ₂ -5% PuO ₂	420-590	9.84	97.7	0.015	< 10	0.04
ThO ₂ -5% PuO ₂	< 44	a		0.17	a	0.24
UO ₂ -20% PuO ₂	420-590 ^b	10.54	95.3	0.02	< 10	0.15
UO ₂ -20% PuO ₂	< 44	8.99	81.3	0.03	< 10	0.42

^aData not available.

^bRod 10 contained a coarse size fraction of 85.5% of 420- to 590- μ spheres and 14.5% of 290- to 420- μ spheres.

at the Idaho hot cells could not be performed because they are not equipped for safe plutonium handling. The capsule has been placed in a sealed heavy-walled aluminum pipe, and arrangements are being made to ship it to ORNL as soon as possible for detailed examination.

Since no plausible explanation for the failure is immediately apparent, continued irradiation of the duplicate capsule 43-100 has been deferred, even though it appears to have performed well and there is no indication of an incipient failure.

Additional capsules in this series will have outer tubes of type 304 stainless steel. Although this aggravates the flux perturbation, the problems associated with autoclave testing of Zircaloy-2 with this capsule design and the unexplained failures of experiments 43-83 and 43-99 justify the use of a material less sensitive to contamination-induced water corrosion.

REFERENCES

¹R. G. Wymer and D. A. Douglas (compilers), Status and Progress Report for Thorium Fuel Cycle Development Dec. 31, 1964, ORNL-3831, pp. 82-116.

²A. R. Olsen, J. W. Ullmann, and E. G. Manthos, Status and Progress Report for Thorium Fuel Cycle Development Dec. 31, 1965, ORNL-4001, pp. 102-112.

³S. A. Rabin, J. W. Ullmann, E. L. Long, Jr., M. F. Osborne, and A. E. Goldman, Irradiation Behavior of High-Burnup ThO₂-4.45% UO₂ Fuel Rods, ORNL-3837 (October 1965).

⁴A. R. Olsen, W. O. Harms, D. B. Trauger, R. E. Adams, and D. A. Douglas, "Irradiation Behavior of Thorium-Uranium Alloys and Compounds," pp. 246-291 in Utilization of Thorium in Power Reactors, Report of a Panel Held in Vienna 14-18 June 1965, International Atomic Energy Agency, Vienna, 1966; ORNL-TM-1142 (June 1965).

⁵A. R. Olsen, D. A. Douglas, Y. Hirose, J. L. Scott, and J. W. Ullmann, "Properties and Prospects of Thoria-Based Nuclear Fuels," Proc. Brit. Ceram. Soc. 7, 289-310 (February 1967); ORNL-TM-1297 (November 1965).

⁶A. R. Olsen, J. H. Coobs, and J. W. Ullmann, "Current Status of Irradiation Testing of Thorium Fuels at Oak Ridge National Laboratory," pp. 475-494 in Proceedings of the Second International Thorium Fuel Cycle Symposium, Gatlinburg, Tennessee, May 3-6, 1966, USAEC, Oak Ridge, Tenn., 1968; ORNL-TM-1631 (September 1966).

⁷A. R. Olsen, J. W. Ullmann, and E. G. Manthos, Status and Progress Report for Thorium Fuel Cycle Development Dec. 31, 1965, ORNL-4001, pp. 102-112.

⁸R. G. Wymer and D. A. Douglas (compilers), Status and Progress Report for Thorium Fuel Cycle Development Dec. 31, 1964, ORNL-3831, pp. 1-32.

⁹J. E. Van Cleve, Jr., and A. L. Lotts, "Operating Experience in a Semi-Remote Facility for Fabrication of Fuel Rods Containing $(U^{233}, Th)O_2$," pp. 257-271 in Proceedings of the 12th Conference on Remote Systems Technology, American Nuclear Society, Hinsdale, Illinois, 1964.

¹⁰J. D. Sease and A. R. Olsen, Fabrication Procedures and Pre-irradiation Data for $(Th, ^{233}U)_2$ -Bearing Irradiation Rods, ORNL-TM-1461 (May 1966).

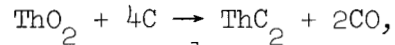
¹¹A. R. Olsen, W. O. Harms, D. B. Trauger, R. E. Adams, and D. A. Douglas, "Irradiation Behavior of Thorium-Uranium Alloys and Compounds," pp. 246-291 in Utilization of Thorium in Power Reactors, Report of a Panel Held in Vienna 14-18 June 1965, International Atomic Energy Agency, Vienna, 1966; ORNL-TM-1142 (June 1965).

8. ADVANCED SOL-GEL STUDIES

K. J. Notz R. L. Hamner W. D. Bond

Preparation of Thorium and Uranium Carbides

Thorium dicarbide can be prepared by the reaction



which is thermodynamically possible¹ above 1430°C at a carbon monoxide pressure below 1 torr. Sol-gel processes under study this past year utilize the above reaction in two ways. In one, dense thoria microspheres are prepared by the usual sol-gel procedure, and then reacted with graphite in a rotating kiln. In the other, thoria and carbon black are combined at the sol stage, then converted to microspheres, and finally caused to react in a suitable furnace. The former method yields a dense product at reaction temperatures near 2150°C, provided the initial carbon content (picked up during sphere formation) is low enough.² The high temperature is required for kinetic reasons, since the process is limited by the rate of diffusion through the dense thoria core and through a dense layer of carbide product. The second method will obviously be far more favorable kinetically, since the carbon and thoria are intimately blended. Both methods are discussed below.

Preparation of ThC₂ Microspheres by Thoria-Carbon Sol Route

Initial work by Kelly, Kleinstaubler, Clinton, and Dean³ showed that carbon black could be incorporated in thoria and thoria-urania sols and the resulting mixed sols formed into microspheres and converted to ThC₂ or (Th,U)C₂ by firing at 1600 to 1750°C under vacuum or in flowing argon. Their feasibility study suggested that the major problems involved in perfecting this process would include minimizing the free carbon content, decreasing the porosity, and attaining a high density. The present work was begun late in 1965, and the early results have been summarized.⁴ This early work affirmed that although reasonably pure ThC₂ could be made by this process, serious problems would be encountered in minimizing free carbon content, residual oxygen, and porosity.

The principal result this past year was the development of a technique that yielded ThC_2 microspheres denser than 90% of theoretical by starting with a gel of an oxide and carbon black. The two critical factors are the use of small microspheres and slow chemical conversion at a critical sintering temperature. To achieve the proper balance between conversion rate and sintering, the reaction is carried out at 1950 to 2000°C under argon until nearly complete and then finished under vacuum. With large spheres and especially with shards the shrinkage pattern is disrupted and large voids appear in the product. Likewise, conversion under vacuum, which occurs at about 1600°C, yields a very porous carbide. Thus, the major potential advantage of the mixed sol route, namely, a much lower reaction temperature, cannot be fully realized in practice. However, a temperature reduction of about 200° can still be realized over the reaction of sintered oxide with graphite, if 7 to 9% porosity (most of it closed) can be tolerated.

Preparation of Carbon-Thoria Sols. — As explained in a later section of this chapter, thoria sols act both as dispersant and stabilizer for carbon blacks. Although both acidic and alkaline carbons are dispersed equally well by thoria, the former yield a more permanent mixed sol; some of the older preparations have been on hand for over a year and are still stable, whereas the alkaline carbons give mixed sols that tend to gel and become lumpy within a week or so. The surface area of the carbon black is not important except for extremes in both directions: if the surface area is very high ($>1000 \text{ m}^2/\text{g}$), the mixed sol is too viscous; if very low ($<30 \text{ m}^2/\text{g}$), the mixed sol is difficult to prepare. For handling convenience, pelletized carbon black is much preferred over the fluffy form. A very suitable carbon black for the present purpose is Spheron 9 (Cabot Corp.). This is a channel black with a specific surface area of $105 \text{ m}^2/\text{g}$, a nominal volatile content of 5%, and an aqueous pH of 4.5.

During the blending process the carbon black pellets must be broken up to the surface area aggregates (see Chap. 9). After the carbon is separated to this degree, the thoria sol acts as a dispersing agent, promoting further separation of the carbon into individual crystallites. Three blending methods have been tested: recirculation through a centrifugal pump recycle loop, ball milling, and ultrasonic agitation. Ultra-

sonic agitation was the most successful. This method had been used earlier to prepare urania-carbon sols.⁵ In the present preparations, a Branson model S-110 sonic generator, with a power output of about 110 w at 20 kHz, achieved good blending of 100-ml batches in about 7 or 8 min. During this time, the dissipated energy heats the sol, and if external cooling is not applied the temperature of the sol rises to about 60 or or 70°C. As long as the sol itself is not heat sensitive, this temperature rise aids the dispersal a little.

Conversion of Oxide Shards to Carbide. - Although the objective of this program is to produce dicarbide microspheres, we felt that a logical approach was to first work with shards, thereby temporarily avoiding the added difficulties associated with sphere forming. We used gel fragments to study empirically the effects of carbon-to-thoria ratio, atmosphere, and temperature on the carbide product. It was soon apparent that gross porosity in the product was a major problem. Figure 8.1 shows the size of the holes present in a typical ThC_2 product prepared from shards. Mixed sols prepared by other blending methods and with different carbon blacks yielded similar products.

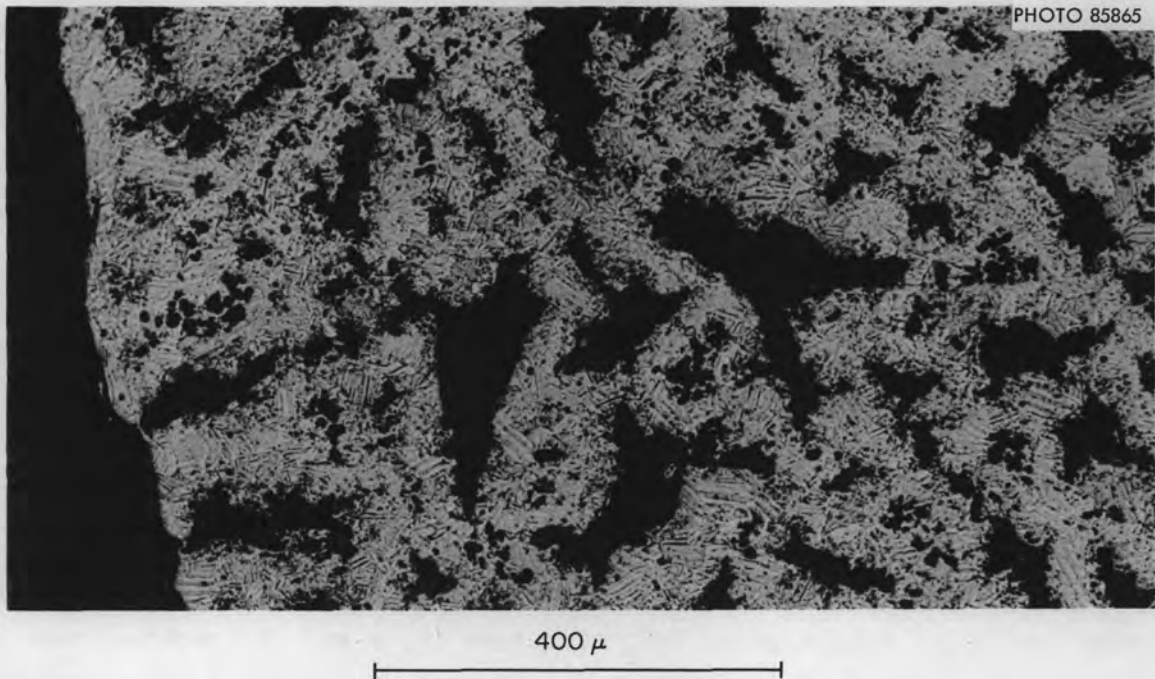


Fig. 8.1. ThC_2 Shard Showing Gross Porosity.

It should be noted that incorporation of carbon in thoria sol-gel practically guarantees a porosity problem. As little as several parts per million of carbon present in dense thoria causes objectionable porosity in carbide made from the sintered oxide and graphite.² Also, in a study related to the oxide-carbon black-gel process, up to 65% porosity was deliberately introduced in sintered thoria through the use of carbon (see later section of this chapter). Therefore, a more reasonable goal for the production of ThC_2 by the oxide-carbon black-gel process is to minimize and control porosity, rather than to eliminate it completely.

Even though shards give a physically unacceptable carbide because of gross porosity, we obtained useful data from shards. Minimum conversion temperatures for both argon atmosphere and vacuum were determined, as shown in Table 8.1. "Soluble Thorium" is a measure of the degree of conversion, since the carbides dissolve in nitric acid but ThO_2 does not. Under argon, complete reaction requires a temperature of at least 1950°C; at 2050°C or above sintering becomes objectionable. Thus, 2000°C is the optimum temperature under argon. At 1550°C no significant reaction had occurred, even after 4 hr. The chemical analyses on the vacuum runs appear to be questionable; however, it seems clear that a minimum temperature of about 1600°C is required. The superior conversion on the 1570°C sample suggests that temperature cycling may be beneficial. Pore volume and pore size distribution measurements (by mercury intrusion) on the vacuum series samples show two interesting trends. The total pore volume remains more or less constant during conversion to carbide, the values being 23, 16, 24, 27, and 16%, respectively, at 1480, 1570, 1680, 1780, and 1900°C; but the size distribution shifts drastically from 100-1000 Å to 1-20 μ between 1480 and 1570° (i.e., as conversion nears completion). Conversion under vacuum also seems to encourage retention of more free carbon than conversion under argon, which in turn causes a higher proportion of monocarbide in the final product.

On 11 other carbide conversions of shards, complete chemical analyses (thorium, oxygen, total carbon, and free carbon) of the products were obtained. Single-phase ThC_2 structure (by x-ray diffraction) was achieved when the ratio of thorium to combined carbon was 1.85 or greater; the maximum thorium-to-carbon ratio found was 1.87. These values are

slightly lower than the lower phase limit of 1.88 to 1.91 reported by Bradley and Ferris,⁶ but this may be caused by the relative insensitivity of x-ray diffraction for detecting minor phases. We encountered problems in getting reliable free-carbon determinations, but in general the free-carbon content was about 400 ppm when ThC was also present and higher than that (up to 7000 ppm) in the single-carbide-phase products. The residual oxygen contents ranged between 200 and 1100 ppm.

Table 8.1. Conversion of ThO₂ Shards to Carbide

Reaction		Chemical Analyses (%)		X-Ray Diffraction ^a		
Temperature (°C)	Time (hr)	Free Carbon	Soluble Th	ThO ₂	ThC	ThC ₂
<u>Under Argon</u>						
1550	4	11.8	0.05	P		
1750	3	10.2	8.62	P		wk
1850	2.5	5.4	44.65	P		wk
1950	1	0.10	83.69		wk	P
2050 ^b	1	0.11	89.59		wk	P
2150 ^c	1	1.82	87.02			P
<u>In Vacuum</u>						
1480	6	3.25	53.1	P		P
1570 ^d	3.5	0.21	74.3	P	P	P
1680	3	1.28	63.3		P	P
1780	2	1.10	69.8		P	P
1900	2	1.07	71.2		P	P

^aP indicates phase present; wk indicates phase was only weakly observed.

^bProduct was lightly sintered.

^cProduct was partially fused. The high free-carbon content is due to reaction with the crucible.

^dDue to power failure, this run was cooled and then reheated.

Since thoria sols contain nitrate, the reaction between carbon and nitrate is of interest because it will influence the effective carbon-to-thoria ratio. Preliminary experiments, which simulated the reaction conditions existing in carbon-thoria gels, showed that the stoichiometry of the carbon-nitrate reaction is a function of the manner in which the nitrate is present. Nitrate in three forms [NH_4NO_3 , HNO_3 , and $\text{Th}(\text{NO}_3)_4$] was added to carbon-thoria sols, which were then dried to gels and heated to 400°C under argon. The residues were analyzed for their remaining carbon, from which the carbon-to-nitrate reaction ratio was calculated. For nitrate present as NH_4NO_3 no carbon was consumed; the ammonium nitrate simply decomposed to water and nitrous oxide. With nitric acid, about one-third carbon atom was consumed per nitrate ion, and with thorium nitrate about $1\frac{1}{3}$. The lower reaction ratio with HNO_3 than with $\text{Th}(\text{NO}_3)_4$ is probably caused by the volatility of the acid at lower temperatures. Work on these reactions is continuing.

Conversion of Microspheres to Carbide. - Microspheres can be formed from mixed carbon-thoria sols in 2-ethyl-1-hexanol in a manner analogous to pure thoria sols, except that the choice of surfactant is more critical and, even under the most favorable conditions, some carbon "shedding" (loss of carbon to the organic phase) occurs. After testing a variety of surfactants, we found the optimum combination was 0.2 vol % Span 80 and 0.2 vol % Ethomeen S/15. The Span 80 controls clustering in the column but causes a rough surface on the spheres. Addition of the Ethomeen S/15 smooths the surfaces. Ethomeen S/15 alone partially controls clustering but not as well as Span 80. Typical spheres are shown in Fig. 8.2.

Once the gel beads have been formed and allowed to harden enough to handle (about 1 hr), further exposure to 2-ethyl-1-hexanol has no effect on either size or carbon-to-thoria ratio. Fresh beads were compared with some that had remained in contact with the solvent for three days. For two different sols, the respective carbon-to-thoria ratios were 4.19 vs 4.24, and 3.79 vs 3.79. The above sols were formed into beads of three sizes: 200, 300, and 400 μ . Aging in solvent for three days caused no detectable change in size. Drying at 110°C caused all three to shrink about 10 vol %. Firing at 1400°C caused a total

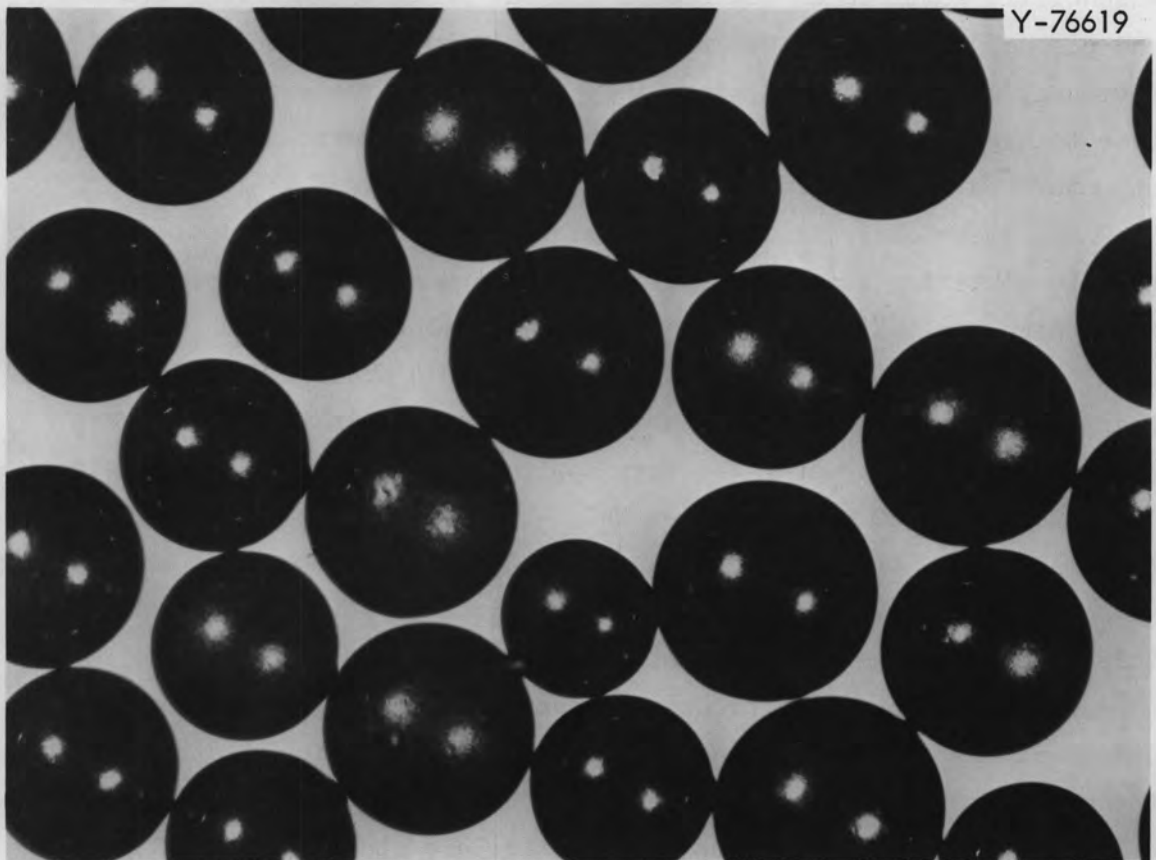


Fig. 8.2. Thoria-Carbon Microspheres Dried at 300°C. 33X.

shrinkage of 39 to 47 vol %, depending on the size. The smaller spheres shrank proportionately more, suggesting that for carbide conversion the smaller spheres are preferable, since they will be less porous at the start of the carbiding reaction.

Several trial conversions of microspheres to carbide showed that there was less porosity in spheres than in shards and that the smaller spheres were the least porous of all. Additional runs were then made, verifying that reasonably dense dicarbide microspheres can be made by this method. At first, we thought that the most favorable conditions for conversion would be a relatively low temperature, under vacuum, with temperature cycling (see Table 8.1, note d). This did not prove to be so. Seven trials were made at temperatures of 1600 to 1750°C under vacuum, using none, one, or two thermal cycles. Chemical reaction was

essentially complete in all cases, but the products were fine-grained and porous, with porosities ranging from 19 to 49%. These products were obviously under-sintered, since they "pop-corned" on exposure to air (due to high internal surface area) and showed a very fine-grained structure on the metallograph.

The above observations suggested the use of a higher temperature to promote sintering and the use of an argon atmosphere to retard the reaction rate. An infrared in-line CO analyzer (Beckman, model 315) was used to monitor the reaction, which took 1 to 4 hr at 1850 to 2050°C. Near the end of the reaction the CO concentration in the argon sweep gas dropped, and a vacuum was then applied to complete the conversion. The equilibrium CO pressure over $\text{ThC}_2 - \text{ThO}_2$ is about 1 atm at these temperatures.⁷ Under the conditions used for these runs, the argon sweep gas contained about 4000 ppm CO at steady state, which is controlled in this case by diffusion of CO out of the sample crucible.

From six such runs, products denser than 90% of theoretical were obtained. Results are summarized in Table 8.2. Taking⁸ 9.60 g/cm^3 as the density of ThC_2 , the observed particulate densities are 91 and 93% of theoretical. Since the open porosities are about 1%, closed porosities are about 6 to 8%. This is evident in cross sections (Fig. 8.3). (Since helium and mercury intrusion densities are the same within experimental error, there are no open pores in the range 5 to 120 Å either.) The crushing strength of these spheres is adequate for most purposes, although less than sometimes obtained with other sol-gel microspheres. The external appearance is not as uniform as would be desired (Fig. 8.4) and might be significant in terms of surface fine structure. Both oxygen and free carbon contents are reasonably low, and it may be difficult to decrease them much further. Considering only the five runs in Table 8.2 conducted at 1950°C or above, the free carbon ranged between 700 and 1900 ppm and oxygen between 300 and 1100 ppm. This aspect of the problem is currently under study.

In general terms, the explanation for the success of the firing method finally adopted must revolve about a critical balance between grain growth, sintering, and chemical conversion. First of all, the

Table 8.2. Properties of Thorium Carbide Microspheres

Run	II-146	II-148	II-150	III-14	III-16	III-18
Max. Temp., °C	2050	1950	1850	1975	1975	2030
Time at temp., hr	1	2.5	4	2.5	2.5	4 ^e
X-ray diffraction ^a						
ThO ₂	?	0	?	0	0	0
ThC	v wk	0	wk	v wk	v wk	v wk
ThC ₂	P	P	P	P	P	P
Thorium, %	90.93	91.25	90.88	91.23	91.23	91.45
Total C, %	9.09	8.74	8.85	8.57	8.52	8.65
Oxygen, %	0.096	0.045	0.360	0.033	0.032	0.106
Material balance	100.12	100.04	100.09	99.83	99.78	100.21
Free C, %	0.12	0.12	0.47	0.066	0.106	0.186
Value of x in ThC _x	1.92	1.83	1.83	1.81	1.79	1.80
Density, g/cm ³ ^b						
Particulate	> 8.75	8.83	8.75	> 8.91	> 8.76	> 8.97
Hg Intrusion	8.84	8.95	8.87	9.00	8.84	9.06
Helium				9.04	8.77	9.10
Open porosity, % ^c	< 1	1.3	1.4	< 1	< 1	< 1
Crushing strength, g ^d	700	790	940	800	700	

^aP indicates phase present; v wk, very weak; wk, weak; ?, may be present; 0, not detected.

^b"Particulate" density means the bulk density of single spheres; "Hg intrusion" density is the density after subtracting the volume occupied by mercury at 15,000 psi. The difference between these two values give the "open porosity" for pores larger than 120 Å. The helium density subtracts all pore volumes down to about 5 Å.

^cDefined in note b.

^dCorrected to 240 μ diameter, by assuming that crushing strength is proportional to the square of the diameter.

^eTemperature was gradually increased from 1700 to 2030°C during the 4 hr.

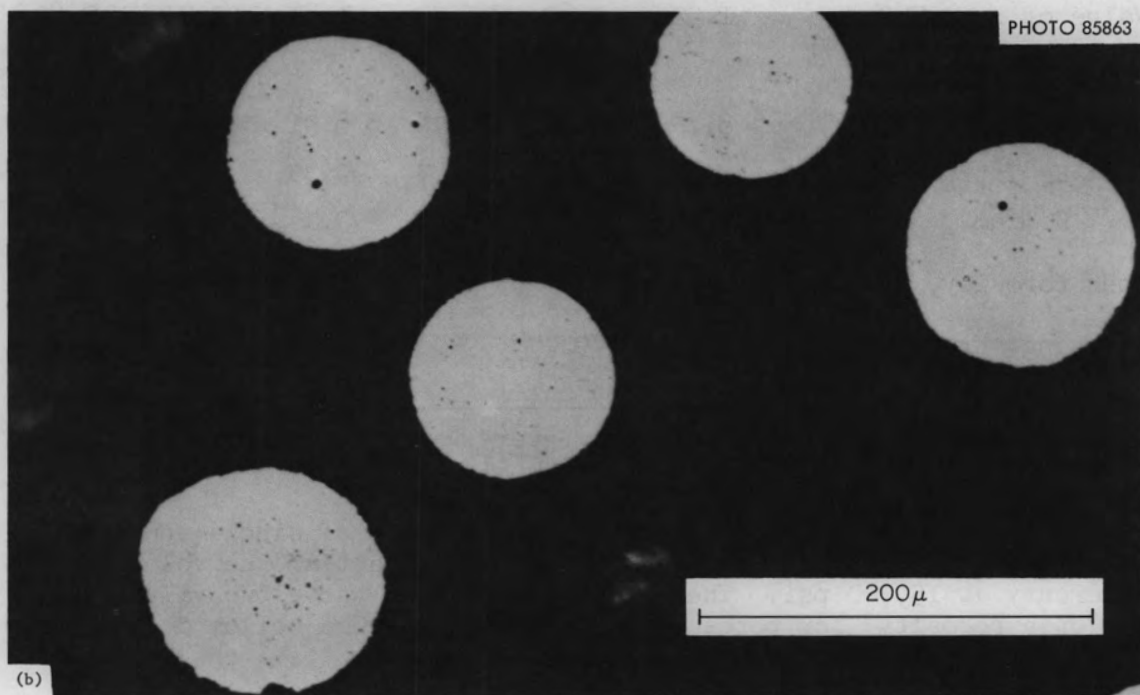
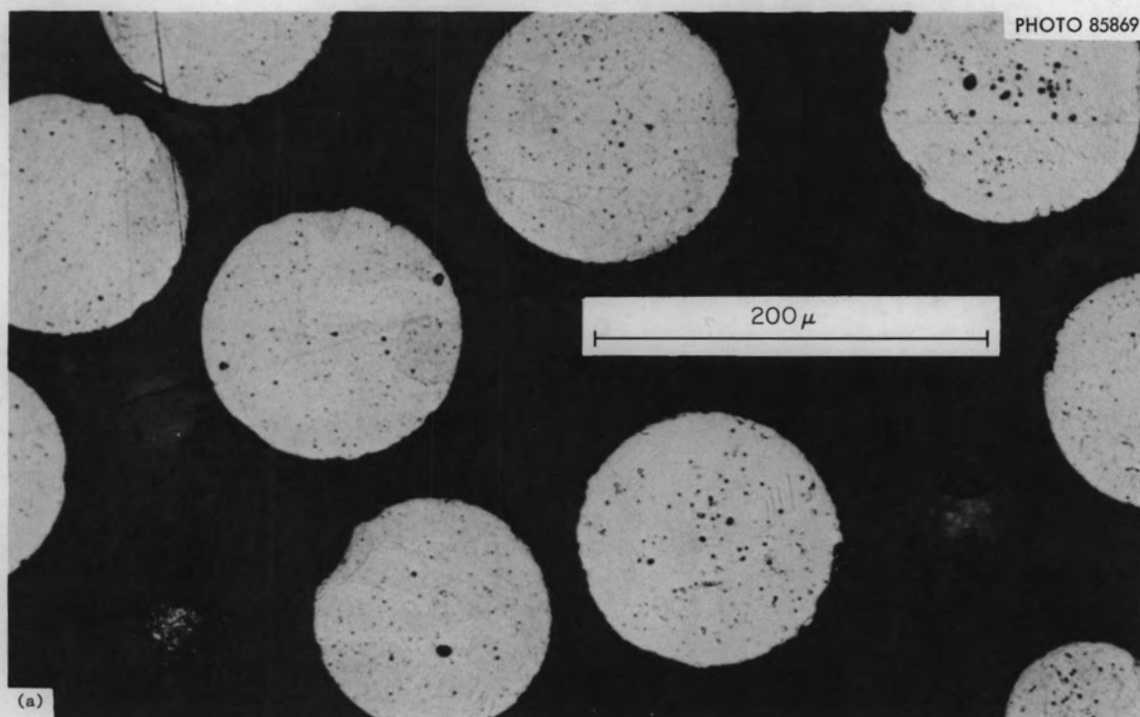


Fig. 8.3. Cross Section of ThC_2 Microspheres. (a) Fired 4 hr at up to 1870°C . (b) Fired 1 hr at up to 2050°C .

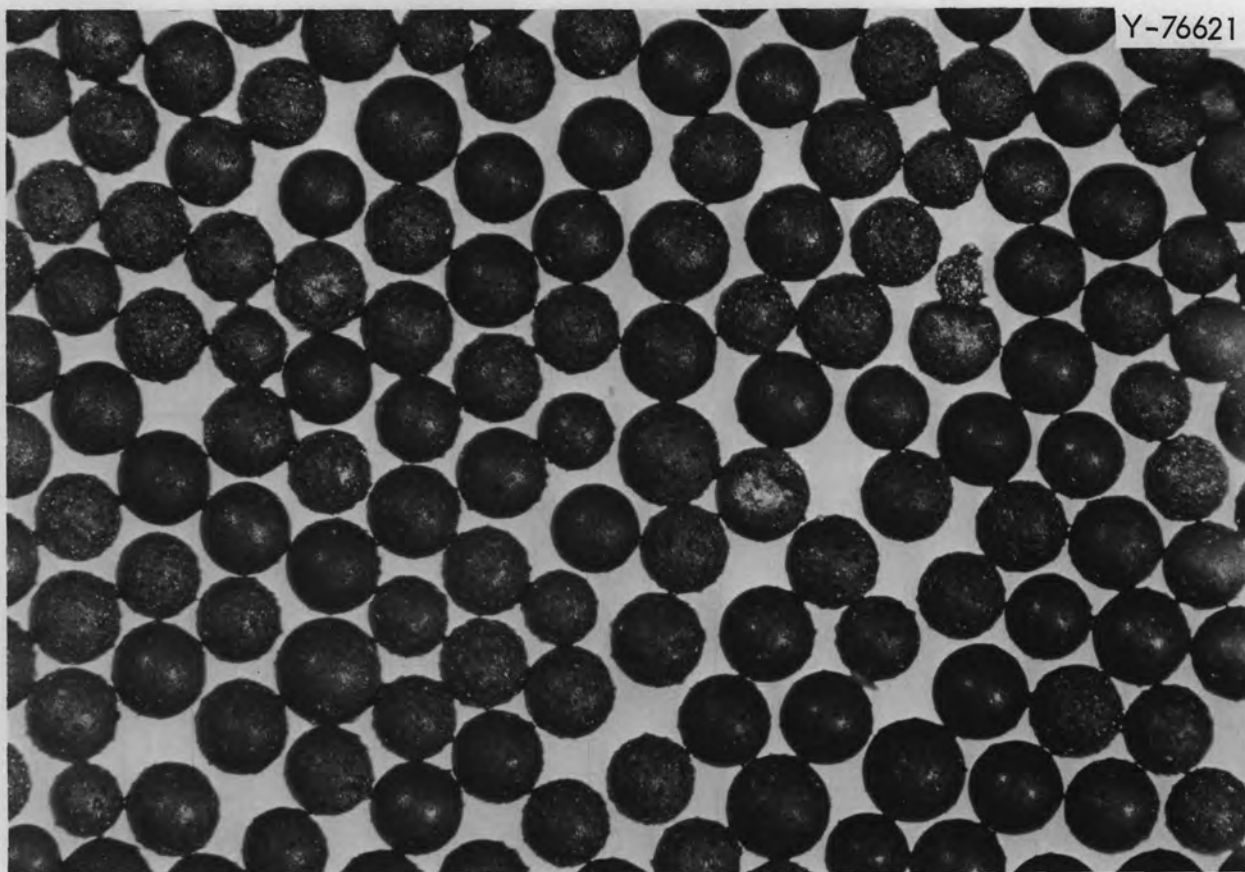


Fig. 8.4. ThC_2 Microspheres.

presence of the carbon greatly retards sintering of ThO_2 ; otherwise this method would not work at all (note, e.g., the permanent porosity left in dense thoria by small amounts of carbon⁹). If conversion to carbide occurs at too low a temperature, sintering of the grains establishes the outside dimensions, and further heating simply consolidates the small pores into large internal pores. Under a carbon monoxide overpressure of about 1 atm, conversion to carbide occurs at a temperature where grain growth is optimized, and the entire particle can shrink to a high density, provided the shrinkage path is not too long. The presence of carbon monoxide during this process may also facilitate grain growth by enhancing diffusion on the solid surfaces.

Preparation of ThC_2 Microspheres by Conversion of Sintered Oxide

The outlook for pyrolytic-carbon-coated UO_2 and $(\text{Th},\text{U})\text{O}_2$ microspheres as potential fuels for high-temperature gas-cooled reactors

continues to be favorable from the standpoint of chemical and radiation stability. However, we must still consider the possibilities of dicarbide fuels for this application and the simplest method for remotely preparing these fuels.

We showed in previous studies⁹ that dense ThC_2 and $(\text{Th,U})\text{C}_2$ microspheres could be prepared by heating dense sol-gel ThO_2 and $(\text{Th,U})\text{O}_2$ microspheres with equal weights of carbon at $2150 \pm 50^\circ\text{C}$; this was accomplished in a graphite crucible rotating at 40 rpm under a flowing argon atmosphere. We prepared hypostoichiometric UC_2 microspheres ($\text{UC}_{1.5}$) in the same manner at a lower temperature (2000°C), but these were porous because of the residual carbon (0.6 wt %) in the starting material.

In our continuing process studies, we were concerned primarily with further simplification of the conversion process. Also, we extended our studies to the preparation of UC microspheres from sol-gel UO_2 microspheres.

The sol-gel microspheres used as starting materials in our previous studies were calcined at 1150°C in air or argon for the removal of volatiles and for densification before conversion. A more efficient process would evolve if the sol-gel microspheres, after drying at 120°C , could be calcined to dense oxide particles and converted to dicarbide particles in the same environment in one operation.

We demonstrated that the combined calcination-conversion approach was feasible, using $600\text{-}\mu$ ThO_2 sol-gel microspheres, provided the heating rate did not exceed $230^\circ\text{C}/\text{hr}$ below a temperature of 700°C and the crucible did not rotate more than about one revolution per hour below a temperature of 1100°C . Excessive heating rates during calcining resulted in cracking of the particles. Excessive rotation of the crucible during the time required for calcination caused packing of carbon against the crucible walls; this reduced oxide-to-carbon contact and the amount of carbon available for particle separation, which, in turn, resulted in sintering of particles together and incomplete conversion of the particles to the dicarbide.

In the combined calcination-conversion process, carbon contained in the starting material is not removed during calcination in the argon

atmosphere and therefore will be present during conversion. We previously noted⁹ that appreciable quantities of residual carbon in UO_2 microspheres resulted in a porous product after conversion to carbide. To study further the effects of residual carbon on the final product, we converted 600- μ -diam sol-gel ThO_2 microspheres containing 1.5 wt % residual carbon to ThC_2 by the combined-operations process; for comparison, the carbon content of oxide particles from the same batch of starting material was reduced to 100 ppm by air calcination at 1000°C before conversion to carbide under the same conditions of time and temperature (6 hr at 2200°C). Metallographic examination (Fig. 8.5) of the products showed the high-carbon-content oxide particles to have much greater porosity after conversion than the low-carbon-content particles.

Conversion of UO_2 to UC

Uranium monocarbide microspheres are of interest for use in metal-clad fuel elements. Harder, Read, and Sowden¹⁰ prepared stoichiometric UC by low-temperature (850°C) hydrogen treatment of hyperstoichiometric UC powder. We are investigating the feasibility of preparing UC microspheres similarly from hypostoichiometric UC_2 .

We prepared $\text{UC}_{1.5}$ microspheres containing platelets of UC by heating UO_2 sol-gel microspheres with carbon at 2000°C. These particles were then heated in hydrogen for 24 hr at the prescribed temperature¹⁰ of 850°C. The treated particles had a dark gray crust of material that was badly cracked and tended to spall. We were unable to identify this material metallographically or by a Debye-Scherrer x-ray diffraction pattern. The unreacted cores of the particles were apparently unchanged by the hydrogen treatment.

Results from heating the $\text{UC}_{1.5}$ microspheres in a tungsten crucible in hydrogen at 1900°C for 1 to 2 hr were encouraging. Metallographic examination showed the material treated under these conditions to be a UC matrix containing thin platelets of UC_2 . Apparently the UC_2 concentration was low, since only UC was detected in a Debye-Scherrer x-ray diffraction pattern. These results appear to be inconsistent with the findings of Harder, Read and Sowden,¹⁰ who reported that 850°C was the optimum temperature and that above 1100°C very little reduction occurred.

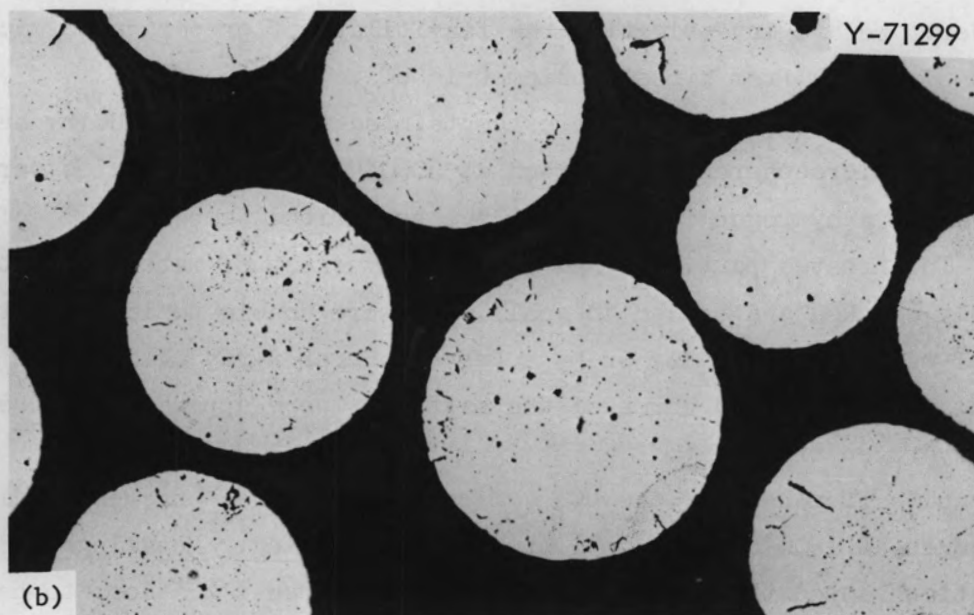
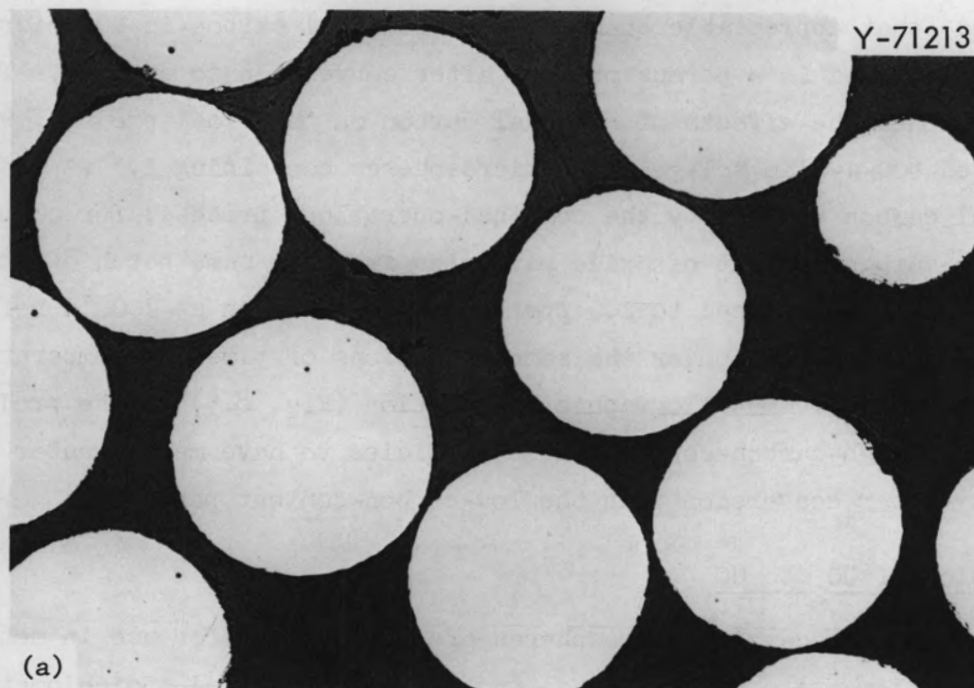


Fig. 8.5. Microstructures of ThC₂ Microspheres Prepared by Heating Oxide Particles of Different Carbon Content with Lampblack at 2200°C for 6 hr. As polished. 75X. (a) 100 ppm initial carbon. (b) 1.5 wt % initial carbon.

To determine whether our results of heating in hydrogen at 1900°C may have been influenced more by the "gettering" of carbon by the tungsten crucible than by the hydrogen treatment, we heated the UC_{1.5} microspheres at 1900°C for 2 hr in a tungsten crucible in an argon atmosphere. Although some increase in UC content was evident by metallographic examination after this treatment, it was not as extensive as that obtained by hydrogen treatment of the UC_{1.5} microspheres. Furthermore, the carbon reduction obtained by hydrogen treatment of UC_{1.5} particles buried in tungsten powder appeared to be insignificant, and we observed in the microstructure of the particles unidentified phases that had not been observed in the previous experiments.

We concluded that the presence of tungsten influenced the carbon reduction in the UC_{1.5} particles but that the hydrogen treatment was the most important factor.

Porous Oxides

K. J. Notz

Laboratory studies are being carried out on methods by which controlled porosity can be built into sol-gel uranium and thorium oxide microspheres. We are presently investigating methods whereby the material to be volatilized is introduced at the sol preparation step and then volatilized in the gel-firing step. We have examined the preparation of porous thoria by the volatilization of carbon by oxidation from thoria-carbon gels, porous UO₂ by chloride volatilization, and porous ThO₂, UO₂, and ThO₂-UO₂ by volatilization of MoO₃ introduced as molybdic acid in the oxide sol.

Preparation of Porous UO₂, ThO₂, and ThO₂-UO₂ by Incorporation of Chloride or MoO₃ (T. A. Gens¹¹)

Urania microspheres with porosities between 1 and 44% (see Fig. 8.6) were made by firing gel spheres prepared from UCl₄. The amount of chloride in the gel spheres, and thus the porosity of the products, could be controlled by varying the volume of ammonium hydroxide solution used as a leachant. Most of the pores were about 1 μ in diameter at porosities above 25%. At lower porosities the pore sizes were distributed over a range from 0.01 to 10 μ.

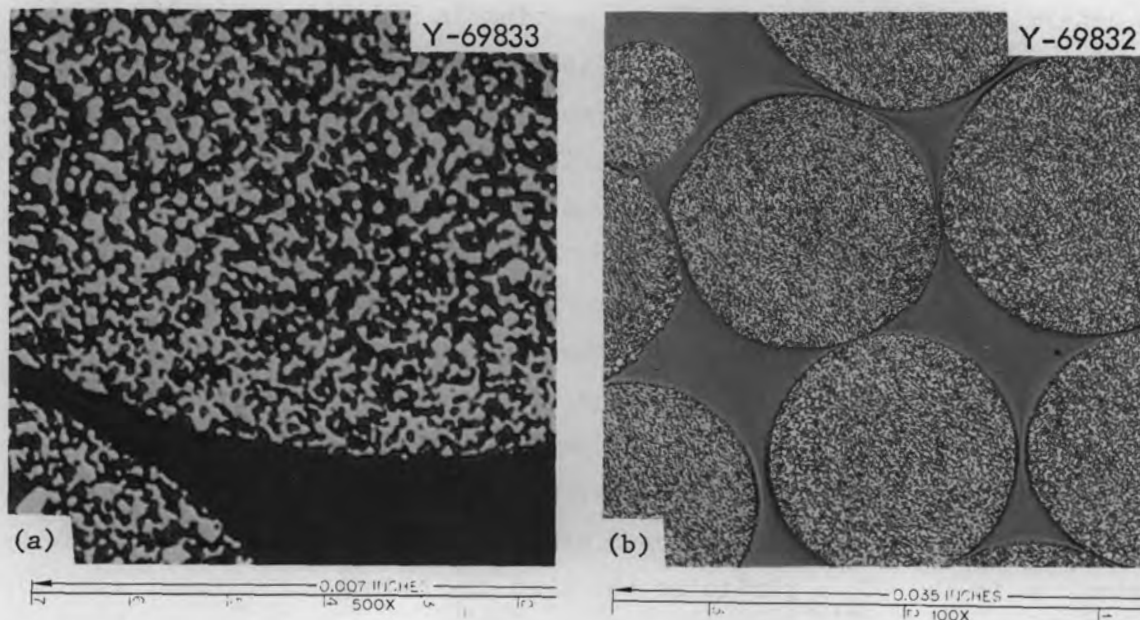


Fig. 8.6. UO_2 Microspheres with 44% Porosity Prepared by Firing Chloride-Containing Gel. The pores are uniformly distributed throughout the microspheres.

Urania or thoria microspheres of 20 to 35% porosity could be prepared from gels containing MoO_3 . Only one UO_2 - ThO_2 preparation was made, and that was at 43% porosity. In the UO_2 preparations, the porosity could be controlled by varying the molybdenum-to-uranium ratio in the sols from 0.1 to 0.8. The final products closely resembled the products described in the preceding paragraph except that the pore sizes tended to be larger and pore size increased with increasing porosity (Fig. 8.7). The porosity introduced in ThO_2 was not reproducible over a range of molybdenum-to-thorium ratios from 0.4 to 0.6. The preparation of porous UO_2 , ThO_2 , and UO_2 - ThO_2 by volatilizing chloride or MoO_3 is described in more detail in topical reports.^{12,13}

Preparation of Porous Thoria by Incorporation of Carbon

(K. J. Notz, A. H. Mesch,¹⁴ C. K. Neulander¹⁴)

For certain nuclear applications, a limited amount of controlled porosity is desirable in ThO_2 . One way of introducing porosity into thoria (and other oxide fuels as well) is to incorporate carbon black in the oxide sol and subsequently burn out the carbon. The feasibility

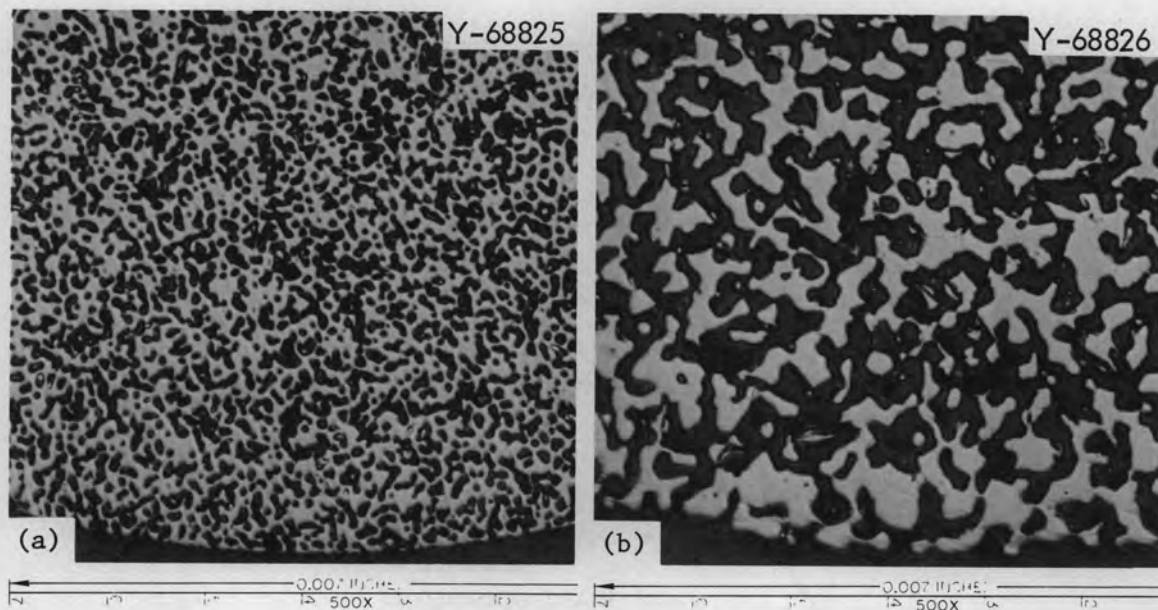


Fig. 8.7. Porous UO_2 Microspheres Made from Chloride-Containing Uranium(IV) Sols. Porosity is 19.2% in (a) and 29.7% in (b). The molybdenum-to-uranium atomic ratios in the respective sols were 0.10 and 0.29.

was demonstrated several years ago¹⁵ at a porosity level of 1 to 4%. During the past year, this work was continued to seek higher porosities and control of the pore size distribution.

In addition to nuclear applications, porous inorganic materials with pore sizes in the 100- to 1000-A range may be useful as chromatographic media for the separation of biologically important compounds. Below 100 A, molecular sieves are available, and above 1000 A conventional filters can be obtained. Therefore, if porous thoria can be made with a controlled pore size in the above range, it may have potential value in other areas of research.

Work on this problem during the past year dealt only with shards; current work is on microspheres. The primary variables studied so far are carbon-to-thoria ratio and variations in the firing cycle that both densifies thoria and burns out the carbon. The best control and maximum porosity for a given carbon content is obtained if the mixed gel is first densified at about 1400°C and the carbon burned out afterward. This method has given porosities up to 64%, with the pore sizes in the 120- to 2000-A range. Typical data are shown in Fig. 8.8. Details of this work will be published as a topical report.¹⁶

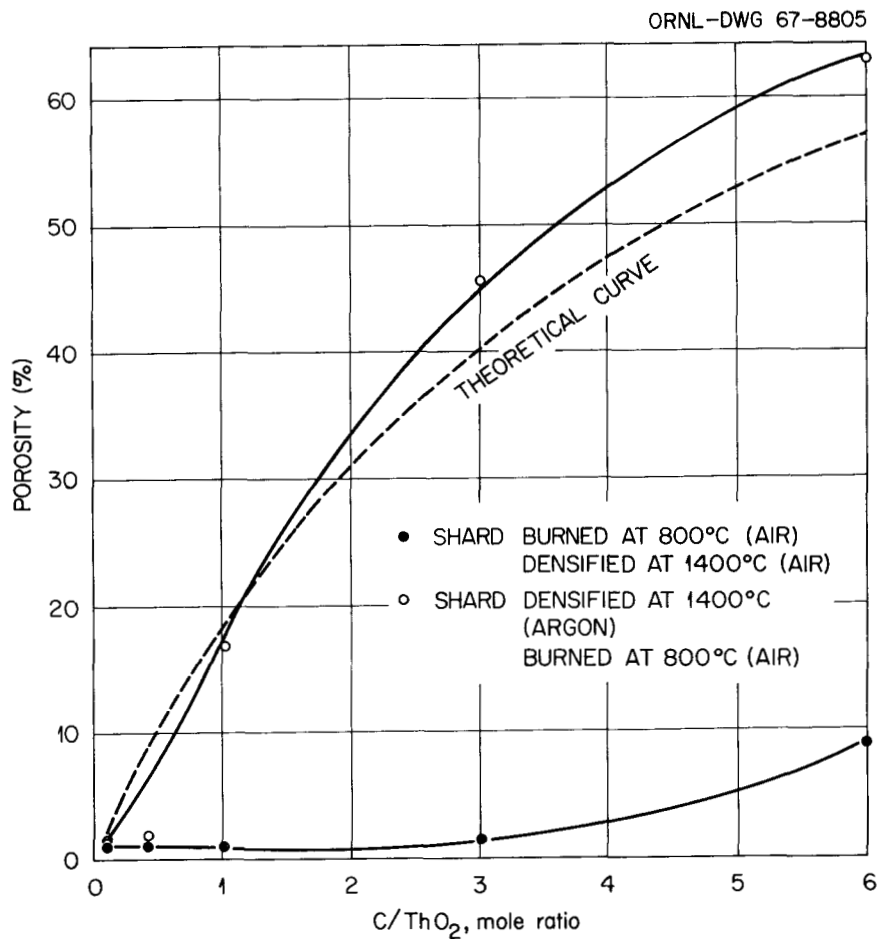


Fig. 8.8. Porosity of Sol-Gel Thoria from Which Incorporated Carbon Was Burned Out.

Properties of Carbon-Metal Oxide Sols

K. J. Notz

To better understand the problems associated with the preparation of carbon-thoria sols, which are subsequently used to make ThC₂ microspheres, we studied the properties of these sols and also of other metal oxide-carbon sols. Electron microscopy, "viscosity titrations", electrophoretic measurements, and other physicochemical methods were employed. So far only urania sols have interacted with carbon blacks in a manner analogous to thoria sols. The other sols that we examined - silica, boehmite (AlOOH), zirconia, and europium hydroxide - behaved differently.

The thoria sols we prepare by steam-stripping of the tetranitrate have a crystallite size of about 70 Å and are acid-stabilized (i.e., positively charged). These sols can disperse and stabilize carbon blacks, thereby forming very stable, very fluid, and relatively concentrated thoria-carbon sols. The rather dramatic effect of a thoria sol on an 8 M carbon black paste is shown in Fig. 8.9. As the thoria concentration is increased, the viscosity decreases greatly, attaining a minimum at a carbon-to-thoria mole ratio of about 8. At higher ThO_2 concentrations the viscosity increases slightly because of the additional thoria. A curve of this type, in which viscosity is used to determine an end point, may be termed a viscosity titration. Similar titrations at other initial concentrations and also in the opposite direction (i.e., adding carbon black to a thoria sol) gave similar curves and end points at carbon-to-thoria mole ratios of about 8. Thus we conclude that there is a fixed carbon-thoria interaction ratio. This ratio is a function of

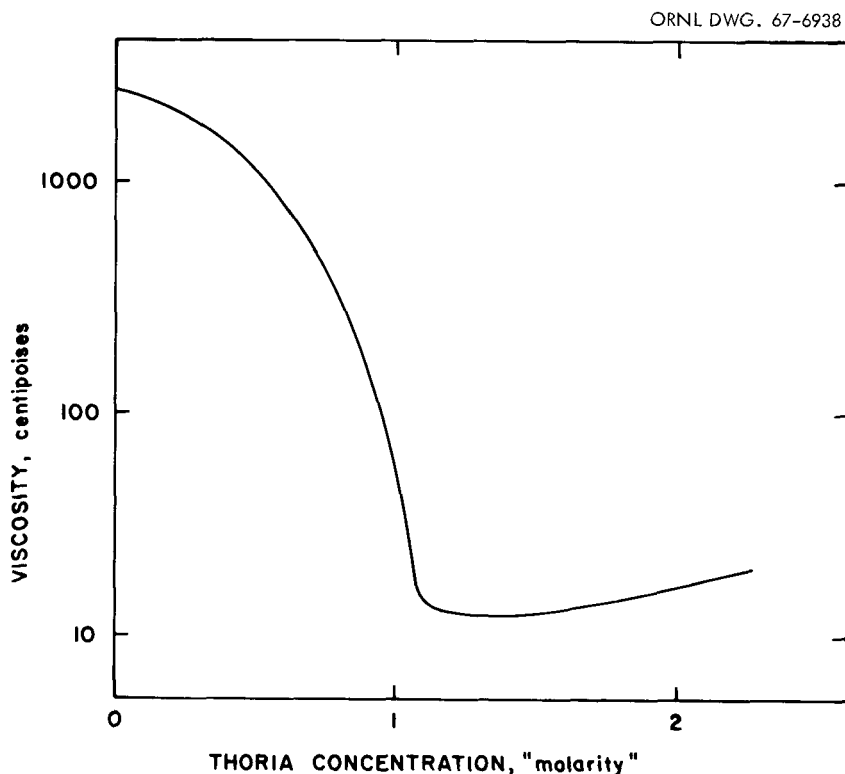


Fig. 8.9. Viscosity Titration of an 8 M Suspension of Spheron 9 (a Carbon Black) by a Thoria Sol.

the specific surface area (or, equivalently, of particle size, since the two are inversely related). When a precipitated thoria with a crystallite size of 35 A -- only half as large as the steam-stripped thoria -- is used, the end point in a viscosity titration occurs at a carbon-to-thoria mole ratio of about 15. The end point also varied with the particle size of the carbon. Thus the thoria-carbon interaction mole ratio is dependent on the particle size of the carbon as well as the crystallite size of the thoria.

Electron micrographs suggest that the ThO_2 particles act as a protective colloid, attaching to the carbon surfaces. This is also borne out by measurements of the zeta potential: the thoria sols have a zeta potential of +67 mv compared to +55 mv for the mixed carbon-thoria sol, whereas conventional aqueous carbon black sols have a negative zeta potential.

The interaction between thoria and carbon black must be fairly strong, since attempts to separate and recover both ThO_2 and carbon from blended sols have not been successful. However, refluxing the mixed sol with approximately 4 M HCl converted the thoria to a soluble chloride, leaving a carbon residue. This residue was then examined under the electron microscope and its specific surface areas was also measured. The recovered carbon, which amounted to 81% of the original amount, was virtually unchanged.

Urania sols behaved in a similar manner toward carbon black. In fact, about the same stabilizing and dispersing effect was noted as for thoria. In viscosity titrations with UO_2 sols, the end point occurred at about the same carbon-to-metal ratio as with thoria after a particle size correction was applied. The urania sols were very much like the thoria sols: the crystallite size of the former was 50 A, and both oxide sols were positively charged.

The other oxide sols tested for their dispersing ability toward carbon black gave negative results. The silica sol had small crystallites (75 A) but was negatively charged. The other sols were positive but had large particle sizes: $\text{Eu}(\text{OH})_3$, 300 x 2000 A; ZrO_2 , 50 x 300 A; and AlOOH , 100 x 1000 A. From these data one would conclude that an oxide sol suitable for dispersing and stabilizing carbon black must consist of small (<100 A in the longest dimension) positively charged particles.

REFERENCES

- ¹Calculated from data given in Fig. 6 of J. L. Kelly, A. T. Kleinsteuber, S. D. Clinton, and O. C. Dean, "Sol-Gel Process for Preparing Spheroidal Particles of the Dicarbides of Thorium and Thorium-Uranium Mixtures," Ind. Eng. Chem. Process Design Develop. 4, 212-16 (1965).
- ²R. L. Hamner, R. L. Pilloton, R. B. Pratt, and J. T. Venard, Status and Progress Report for Thorium Fuel Cycle Development Dec. 31, 1965, ORNL-4001, pp. 70-76. See also next subsection of this report.
- ³J. L. Kelly, A. T. Kleinsteuber, S. D. Clinton, and O. C. Dean, "Sol-Gel Process for Preparing Spheroidal Particles of the Dicarbides of Thorium and Thorium-Uranium Mixtures," Ind. Eng. Chem. Process Design Develop. 4, 212-16 (1965).
- ⁴W. D. Bond and K. J. Notz, Status and Progress Report for Thorium Fuel Cycle Development Dec. 31, 1965, ORNL-4001, pp. 120-22.
- ⁵T. A. Gens, D. M. Helton, and S. D. Clinton, Laboratory Preparation of Uranium Nitride Microspheres by a Sol-Gel Technique, ORNL-3879 (November 1965).
- ⁶M. J. Bradley and L. M. Ferris, "Hydrolysis of Thorium Carbides Between 25 and 99°C," J. Inorg. Nucl. Chem. 27, 1021 (1965).
- ⁷Calculated from data given in Fig. 6 of J. L. Kelly, A. T. Kleinsteuber, S. D. Clinton, and O. C. Dean, "Sol-Gel Process for Preparing Spheroidal Particles of the Dicarbides of Thorium and Thorium-Uranium Mixtures," Ind. Eng. Chem. Process Design Develop. 4, 212-16 (1965).
- ⁸E. B. Hunt and R. E. Rundle, "The Structure of Thorium Dicarbide by X-Ray and Neutron Diffraction," J. Am. Chem. Soc. 73, 4777-81 (1951).
- ⁹R. L. Hamner, R. L. Pilloton, R. B. Pratt, and J. T. Venard, Status and Progress Report for Thorium Fuel Cycle Development Dec. 31, 1965, ORNL-4001, pp. 70-76.
- ¹⁰B. R. Harder, J. Read, and R. G. Sowden, The Reduction and Sintering of Hyperstoichiometric Carbides in Hydrogen, AERE-R-4877 (1965); J. Nucl. Mater. 17, 203-14 (1965).
- ¹¹Present address: Union Carbide Research Laboratory, Tarrytown, N. Y.
- ¹²T. A. Gens, Preparation of Uranium and Thorium Oxide Microspheres with Controlled Porosity by a Sol-Gel Process, ORNL-TM-1530 (May 31, 1966).
- ¹³T. A. Gens, Laboratory Preparation of Several Kinds of Nuclear Fuel Microspheres Using a Sol-Gel Method, ORNL-TM-1785 (Mar. 10, 1967).

¹⁴MIT Practice School participant.

¹⁵Chem. Technol. Div. Ann. Progr. Rept. May 31, 1965, ORNL-3830, p.
p. 176.

¹⁶K. J. Notz, Preparation of Porous Thoria by Incorporation of
Carbon in Sols, ORNL-TM-1780 (in press).

9. DRYING, SINTERING, AND GAS EVOLUTION STUDIES
ON SOL-GEL UO_2 MICROSPHERES

W. D. Bond

Drying and sintering studies are being made on sol-gel UO_2 microspheres to establish firing conditions that yield products having low carbon content (< 100 ppm) and near-theoretical density. The major problem in firing UO_2 gel microspheres resides in the removal of carbon, which is introduced by the microsphere-forming step as sorbed 2-ethyl-1-hexanol and surfactant. Low-temperature drying methods, such as steam drying to 200°C or washing at room temperature with acetone or methanol, did not remove carbon to acceptable levels. We find a mild oxidizing gaseous atmosphere is required to remove carbon and achieve high density during the firing. It appears that chemical reaction with either steam or carbon dioxide is required to remove the final traces of carbon compounds. Reducing atmospheres, such as hydrogen, or neutral atmospheres, such as argon, do not achieve the desired carbon levels. Firing in an atmosphere containing steam has been far more successful than in one containing carbon dioxide, although in many cases carbon dioxide has yielded adequate results. The difficulty in removing carbon with these atmospheres resides in the fact that the maximum shrinkage rate and pore closure occur in the temperature interval 400 to 600°C , where carbon is oxidized. Carbon dioxide is more effective in promoting sintering and pore closure than is steam, and we consider this to be a disadvantage in that it leads to trapping of the carbon compounds and hence tends to block densification. The enhancement of sintering may be due to oxidation of the UO_{2+x} by carbon dioxide or steam. Studies by thermogravimetric analysis (TGA) show that the UO_{2+x} is oxidized by carbon dioxide or steam at temperatures below which the carbon is oxidized. This result is in agreement with thermodynamic calculations.

The most effective atmosphere that we have used for attaining low carbon and high density is Ar- H_2 - H_2O . We have been using Ar-4% H_2 saturated with water vapor at 90°C (~ 40 moles H_2O /mole H_2) and have found it to be effective in small-scale firings. We have not as yet investigated other proportions of Ar-4% H_2 and steam. Thermodynamic

calculations show that the composition presently used reduces UO_{2+x} up to 1000°C at all values of x from 0.05 or greater (x in our UO_{2+x} gels ranges from 0.1 to 0.35), but it oxidizes carbon or hydrocarbons. On the other hand, argon-steam or carbon dioxide atmospheres are oxidizing to the UO_{2+x} under the same conditions.

In the past year, we performed basic studies on the effects of various atmospheres on the sintering of UO_{2+x} gels in an attempt to understand both carbon removal and UO_2 densification. Fundamental studies of the variables of isothermal shrinkage rate, crystallite growth, and surface area decrease were made. Data on differential thermal analysis (DTA), thermogravimetric analysis (TGA), and gases evolved on heating were used also to study reactions and phenomena occurring during the firing of UO_2 gels in various atmospheres. Based on the fundamental studies, we specified a drying and firing schedule, which on a laboratory (5- to 10-g) scale yielded microspheres of low carbon content and high density. Firing procedures involving a variety of semiempirically chosen atmospheres and soaking conditions were evaluated for their effectiveness in carbon removal and densification in 10- to 300-g firings. Low-temperature drying conditions were again examined for their effectiveness in carbon removal.

Isothermal Shrinkage of Sol-Gel Urania Microspheres

H. Beutler¹

R. L. Hamner

Individual urania gel microspheres were held at carefully controlled temperatures in a hot-stage microscope, and the process of shrinkage was followed by sequence photography. We determined isothermal shrinkage on six spheres in dry hydrogen in the temperature range 680 to 1000°C . To differentiate between dimensional changes due to drying and sintering we soaked the spheres for 12 hr at 400°C before each determination. During this soaking treatment, in which the volatiles were removed, we observed consistently a linear shrinkage of 8 to 10%. Results of our experiments are shown in Fig. 9.1. As in the case of thoria particles, the shrinkage followed a law of the form $\Delta L/L_0 \propto t^n$ at constant temperature. The isotherms differ, however, from those expected from simple

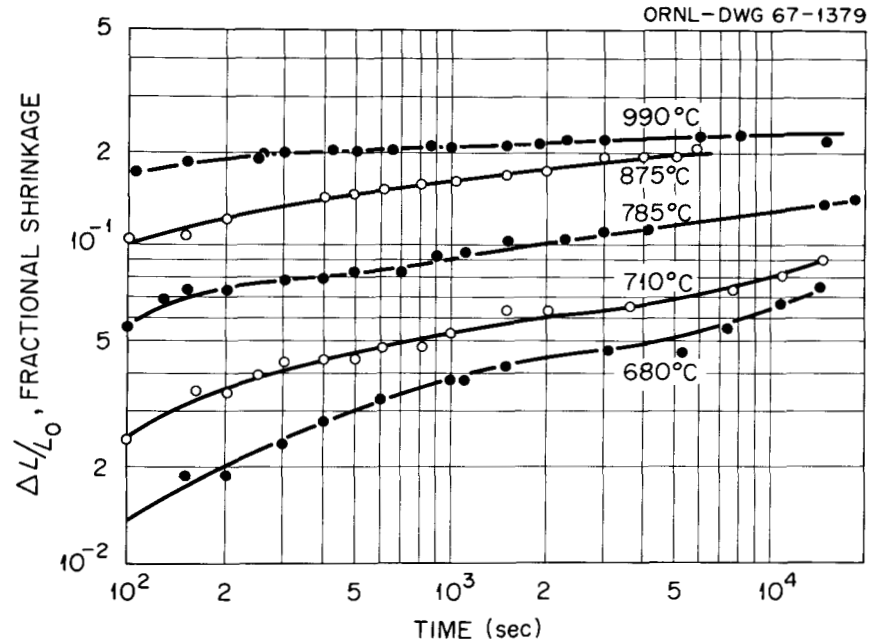


Fig. 9.1. Isothermal Shrinkage of Sol-Gel UO_2 Microspheres in Hydrogen.

sintering theory in that log-log plots of the fractional shrinkage vs time are not linear but decrease in slope with increasing shrinkage. The slope of the shrinkage isotherms decreases from 0.20 to 0.1 as $\Delta L/L_0$ values increase from 0.04 to around 0.1. Maximum linear shrinkage observed was 24% after 1 hr at 990°C, compared to 26% predicted for theoretical density.

Changes of Crystallite Size, BET Surface Area, and Bulk Density During Drying and Sintering of Urania Microspheres

H. Beutler¹

R. L. Hamner

We carried out two series of isothermal heat treatments on sol-gel UO_2 microspheres to investigate the effects of time and temperature on crystallite size, BET surface area, and bulk density. We selected temperatures of 300, 500, 700, and 900°C and heat treatment times of 1 to 24 hr. The sintering atmosphere for the first series was dry Ar-4% H_2 . In the second series the argon-hydrogen mixture was saturated with water at room temperature. The microspheres were contained in fused silica boats and heat treated inside a silica carrier tube in a

laboratory muffle furnace. All the samples heat treated at one temperature were initially charged together into the cold furnace. The temperature was raised to the required level and controlled to $\pm 10^\circ\text{C}$. After intervals of 1, 2, 5, and 24 hr, the samples were moved into the cold end of the carrier tube. By this means all the samples heat treated at one temperature were exposed to the same heatup cycle. For each heat treated sample we determined the x-ray crystallite size (from the broadening of 111, 220, 311 reflections), the BET surface area, and the bulk density by mercury porosimetry. Experimental results are summarized in Fig. 9.2. In dry Ar-4% H_2 we did not observe crystallite growth or

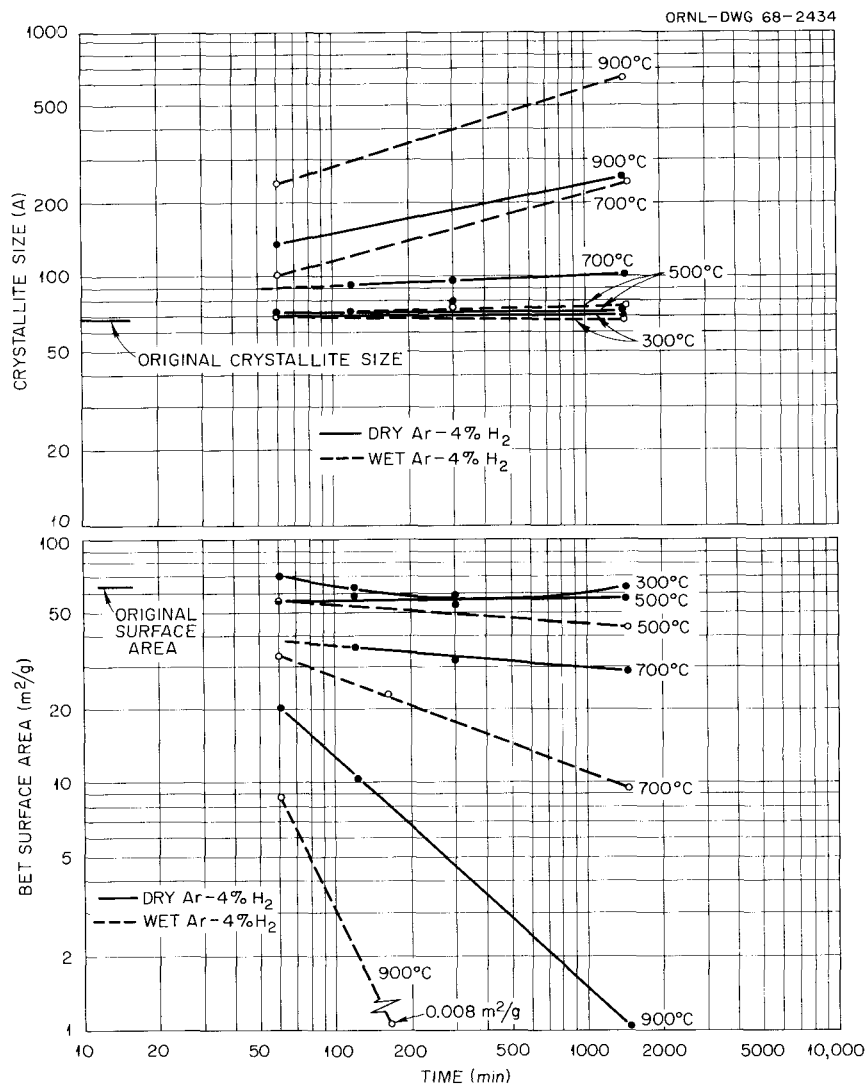


Fig. 9.2. Effect of Time and Temperature on Crystallite Size and BET Surface Area of Sol-Gel UO_2 in Dry and Wet Ar-4% H_2 .

change in surface area at heat treatments for 24 hr at 500°C and below. Above 500°C the crystallite size increased and the BET surface area decreased with both time and temperature.

When the materials were heated for 24 hr at 900°C the average crystallite size increased from 69 Å (crystallite size of original gel) to 247 Å, and the surface area decreased from 69.7 m²/g (BET surface area of original gel) to 1.03 m²/g, which is approximately 500 times larger than the geometrical surface area of the microspheres used. The bulk density increased even after heat treatments at 300°C, although crystallite size and BET surface area did not change. As previously discussed, the density increase at low temperature is associated with the removal of volatiles and subsequent reordering of crystallites and agglomerates thereof to a closer packing. The change in bulk density with both time and temperature is in good agreement with our previously discussed shrinkage data obtained by hot-stage microscopy on single microspheres.

The relationship between fractional shrinkage, crystallite growth, and surface area decrease is shown in Fig. 9.3. Data previously² obtained for the densification of thoria are shown for comparison. The relationships between shrinkage, crystallite growth, and surface area decrease for both thoria and urania are remarkably similar and appear independent of temperature. This suggests a similar activation energy for both densification and crystallite growth.

The presence of water vapor lowered the temperature at which crystallite growth and surface area reduction started and enhanced the process of densification over the whole range of conditions investigated. After a heat treatment for 24 hr at 900°C in wet Ar-4% H₂, the density increased to 10.14 g/cm³, the crystallite size increased to 620 Å, and the surface area decreased to 0.008 m²/g, a value only 4 times higher than the geometrical surface area of the spheres used.

The increase in densification rate due to the addition of water vapor - which we observed either directly in changes of bulk density or indirectly in changes of crystallite growth and surface area reduction with time - corresponds to a temperature increase of 100 to 150°C in treatments in a dry atmosphere.

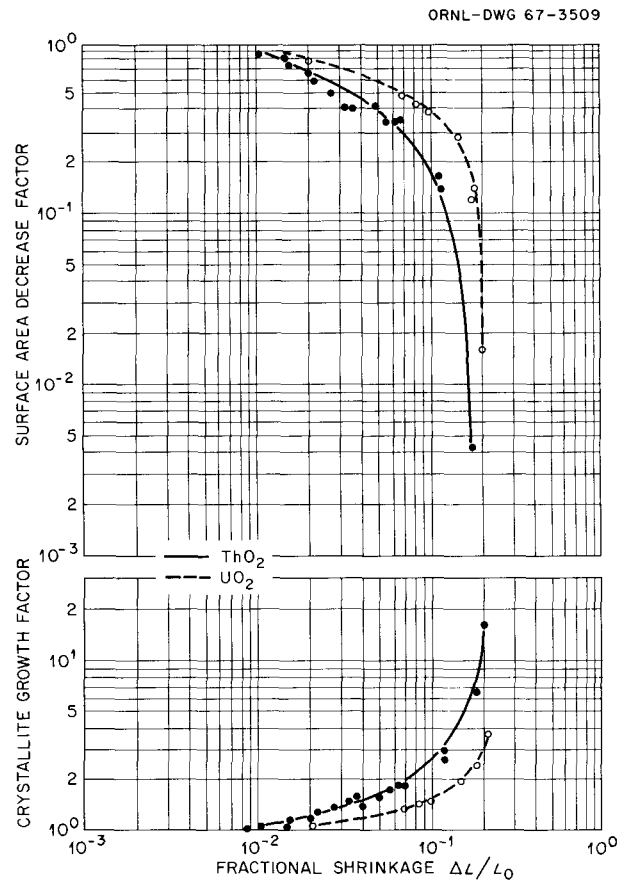


Fig. 9.3. Relationship Between Changes in BET Surface Area, Crystallite Size, and Fractional Linear Shrinkage of Sol-Gel UO_2 and ThO_2 .

Differential Thermal Analyses of Sol-Gel Urania

H. Beutler¹

R. L. Hamner

We employed differential thermal analyses (DTA) as additional means of investigating the drying and sintering behavior of sol-gel urania. A typical DTA pattern, which we obtained during the heating of crushed UO_2 microspheres in Ar-4% H_2 at a uniform rate of $10^\circ\text{C}/\text{min}$, is shown in Fig. 9.4. Two pronounced energy-absorption peaks at 170°C and 470°C are interrupted by a strong energy-release peak at 220°C . A release of surface energy is detected at 730°C and peaks at 870°C . We attribute the endothermic peaks to the evaporation of residual volatiles. The sharp exotherm starting at 220°C is typical of both thoria and urania

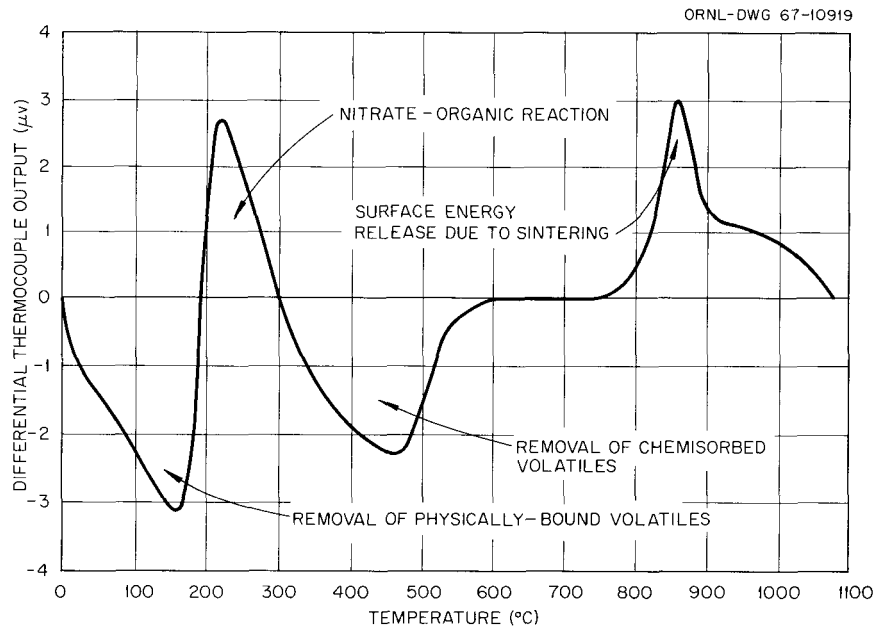


Fig. 9.4. Differential Thermal Analysis Pattern of Sol-Gel UO_2 Microspheres.

microspheres. Since this exotherm is observed only for gels that contain residual organic solvents and surfactants, we attribute this energy release to the oxidation of organic compounds by nitrate. This reaction has caused severe cracking of ThO_2 microspheres heat treated in bulk charges. We have demonstrated by DTA that the organic-nitrate reaction can be successfully suppressed by exposing the microspheres to superheated steam at $150^\circ C$ for 8 hr before the critical temperature region (200 to $250^\circ C$) is passed.

On the basis of our previously discussed study of changes in BET surface area and crystallite growth, we expected the energy release peak due to sintering to start at a lower temperature. We suspected that concurrent removal of residual volatiles during the initial states of sintering resulted in an apparent shift of the surface energy release peak. We subsequently investigated the surface energy release pattern of urania gel fragments that did not contain residual organics. In addition we precalcined the sample in the DTA apparatus for 4 hr at $400^\circ C$ before final heatup to remove residual volatiles. The release of surface energy started at $600^\circ C$ and peaked at $700^\circ C$, in agreement with crystallite growth and surface area decrease measurements.

We investigated the effect of steam-Ar-4% H₂ and carbon dioxide atmospheres on the surface energy release pattern. The addition of water vapor shifted the surface energy release peak approximately 100°C downward in temperature, but the intensity and general pattern of the peak remained remarkably similar to the one obtained in dry Ar-4% H₂. The carbon dioxide atmosphere caused a drastic lowering of the temperature where surface energy release started (see Fig. 9.5). The release occurred within a very narrow temperature range and was completed at 650°C. An isothermal heat treatment of microspheres at 650°C for 24 hr in carbon dioxide confirmed that both sintering and crystallite growth were greatly enhanced. As measured by both mercury porosimetry and helium pycnometer, the bulk density of the microspheres after this treatment was 10 g/cm³, indicating complete closure of surface pores. X-ray diffraction revealed preferential crystallite alignment in the [220] direction. So far we have not been able to demonstrate whether these effects are associated with oxidation of urania during sintering

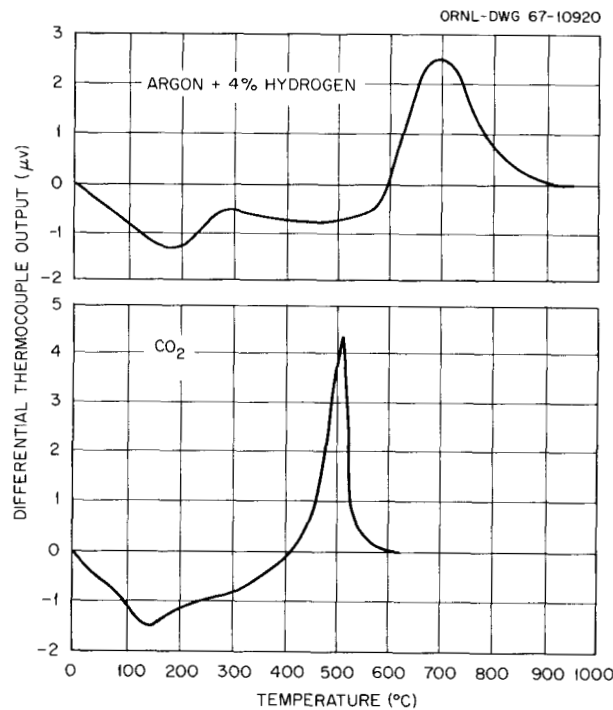


Fig. 9.5. Comparison of Differential Thermal Analysis Patterns of Sol-Gel UO₂ Fragments Heated at 10°C/min in Two Atmospheres. Samples had been precalcined 4 hr at 400°C in Ar-4% H₂.

in CO_2 . We consider the drastic acceleration of the sintering process due to CO_2 a disadvantage. Removal of carbon by CO_2 before sintering (below 400°C) is extremely slow, and removal during sintering appears to lead sometimes to low densities (see previous section).

We conclude that the study of the surface energy release by DTA is a convenient means to characterize the sinterability of sol-gel materials. It enables the determination of upper temperature limits for removal of residues before sintering. For the particular UO_2 sol-gel material investigated, these temperature limits are:

<u>Drying Atmosphere</u>	<u>Maximum Drying Temperature</u>
Dry Ar-4% H_2	550°C
Steam-Ar-4% H_2	450°C
Carbon dioxide	400°C

UO_2 Oxidation Studies by Thermogravimetric Analysis

W. D. Bond

Additional thermogravimetric analysis experiments were performed beyond those previously reported.³ We showed that the UO_{2+x} gels are readily oxidized by carbon dioxide or argon-steam mixtures in the range 400°C and up, but carbon oxidation is not very rapid until the temperature reaches 500°C . The weight change pattern at constant temperatures above 500°C indicated that the UO_{2+x} and the sorbed carbon-bearing species were simultaneously oxidizing. In the initial stages the rate of UO_{2+x} oxidation apparently exceeded the rate of carbon oxidation, but after 2 to 5 min the carbon oxidized faster. After oxidation in CO_2 to 650°C , the UO_2 samples had lost 90% of their BET surface areas. The oxidation of UO_{2+x} with carbon dioxide or steam is in agreement with thermodynamic calculations.^{4,5} The thermodynamic calculations also indicate⁵ that the oxidation of UO_{2+x} can be prevented during the carbon removal step by using as little as 0.1% CO in the carbon dioxide or 0.1% H_2 in steam. Future TGA studies will seek the effect of the hydrogen-steam atmosphere.

Firing in Various Atmospheres

W. D. Bond

In the firing of UO_2 gel microspheres, we heat up and soak the gel in atmospheres that can potentially react with and remove the carbon and then densify the gel. The final sintering is then done in Ar-4% H_2 to reduce the UO_{2+x} to $\text{UO}_{2.00}$. We performed additional studies beyond those previously reported for CO_2 and Ar-4% H_2 atmospheres. In addition we studied Ar- H_2O , Ar- H_2 - H_2O , and room-temperature exposure to air followed by firing in an Ar-4% H_2 atmosphere. We observed effects with carbon dioxide firings that we did not encounter in our earlier work. In the present work with carbon dioxide, we nearly always obtain a mixture of brown and black spheres, and the particle density of this mixture is frequently less than the minimum desired 95% of theoretical. We never observed this in our earlier work, where the fired spheres were always a uniform black. The brown spheres appear to be less dense than the black ones and generally contained fine, closed porosity. We are at present attempting to determine what causes this previously unobserved phenomenon. We also observe this effect in Ar-4% H_2 - H_2O atmospheres when we fire in large batches (>100 g) but not in small batches (<10 g).

Typical Firing Results

Some typical results of the firings using various atmospheres are shown in Table 9.1. The exact time schedules of firings are given in Table 9.2. It is evident from the data that firing in Ar-4% H_2 is only effective for gels having oxygen-to-uranium ratios greater than 2.3, and even this may depend on the amount of excess oxygen in UO_{2+x} relative to the amount of sorbed carbon compounds. Apparently, the excess oxygen can react with the sorbed organic materials. Exposure of the gels to air at room temperature before firing in Ar-4% H_2 was also effective only for the gels with the higher oxygen-to-uranium ratios. Firing in argon rather than in Ar-4% H_2 does not improve the carbon removal. We thought that argon would be more effective than Ar-4% H_2 , because excess oxygen is retained to higher temperatures in the argon atmospheres. With the Ar-3% H_2O , excellent density was always attained, but the carbon content was most often 100 to 200 ppm. With argon-hydrogen-steam mixture,

Table 9.1. Firing of UO₂ Gel Microspheres in Various Atmospheres^a

Microsphere Preparation	Gel Analysis ^b		Firing ^c Code	Carbon (ppm)	Final Product Analysis ^d		
	O/U	Net C (ppm)			Density ^e (g/cm ³)		Helium
					Hg at 210 psi	Hg at 15,000 psi	
11-15-1550	2.37	0.50	Ar-4% H ₂	70	10.83	10.83	10.94
			Air(Ar-4%H ₂)	30	10.90		
			Ar	< 20	10.80		
			CO ₂ -1	< 20	10.84		
			CO ₂ -B	< 20	10.37	10.59	
11-10-1215	2.34	1.02	Ar-4% H ₂	50	10.81		
			Ar	90	10.77		
			CO ₂ -1	< 20	10.70		
			Ar-4%H ₂ -H ₂ O	60	10.6		10.8
10-20-1600	2.27	1.94	Ar-4% H ₂	5500	10.4	10.6	10.6
			CO ₂ -1	120	10.70		10.81
			Ar-3% H ₂ O	110	10.72		10.90
11-7-1545	2.23	1.75	CO ₂ -1	160	10.90		10.94
			CO ₂ -B	50	10.79		11.02
10-19-2310	2.20	0.93	Ar-4% H ₂	2340	10.5	10.5	
11-4-1530	2.19	1.52	Ar-4% H ₂	2320	10.3		
			Ar	3100	10.7		
			CO ₂ -1	90	10.71		
			Ar-3% H ₂ O	180	10.70		
11-2-1504	2.18	2.26	Ar-4% H ₂	5700	10.5		
			Air-Ar-4%H ₂	3900	10.4		
			CO ₂ -1	80	10.07		10.45
			CO ₂ -B	< 20	10.44		
			Ar-3% H ₂ O	< 20	10.58		
47-56-93	2.18		Ar-4% H ₂	8000	10.1		
			CO ₂ -1	810	9.93	9.93	10.01

^aMicrospheres were ~600 μ in diameter. Samples were 100 to 300 g for firings in CO₂ or H₂O atmospheres and were 10 to 25 g for firings in Ar-4% H₂ or Ar atmospheres.

^bFormate-derived carbon is subtracted from the total carbon.

^cFiring conditions defined in Table 9.2.

^dOxygen-to-uranium ratios on final material were 2.002 or less.

^eTheoretical density is 10.97 g/cm³.

Table 9.2. Firing Schedules for Table 9.1.

Firing Code	Heating Conditions			Hold Conditions		
	Atmosphere	Rise Rate (°C/hr)	Temperature Range (°C)	Atmosphere	Temperature (°C)	Time (hr)
Ar-4% H ₂	Ar-4% H ₂	300	25-1200	Ar-4% H ₂	1200	4
Air-Ar-4% H ₂				Air	25	24
	Ar-4% H ₂	300	25-1200	Ar-4% H ₂	1200	4
Ar	Ar	300	25-1000	Ar-4% H ₂	1000	4
CO ₂ -1	Ar-4% H ₂	450	25-450	Ar-4% H ₂	450	0.5
	CO ₂	300	450-850	CO ₂	850	1.5
	Ar-4% H ₂	200	850-1100	Ar-4% H ₂	1100	2-4
CO ₂ -B	CO ₂	50	25-400			
	CO ₂	25	400-600			
	CO ₂	50	600-950			
	Ar-4% H ₂	300	950-1200	Ar-4% H ₂	1200	2-4
Ar-4% H ₂ -H ₂ O ^a	Ar-4% H ₂	300	25-150	Ar-4% H ₂ -H ₂ O	150	2
	Ar-4% H ₂ -H ₂ O	200	150-450	Ar-4% H ₂ -H ₂ O	450	20
	Ar-4% H ₂ -H ₂ O	300	450-1000	Ar-4% H ₂	1000	2
Ar-3% H ₂ O ^b	Ar-3% H ₂ O	50	25-400	Ar-3% H ₂ O	400	20
	Ar-3% H ₂ O	25	400-1000	Ar-4% H ₂	1000	2-4

^aAr-4% H₂ saturated at 90°C.

^bArgon saturated at room temperature.

the P-11-10-1215 product was multicolored like the products fired in carbon dioxide. This was not observed in smaller-scale firings.

The firings in carbon dioxide almost invariably produced mixtures of black and brown spheres, and only with the 11-7-1545 gel did we obtain a uniform black product. In general, the greater the percentage of the brown spheres, the lower was the density. The firings in carbon dioxide atmospheres appear to be reproducible within a given batch preparation but not on different batches of practically the same O/U ratio. Occasionally, we obtain very low-density material, in which the pores are closed, with firing in carbon dioxide. Refiring these low-density spheres to 1500°C in Ar-4% H₂ produces practically no increase in density. We do not understand this variability in the carbon dioxide firings, but we suspect it may have to do with the nature of the excess

oxygen in the UO_{2+x} and variations in the degree of sorption of organic compounds in different microsphere preparations. The excess oxygen in some cases could possibly be mainly on the surface of the 50- to 100-Å UO_2 crystallites, whereas in other cases it may be uniformly distributed through the UO_{2+x} crystalline lattice.

Since excellent results have been obtained on small-scale firings with Ar-4% H_2 - H_2O atmospheres, this work will be extended to the 300- to 500-g scale in the coming year. We believe that the chemical variation kinetics, mass transfer kinetics, or both can be adjusted for larger-scale preparations. Some of the other atmospheres such as carbon dioxide, argon, or argon-steam might well work if the proper soaking conditions are used. However, we do not plan to investigate them thoroughly unless the Ar-4% H_2 - H_2O atmosphere requires unusually long soaking periods.

Low-Temperature Drying Studies (W. D. Bond)

Studies of low-temperature drying in argon or steam show that carbon is not effectively removed by these atmospheres (Table 9.3). Even after drying to 350 or 400°C the gels still contained about 0.5% net carbon. The drying results show that steam is slightly more effective than argon. The measured nitrate-to-uranium ratios show that nitrate removal is nearly complete at 180 to 200°C. The ratio in the original sols is about 0.15. For gels treated below 200°C, the amount of steam used did not appear to be critical, as long as at least 2 g of steam was used for each gram of UO_2 gel. The rate of removal became very slow when more steam was used. The drying results indicated that the carbon-bearing substances are very strongly sorbed.

Drying and Sintering Schedule for Sol-Gel Urania Microspheres

R. L. Hamner H. Beutler⁶

Based on our preliminary characterization studies of sol-gel urania microspheres by differential thermal analyses (DTA), hot stage microscopy, crystallite size determinations, and BET surface area measurements, we sought to establish a drying and sintering schedule designed to obtain high-density low-carbon-content urania microspheres. Our approach was

Table 9.3. Drying of UO₂ Gel Microspheres^a

Gel Microsphere Preparation	Drying Conditions ^b				Gel Analysis				
	Atmosphere	Total Time (hr)	T Max (°C)	Steam Time (hr)	Bulk Density by Hg (g/cm ³)	O/U	NO ₃ ⁻ /U	Carbon (wt %) Total	Net ^c
10-19-2340	Argon	16.0	195	0	4.65	2.20	0.002	1.92	0.93
10-20-1600	Argon	6.5	182	0	4.34	2.27	0.008	2.73	1.94
11-2-1504	Argon	5.5	188	0	3.90	2.18	0.004	2.75	2.26
11-4-1530	Steam	22	180	4	4.03	2.19	0.001	2.22	1.52
11-7-1545	Steam	22	160	4	4.45	2.23	0.004	1.92	1.75
11-8-1400	Steam	22	157	4	4.64	2.34	0.01	1.51	1.44
11-9-1301	Steam	22	152	4		2.30	0.005	1.60	1.45
11-10-1215	Steam	24	160	4	4.72	2.34	0.009	1.44	1.02
11-10-1520	Steam	24	140	2.5	5.09	2.36	0.016	1.14	
11-15-1550	Steam	48	154	2.7	4.63	2.37	0.02	1.08	0.56
3-3-1515	Steam	20	105	4		2.18		2.90	2.00
3-3-1515	Steam	20	350	4				1.05	0.62
47-24-97	Argon	21.5	400	0				1.20	0.50

^aTested in 100- to 300-g batches at flow rates of Ar, 1 liter/min; steam, 2 to 3 g/min.

^bSamples reported dried in steam were first heated to 120°C in argon; then steam was introduced.

^cFormate-derived carbon is subtracted from total carbon. Work on dried gel fragments shows that formate does not contribute carbon to a product fired at 1100°C.

to remove as large a quantity of residuals (nitrates, organics, carbon) as possible during the drying step, before the beginning of sintering. The atmosphere and the heating schedule were the major variables considered.

In the past, carbon dioxide has been used extensively as the atmosphere for sintering urania microspheres, mainly because it is effective in removing carbon. However, microspheres sintered in a carbon dioxide atmosphere often have low densities (<95% of theoretical). Our hypothesis regarding these low densities is that the residuals in urania microspheres are not removed to an appreciable degree in carbon dioxide before the beginning of sintering at a temperature just above 400°C; consequently, they become trapped during the early stages of sintering and cause low densities.

Sintering of urania microspheres in steam-Ar-4% H₂ begins just above 450°C. However, in preliminary experiments on one batch of UO₂ gel the nitrate content was reduced from 0.26% (2600 ppm) to 40 ppm and the carbon content from 1.6% to 400 ppm by soaking urania microspheres for 16 to 24 hr at 450°C (before sintering began) in this atmosphere. For this reason, we selected steam-Ar-4% H₂ as the atmosphere for our drying and sintering schedule for urania microspheres.

Another important point to be considered in drying urania microspheres during the heating schedule is the exothermic reaction (we believe between organic material and nitrate) shown by differential thermal analysis (Fig. 9.5) to occur at 220°C. This reaction might lead to a temperature excursion in which the temperature of sintering may be reached quickly before the residuals are removed. We demonstrated by differential thermal analysis that this exotherm could be suppressed by soaking in steam-Ar-4% H₂ at 150°C, just below the temperature at which the exotherm begins.

Based on these considerations, we designed a tentative schedule for drying and sintering urania microspheres as follows:

1. As a precaution against oxidation of urania, the residual organics, or both, deoxygenate the water in the steam generator for 16 hr by passing Ar-4% H₂ through the water heated at 90°C.

2. Heat the microspheres to 150°C in a dry gas, introduce steam at this temperature, and soak for 2 hr to suppress the nitrate-organic reaction.

3. Heat to 450°C and soak for 16 hr at this temperature (just below the threshold temperature for sintering) to remove residual nitrates and carbon.

4. Heat to 1000°C and soak for 1 hr to densify the particles.

5. Cool to room temperature in dry gas.

Four 10-g samples of urania sol-gel microspheres, approximately 600 μ in diameter, from different batches, were heated according to the schedule described. We observed no cracked particles after sintering, and the particles were glossy black. Figure 9.6 shows the microstructure of particles from one of the batches after sintering at 1000°C. Other results of sintering the particles according to the prescribed schedule

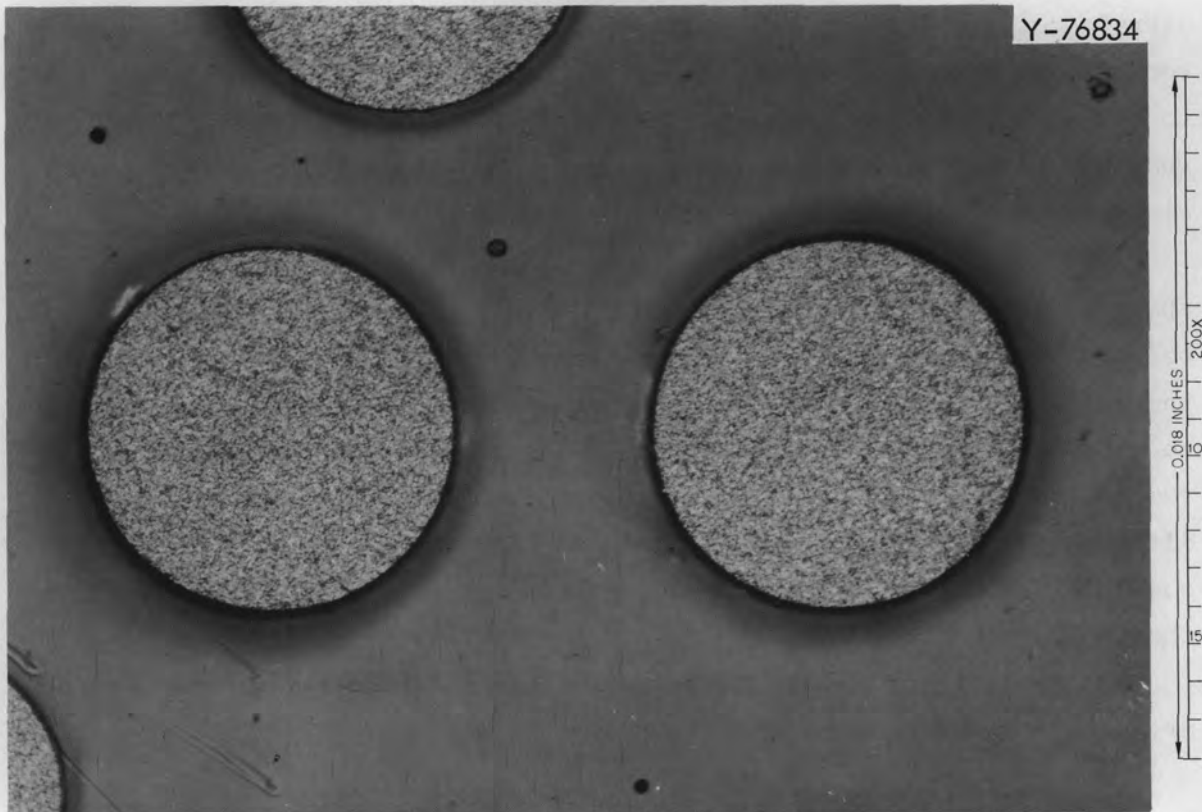


Fig. 9.6. Microstructure of Urania Sol-Gel Microspheres Sintered in Steam-Ar-4% H_2 to 1000°C. Etchant: 70 H_2O -20 H_2O_2 -10. H_2SO_4 .

are shown in Table 9.4. These results show that for small samples, sound high-density low-carbon-content urania microspheres can be obtained by drying and sintering in steam-Ar-4% H₂.

We are now studying the rate of carbon and nitrate removal from the microspheres as a function of time and temperature to optimize the sintering schedule.

Gas Evolution from Sol-Gel Microspheres⁷

D. N. Hess C. F. Weaver B. A. Soldano H. F. McDuffie

Sol-gel microspheres of ThO₂ and UO₂ evolved gases when heated, as did the ThO₂-3% UO₂ sol-gel materials previously reported.^{8,9} We tried to remove these gases and carbon, which are generated by interaction and pyrolysis of the water, nitrates, organic solvents, and surfactants included in the sol-gel materials during their preparation. Such removal is considered desirable because excess gas pressure or reactions between the gas and metal might occur in sealed fuel elements and cause rupture during reactor operation.

Table 9.4. Results of Heating Urania Sol-Gel Microspheres to 1000°C in Steam-Ar-4% H₂

O/U Ratio		Carbon Content (%)		Density ^a (g/cm ³)
Initial	Final	Initial	Final	
b	2.003	b	0.004	10.45
2.303	2.001	1.60	0.003	11.0
2.354	<2.001	1.51	<0.002	10.93
2.326	2.002	0.72	<0.002	10.87

^aAs determined by mercury porosimetry. Theoretical density is 10.97 g/cm³.

^bNot determined.

The following conditioning scheme, comprising a sequence of exposures to flowing gases at atmospheric pressure, successfully produced a low carbon content, a low oxygen-to-uranium ratio, and a high density:

Treatment Time (hr)	Temperature (°C)	Gas
16	170	Ar-H ₂ O
2	250	Ar-4% H ₂ -H ₂ O
2	350	Ar-4% H ₂ -H ₂ O
2	450	Ar-4% H ₂ -H ₂ O
	Cool	Ar-4% H ₂ -H ₂ O
16	Store	He
	25 → 550	Ar-4% H ₂ -H ₂ O
2	550	Ar-4% H ₂ -H ₂ O
2	650	Ar-4% H ₂ -H ₂ O
	Cool	Ar-4% H ₂ -H ₂ O
16	Store	He
	25 → 850	Ar-4% H ₂ -H ₂ O
1 2/3	850	Ar-4% H ₂ -H ₂ O
2	850	CO ₂ -75% H ₂ O
1/2	850	H ₂
3/4	1000	H ₂

The wet gas used was prepared by saturation with water at about 95°C, giving about 3 moles H₂O to 1 mole Ar-4% H₂. The flow of water vapor was necessary to remove carbonaceous material and thus produce a low final concentration of carbon in the UO₂ microspheres. The initial 16 hr at 170°C was a convenient (overnight) period but probably can be reduced to as little as 2 hr. The water vapor also seems to prevent fragmentation of the spheres. The 9.976-g sample lost 15% of its weight. Its final oxygen-to-uranium ratio was 2.001, its carbon content 0.008%, and its density 10.82 g/cm³ (measured with 210 psi Hg). The product was shiny and black with no fines but of nonuniform size.

The mixture of carbon dioxide and steam was superior to either compound used alone for increasing the rate of sintering. Carbon removal

had to be complete before the mixture was added, since the densification trapped any remaining carbonaceous material either mechanically or by carbide formation.^{10,11} The final use of pure hydrogen to counter the oxidizing effect of the mixture of carbon dioxide and steam produced the low oxygen-to-uranium ratios.

We expect that the same processing scheme would be applicable to microspheres consisting of any ThO₂-UO₂ solid solution, although no experimental information is available for such materials. For the pure ThO₂, the hydrogen in the processing scheme is both unnecessary and harmless. Since excess oxygen in UO_{2+x} aids sintering,¹² longer densification times would be required for ThO₂-rich samples.

Experiments have been performed to help understand the complex chemistry of the conditioning scheme described previously. Primary attention was given to identification of off-gases and to oxidation-reduction reactions involving the processing gases H₂O, CO₂, and H₂.

The air-dried ThO₂ microspheres yielded CO₂, CO, H₂, NO, N₂, and organics upon heating in vacuum. The first three predominated. The largest amount of gas evolution occurred at the following temperature intervals: 240 to 260, 400 to 460, and 700 to 760°C. Above 760°C, only a negligible amount of gas remained.

The wet UO₂ microspheres yielded CO₂, CO, H₂, N₂, O₂, NO, and organics when heated with steam and evacuated. The temperature intervals of maximum gas evolution appeared to be 150 to 250 and 400 to 650°C. The principal organic gas evolved (primarily in the 300 to 350°C range) was CH₄. This is in contrast to the production of higher-molecular-weight organic products previously noted with ThO₂ microspheres.

A possible explanation¹³ for the difference is that in dry ThO₂ thermal cracking of the organics occurs, while in the wet UO₂ matrix catalytic cracking is dominant. The latter case is expected to produce lower-molecular-weight products. That the lighter products would be more easily removed from the microspheres provides a partial explanation of why water vapor enhances the removal of carbonaceous materials.

The oxidation-reduction reactions



are intimately involved in the processing chemistry. We have observed that $\text{UO}_2\text{-ThO}_2$ (Kilorod material) as well as UO_{2+x} microspheres usually, but not always, react with water vapor to produce hydrogen. This reaction has recently been reported in the literature, and its thermodynamics are well described.¹⁴ It is clear that whether or not reaction (1) proceeds to a measurable extent depends on the value of x . This explains why on occasion the UO_{2+x} microspheres will not reduce water vapor or carbon dioxide. An experiment was carried out to confirm that UO_{2+x} from a sol-gel source is not prevented kinetically from reacting according to Eqs. (1) and (2) by its chemical impurities. A sample was ground to -270 mesh and reacted with carbon monoxide at 1200°C until no further reduction occurred. This product was readily oxidized by either water vapor or carbon dioxide producing hydrogen or carbon monoxide respectively. Once the oxidizing reaction had proceeded to its limit the solid product could again easily be reduced with carbon monoxide. These results and those in the literature indicate that there are probably no kinetic barriers associated with using these reactions, so we have a firm base for studying their rates and optimizing the processing scheme for the sol-gel UO_2 microspheres.

REFERENCES

- ¹Noncitizen employee from Switzerland.
- ²M. J. Bannister, Status and Progress Report for Thorium Fuel Cycle Development Dec. 31, 1965, ORNL-4001, pp. 113-116.
- ³J. P. McBride (compiler), Preparation of UO_2 Microspheres by a Sol-Gel Technique, ORNL-3874 (February 1966).
- ⁴R. E. Wilson, C. Barnes, and L. Baker, Jr., Chemical Engineering Division Semiannual Report July-December 1965, ANL-7125 (May 1966), pp. 159-63.
- ⁵W. D. Bond, unpublished results (1966).
- ⁶Noncitizen employee from Switzerland.
- ⁷Contribution from the Reactor Chemistry Division.
- ⁸D. N. Hess, W. T. Rainey, and B. A. Soldano, Reactor Chem. Div. Ann. Progr. Rept. Jan. 31, 1965, ORNL-3789, p. 177.

⁹D. N. Hess and B. A. Soldano, Reactor Chem. Div. Ann. Progr. Rept. Dec. 31, 1965, ORNL-3913, p. 72.

¹⁰J. R. Hollahan and N. W. Gregory, "A Torsion Effusion Study of the Reaction of Graphite with Oxides of Thorium and Zirconium," J. Phys. Chem. 68, 2346 (1964).

¹¹T. C. M. Pillay and N. W. Gregory, "A Torsion Effusion Study of the Reaction of Graphite with Hafnium and Uranium Dioxides," J. Phys. Chem. 70, 3140 (1966).

¹²W. E. Bailey et al., "Steam Sintering of Uranium Dioxide," Am. Ceram. Soc. Bull. 41, 768 (1962).

¹³P. H. Emmett, consultant, personal communication (1966).

¹⁴R. E. Wilson, C. Barnes, and L. Baker, Jr., Chemical Engineering Division Semiannual Report July-December 1965, ANL-7125 (May 1966), pp. 159-63.



INTERNAL DISTRIBUTION

- | | |
|-------------------------------------|-----------------------|
| 1-3. Central Research Library | 93. J. P. Jarvis |
| 4-5. ORNL - Y-12 Technical Library | 94. P. R. Kasten |
| Document Reference Section | 95. F. J. Kitts |
| 6-50. Laboratory Records Department | 96. C. E. Larson |
| 51. Laboratory Records, ORNL R.C. | 97. J. M. Leitnaker |
| 52. MIT Practice School | 98. T. B. Lindemer |
| 53. R. E. Adams | 99. C. S. Lisser |
| 54. G. M. Adamson | 100. R. E. Leuze |
| 55. S. E. Beall | 101. M. H. Lloyd |
| 56. R. E. Blanco | 102. J. T. Long |
| 57. J. O. Blomeke | 103. A. L. Lotts |
| 58. E. S. Bomar | 104. R. S. Lowrie |
| 59. W. D. Bond | 105. H. G. MacPherson |
| 60. G. E. Boyd | 106. J. P. McBride |
| 61. R. A. Bradley | 107. R. W. McClung |
| 62. R. E. Brooksbank | 108. K. H. McCorkle |
| 63. K. B. Brown | 109. W. T. McDuffee |
| 64. F. R. Bruce | 110. A. B. Meservey |
| 65. W. L. Carter | 111. J. G. Moore |
| 66. J. M. Chandler | 112. J. P. Moore |
| 67. S. D. Clinton | 113. W. L. Moore |
| 68. C. F. Coleman | 114. C. S. Morgan |
| 69. J. H. Coobs | 115. L. E. Morse |
| 70. D. J. Crouse | 116. J. P. Nichols |
| 71. F. L. Culler | 117. E. L. Nicholson |
| 72. J. E. Cunningham | 118. K. J. Notz |
| 73. F. L. Daley | 119. A. R. Olsen |
| 74. D. E. Ferguson | 120. J. R. Parrott |
| 75. L. M. Ferris | 121. W. A. Pate |
| 76. B. C. Finney | 122. P. Patriarca |
| 77. R. B. Fitts | 123. W. L. Pattison |
| 78. J. H. Frye, Jr. | 124. W. H. Pechin |
| 79. F. J. Furman | 125. S. Peterson |
| 80. H. E. Goeller | 126. R. B. Pratt |
| 81. J. H. Goode | 127. J. M. Robbins |
| 82. A. T. Gresky | 128. A. D. Ryon |
| 83. W. R. Grimes | 129. J. L. Scott |
| 84. P. A. Haas | 130. J. D. Sease |
| 85. R. G. Haire | 131. R. J. Shannon |
| 86. J. P. Hammond | 132. M. J. Skinner |
| 87. R. L. Hamner | 133. J. W. Snider |
| 88. W. O. Harms | 134. D. A. Sundberg |
| 89. F. E. Harrington | 135. O. K. Tallent |
| 90. C. C. Haws, Jr. | 136. E. H. Taylor |
| 91. M. R. Hill | 137. D. B. Trauger |
| 92. A. R. Irvine | 138. W. E. Unger |

- | | |
|-----------------------|------------------------------------|
| 139. J. E. Van Cleve | 148. C. M. Adams, Jr. (consultant) |
| 140. V. C. A. Vaughen | 149. L. Brewer (consultant) |
| 141. T. N. Washburn | 150. L. S. Darken (consultant) |
| 142. C. D. Watson | 151. J. A. Krumhansl (consultant) |
| 143. G. M. Watson | 152. P. H. Emmett (consultant) |
| 144. A. M. Weinberg | 153. J. J. Katz (consultant) |
| 145. J. R. Weir | 154. J. L. Margraves (consultant) |
| 146. M. E. Whatley | 155. E. A. Mason (consultant) |
| 147. R. G. Wymer | 156. R. B. Richards (consultant) |

EXTERNAL DISTRIBUTION

157. A. Amorosi, Argonne National Laboratory, LMFBR Program Office
158. G. E. Ashby, W. R. Grace and Company, Washington Research Center, Clarksville, Maryland
159. J. E. Ayer, Argonne National Laboratory
160. E. E. Bain, Nuclear Fuel Service, Erwin, Tennessee
161. J. Crawford, AEC, Washington
162. P. Clark, AEC, Washington
163. D. F. Cope, RDT Site Office, ORNL
164. G. W. Cunningham, AEC, Washington
165. C. B. Deering, RDT Site Office, ORNL
166. Donald de Hales, Pacific Northwest Laboratory, Richland, Washington
167. W. Devine, Jr., Production Reactor Division, P.O. Box 550, Richland, Washington
168. E. W. Dewell, Babcock and Wilcox Co., Lynchburg, Virginia
- 169-173. T. D. Edwards, Gulf General Atomic, San Diego, California
174. R. Fryar, Kerr-McGee Corporation, Oklahoma City, Oklahoma
175. J. Giambusso, AEC, Washington
- 176-177. R. H. Graham, Gulf General Atomic, San Diego, California
178. J. S. Griffio, AEC, Washington
179. N. Haberman, RDT, AEC, Washington
180. C. J. Hardy, AERE, Harwell, England
181. P. G. Holstead, RDT-OSR, P.O. Box 550, Richland, Washington
- 182-183. S. Jaye, Gulf General Atomic, San Diego, California
184. Donald Keller, Battelle Memorial Institute, Columbus, Ohio
185. W. J. Larkin, AEC, ORO
186. K. Laughan, RDT Site Office, ORNL
187. S. Marshall, National Lead Company of Ohio
188. G. L. Mercer, Division of International Affairs, AEC, Washington
189. T. McIntosh, AEC, Washington
190. W. H. McVey, AEC, Washington
191. E. C. Moncrief, Babcock and Wilcox Co., Lynchburg, Virginia
192. R. L. Morgan, AEC, Savannah River Operations Office
193. Peter Murray, Westinghouse Atomic Power Division, P.O. Box 355, Pittsburgh, Pennsylvania
194. M. V. Nevitt, Argonne National Laboratory, Argonne, Illinois
195. R. I. Newman, Nuclear Fuels Department, Allied Chemical Co., P.O. Box 70, Morristown, New Jersey
196. R. E. Pahler, AEC, Washington

197. R. L. Philippone, RDT Site Office, ORNL
198. C. W. Richards, AEC, Canoga Park
199. H. Schneider, AEC, Washington
200. M. Shaw, AEC, Washington
201. J. M. Simmons, Division of Reactor Development and Technology, AEC, Washington
202. E. E. Sinclair, AEC, Washington
203. K. G. Steyer, Gulf General Atomic, San Diego, California
204. C. L. Storrs, HPO-AI/CE
205. A. A. Strasser, United Nuclear Corporation, 5 New Street, White Plains, New York
206. J. A. Swartout, Union Carbide Corporation, New York
207. C. A. Trilling, Atomics International
208. R. P. Varnes, Combustion Engineering, Windsor, Connecticut
209. W. R. Voigt, AEC, Washington
210. B. L. Vondra, NUMEC, Apollo, Pennsylvania
211. M. J. Whitman, AEC, Washington
212. E. L. Zebroski, General Electric Co., 310 DeGuigne Drive, Sunnyvale, California
213. M. A. Khan, Division of Nuclear Power and Reactors, International Atomic Energy, Karntner Ring 11, 1010 Vienna, Austria
214. M. E. A. Hermans, KEMA, The Netherlands
215. Laboratory and University Division, AEC, ORO
- 216-437. Given distribution as shown in TID-4500 under Metals, Ceramics, and Materials category (25 copies - CFSTI)